THE ANALYTIC SCIENCES CORPORATION

TR-1001-1-1

SPACE SHUTTLE NAVIGATION ANALYSIS
FINAL REPORT
VOLUME I - GPS AIDED NAVIGATION

31 May 1980

Prepared under

Contract No. NAS 9-15151

for

NATIONAL AERONAUTICS AND SPACE ADMINSTRATION
Johnson Space Center
Houston, Texas

Prepared by:

G.A. Matchett
M.A. Vogel
T.J. Macdonald

Approved by:

H.L. Jones
E.W. Vinje

THE ANALYTIC SCIENCES CORPORATION
Six Jacob Way
Reading, Massachusetts 01867

FOREWORD

The work for this report was performed under contract number NAS 9-15151. The authors acknowledge the guidance and assistance of the Contract Technical Monitors, Messrs. R.T. Savely and E.R. Schiesser of the Math Physics Branch of the Mission Planning and Analysis Division of NASA/JSC. Assistance and cooperation were also received from Messrs. H.G. DeVezin and T.J. Blucker.

ABSTRACT

This report presents the results of several analytical studies related to Space Shuttle navigation. It is divided into two Volumes, the first dealing with studies related to the addition of NAVSTAR Global Positioning System user equipment to the Shuttle avionics suite, and the second dealing with studies of the baseline avionics suite without GPS. The GPS studies center about navigation accuracy covariance analyses for both developmental and operational phases of GPS, as well as for various Orbiter mission phases. The baseline navigation system studies include a covariance analysis of the Inertial Measurement Unit calibration and alignment procedures, postflight IMU error recovery for the Approach and Landing Phases, on-orbit calibration of IMU instrument biases, and a covariance analysis of entry and prelaunch navigation system performance.

TABLE OF CONTENTS

TABLE OF CONTENTS (Continued)

LIST OF FIGURES

LIST OF FIGURES (Continued)

LIST OF FIGURES (Continued)

LIST OF FIGURES (Continued)

LIST OF FIGURES (Continued)

LIST OF FIGURES (Continued)

LIST OF TABLES

LIST OF TABLES (Continued)

LIST OF TABLES (Continued)

1. INTRODUCTION

For the past six years TASC has participated in the development and evaluation of the navigation software for the Space Shuttle. The earliest studies, summarized in Refs. 1 and 2, involved development of error models for a variety of navigation aids and generation of detailed performance projections for candidate navigation systems for the entry and landing mission phases. Studies that followed, summarized in Refs. 3 and 4, expanded on the earlier studies to encompass navigation performance analyses for hangar and preflight phases (IMU calibration and alignment), for the ascent phase, and for the landing phases (from the termination of entry through touchdown). In the current study, TASC has revised its assessment of preflight IMU calibration and alignment to keep pace with changes in the software procedures, and has expanded the scope of its analytic support to encompass baseline navigation performance analysis for

- Post flight IMU error recovery for ALT
- On orbit calibration of IMU accelerometer and gyroscope biases
- Entry and preland baseline navigation.

As a major addition to these baseline navigation system studies, much of the current effort has focused on consideration of the NAVSTAR Global Positioning System (GPS) as a Space Shuttle navigation aid. This work grew out of the ascent studies reported in Ref. 4, and now includes on-orbit and deorbit/entry mission phases as well. The principal objective of the GPS study effort was to support the Mission Planning and Analysis Department (MPAD) in its work with the Space Shuttle/GPS Panel.

This involved numerous Panel and working group meetings to prepare for the generation of procurement specifications for GPS user equipment hardware and software and to prepare interface specifications between the GPS user equipment and the General Purpose Computer (GPC) of the Space Shuttle. One output of this effort was a series of working papers and recommendations of an informal nature impacting the Panel studies. Another output was the formal, connected performance studies presented in Volume I of this report.

1.1 OVERVIEW

The various studies contained in this report all relate to Space Shuttle navigation during the several Orbiter mission phases, either with the equipment of the baseline navigation system, or with the addition of GPS user equipment to the Orbiter. Figure 1.1-1 summarizes these studies. Most of them were previously reported in Quarterly Progress Reports (Refs. 5 to 16), but they have, in some cases, been updated, reworked, and combined for this final report.

1.1.1 GPS as a Space Shuttle Navigation Aid

While it is not part of the baseline navigation system, GPS user equipment (consisting of antennas, preamplifiers, cabling, receivers, and associated interface equipment) is currently being planned for addition to the Orbiter avionics suite. GPS will have a major impact on Shuttle navigation performance. Once GPS itself is fully operational (Phase III) the passive system aboard the Orbiter will provide a semi-autonomous source of highly accurate navigation data at almost all times, depending on acceptable antenna coverage. The only outages in coverage will come during reentry blackout and during

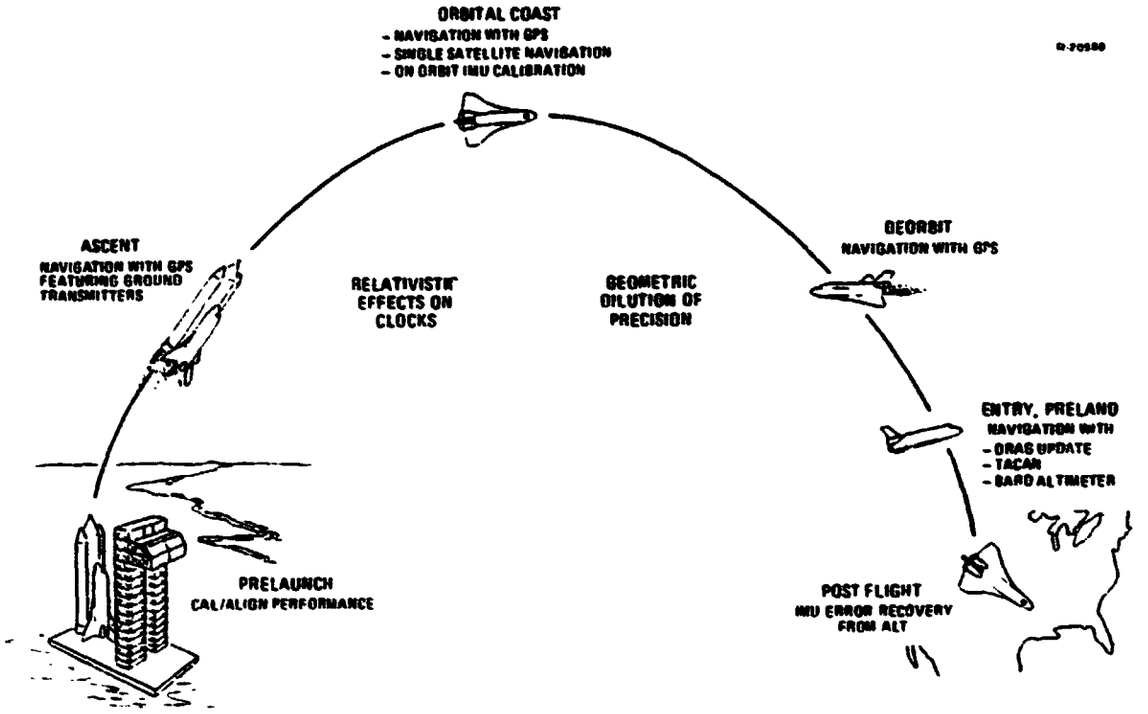

Figure 1.1-1 Summary of TASC Studies Relative to Space Shuttle Navigation (1976-1979)

ascent, where the external fuel tank may block antenna coverage. During the GPS Phases I and II, satellite coverage will be quite limited, but will still support accurate Orbiter navigation on orbit and at times of good satellite visibility during deorbit.

The GPS user equipment differs from the baseline navigation equipment in that it will incorporate an extensive amount of internal software in the receiver/processor assembly (R/PA) and will interface on a computer-to-computer basis with the Shuttle General Purpose Computers. A multiplicity of issues related to software and to navigation system performance need resolution as part of the planning process to incorporate GPS user equipment aboard the Orbiter. Many of these were addressed during the course of this study.

Since the initial utilization of GPS as a Shuttle navigation aid is expected to occur before GPS is fully operational, an extensive study of navigation during GPS Phases I and II was performed. That study features signal coverage analysis as well as covariance analysis of integrated navigation system performance. To look at a limiting case, a situation was examined with only one GPS satellite assumed to be available. The on-orbit navigation performance of the Shuttle was estimated for this condition.

Since navigation performance with Phase III GPS is expected to be very good at almost all times, the study here focuses on the exceptional circumstances associated with reentry blackout, when the GPS signals will not be available. The other situation with potentially limited GPS signal availability during GPS Phase III is Shuttle ascent, when the external fuel tank may block receiving antennas. A study was performed to see if the satellite constellation could be usefully augmented with ground-based GPS transmitters for the ascent and post-blackout mission phases.

There is a considerable connection between the R/PA software and the hardware signal tracking loops. To shed further light on this interaction and on the performance potential of the tracking loops, a study of one mechanization of the tracking loops was performed. That mechanization is associated with the GPSPAC receiver (being developed for space applications by Magnavox) which was an early candidate for a place aboard the Orbiter.

Finally, two special topics related to Orbiter use of GPS were studied. One is the relativistic effects on the Orbiter clock used in the receiver to make GPS measurements. Due to the very large changes in velocity and gravitational

potential experienced by the Shuttle, the relativistic effects are much larger than they would be for earth-based users. Since an atomic time standard is being considered for Shuttle R/PA application, it may be desirable to explicitly account for these effects in the R/PA software. The other special topic addressed is geometric dilution of precision (GDOP). GDOP is not so meaningful for Shuttle operations as it is for other applications, since the anticipated receiver configuration for the Orbiter is a two-channel sequential set, since four GPS satellites may not always be available during the initial usage of GPS on the Orbiter, and since the potential exists for use of an atomic time standard in the receiver. Nonetheless, it is useful as a measure of relative navigation performance potential.

1.1.2 Baseline System Navigation Studies

In addition to the GPS studies, several of the studies summarized in this report address the baseline navigation system. Four specific areas are addressed; three of them involve calibration of the IMU, while the fourth centers on navigation performance.

Preflight calibration and alignment of the IMU's has been studied in prior contracts, but this report contains the first (final) report on covariance analysis of the current cal/align procedure. The previous efforts utilized monte carlo techniques to generate an overall performance projection for the Approach and Landing Tests (ALT) and to identify potential risk areas. The current effort uses covariance techniques to develop a detailed error budget for the Orbital Flight Tests (OFT's, now called Space Transportation System, or STS, missions) and to identify the major error mechanisms that limit calibration and alignment performance.

The ALT's provided NASA's first opportunity to evaluate both the navigation performance achievable with the IMU and the true calibration and alignment uncertainties in a flight environment. TASC's study of postflight IMU error recovery provided a preliminary assessment of the potential accuracy of recovering IMU errors from ALT's.

After lengthy periods on-orbit, the IMU gyros and accelerometers will need recalibration of their only observable characteristics in the weightless environment: their biases. The study of just how to best perform such a calibration recommends procedures, timings, and analytical techniques based on laboratory models of the instruments.

The final baseline navigation topic is the assessment of navigation performance during entry, prior to the landing phase. This work, too, was begun under the previous contract, but is substantially revised here, based on more recent assumptions of initial errors and sensor performance. A candidate, baseline navigation filter is examined in detail.

1.2 ORGANIZATION OF THE REPORT

This report is divided into two volumes. Volume I contains all the GPS-associated studies, while Volume II presents those studies addressing the baseline system.

In Volume I, Chapter 2 summarizes results pertaining to Shuttle navigation with Phase I and II GPS, the test constellations of navigation satellites. Chapter 3 is a study of Shuttle navigation on orbit with a single GPS satellite. Chapter 4 discusses post-blackout navigation with the fully

operational, Phase III GPS constellation. Chapter 5 considers possible augmentation of the GPS satellite constellation with GPS ground transmitters for the ascent and post-blackout mission phases. Chapter 6 contains an analysis of a particular version of a GPS receiver, the GPSPAC receiver, discussing tracking loop performance in the Shuttle environment. Chapter 7 summarizes the most significant conclusions of Volume I. Appendix A considers the relativistic effects on the Space Shuttle GPS clock that must be part of the GPS user equipment. Appendix B is a tutorial discussion of the subject of dilution of precision as it applies to GPS.

In Volume II, Chapter 2 reports the final results of the revised IMU calibration and alignment covariance analysis. Chapter 3 considers postflight IMU error recovery for ALT. Chapter 4 summarizes the study of on orbit calibration of IMU accelerometer and gyroscope biases. Chapter 5 discusses the baseline entry and preland navigation performance. Finally, Chapter 6 summarizes the most significant conclusions of Volume II.

2. NAVIGATION WITH PHASE I AND II GPS

This chapter considers the problem of navigating the Space Shuttle with the developmental satellites of the Phase I and II GPS constellation. During the time in which much of the analysis was being done (Refs. 5 through 8), the concept of using GPS aboard the Space Shuttle was evolving rapidly, and the analytical baseline was changing in parallel. Those study results still relevant to the Space Shuttle program are presented in this chapter, accompanied by some partly outdated, isolated segments believed to still have current, if limited, value.

Section 2.1 provides a brief introduction to the remainder of the Chapter. Section 2.2 is a lengthy summary of GPS satellite visibility with the Phase I and II GPS constellations. Sections 2.3 and 2.4 summarize navigation performance results for the deorbit and on-orbit Shuttle mission phases.

2.1 INTRODUCTION

Both the plans for the GPS itself and for its use aboard the Space Shuttle have been evolving over the three year period encompassed by this report. It is still expected that there will be a period, possibly of several years duration, in which the GPS user equipment will be aboard the Orbiter, but the fully operational GPS satellite constellation of Phase III will not be in place. The ability of the Shuttle to navigate during this period with GPS is open to considerable question, as there will generally be fewer satellites available than are sufficient to support accurate navigation.

This chapter assesses the navigation performance achievable before the Phase III GPS constellation is available. Since the navigation performance depends so much on the limited GPS signal availability, that issue -- satellite visibility -- is treated at some length. Visibility results for an example of the deorbit and on-orbit mission phases are used as inputs to statistical simulations of navigation performance. In addition, the effects of antennas on the visibility situation are examined (although the antennas considered here do not match those currently planned for the Orbiter), and a parametric study of orbital visibility is made covering the constellation options for GPS Phase II.

The navigation performance studies posit navigation filter algorithms for the Shuttle GPS receiver and evaluate those algorithms via a filter-model-versus-truth-model covariance analysis approach. Sensitivity studies are done on some key assumptions. Both the deorbit and on-orbit flight phases are considered.

A previous report (Ref. 4) considered GPS-aided navigation in the ascent phase, but without regard to GPS receiving antenna blockage by the external fuel tank of the Orbiter. The presence of the tank makes the use of GPS during ascent more difficult. Chapter 5 of this report considers augmenting the satellite constellation with ground GPS transmitters to support the Shuttle ascent phase.

2.2 PHASE I AND II GPS SATELLITE VISIBILITY

GPS transmitting antennas are pointed at the earth and have beamwidths adequate to cover the entire earth and near-earth region, including the outer limits of Space Shuttle

travel. The L-band GPS signals have wavelengths of about 20 cm, long enought to penetrate almost all weather conditions, but short enough so that signal transmission is largely a line-of-sight matter. To users with full, spherical, receiving antenna coverage, signal availability is a simple matter of satellite visibility. If a satellite is visible from the user's antenna position, then its signal is available to the user's receiver. The only reason the satellite might not be visible is that the earth or some other body is blocking the signal path.

The ability of GPS to aid in Space Shuttle navigation depends strongly on the number of signals available to the receiver. Having four signals available implies good navigation, except for situations of singular or nearly-singular geometry.* Having more than four signals available increases the likelihood of finding a suitable subset of four. When fewer than four satellites are available, however, the situation is more complex.

When fewer than four GPS signals are available to the Shuttle receiver, the quality of navigation will depend on

- The past history of signal availability
- The quality of the clock (oscillator) in the receiver
- The magnitude of the unaccountable portion of disturbing accelerations on the Orbiter (due primarily to venting on orbit or to IMU errors during dynamic flight phases)
- The degree to which the satellite-to-Orbiter geometry has varied in the recent past
- The type of navigation filter in the GPS receiver.

*See Appendix B for a discussion of such situations.

Since navigation performance depends so strongly on signal availability, visibility studies are an important prelude and accompaniment to navigation performance studies. Such signal availability studies are all termed here "visibility" studies, although they sometimes go beyond the simple concept of line-of-sight visibility into signal availability, and even into signal usability, if necessary. The main factors in the visibility analyses are:

For line-of-sight visibility

- The positions of the GPS satellites
- The position of the Orbiter
- The location of the earth and other signal blocks such as the vehicle structure, the external fuel tanks, and the reentry plasma sheath.

When antenna effects are considered

- The locations of the antennas on the Orbiter
- The attitude of the Orbiter
- The gain patterns of the antennas.

When signal dynamics are considered

- The capability of the receiver tracking loops
- The ability to switch from one antenna to another.

2.2.1 GPS Satellite Positions

The GPS is undergoing a phased development. In the final, operational, Phase III, there are to be 24 satellites*

*A proposed program restructuring would reduce the number of satellites to 18.

"evenly" distributed in a constellation that will provide good signal coverage everywhere on the earth's surface at all times. Once this constellation is achieved, any limitations on satellite visibility from the Space Shuttle will come from less than full coverage by the receiving antennas, or from antenna blockage by the external fuel tank during ascent or by the plasma sheath during reentry blackout.

Schedules for GPS development and for Shuttle GPS user equipment development are still in flux, but it is expected that there may be a considerable period of operation of GPS user equipment aboard the Orbiter before the operational constellation is achieved. During GPS developmental Phases I and II (Phase II began in 1979) there will be from four to six satellites "bunched together" so that four or more are visible at certain times and places, while fewer or none may be visible at other times and places. Generally speaking, good visibility will be obtained from four broad areas of the earth (one of which is the Yuma, Arizona GPS testing grounds) for periods of a few hours each day.

GPS satellite orbits are all norminally circular with radius somewhat over four earth radii, selected so that the satellite period is almost exactly one half of a sidereal day. Each sidereal day, the satellites make two complete revolutions while the earth completes one rotation on its axis, so the ground tracks of the satellites repeat. In fact, the orbital periods are adjusted so that the satellite ground tracks do repeat, taking into consideration a small retrograde movement of the satellite orbital planes brought about by the oblateness of the earth. Each ordinary, solar, day each satellite will appear over any given point on its repeating ground track just 4 min, 3.4 sec earlier than it did the day before. Viewed from

any point on the earth, the time when the Phase II satellites bunch together for multiple signal availability steadily gets earlier each day, taking a little over a year to come full cycle through a complete solar day.

For most of the visibility studies reported here, the trajectory of the Space Shuttle is related to features fixed to the earth, but the time and date of the mission are completely unknown. It is impossible to predict, then, what the visibility situation will be, even approximately. A complete range of visibility situations must be examined, parameterized on the time connection between the Shuttle and GPS satellite orbits. This time connection is termed "offset time" and runs through one full day before the visibility situation approximately repeats. That is, if the "starting time" of a mission under consideration were to vary over a span of one day, then a range of visibility situations would be encountered, with offset time being related directly to the mission starting time. Another useful interpretation of offset time is this: if the mission starting time is a fixed time of day, but the date of the mission were to vary over the span of one year, then the same range of visibility situations would be encountered, with offset time now corresponding to the mission date in an obvious, if indirect, manner. The initialization of the parameter "offset time" for the studies reported here is generally based on a nominal mission starting time and a satellite constellation epoch time that are no longer meaningful. No importance is ever attached to results for such arbitrary times; rather, the range of results is considered for variations.

All of the satellite orbits have the same nominal inclination angle to the earth's equator. Initially, this

inclination angle was planned to be 63 deg, and the satellites of the Phase I & II constellation have (or will have) this nominal inclination. Many of the results reported in Chapter 4 for the Phase III constellation also assume a 63 deg inclination. Recent planning for Phase III, however, calls for a 55 deg inclination angle to improve visibility from middle latitudes while sacrificing some visibility from polar regions. Only minor differences in visibility are observable between these two inclination angles.

The Phase III constellation has its 24 satellites arrayed as eight satellites in each of three orbit planes. The eight satellites are equally spaced, 45 deg from one to the next, in an orbit plane. The three planes are equally spaced, 120 deg from one to the next, in right ascension from the vernal equinox. The relative positions of the eight satellites in one plane, compared to those in another, are offset by 15 deg, so that each satellite has a unique ground track on the earth, although there are only three orbital planes in inertial space. Table 2.2-1 shows the initial right ascensions and initial anomalies of the 24 Phase III satellites. Both the initial epoch (the time at which the values the table are valid) and the reference point for the right ascensions are regarded as arbitrary for purposes here.

The plans during Phase I were to array six satellites as three in each of two orbit planes. The three satellites in each plane were to be separated by 40 deg, the right ascensions of the planes were to be separated by 120 deg, and the relative positions of satellite anomalies in one plane versus those in the next were to be 40 deg different. Table 2.2-2 summarizes this situation, and is the constellation assumed in this report whenever Phase I is referenced without qualification.

TABLE 2.2-1

RIGHT ASCENSIONS AND INITIAL ANOMALIES
FOR THE PHASE III CONSTELLATION

ORBIT PLANE 1 RIGHT ASCENSION* 0 deg		ORBIT PLANE 2 RIGHT ASCENSION 120 deg		ORBIT PLANE 3 RIGHT ASCENSION 240 deg	
SATELLITE NUMBER	INITIAL ANOMALY	SATELLITE NUMBER	INITIAL ANOMALY	SATELLITE NUMBER	INITIAL ANOMALY
1	0	9	15	17	30
2	45	10	60	18	75
3	90	11	105	19	120
4	135	12	150	20	165
5	180	13	195	21	210
6	225	14	240	22	255
7	270	15	285	23	300
8	315	16	330	24	345

*Arbitrarily chosen reference point, not necessarily referenced to the vernal equinox.

TABLE 2.2-2

RIGHT ASCENSIONS AND INITIAL ANOMALIES
OF THE PHASE I CONSTELLATION
(BASED ON 1978 PROJECTIONS)

ORBIT PLANE 1* RIGHT ASCENSION -130 deg		ORBIT PLANE 2 RIGHT ASCENSION +110 deg	
SATELLITE NUMBER	INITIAL ANOMALY	SATELLITE NUMBER	INITIAL ANOMALY
1	0	4	40
2	40	5	80
3	80	6	120

*Referenced to the location of the Greenwich Meridian at 2 hours GMT on 26 August 1977.

Figure 2.2-1 illustrates the ground tracks of the Phase I satellites. The circles on the ground tracks correspond to the satellite positions at the beginning of the Orbiter deorbit trajectory segment considered in the next section.

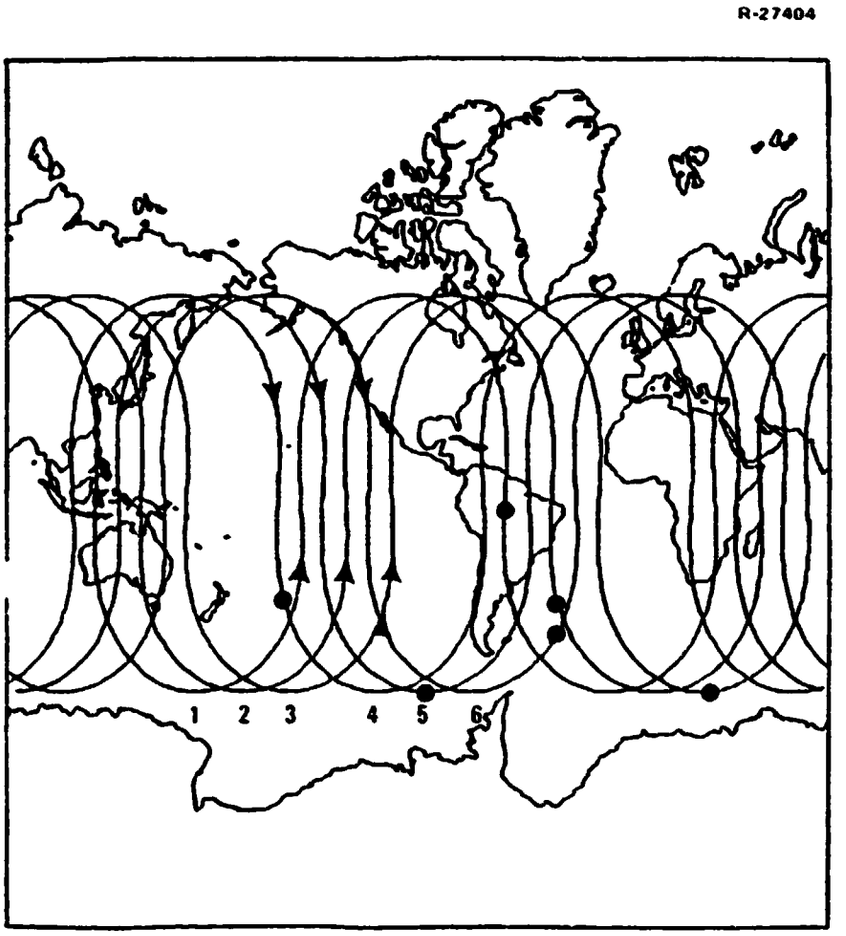

Figure 2.2-1 Ground Tracks of the Phase I GPS Satellites

The tolerances on the orbital parameters of the GPS satellites at the Phase I epoch are shown in Table 2.2-3. The variation in the orbital period is especially important. During

TABLE 2.2-3

TOLERANCES ON THE GPS PHASE I CONSTELLATION AT EPOCH (Ref. 6)

Period	±2 sec
Inclination	±2 deg
Eccentricity	< 0.02
Longitude of the Ascending Node	±2 deg
Angle Between Any Two Satellites	±5 deg

the approximately 580 days from the GPS Phase I epoch to the nominal mission dates considered in the following sections, the orbital period variations could cause satellite mean anomaly variations of over 19 deg.

GPS program plans were revised before all of the satellites were launched. Table 2.2-4 summarizes the revised Phase I constellation, having 42 and 43 deg separations between satellites in one orbit plane and a 47 deg difference in relative anomalies from satellites in one plane to those in the other. The initial anomalies of the table apply at the epoch time of midnight GMT on 21 March 1977. At this time the right ascension of the Greenwich meridian was 178.4 deg.

The four satellites actually launched to date were to nominal positions corresponding to those characteristic of Table 2.2-4, and they are identified by the "NS" numbers in parentheses in the table. Where only four satellites are considered as a constellation in this chapter, it is these four.

TABLE 2.2-4

RIGHT ASCENSIONS AND INITIAL ANOMALIES
FOR THE REVISED PHASE I CONSTELLATION

ORBIT PLANE 1* RIGHT ASCENSION* 219.49 deg		ORBIT PLANE 2 RIGHT ASCENSION 99.49 deg	
SATELLITE NUMBER	INITIAL ANOMALY	SATELLITE NUMBER	INITIAL ANOMALY
1(NS-1)	-29	4	18
2	14	5(NS-2)	61
3(NS-4)	56	6(NS-3)	103

*Referenced to the mean vernal equinox of 1950.0.

2.2.2 Phase I Deorbit Visibility

Satellite visibility during the deorbit segment of a Space Shuttle trajectory is considered in this section. Only one trajectory is used for analysis, and that is to a temporary landing site, but the results should be indicative of performance on most deorbit trajectories from similar orbital inclinations. Using only one trajectory has the advantage that direct comparisons of results obtained under a variety of assumptions is not further complicated by trajectory differences. Navigation performance associated with these visibility results is reported in Section 2.3.

Deorbit Trajectory - A single, simulated Orbiter trajectory generated at JSC is used throughout this report for all studies of deorbit navigation. This trajectory was generated as a candidate for an OFT-1 (STS-1) mission segment, and covers the span from just prior to the deorbit burn at 655 kft of altitude, through touchdown at Edwards AFB runway 17.

The trajectory ground track is plotted on a world map in Fig. 2.2-2, beginning in Australia and continuing to California. Also plotted are the nominal ground tracks of the Phase I GPS satellites over the same period. Figure 2.2-3 is a plot of Orbiter altitude versus time. Both figures show a nominal span labeled "blackout" referring to an assumed loss of L-band (GPS and TACAN) signals during reentry. Additional information relevant to this trajectory is found in Chapters 4 and 5 of this volume, in Chapter 5 of Volume 2, and in Refs. 1 through 4, and 17 through 19.

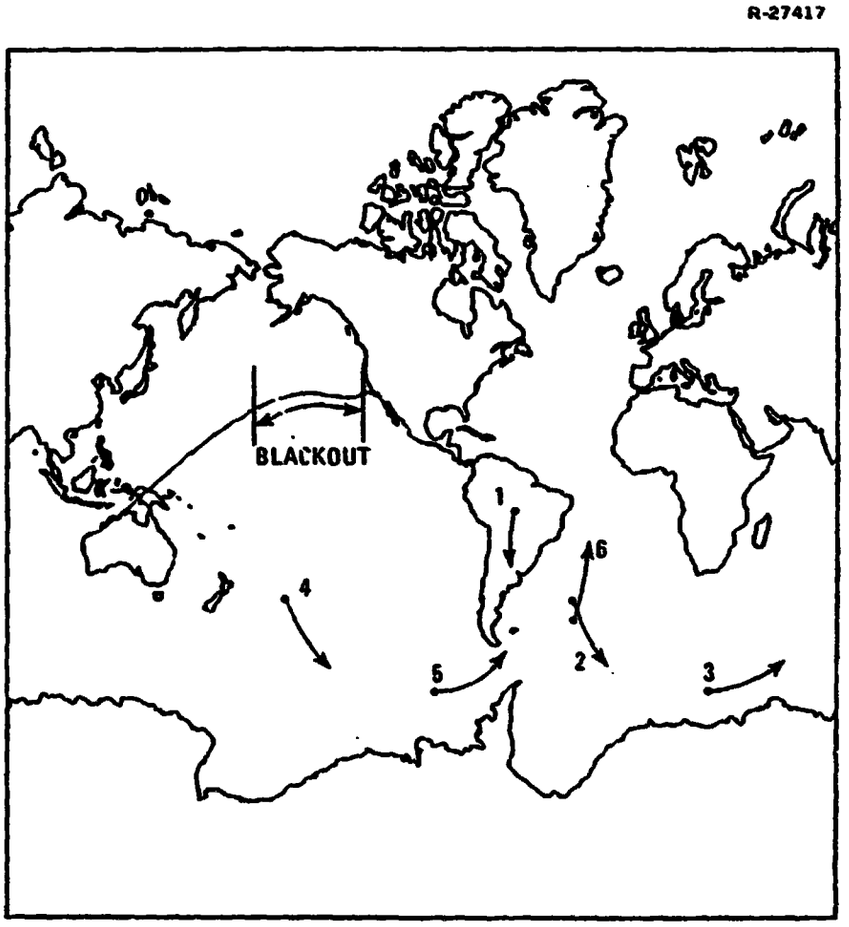

Figure 2.2-2 Ground Tracks of the Shuttle Deorbit Trajectory and Phase I GPS Satellites

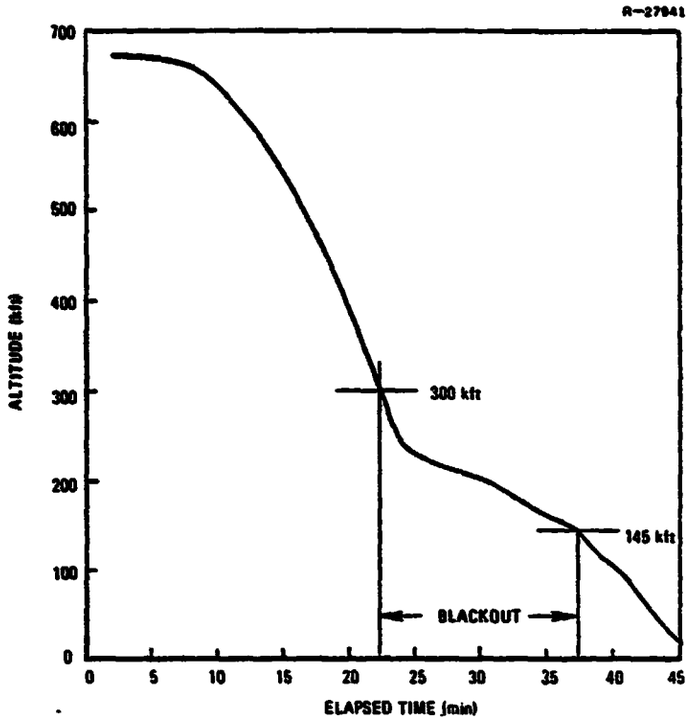

Figure 2.2-3 Altitude versus Elapsed Time for the Deorbit Trajectory

The specific epoch assigned to this trajectory is 16 March 1979 at 19:16:40.4 GMT, and this epoch is used for the Phase I and II visibility studies of this chapter. While the trajectory continues down to a landing, it is sometimes truncated at 20 kft of altitude in this report when the landing phase is not of interest. Besides including Orbiter position, velocity, and sensed acceleration as functions of time, the trajectory tape contains a time history of Orbiter attitude (and numerous other quantities) useful in assessments of visibility with specific antenna locations.

Deorbit Visibility Results - In the visibility results presented in this section, a satellite is assumed visible from the Orbiter if it is more than 10 deg above the Orbiter's

horizon. No antenna limitations are considered. The figure of 10 deg, called the visibility mask angle or the earth mask angle, is somewhat arbitrary; values from 5 deg to 15 deg are reasonable, depending on such factors as antenna gain and atmospheric attenuation of the GPS signals. An approximation to the ellipsoidal earth was used which yields horizon angle computation accuracy of 0.1 deg or better.

Figure 2.2-4 shows how many satellites were visible at each minute from the deorbit epoch down to touchdown on runway 17 at Edwards AFB, assuming the nominal epoch times for the trajectory segment and for the Phase I constellation. As illustrated later, the touchdown time selected for the trajectory tape corresponds to a period of extremely poor GPS satellite visibility along the approach path.

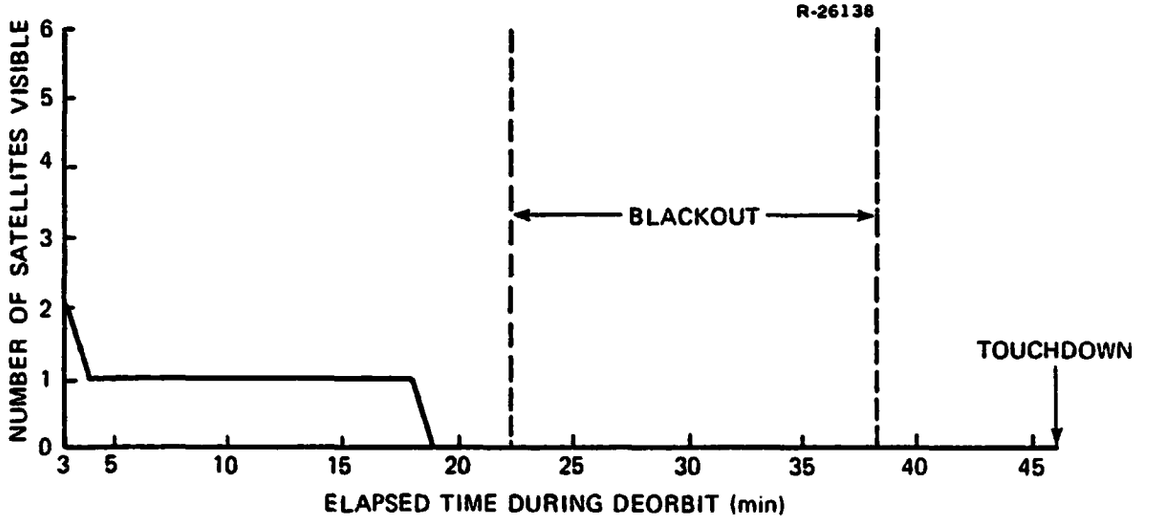

Figure 2.2-4 Satellite Visibility During the Deorbit Phase at Nominal Epochs

During a portion of the deorbit phase of the test, there may be a blackout of radio communications, meaning that

measurements to the GPS satellites are not possible, whatever the geometry for visibility. The blackout portion of the test is indicated in Fig. 2.2-4, based on the assumption of blackout conditions between 300,000 ft and 130,000 ft of altitude during deorbit.

If the mission timeline were advanced so that the deorbit epoch and touchdown occurred at some later time than the one given, then the satellite positions in inertial space would be different, as the satellites advance in their orbits. Also, the Orbiter position in inertial space (given on the trajectory tape) would have to be rotated with the earth so that the Orbiter would still land at Edwards AFB. Precisely these calculations were carried out for a sequence of possible offset times, a sequence spanning one day in steps of 30 min. The calculations leading to the visibility plot of Fig. 2.2-4 were repeated for each offset time to examine satellite visibility as a function of deorbit epoch. Figure 2.2-5 presents all these results.

A vertical line in Figure 2.2-5 shows how many satellites would be visible to the Orbiter as a function of elapsed time since the deorbit epoch, for one particular deorbit epoch. The leftmost vertical line corresponds to the originally quoted epoch, and thus reproduces the data of Fig. 2.2-4. Each succeeding vertical line corresponds to a 30 min offset of the epoch. As the figure shows, if the deorbit epoch were chosen to maximize GPS satellite visibility, it would be about 16 hours later than the time quoted. Figure 2.2-6 shows the visibility for the deorbit phase if the deorbit epoch were offset 16 hours, and the figure includes a bar plot showing which satellites are visible at which times. Figure 2.2-7 is a second such plot showing reduced satellite visibility for an offset time of 21 hr 43 min. Both the good visibility segment and the reduced visibility segment are used in the deorbit navigation studies of Section 2.3.

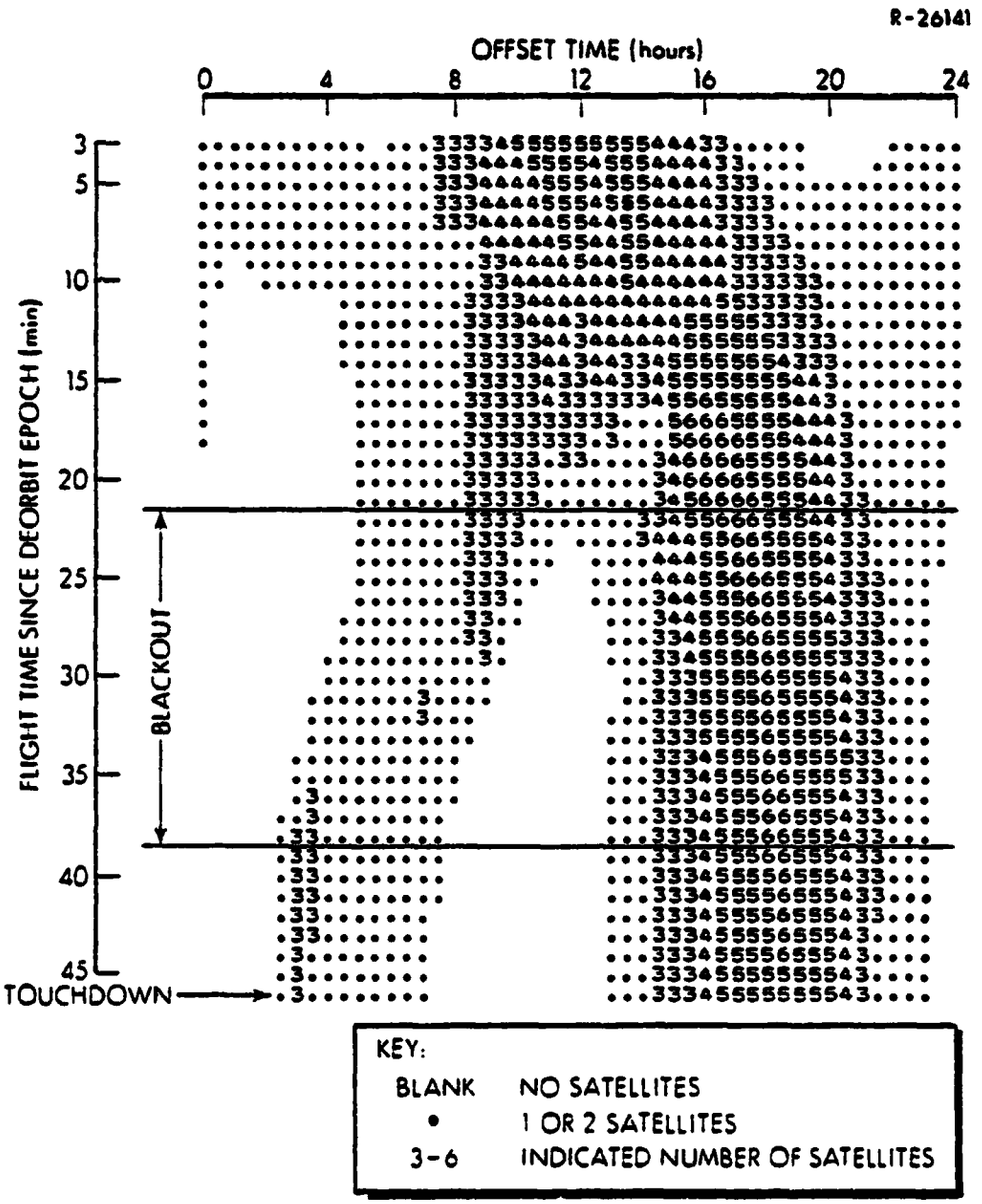

Figure 2.2-5 Satellite Visibility During the Deorbit Phase as a Function of Offset Time

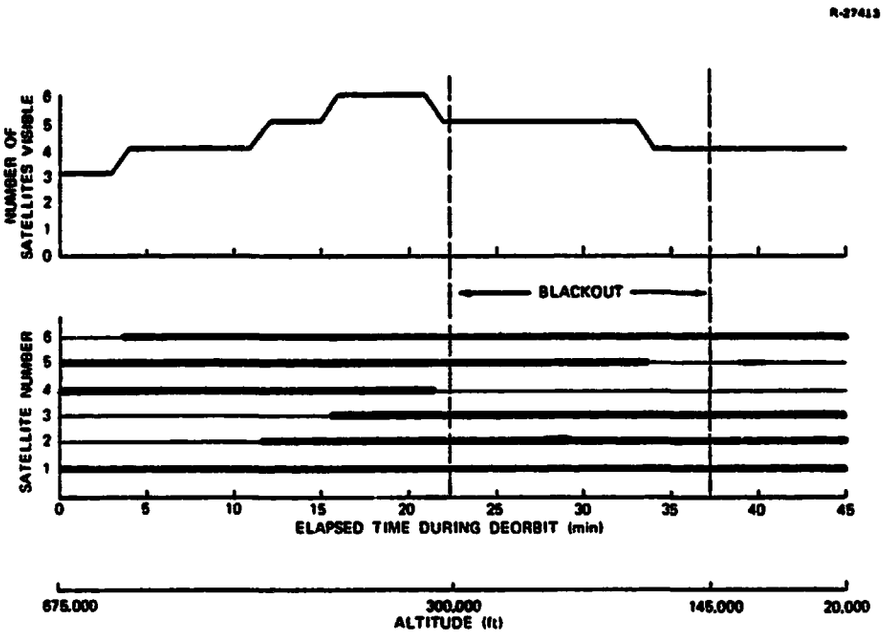

Figure 2.2-6 Good Satellite Visibility During Deorbit for a 16 hr Offset Time

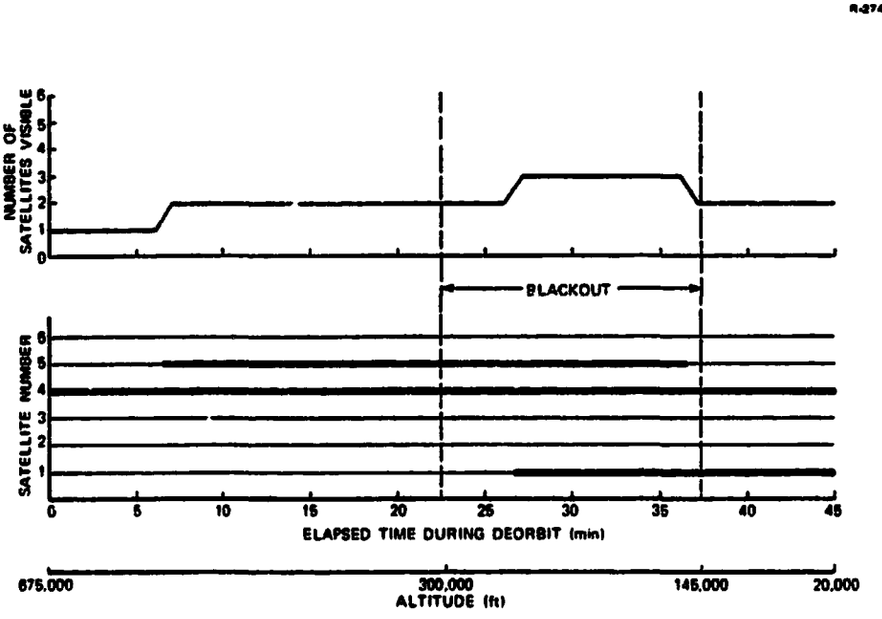

Figure 2.2-7 Reduced Satellite Visibility During Deorbit for a 21 hr 43 min Offset Time

Instead of considering the offset time as an advance in the Orbiter epoch, it is equally valid to consider it as a regression of the GPS Phase I epoch, or as a combination of the two. Because the satellite constellation at epoch was described in earth relative terms, the visibility results are quite the same if the Orbiter is late as they are if the satellites are early; it is only the elapsed time from the satellite epoch to the Orbiter epoch that determines satellite visibility.

2.2.3 Phase I Orbital Visibility

Visibility results for the Shuttle on orbit are reported in this section in a manner similar to that used for the deorbit results of the previous section. One orbital trajectory is baselined for visibility results that are later input to navigation performance analyses. Visibility results for the Shuttle over a range of other orbits, considering antenna effects explicitly, are presented in Sections 2.2.4 and 2.2.5.

Orbital Trajectory - The orbital trajectory used in the study of orbital navigation is extrapolated from a set of initial conditions (position and velocity) by assuming a simple earth gravity model (the same one used for GPS satellite orbit propagation) with no sensed acceleration. Table 2.2-5 summarizes the orbital initial conditions, while Fig. 2.2-8 plots a 90 min segment of the orbit ground track on a world map.

Orbital Visibility Results - Figure 2.2-9 shows how many satellites were visible at 5 min intervals over the 12 hour (8 orbit) period commencing at orbital epoch. Since the GPS satellites have periods of almost exactly 12 hours, which

TABLE 2.2-5
ORBITAL TRAJECTORY PARAMETERS

T-1151

ORBIT DATA	30 March 1979
INITIAL TIME	13:15:38.8 GMT
INITIAL POSITION*	(-2081432, 20009848, - 8493118) ft
INITIAL VELOCITY*	(-21116, -7323, -12066) fps
ALTITUDE AT APOGEE	155.3 n mi
ALTITUDE AT PERIGEE	149.9 n mi
ORBITAL INCLINATION	37.9 deg

*With respect to Aries-Mean-of-1950 coordinates.

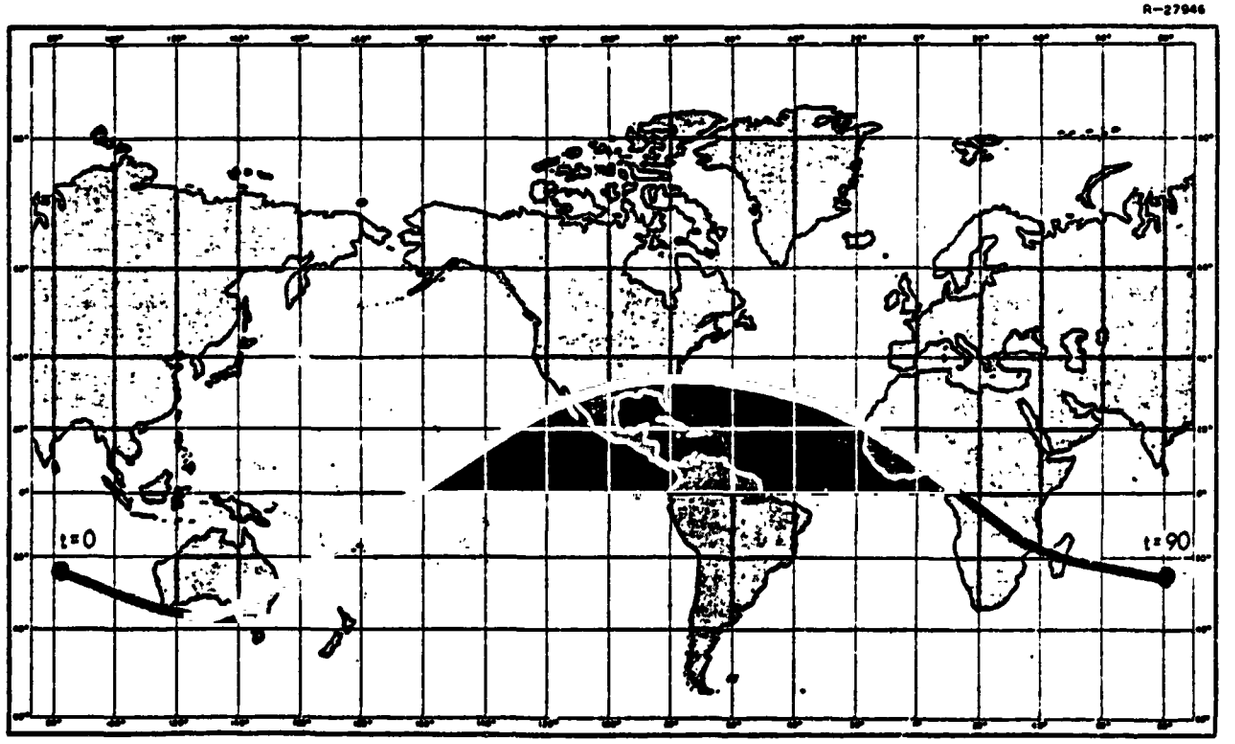

Figure 2.2-8 Shuttle Orbital Trajectory

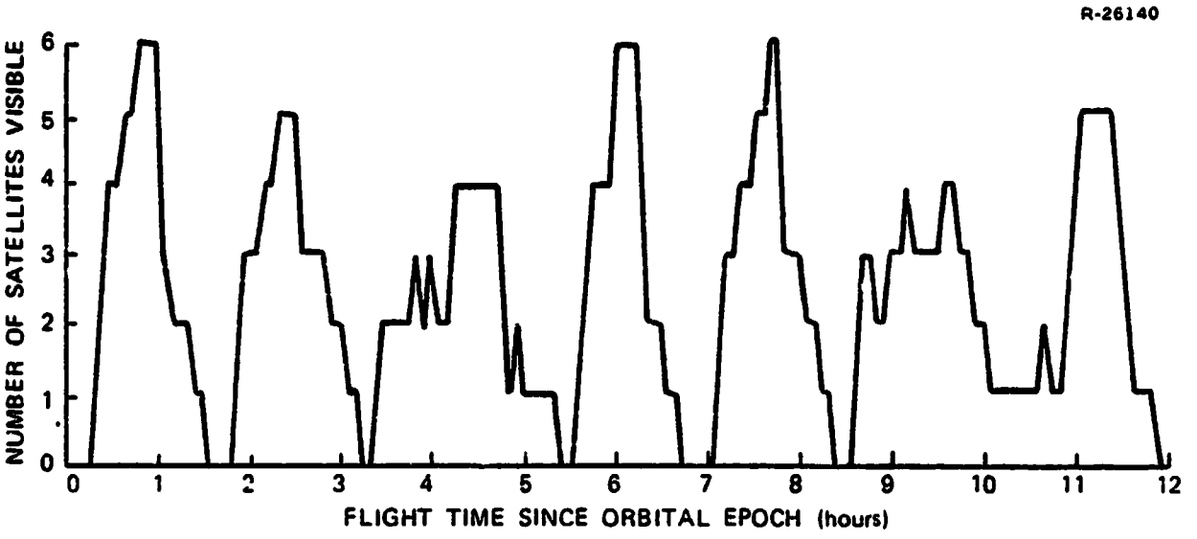

Figure 2.2-9 Satellite Visibility During the Orbital Phase

also corresponds to an integral number of Orbiter revolutions, the visibility patterns should almost repeat every 12 hours. The figure indicates that, in most instances, four or more satellites are simultaneously visible at some time during each orbit. Three or more satellites are visible about 50% of the time.

As was done for the deorbit phase, the orbital results were recomputed for a 24 hour sequence of offset times at 30 min intervals to assess visibility if the orbital epoch or the GPS Phase I epoch should change. Figure 2.2-10 (2 pages) presents these orbital visibility results in the same form that Fig. 2.2-5 used for the deorbit phase.

Visibility on orbit, while it depends in detail on the offset time, is usually good for a significant portion of each orbit whatever offset time is chosen. In order to make

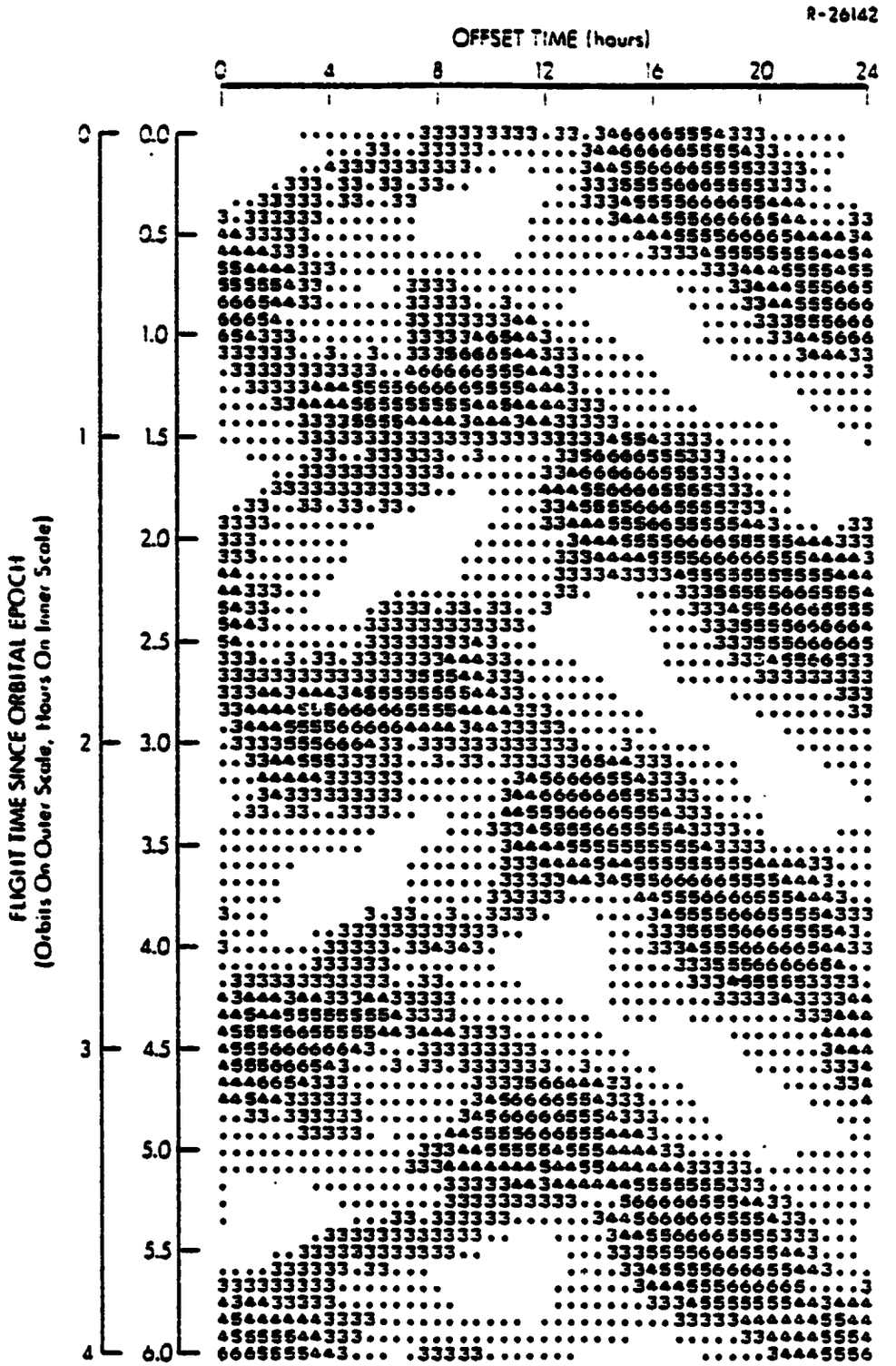

Figure 2.2-10 Satellite Visibility During the Orbital Phase as a Function of Offset Time (See key on Fig. 2.2-5)

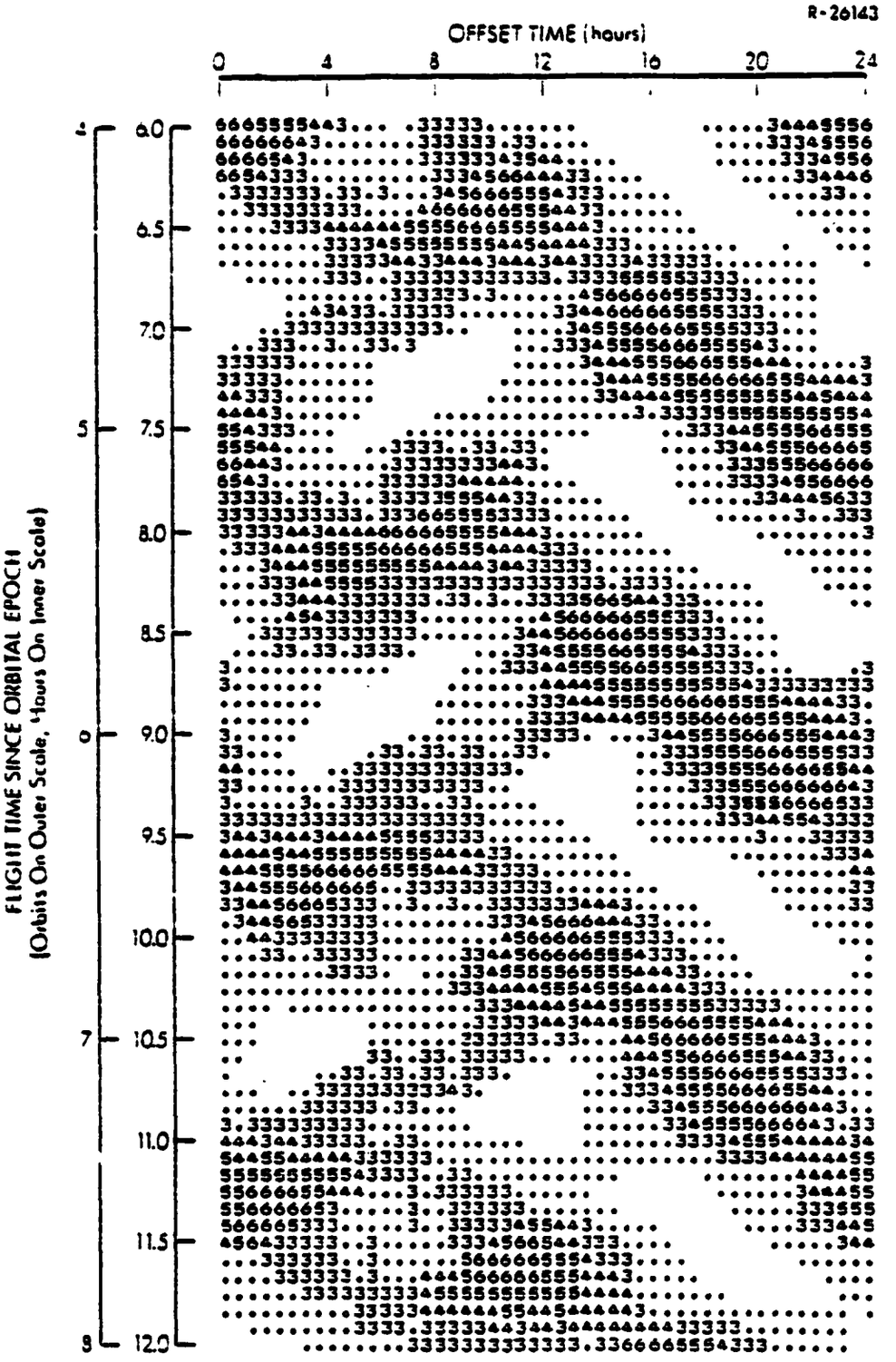

Figure 2.2-10 Satellite Visibility During the Orbital Phase as a Function of Offset Time (Cont.)

use of the results of a detailed statistical simulation of the GPS satellite ephemeris and clock errors done for the deorbit navigation study it was necessary to assume an offset time of $16^h58^m58^s.4$ (not plotted in Fig. 2.2-10) for use in the orbital navigation study. For the most part, this assumption has little effect on the significant features of orbital navigation. The visibility situation for the above offset time is illustrated in Fig. 2.2-11. The lower half of the figure shows which satellites are available at which times and also indicates, by the tic marks, a measurement schedule used in the orbital navigation study of Section 2.4.

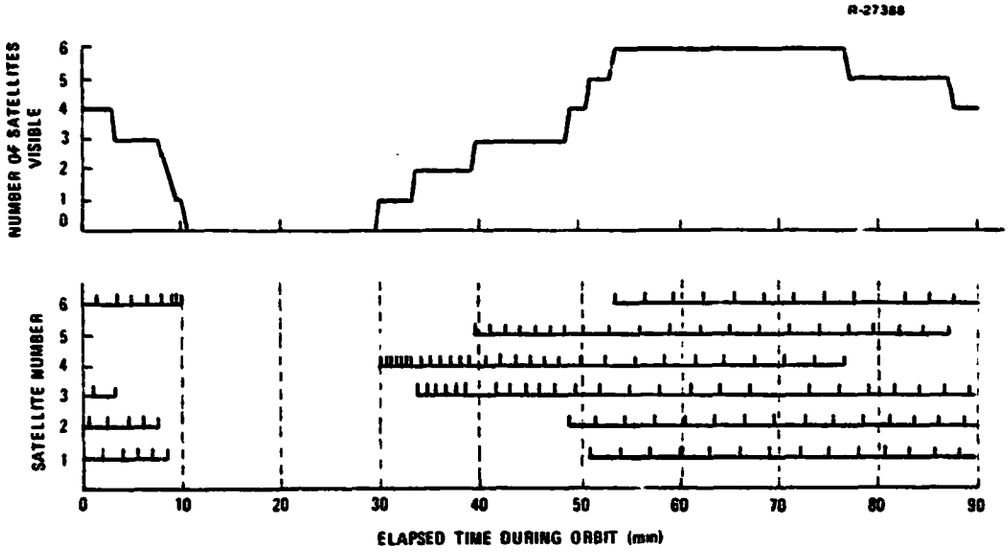

Figure 2.2-11 Orbital Satellite Visibility and Measurement Schedule

2.2.4 Antenna Effects on Phase I Orbital Visibility

During the evolution of the concept of Space Shuttle navigation using GPS, there was an experimental stage considered as a part of a phased development plan. That phased plan

was later dropped, as was the experiment. Some of the visibility results developed for the experiment are reported here for their general insight into orbital visibility considering antenna effects. These results are isolated to this section, and do not form the basis for further analysis in this volume.

Experimental Antenna Types and Locations - Two types of GPS antennas were considered for experimental use aboard the Orbiter. One type is an antenna being constructed by APL for use with the GPSPAC receiver under development by NASA Goddard and the DMA for use in satellites. The gain pattern of this antenna is shown in Fig. 2.2-12 for right hand circularly polarized signals at the L_2 GPS frequency. (Since L_2 signals were originally planned to be weaker than L_1 signals, the L_2 performance was deemed more critical than the L_1 performance.) The coverage of this antenna may be approximated by the specification, which calls for a conical zone of coverage with half-cone angle of 100 deg. This antenna would have to be located in the payload bay of the Orbiter or be deployed from the bay on a boom.

The second type of antenna considered is a stripline antenna that would be mounted on the inside of a window into the crew area. The coverage zone of such an antenna is uncertain without testing. It is modeled here as having a conical coverage zone with a 45 to 75 deg half-cone angle.

Figure 2.2-13 shows five locations considered for placement of the experimental antennas. Locations I and II are on pallets in the payload bay, appropriate for the APL antenna. Locations III and IV are alternate positions of a boom extending from the payload bay, also for the APL antenna. Location V is a window into the crew area, appropriate for the stripline antenna.

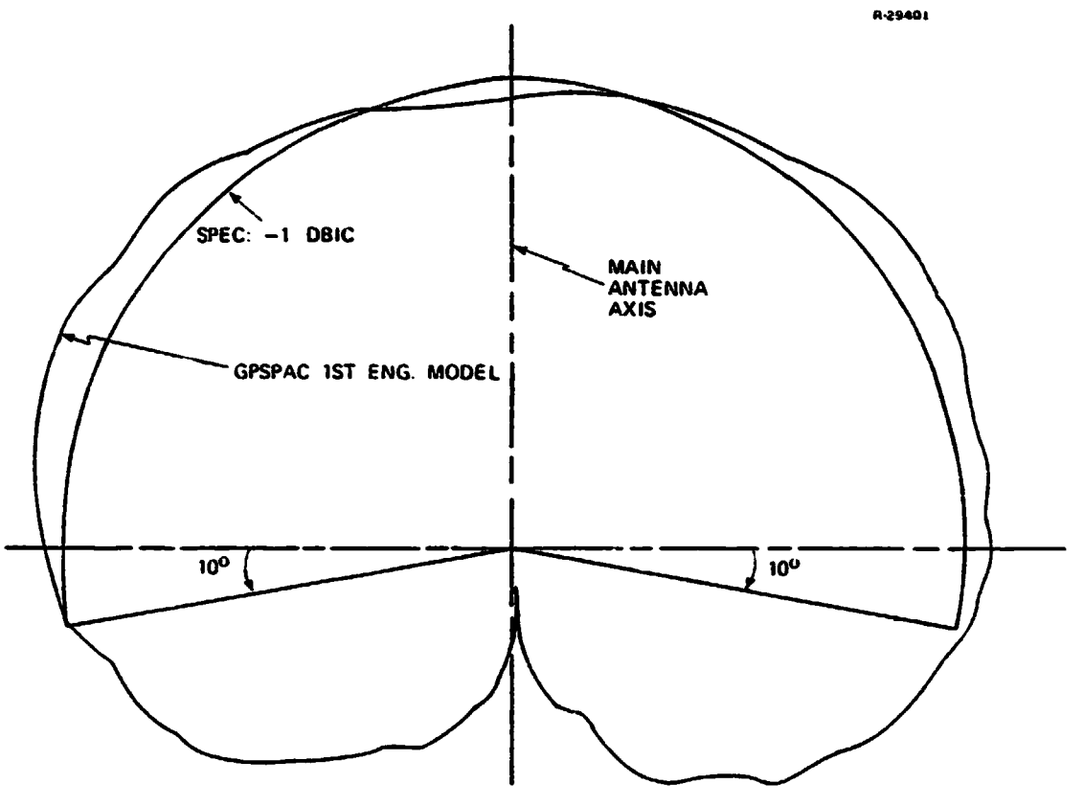

Figure 2.2-12 APL Antenna Pattern (RHC Gain for L_2)

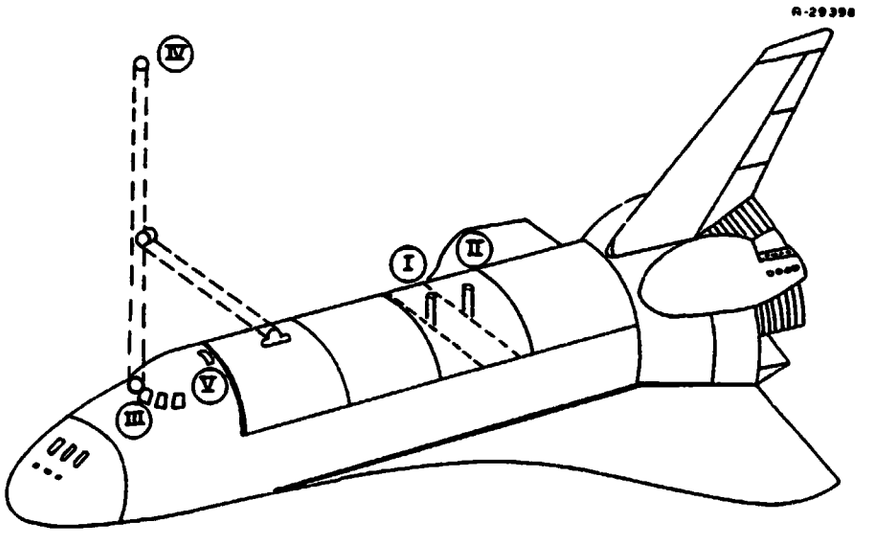

Figure 2.2-13 Alternate Experimental GPS Antenna Locations

The locations I and II in the payload bay suffer from masking caused by the Orbiter structure. Figures 2.2-14 and 2.2-15 show the antenna masking by the Orbiter for the APL antenna in locations I and II. Any direction from the antenna may be described by two angles termed "look angles." Referring to the standard Orbiter body coordinate system with its x axis out the nose, the y axis out the right wing, and the z axis out the bottom, the look angles are defined as: pitch look is the elevation angle of the antenna look direction above the xy body plane; yaw look is the angle the projection of the look direction from the antenna onto the xy plane is rotated about the positive z axis from the x axis toward the y axis. The figures consider all possible directions from the antenna and show which are masked by the vehicle itself (the hatched region at the bottom of the figure) and which, although not masked, are outside the 100 deg half cone angle limit for the APL antenna (the shaded region below -10 deg of pitch look angle). The Orbiter tail is evident in the figures on the left hand side; it is not symmetrically located about the 180 deg yaw look angle because the antenna locations are slightly to the right of the Orbiter centerline (i.e., have +y components of location in body coordinates). The figures were prepared from equivalent data in a different form (Ref. 20).

Experimental Orbiter Trajectories - The missions assumed for the Shuttle GPS experiment were denoted as OFT-5 and OFT-6. OFT-5 was to have been a Skylab revisit launched on 3 February 1980. Even as this work was progressing, the mission plans were changing. Originally the OFT-5 mission was to contain lengthy segments with the Orbiter in a bottom-down, earth oriented attitude, and some of the results reported here assume such an attitude. The plans changed so that during most of OFT-5 the Orbiter would be stabilized in inertial space with its wing toward the sun or with its tail toward the sun. At this point,

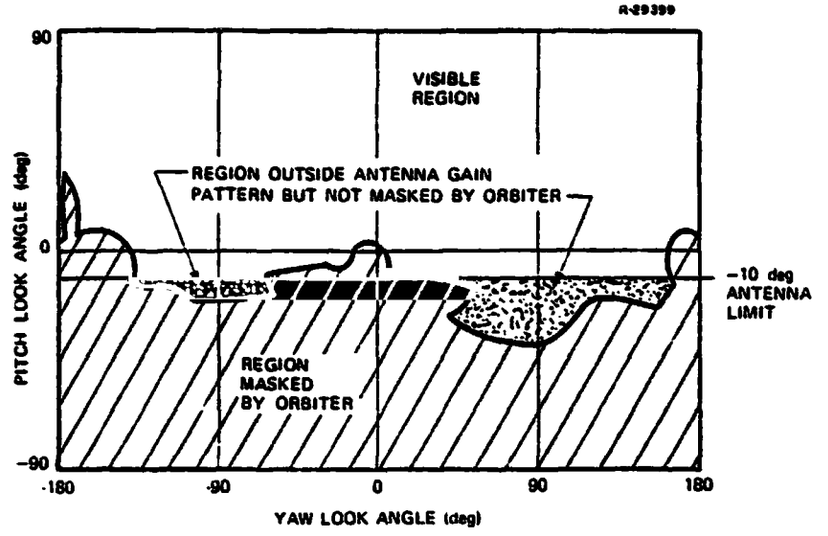

Figure 2.2-14 APL Antenna Masking Due to the Orbiter -- Location I

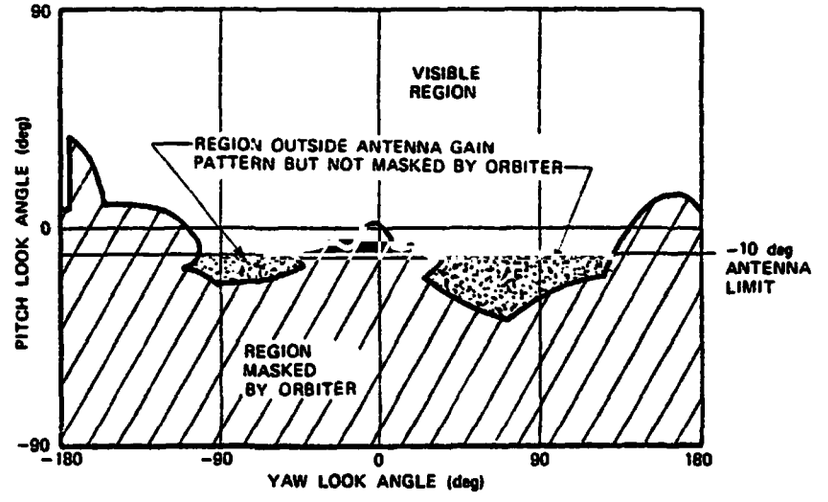

Figure 2.2-15 APL Antenna Masking Due to the Orbiter -- Location II

interest was expressed in OFT-6, since it was to have lengthy segments of the desirable, bottom-down, attitude stabilization that improves satellite visibility from topside antennas. Table 2.2-6 shows the basic orbital parameters for the two missions.

TABLE 2.2-6
ORBITAL PARAMETERS FOR OFT-5 AND OFT-6

PARAMETER	OFT-5	OFT-6
Altitude	175 nm	160 nm
Eccentricity	0	0
Inclination	50 deg	57 deg
Period	90.9 deg	90.45 min

Experimental Orbital Visibility Results - Figure 2.2-16 shows the nominal satellite visibility from the Orbiter for OFT-5 without regard to antenna considerations. The only visibility criteria is a 10 deg earth mask angle. To see how such full coverage visibility changes with offset time, Fig. 2.2-17 is a visibility density plot showing the number of satellites visible as functions of both time on orbit and offset time.

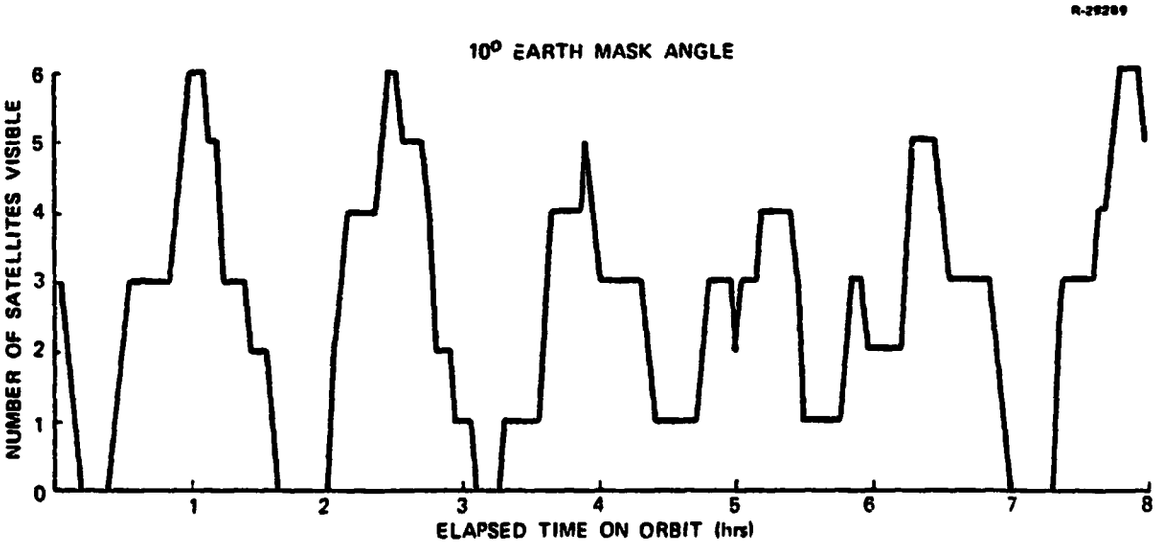

Figure 2.2-16 GPS Phase I Satellite Visibility During OFT-5 Orbit

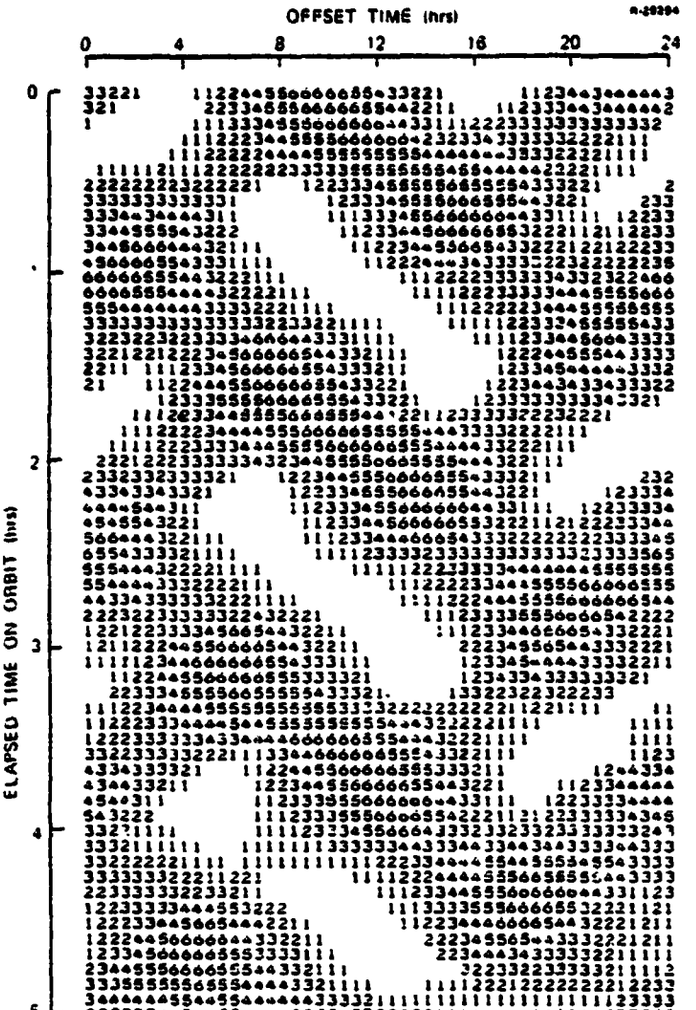

Figure 2.2-17 GPS Phase I Visibility from OFT-5 on Orbit as a Function of Elapsed Time and Offset Time

To confirm that important orbital visibility conclusions are largely independent of offset time, some average visibility results were prepared. Figure 2.2-18 shows the average number of satellites visible (averaged over time on orbit) as a function of offset time. Figure 2.2-19 shows what percentage of time on orbit three or four satellites are visible as a function of offset time. The relatively small variations in these plots confirm that while visibility is a detailed function of offset time, the averages are much less sensitive to offset time.

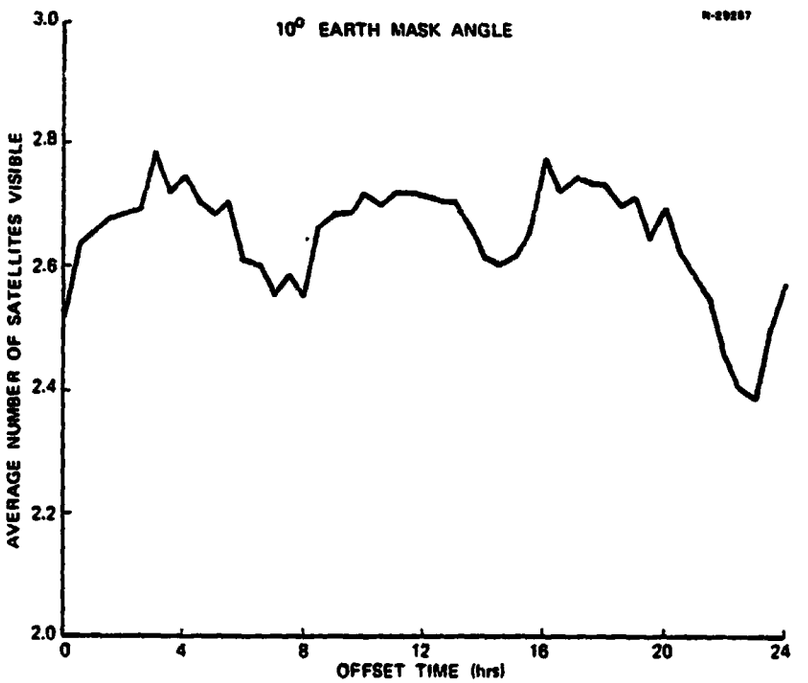

Figure 2.2-18 Average Visibility for OFT-5 as Function of Offset Time

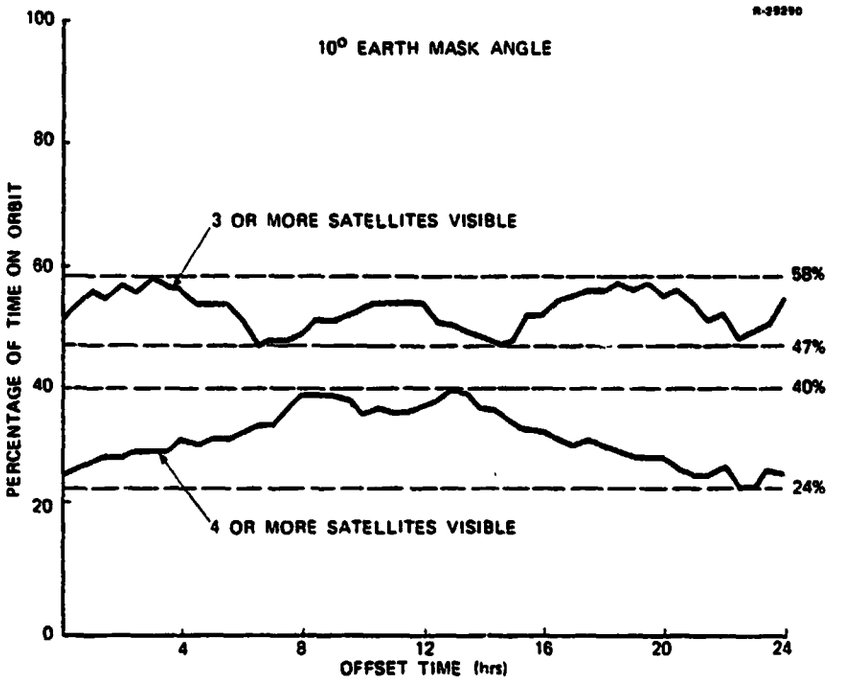

Figure 2.2-19 Percentage Visibility for OFT-5 as Function of Offset Time

Figures 2.2-20 and 2.2-21 show example visibility penalities associated with the APL antenna placed in locations I and II. These figures were prepared when the baseline for OFT-5 was a bottom-down attitude. The "top side" of the plot is the same in both figures and is identical to Fig. 2.2-16, for it represents full coverage visibility considering only earth masking with the 10° mask angle above the Orbiter's horizon. The shaded portions of the figures represent satellites "lost" to the two antenna placements due to Orbiter masking (the antenna beam pattern was never a factor). Both locations offer nearly full coverage, with placement I being slightly superior as it is farther from the tail and suffers less from tail masking.

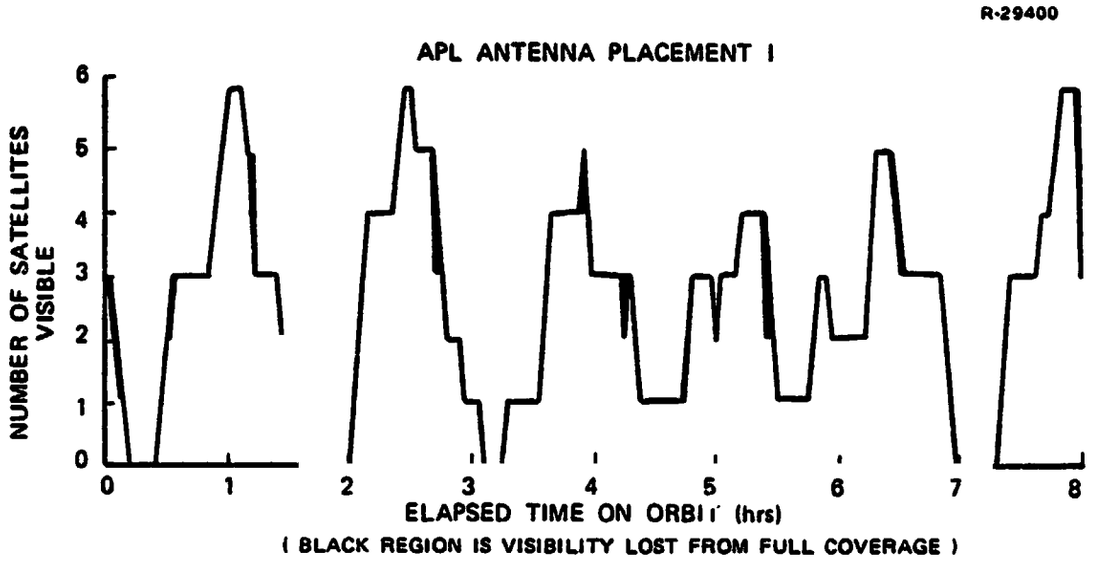

Figure 2.2-20 Example of Orbiter Masking Visibility Penalty for Bottom-down Attitude -- Location I

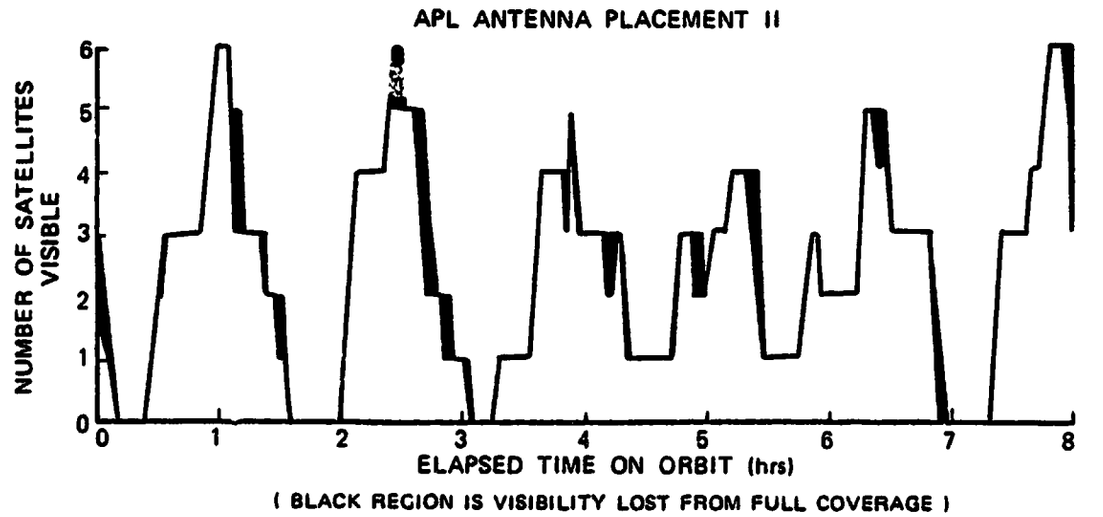

Figure 2.2-21 Example of Orbiter Masking Visibility Penalty for Bottom-down Attitude -- Location II

Table 2.2-7 compares full coverage visibility with that from locations I and II and from a location V window antenna of three possible different half-cone angles. This table still assumes that the OFT-5 mission would be flown bottom-down.

TABLE 2.2-7

ANTENNA EFFECTIVENESS COMPARISON FOR PRIOR OFT-5 BASELINE (BOTTOM-DOWN)

T-1477

ANTENNA	AVERAGE NUMBER SATS VISIBLE	% TIME NONE VISIBLE	% TIME 3 OR MORE	% TIME 4 OR MORE
IDEAL (APL IV)	2.52	12	51	26
APL I	2.39	13	49	22
APL II	2.27	15	45	20
75° HCA	1.16	38	12	2
60° HCA	0.69	54	3	0
45° HCA	0.37	70	0	0

HCA - HALF-CONE-ANGLE WINDOW ANTENNA (V)

Before proceeding with visibility results, the related matter of kinematic ranges should be discussed. Any GPS receiver will have limitations on the signal dynamics that it can handle. These limits may usually be expressed in terms of the range from the receiver to the satellite and the first three derivatives of this range: range-rate, range-acceleration, and range-jerk. Table 2.2-8 gives the extreme values of range (and its first three derivatives) from the Orbiter to the visible satellites for a 12 hr segment of the OFT-5 orbit. The effect of vehicle maneuvers are not included in the values given in the table. Due to unbalanced attitude thrusting or to high attitude rates, the range jerk might, for very short periods of time, be significantly larger than the tabulated values, but the other variables should be largely unaffected.

TABLE 2.2-8
KINEMATIC RANGES

KINEMATIC VARIABLE	OFT-5 ON ORBIT EXTREMES	
	MINIMUM	MAXIMUM
Range (10^6 ft)	65.1	87.6
Range Rate (10^3 ft/sec)	-25.9	26.0
Range Acceleration (ft/sec^2)	-5.3	41.2
Range Jerk (10^{-3} ft/sec^3)	-49.9	49.8

Figures 2.2-22 through 2.2-24 show what nominal visibility may be expected on the OFT-5 orbit with the stripline window antenna in location V. Various values for the antenna half-cone angle are considered. These figures should be compared with Fig. 2.2-16 showing visibility for the same orbital

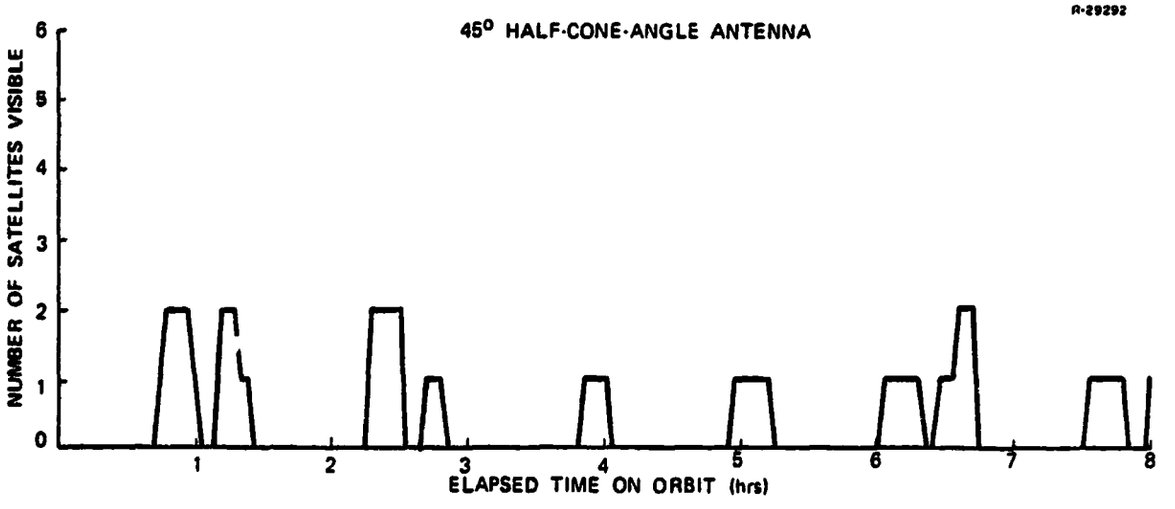

Figure 2.2-22 GPS Phase I Satellite Visibility from OFT-5 Orbit with a 45° Half-Cone Window Antenna

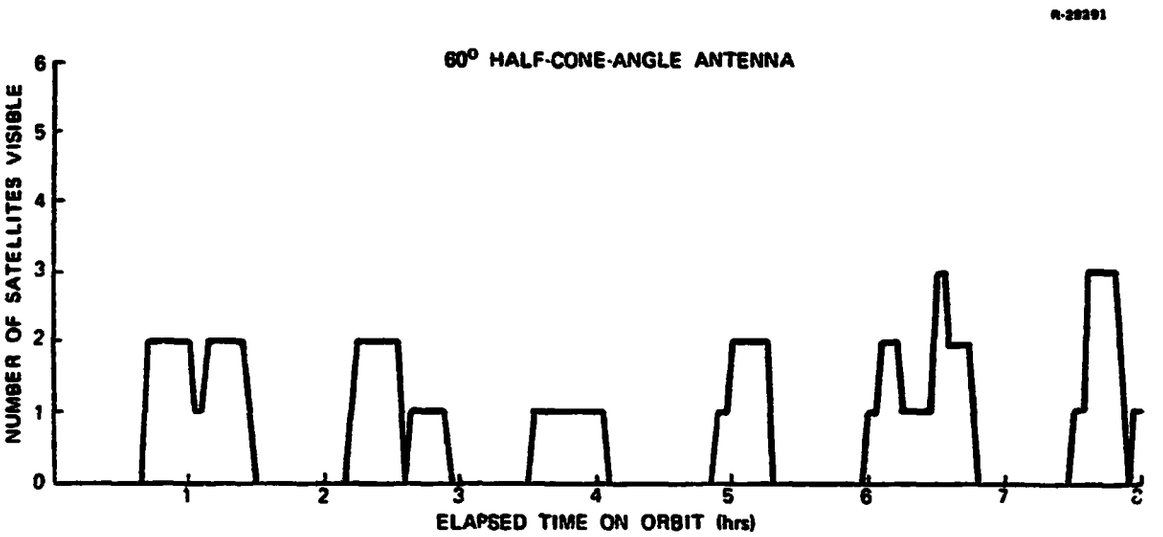

Figure 2.2-23 GPS Phase I Satellite Visibility from OFT-5 Orbit with a 60° Half-Cone Window Antenna

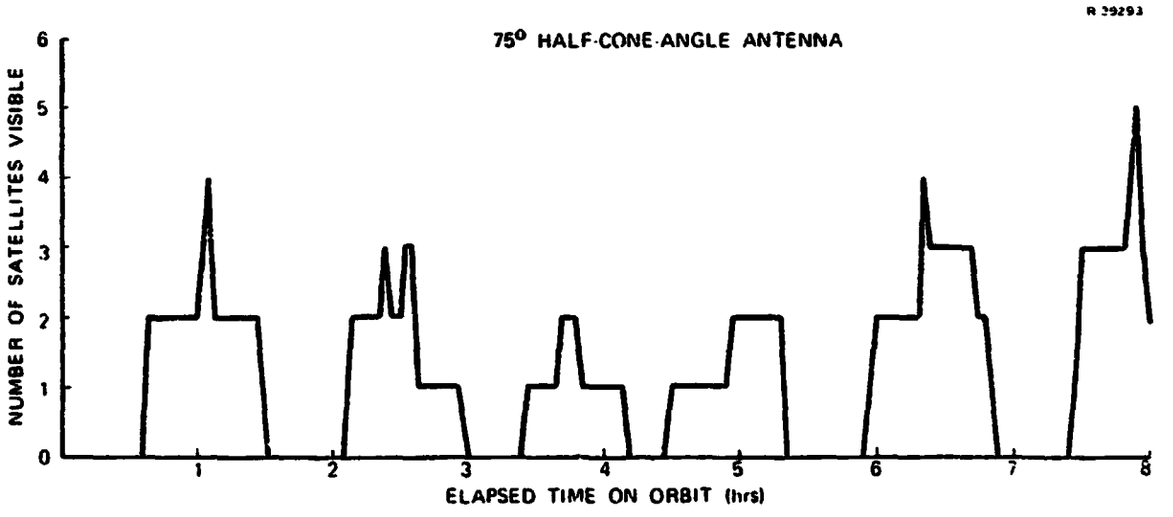

Figure 2.2-24 GPS Phase I Satellite Visibility from OFT-5 Orbit with a 75° Half-Cone Window Antenna

segment without regard to antenna limitations. Again, a bottom-down attitude of the Orbiter is assumed. Note that no more than two satellites can ever be seen at once with a 45 deg half-cone-angle antenna, and that 70% of the time none are visible.

Figure 2.2-25 shows a six hour segment of visibility on orbit for OFT-6 as a function of both elapsed time and off-set time. Omitting some of the detailed results, Table 2.2-9 summarizes visibility for OFT-5 and OFT-6 for antenna locations I and II, now assuming that the Orbiter attitude on OFT-5 will be space stable while on OFT-6 it will be earth stabilized bottom-down. The conclusion to be drawn is that the space stable attitudes cut average visibility by 50% and reduce the amount of time 4 or more GPS satellites are visible by a factor of 3 to 4, so that bottom-down, earth stabilized attitude is desirable for a GPS demonstration.

2.2.5 Phase II Orbital Visibility

This section summarizes the results of a parametric look at GPS satellite visibility from the Space Shuttle on orbit. The satellite constellation used is an approximation to the GPS Phase II constellation of six satellites, with results also for a four satellite subset to illustrate a minimum visibility situation. Full coverage antennas are assumed for the Orbiter, and a 5 deg earth mask angle is used. This study is separate from the other results of this chapter in that these particular visibility results were not used to generate navigation performance results.

A conceptually straightforward way to organize a study of orbital visibility would be to fix a satellite constellation and then vary the orbit of the Space Shuttle. In general,

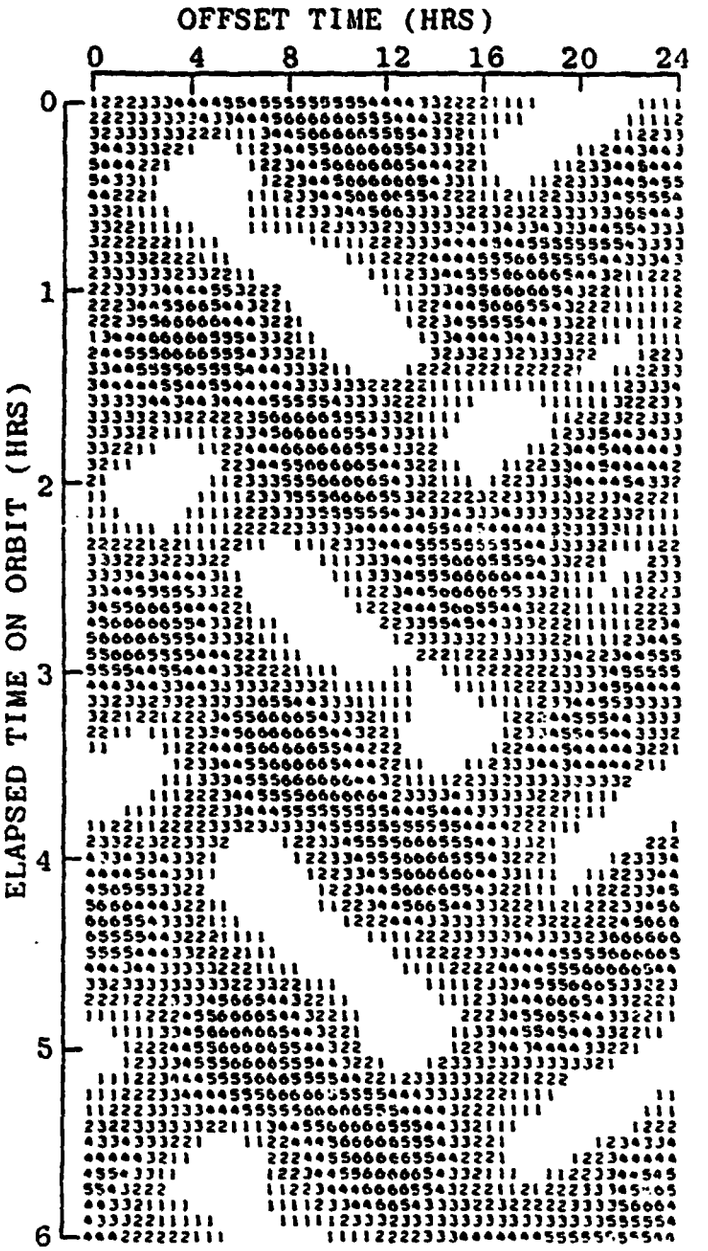

Figure 2.2-25 GPS Phase I Visibility from OFT-6 On Orbit as a Function of Elapsed Time and Offset Time

TABLE 2.2-9

VISIBILITY COMPARISON FOR CURRENT
OFT-5 AND OFT-6 MISSIONS
(FOR NOMINAL ORBITS OF 12 HR DURATION)

T-1478

MISSION (ATTITUDE)	ANTENNA LOCATION	AVERAGE NO. SATS VISIBLE	% TIME NONE VISIBLE	% TIME 3 OR MORE	% TIME 4 OR MORE
OFT-5	Ideal	2.5	12	51	26
Wing to Sun	I	1.2	41	21	8
	II	1.2	42	20	6
Tail to Sun	I	1.3	39	22	8
	II	1.2	40	22	7
OFT-6	Ideal	2.7	11	53	30
Bottom to Earth	I	2.5	13	50	28
	II	2.3	16	46	23

there are six parameters necessary to describe the Shuttle orbit, far too many to consider in this study. That number may be reduced by two by considering only circular Shuttle orbits, thus eliminating orbital eccentricity and argument of perigee from consideration. An additional parameter may be removed by fixing the orbit altitude at the typical value of 150 nm, as altitude does not strongly affect visibility. Orbital inclination is a significant factor in the visibility patterns, so it must be retained as a variable parameter. Similarly, the right ascension of the Space Shuttle orbit with respect to the GPS satellite orbits is quite significant and must be retained as a variable.

The initial anomaly of the Shuttle in its orbit is a significant factor in the visibility. When visibility is also parameterized as a function of time in orbit, however, and that time is carried over several complete revolutions of the Orbiter, then the resulting visibility patterns are nearly cyclical. The general pattern features under these conditions are not strongly dependent on the initial Shuttle anomaly, so it may

be removed as a free parameter. Thus, only two free parameters, inclination and right ascension, remain besides the independent variable of time in orbit.

The Phase II visibility results were generated in a manner similar to that discussed above, but are organized differently. The concept of restriction to circular Shuttle orbits at 150 nm altitude was assumed. Shuttle orbital inclination was varied over the discrete values of 0, 30, 45, 60, and 90 deg. The initial anomaly of the Shuttle orbit was fixed at 0 deg., so the Orbiter is always crossing the equator from south to north at time zero.

The absolute right ascension of the Orbiter was not varied, always being assumed to be 0 deg with respect to the Greenwich meridian at time zero. In order to vary the Shuttle orbit right ascension with respect to the GPS satellite orbit right ascensions, the concept of "offset time," previously built into the software, was used. By specifying the initial longitudes of the ascending nodes of the GPS satellite orbits with respect to the Greenwich meridian, the right ascensions with respect to the vernal equinox vary with the satellite epoch time. Offset time is the span from the satellite epoch time to the time zero of the "time-on-orbit" parameter, so a positive offset time implies that the satellite epoch precedes the time zero.

Table 2.2-10 gives the satellite constellation initial longitudes of the ascending nodes and initial anomalies at the satellite epoch time. This constellation of six satellites is unique to this section; it approximates the Phase II constellation. The satellite inclinations are assumed to be 63 deg. A reduced constellation of four satellites, omitting satellites 2 and 4, is used to simulate a possible reduction of the Phase II constellation.

TABLE 2.2-10
SATELLITE CONSTELLATION FOR SAMPLE ORBITAL VISIBILITY RESULTS

SATELLITE NUMBER	INITIAL LONGITUDE OF THE ASCENDING NODE (wrt GREENWICH, deg)	INITIAL ANOMALY (deg)
1	0	0
2*	0	45
3	0	90
4*	240	30
5	240	75
6	240	120

*These satellites are omitted for the four satellite version of this constellation.

When the offset time parameter of the results is zero, the Shuttle begins its orbital travel directly beneath the Number 1 GPS satellite. As the offset time varies through 24 hours (less 4 min, 3.4 sec), the right ascension of the Shuttle orbit varies through 360 deg with respect to that of the number 1 GPS satellite. The offset time parameter also affects the time zero anomalies of the GPS satellites with respect to that of the Shuttle, but as previously noted, this variation has little effect on the general properties of the results.

Figures 2.2-26 through 2.2-35 are visibility density plots for the orbital visibility studies. The title of each figure specifies the number of GPS satellites assumed to be in the constellation and the orbital inclination of the Space Shuttle. The vertical axes are time on orbit, from 0 to 3 hours, spanning two complete Shuttle orbits. The horizontal

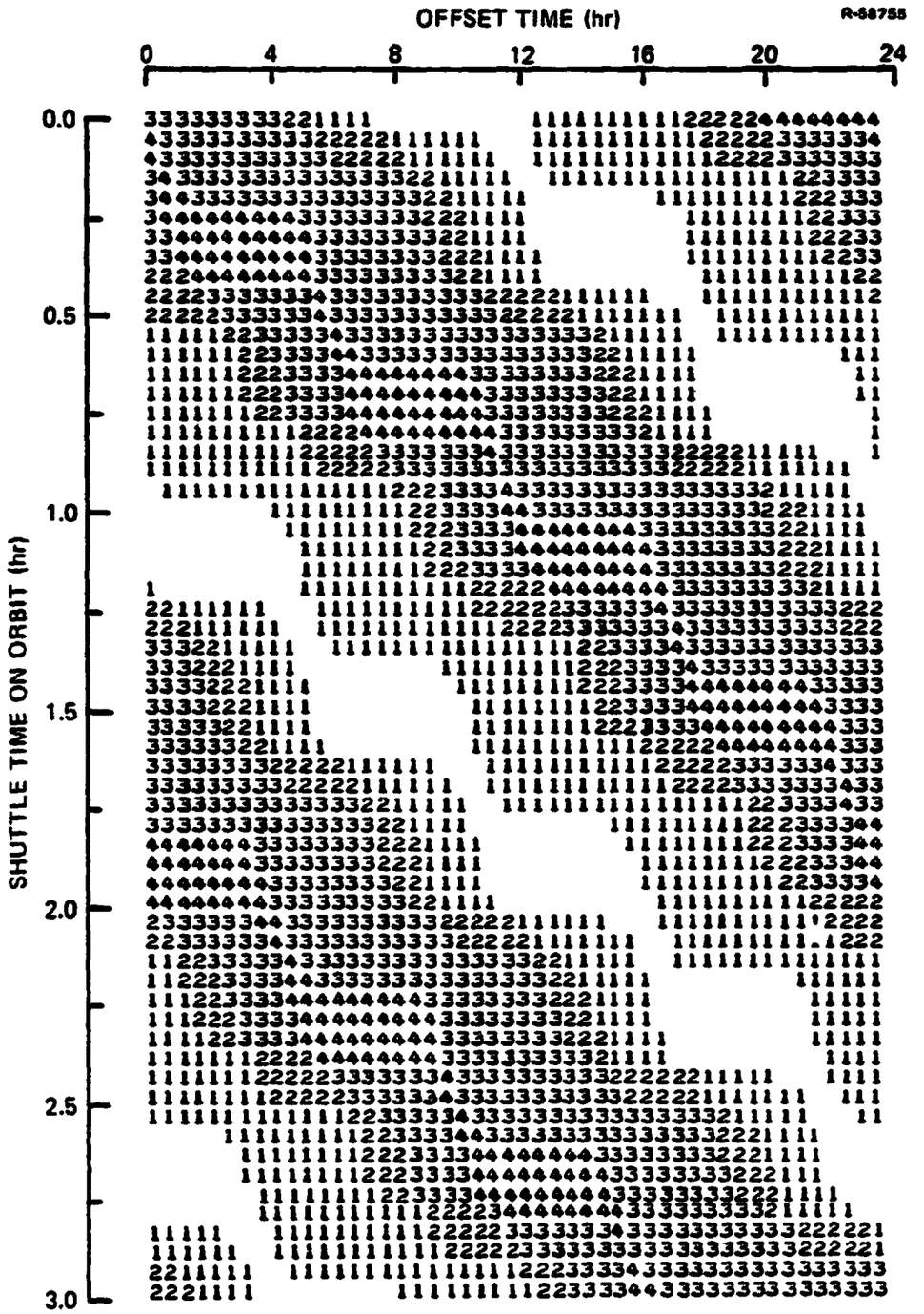

Figure 2.2-26 Orbital Visibility, 0 Deg Inclination, 4 Satellites

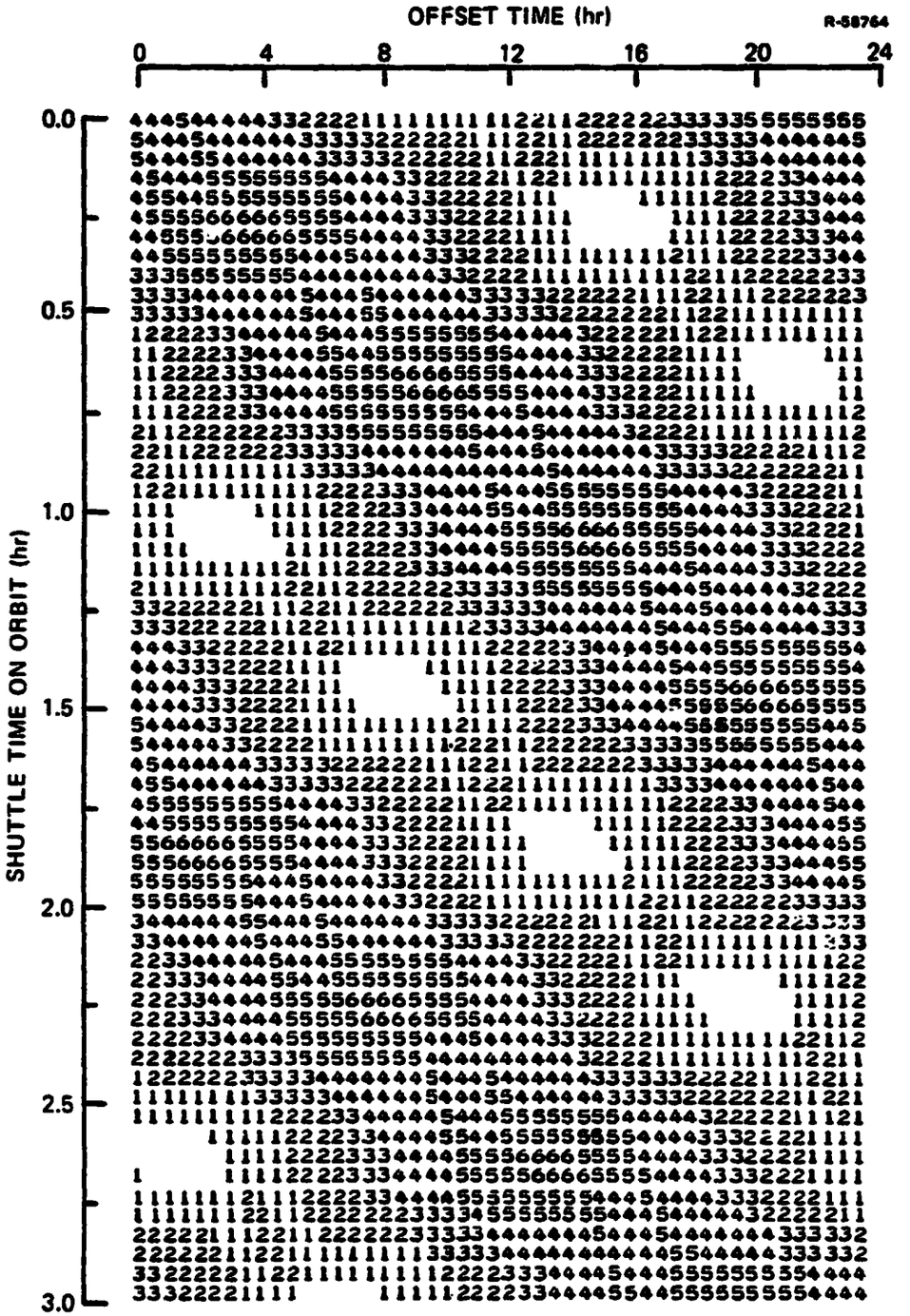

Figure 2.2-27 Orbital Visibility, 0 Deg Inclination, 6 Satellites

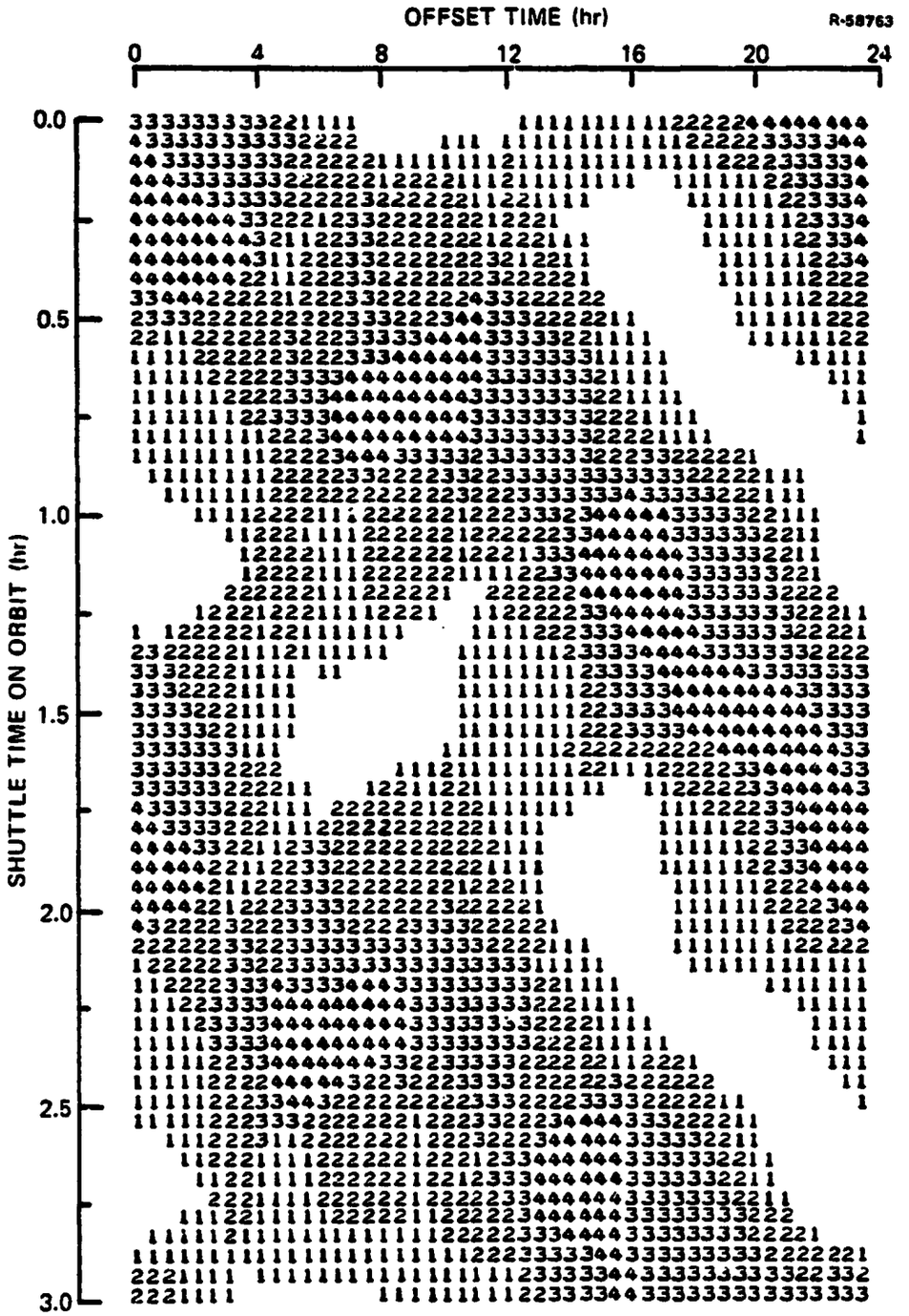

Figure 2.2-28 Orbital Visibility, 30 Deg Inclination, 4 Satellites

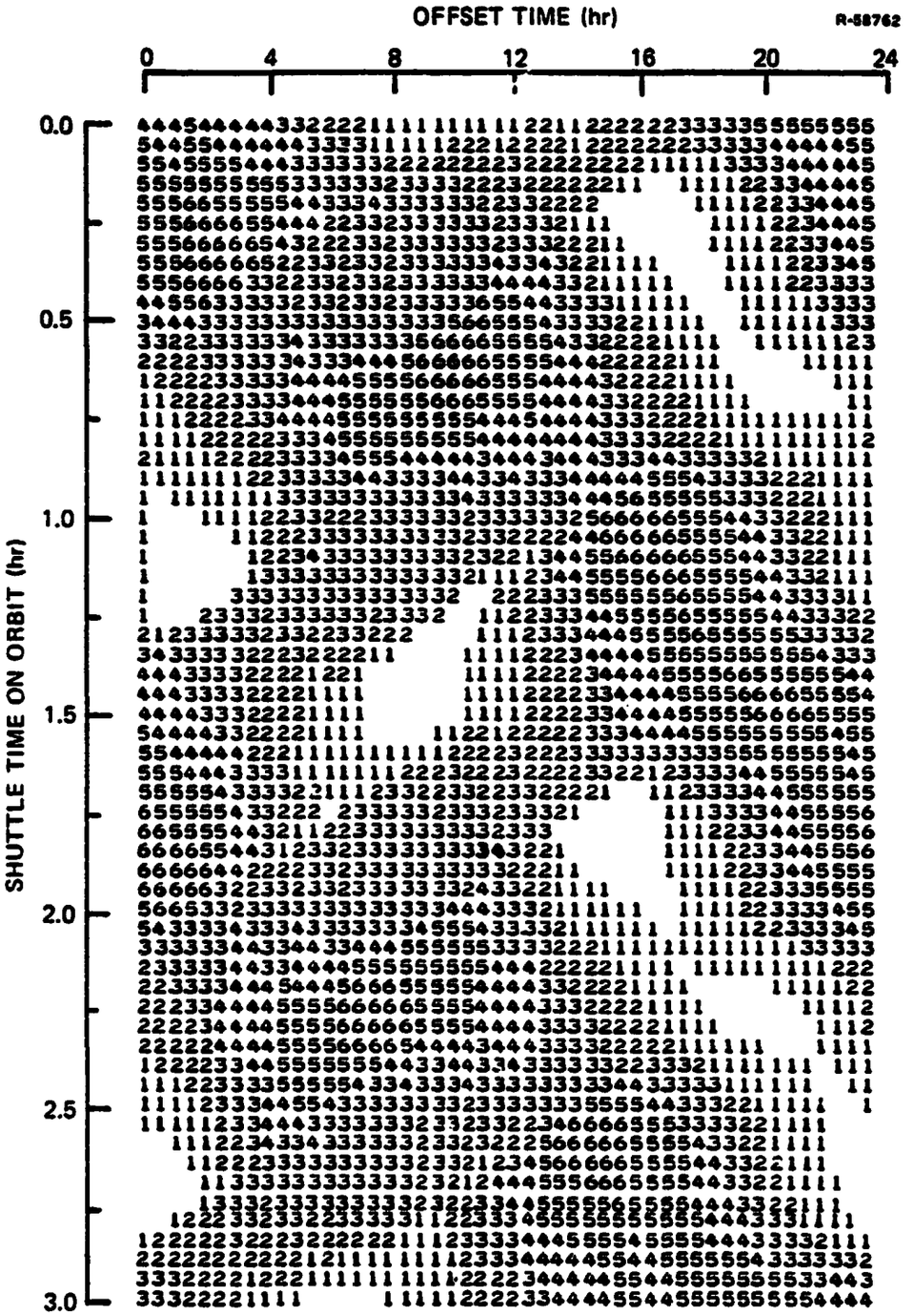

Figure 2.2-29 Orbital Visibility, 30 Deg Inclination, 6 Satellites

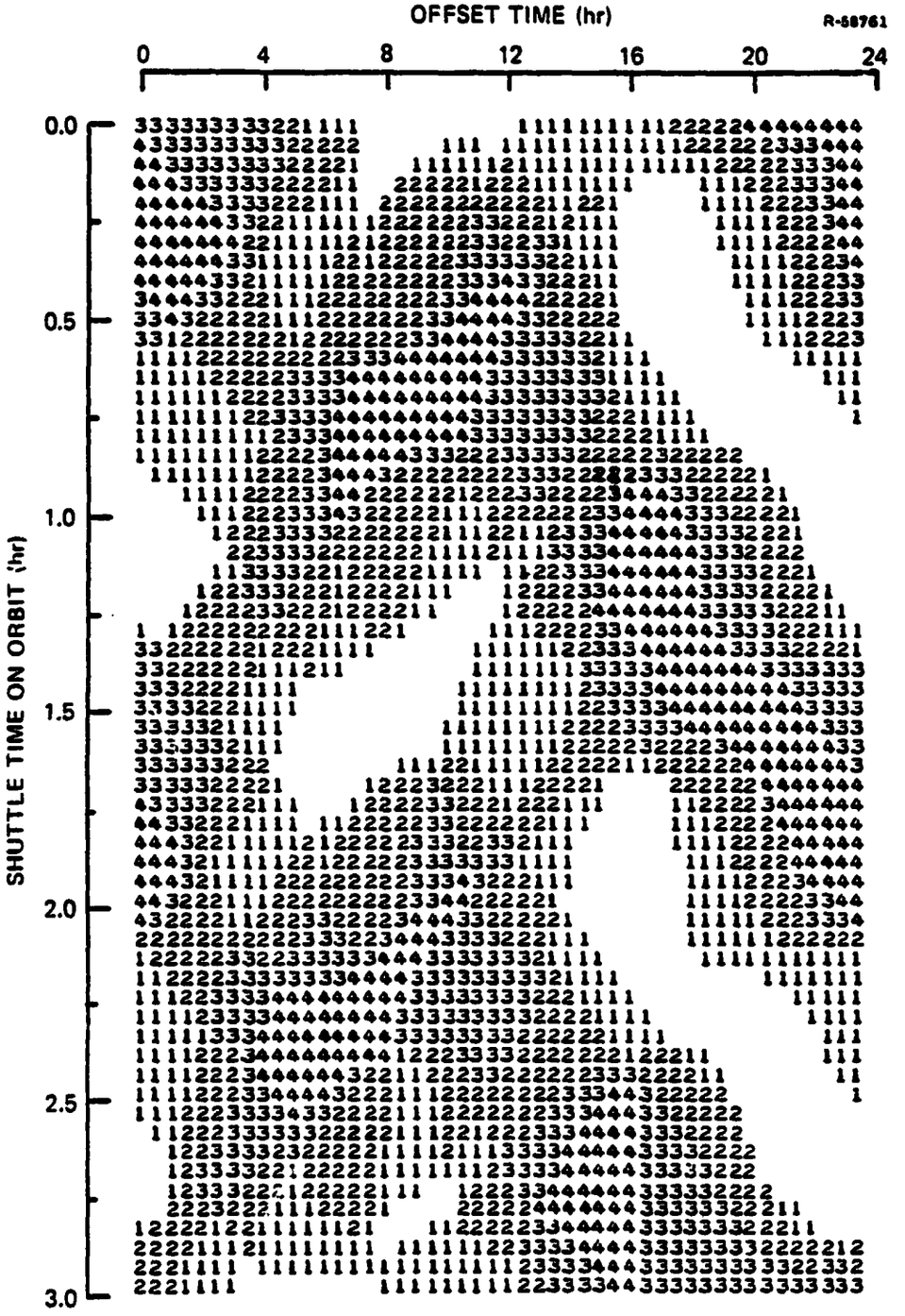

Figure 2.2-30 Orbital Visibility, 45 Deg Inclination, 4 Satellites

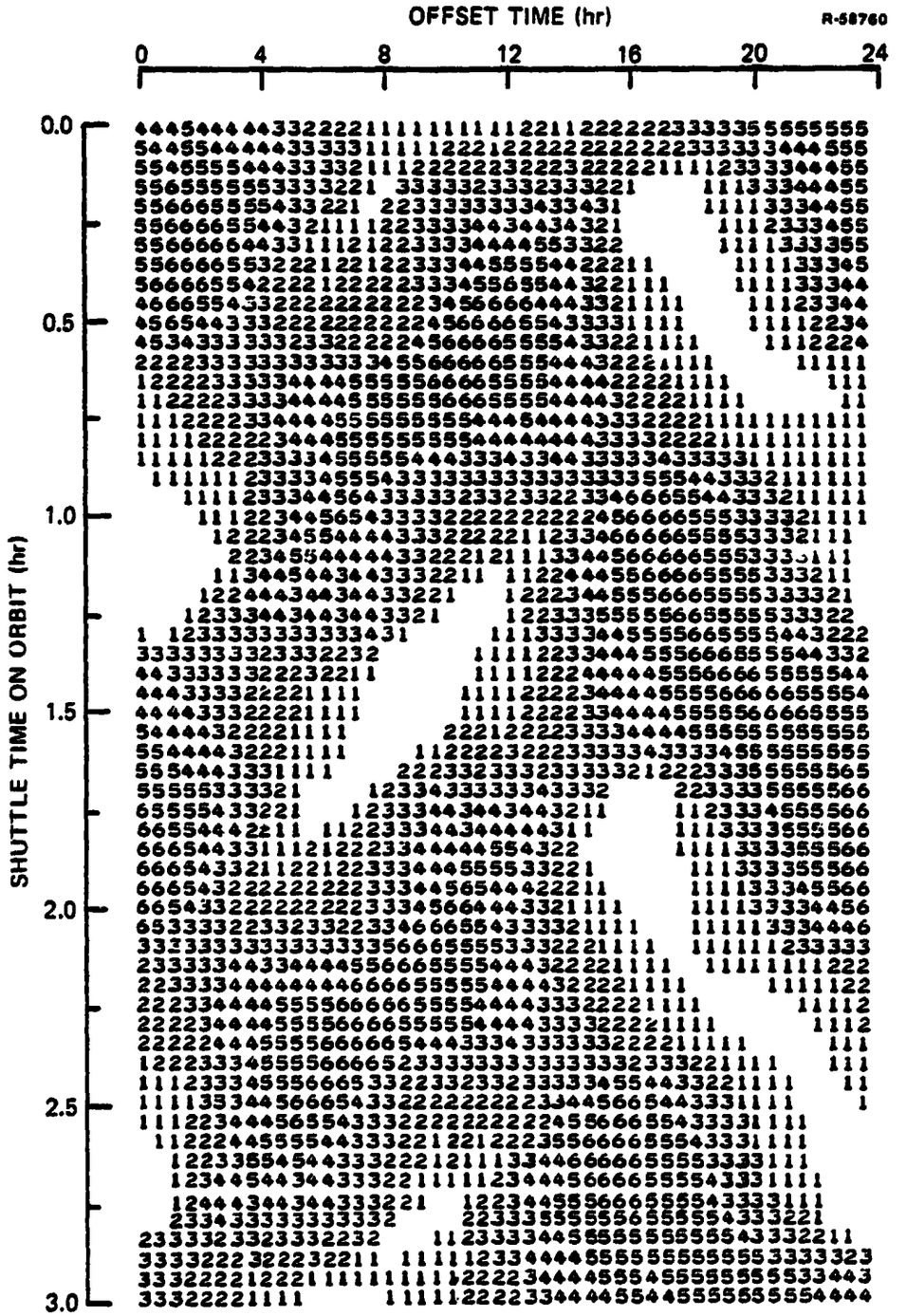

Figure 2.2-31 Orbital Visibility, 45 Deg Inclination, 6 Satellites

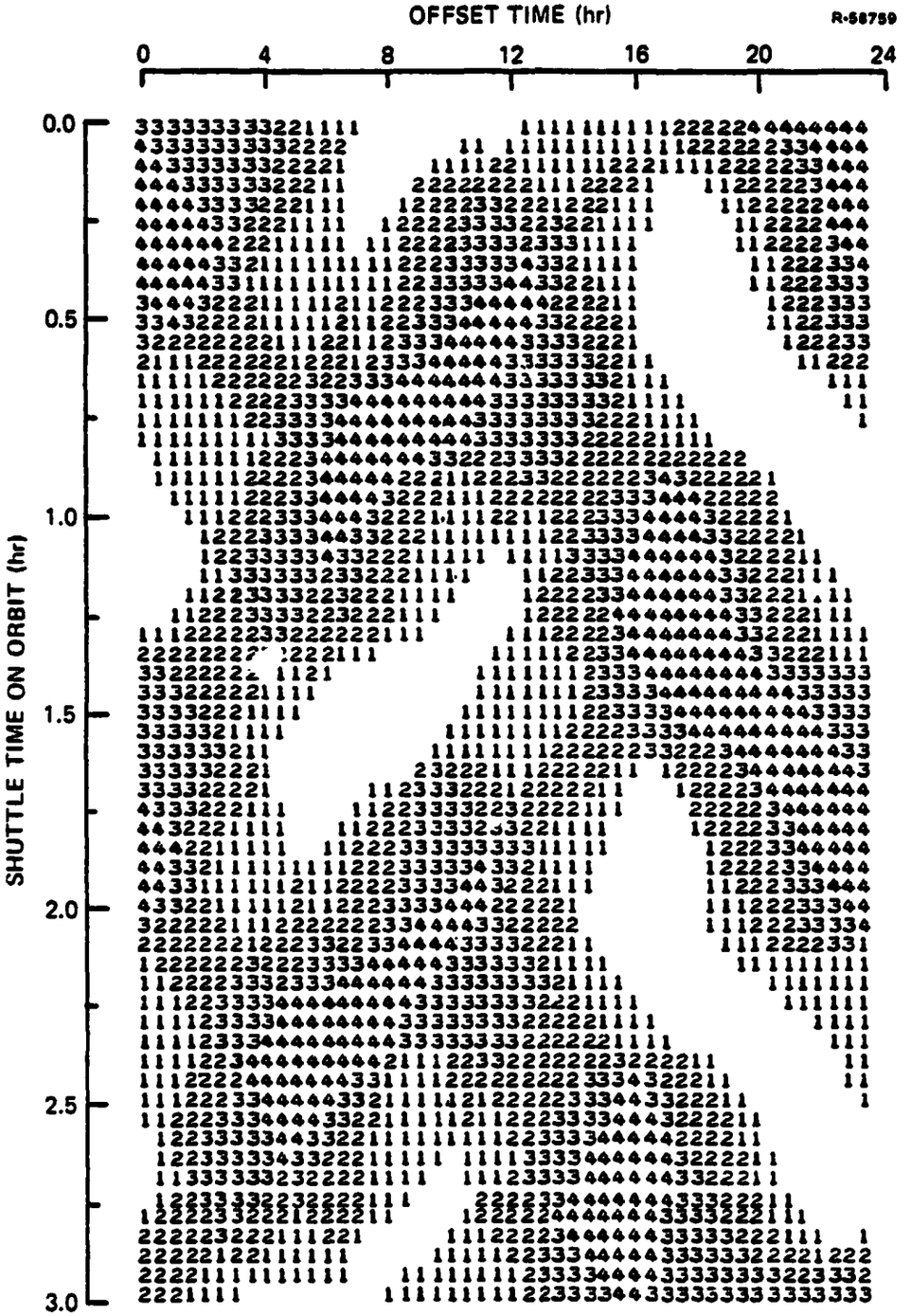

Figure 2.2-32 Orbital Visibility, 60 Deg Inclination, 4 Satellites

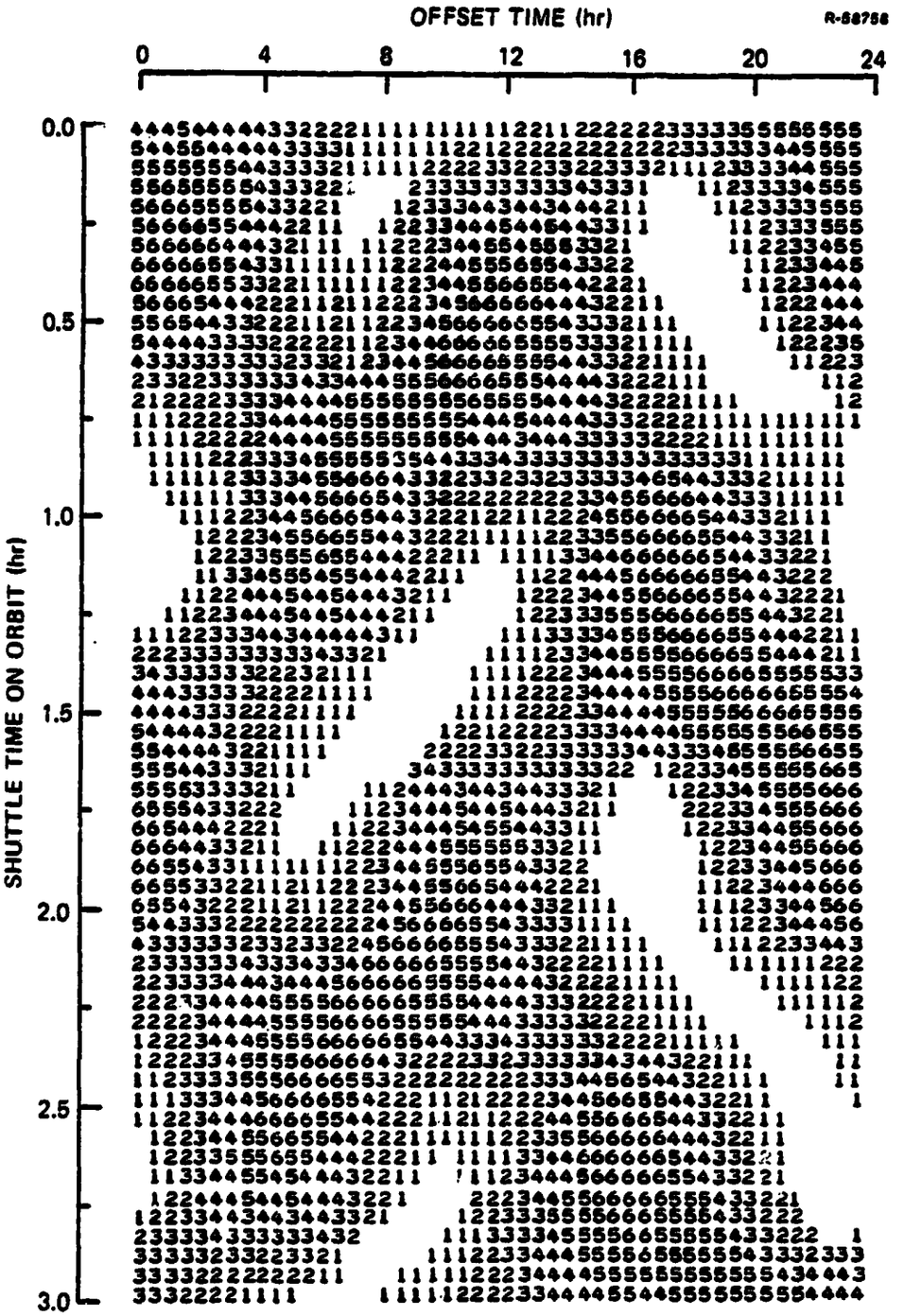

Figure 2.2-33 Orbital Visibility, 60 Deg Inclination, 6 Satellites

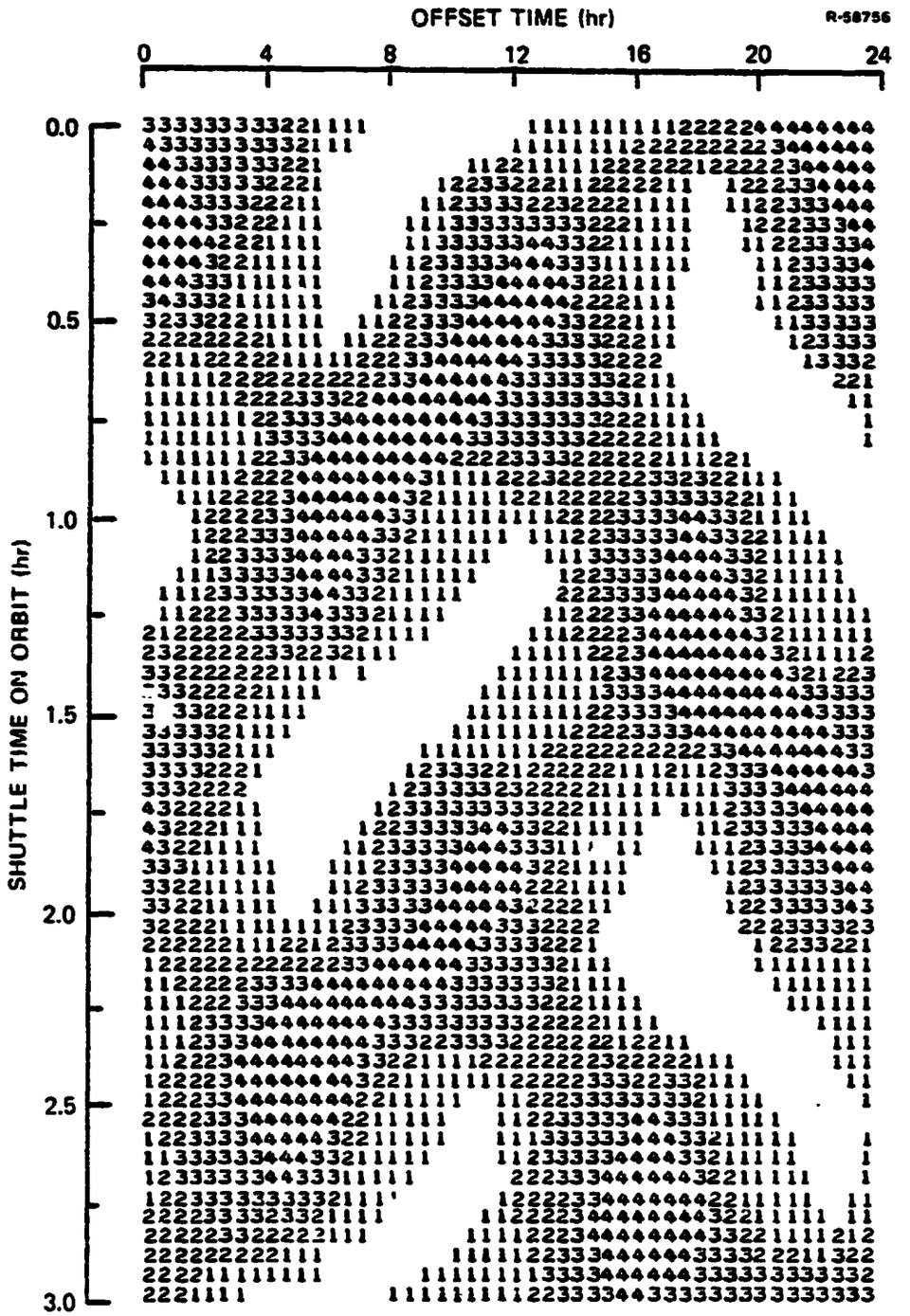

Figure 2.2-34 Orbital Visibility, 90 Deg Inclination, 4 Satellites

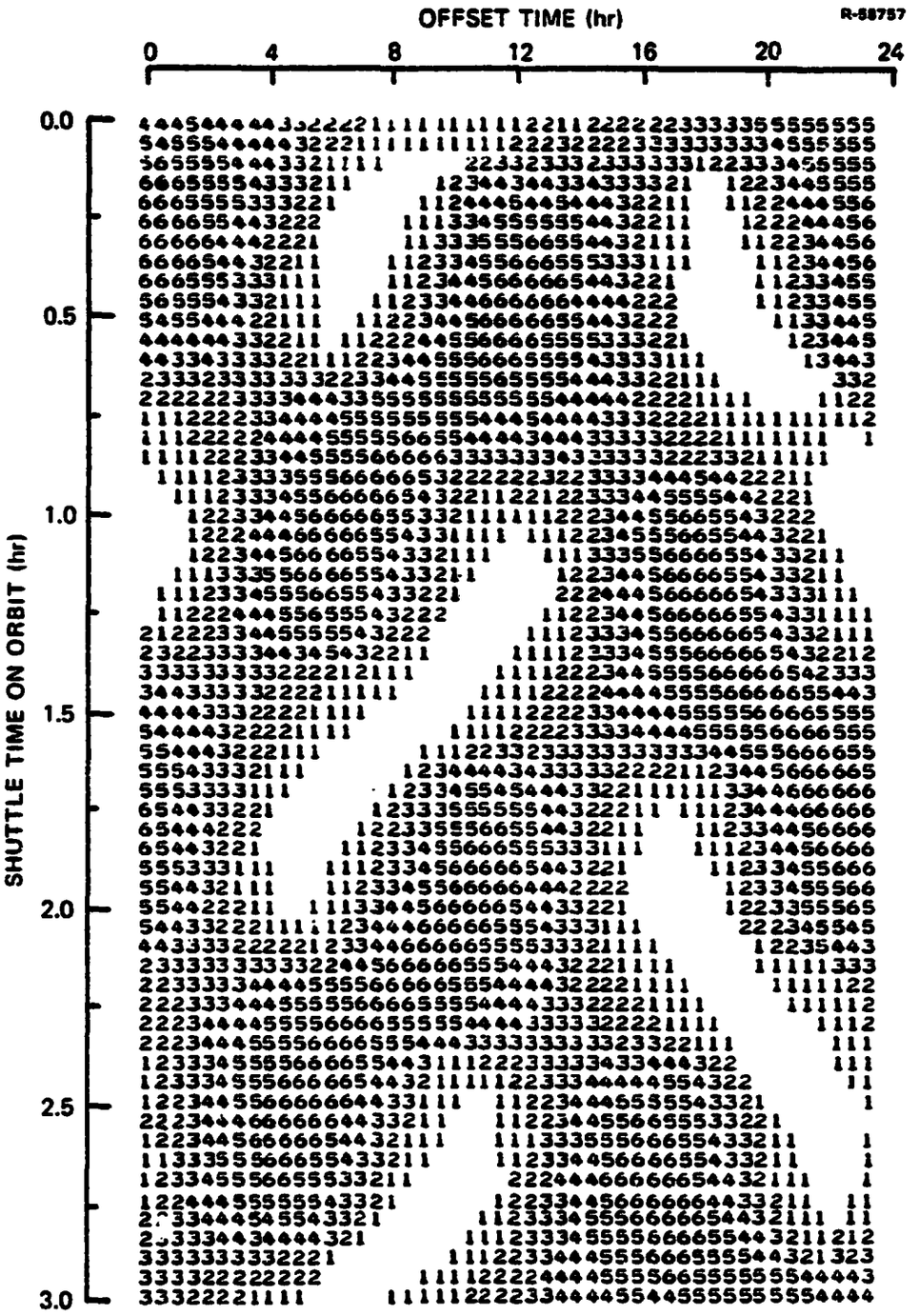

Figure 2.2-35 Orbital Visibility, 90 Deg Inclination, 6 Satellites

axes are offset time, spanning a complete 24 hrs. The numbers in the figures show how many satellites are visible for the particular time on orbit and offset time. Zeros, indicating no satellites visible, have been replaced by blanks. Visibility patterns observed by the Orbiter are given in the vertical columns, a different pattern for each offset time.

The only criterion for visibility used in this study was that to be visible, a satellite must have been above 5 deg above the Orbiter's horizon. (At 150 nm of altitude, the Orbiter's horizon is about 16.5 deg below the local horizontal plane.) No limitations of the Shuttle GPS receiving antennas were assumed, thus removing antenna considerations and Orbiter attitude considerations from the study. Actual visibility with less than full coverage antennas will often be reduced from the values given in the figures, but by adjusting the attitude of the Orbiter, if necessary, all the satellites indicated in the figures may be seen by the Orbiter antennas.

Tables 2.2-11 and 2.2-12 summarize some statistics relating to the orbital visibility study. They show percentages of the time that a given number of satellites are visible. The percentages represent averages over both time on orbit and over offset time. They may not apply on any particular orbit, but the doubly periodic nature of the visibility density figures implies that they should be nearly correct for any orbit at the given inclination. The time percentage visibility figures are generally smoothly varying with orbital inclination, except that the 0 deg orbit shows some sharp changes that may be real or may be an accident of the discrete and limited nature of the simulations. These summary tables show that three or more satellites are available significantly more often than are four or more, especially with the reduced, four satellite constellations.

TABLE 2.2-11

TIME AVERAGE ORBITAL VISIBILITY, 4 SATELLITES

TIME PERCENTAGES FOR ORBITAL GPS SATELLITE VISIBILITY (CONSTELLATION OF 4 PHASE I GPS SATELLITES, 5 deg MASK ANGLE) (SHUTTLE ORBITS ARE CIRCULAR AT 150 nm ALTITUDE)									
SHUTTLE ORBITAL INCLINATION (deg)	NUMBER OF SATELLITES VISIBLE								
	0	1	2	3	4	5	6	3 OR MORE	4 OR MORE
0	14	31	13	31	10			41	10
30	15	25	27	21	12			33	12
45	16	22	28	20	13			33	13
60	17	23	25	20	14			35	14
90	17	25	20	23	15			38	15

TABLE 2.2-12

TIME AVERAGE ORBITAL VISIBILITY, 6 SATELLITES

TIME PERCENTAGES FOR ORBITAL GPS SATELLITE VISIBILITY (CONSTELLATION OF 6 PHASE I GPS SATELLITES, 5 deg MASK ANGLE) (SHUTTLE ORBITS ARE CIRCULAR AT 150 nm ALTITUDE)									
SHUTTLE ORBITAL INCLINATION (deg)	NUMBER OF SATELLITES VISIBLE								
	0	1	2	3	4	5	6	3 OR MORE	4 OR MORE
0	4	20	21	13	23	16	2	55	41
30	7	17	17	27	13	15	4	59	32
45	9	16	17	22	14	15	6	58	36
60	11	16	17	18	15	15	8	56	39
90	13	16	15	17	14	15	10	56	40

2.3 DEORBIT NAVIGATION

2.3.1 Introduction

The performance levels to be expected in using Phase I GPS for deorbit navigation are given in this section. It first examines the issues of GPS satellite uploading and clock quality, the receiver measurement schedule, the receiver navigation filter, and the "truth model" used to assess filter performance. Nominal results are then presented, followed by sensitivity studies considering effects on performance due to the duration of blackout, to having IMU platform misalignment states in the navigation filter, and to adding drag update and baro-altimeter measurements. Conclusions are summarized in Subsection 2.3.11.

The deorbit visibility results of Section 2.2.2 are used here as input to a navigation performance study of the deorbit mission phase. The Phase I GPS satellite constellation and the Shuttle deorbit trajectory have already been presented along with the visibility results. The method used to generate performance predictions is one of covariance analysis. A reasonable navigation filter consistent with flight software limitations is postulated, and its statistics are simulated. A much more comprehensive "truth model" is then statistically simulated to provide an assessment of filter performance considering all important error sources, including many not acknowledged by the filter itself. Finally, key assumptions (including filter design) are varied to assess their impact on the results in a sensitivity study. A similar approach has been used in the past for studies of the integrated landing navigation system of Refs. 1 through 4.

2.3.2 GPS Satellite Uploading

Four ground tracking stations track all of the GPS satellites, and current best estimates of the satellite ephemerides and clock states are maintained on the ground. As each satellite makes its closest approach to Vandenberg AFB (once per day) the ground estimate of ephemeris and clock errors for that satellite are uploaded to the satellite. For the next 24 hours, the satellite then broadcasts this estimate as part of its GPS signal.

Because the Phase I satellites are intentionally bunched, they are all uploaded during a five hour period each day. Since the satellite ground tracks move from west to east and the deorbit trajectory is west of Vandenberg, the period of good visibility selected in Section 2.2.2 takes place prior to the five hour uploading interval (with one exception), while the period of reduced visibility takes place after the uploading interval.

2.3.3 Phase I Satellite Clock Quality

Depending primarily upon the quality of the satellite clocks, the GPS measurements may degrade rapidly with time since uploading. Phase I GPS will utilize rubidium clocks, while in Phase III more accurate cesium clocks are planned. The specified accuracy of the Phase I rubidium clocks, the accuracy of a 5-state model used in this study to simulate them, and some current data from laboratory tests of the rubidium clocks are all presented in Fig. 2.3-1 for comparison. As the figure shows, the test data is significantly better than either the specification or the assumed math model.

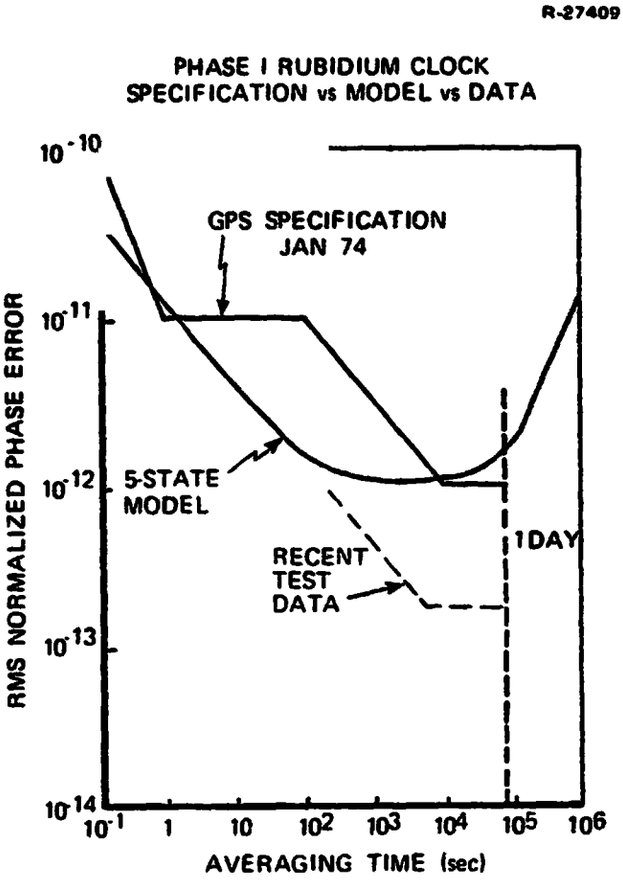

Figure 2.3-1 Phase I Rubidium Clock Model vs Specification and Test Data

From the mathematically modeled clock performance it is possible to extract a good approximation to the satellite clock contribution to pseudo range measurement error. A graph of that contribution for a typical satellite, as a function of the time since uploading, is given in Fig. 2.3-2. It should be noted that the value of about 130 ft of error at the end of one day since uploading is not all due to clock inaccuracy accumulated during the day. Part of the error is due to an inability of the ground network to accurately calibrate the clock frequency at the beginning of the day. This inability, itself, is partly related to clock quality, and accounts for

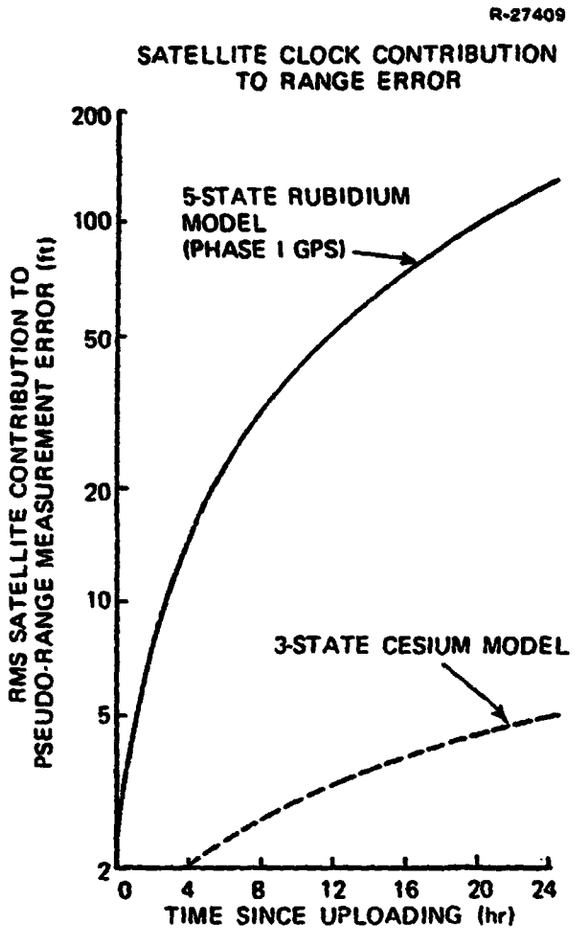

Figure 2.3-2 Satellite Clock Contribution to Range Error

about as much of the error as does the clock error buildup since uploading. Also included in Fig. 2.3-2 is a similar graph applying to a 3-state model used to represent the Phase III cesium clocks. The current* rubidium clock test data is closer to the performance of the modeled cesium clocks than it is to that of the modeled rubidium clocks.

With the modeled clock performance, the accuracy of the GPS measurements varies considerably with time since uploading, and the two segments of satellite visibility postulated earlier,

*Ground test data circa 1978.

coming just before (good visibility) and just after (reduced visibility) the uploading interval, represent the extremes of such accuracy variation.

2.3.4 GPS Measurement Schedule

A GPS receiver that makes sequential pseudo range and pseudo range-rate measurements to single GPS satellites is assumed in this study. The receiver makes measurements at a constant rate (one every 12 sec) by cycling among the set of visible satellites. Measurement intervals ranging between one sec and one min are discussed in planned receiver designs, but for a user with an inertial system of the quality of that planned for the Orbiter, the measurement rate makes very little difference within these limits, provided that initial transient error reduction using GPS (for the first 8 measurements or so) is considered on a "number-of-measurements" basis and not on a time basis. That is, after the fifth measurement, say, results are likely to be very similar whether the five measurements took five sec or five min. Considered on a time basis, a higher measurement rate is always better.

2.3.5 Deorbit Navigation Filter

The filter chosen for GPS-aided deorbit navigation is an 11-state Kalman filter containing 3 positions states, 3 velocity states, 3 platform alignment states (all in inertial coordinates), and 2 clock states (phase and frequency). Table 2.3-1 summarizes the initial state standard deviations and the process noise densities for the filter.

Measurement noise values for GPS measurements are shown in Table 2.3-2. Note that there are two sets of values, one appropriate for use prior to updating and another set with

TABLE 2.3-1

DEORBIT NAVIGATION FILTER INITIAL CONDITIONS AND PROCESS NOISES

T-1138

		AXIS		
		DR*	CR*	R
INITIAL RMS ERROR	Position (ft)	25000†	2500	2500
	Velocity (fps)	3.3	3.3	26.3†
	Alignment ($\widehat{sec}$)	729	729	729
PROCESS NOISE SPECTRAL DENSITY	Position (ft^2/sec)	--	--	--
	Velocity (fps^2/sec)	0.1076	0.1076	0.1076
	Alignment ($\widehat{sec}^2/sec$)	4.41	4.41	4.41
INITIAL RMS CLOCK ERROR	Phase (ft)	1200‡		
	Frequency (fps)	0.25 ‡		
CLOCK PROCESS NOISE SPECTRAL DENSITY	Phase (ft^2/sec)	0.1		
	Frequency (fps^2/sec)	3.0×10^{-5}		

*Referenced to inertial velocity.
†Initial downrange position and radial velocity errors are -90% correlated
‡Initial clock phase and frequency errors are +50% correlated.

TABLE 2.3-2

DEORBIT FILTER MEASUREMENT NOISE

RMS MEASUREMENT ERROR	PRIOR TO UPLOADING	AFTER UPLOADING
Pseudo Range (ft)	100	12
Pseudo Range-Rate (fps)	0.05	0.05

a much reduced pseudo range error appropriate for use after updating. These variations are an attempt to account for the unmodeled (in the filter) effect of satellite states on pseudo range measurements as discussed in Section 2.3.3.

The deorbit filter incorporates underweighting as discussed in Section 2.3 of Ref. 4. Underweighting reduces the possibility of filter divergence due to nonlinear effects and also reduces the sensitivity of the filter to a single bad measurement. It slows convergence when all is well, however. An underweighting factor of 1.2 is used until the root sum of the three position variances falls to less than 3281 ft (1000 meters), at which point the underweighting is turned off. Due to the error growth during the blackout zone of deorbit, the underweighting is turned back on subsequently, and then, finally, turned off again if and when the position error falls back below the limit above.

When drag updating and baro-altimeter aids are added to GPS aiding, the filter includes an additional state. This state represents either drag altitude error or barometric altitude error, depending on whichever aid is currently being used, since the time periods when the two additional aids are being used does not overlap. Numerical values appropriate to this filter are those discussed in Chapter 5 of Volume 2.

2.3.6 Deorbit Navigation Truth Model

The truth model used to evaluate deorbit navigation with GPS aiding alone is similar to that described in Section 2.4.1 of Ref. 4. In particular, the 20-state model for the inertial measurement unit (IMU) and the 6-state model for the

master timing unit* (MTU, also called the Orbiter clock) are identical. The gravity model error section of the earlier study is not exercised here due to the negligible effect of gravity errors in past studies at lower altitudes where such errors would be even larger. The satellite states in the truth model are changed because a 5-state rubidium clock model is used here for Phase I GPS instead of the 3-state cesium model used for Phase III GPS in the earlier study, and because there are only 6 Phase I satellites considered here. Thus, there are a total of 78 satellite states (6 satellites × 13 states per satellite). Including the 11 filter states, the current truth model contains 115 states.

The data base for the current truth model reflects the likely initial values for the filter states and for the MTU for deorbit navigation, assuming GPS had not been used for the two hours preceding deorbit. The IMU values are identical to those assumed in Table 4.2-2 of Volume 2. The GPS satellite state numerical values are used in the NESA program (described in Section 2.2 of Ref. 4) and are appropriate to Phase I GPS. Table 2.3-3 summarizes the data base for the deorbit navigation truth model.

When drag updating and baro-altimeter measurements are taken along with the GPS measurements, the truth model necessarily becomes more complex. The additional models are described in Sections 4.3-1 and 4.3-2 of Ref. 4. The truth model data base for these additional states includes all drag and baro-related error sources as presented in Ref. 4 and used in generating the baseline error budgets of that report. Table 4.3-4 and a portion of Table 4.3-5 of Ref. 4 summarize the added data base.

*When this study was done, it was thought that the MTU would serve as the GPS receiver clock. This is no longer the case.

TABLE 2.3-3
DATA BASE FOR DEORBIT NAVIGATION TRUTH MODEL

T-1140

ERROR SOURCE	STANDARD DEVIATION
0. Uncorrelated GPS Receiver Measurement Errors	
Pseudo Range	12 ft
Pseudo Range-Rate	0.05 fps
1. Initial Filter State Errors	
Position	(11265, 866, 1036) ft*
Velocity	(1.086, 0.942, 12.468)fps*
Alignment	284 sec each of 3 axes
2. IMU Errors	
Accelerometer	
Biases	50 ug each of 3 axes
Scale Factors	100 ppm each of 3 axes
Asymmetries	100 ppm each of 3 axes
Nonorthogonalities	15 sec each of 3 axes
Gyro	
Bias Drifts	0.035 deg/hr each of 3 axes
Mass Unbalances	0.025 deg/hr/g each of 5 components
3. Shuttle MTU Errors	
Initial Phase	1130 ft+
Initial Frequency	0.142 fps
Aging	3.86×10^{-6} ft/sec^2
Random Frequency	20.2 fps#
Random Frequency Rate	1.37 ft/sec^2#
Acceleration Sensitivity	0.1 ft/sec^2/g
4. GPS Satellite Errors	See Text

*Given in downrange-crossrange-radial coordinates referenced to inertial velocity; significant cross correlations exist among initial position and velocity errors

+Correlations among initial clock errors exist; also, clock process noises exist as given in Section 2.4.1 for Ref. 2

#Clock flicker noise is attenuated by a factor of 100 before combining with ordinary frequency error

2.3.7 Results of GPS Aiding Alone

Position and velocity error results of a truth model evaluation of GPS aiding during deorbit, assuming good visibility prior to satellite uploading, are presented in Figs. 2.3-3 and 2.3-4. Similar results for a period of reduced visibility after satellite uploading are presented in Figs. 2.3-5 and 2.3-6. The figures are largely self-explanatory, but because

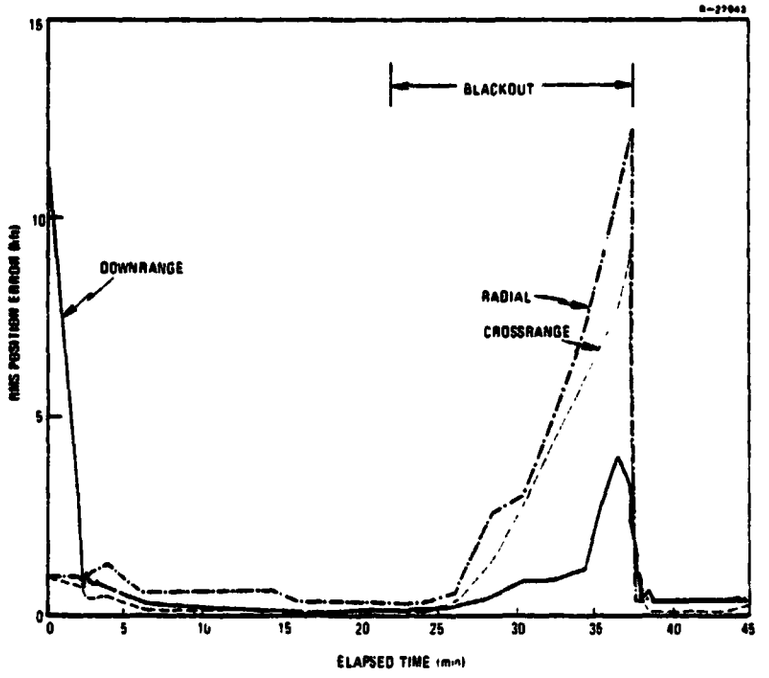

Figure 2.3-3 RMS Position Error versus Time for GPS-Aided Deorbit Navigation with Good Visibility Prior to Satellite Uploading

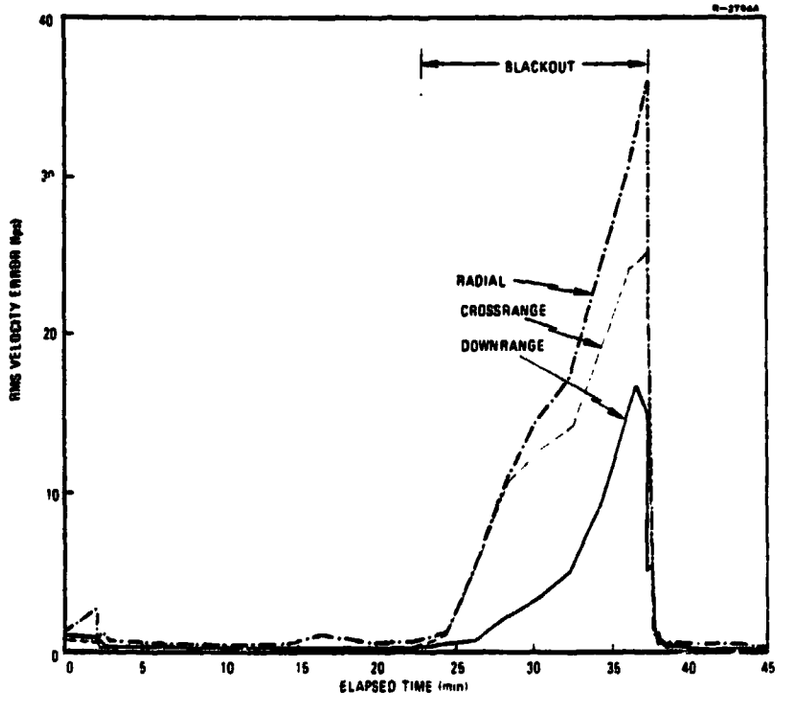

Figure 2.3-4 RMS Velocity Error versus Time for GPS-Aided Deorbit Navigation with Good Visibility Prior to Satellite Uploading

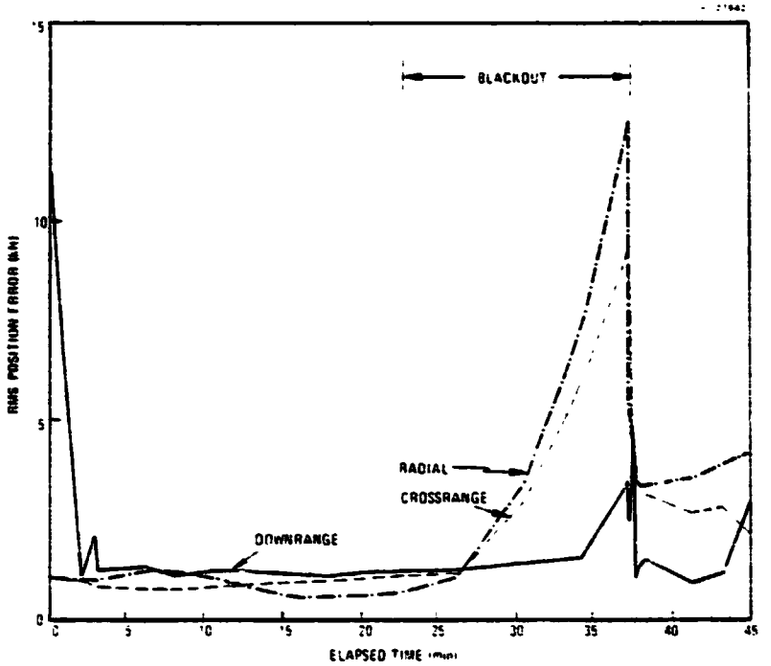

Figure 2.3-5 RMS Position Error versus Time for GPS-Aided Deorbit Navigation with Reduced Visibility After Satellite Uploading

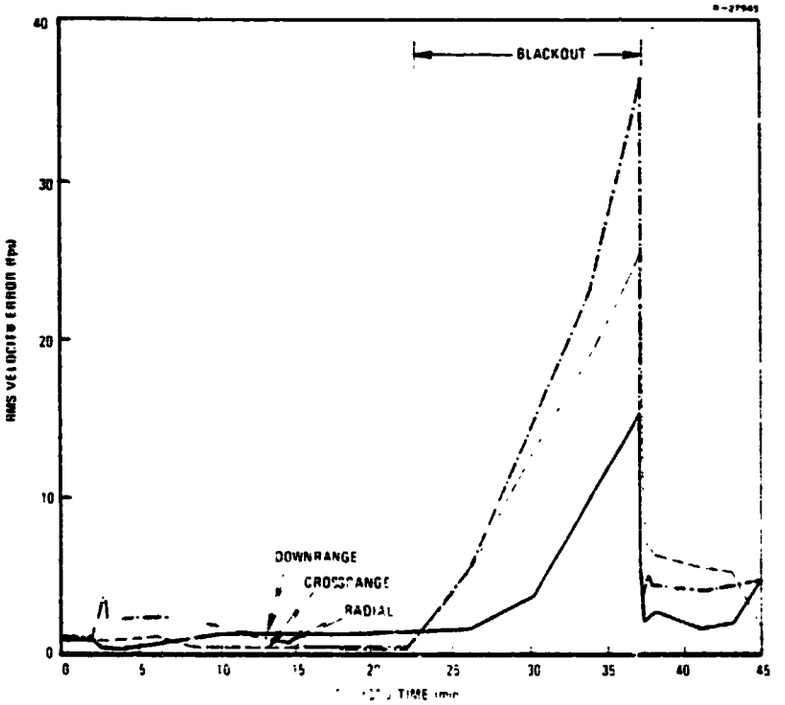

Figure 2.3-6 RMS Velocity Error versus Time for GPS-Aided Deorbit Navigation with Reduced Visibility After Satellite Uploading

of the scales necessary to present all of the results on a linear graph they tend to obscure some details of the transient error reductions, both the initial reductions and the reductions following the blackout period. Figures 2.3-7 and 2.3-8 show these initial reductions of position errors on a logarithmic scale and on a number-of-measurements basis rather than a time basis. It should be pointed out that during the initial portion of deorbit with good visibility there are only three satellites visible, fewer than are needed for complete position determination based on GPS alone.

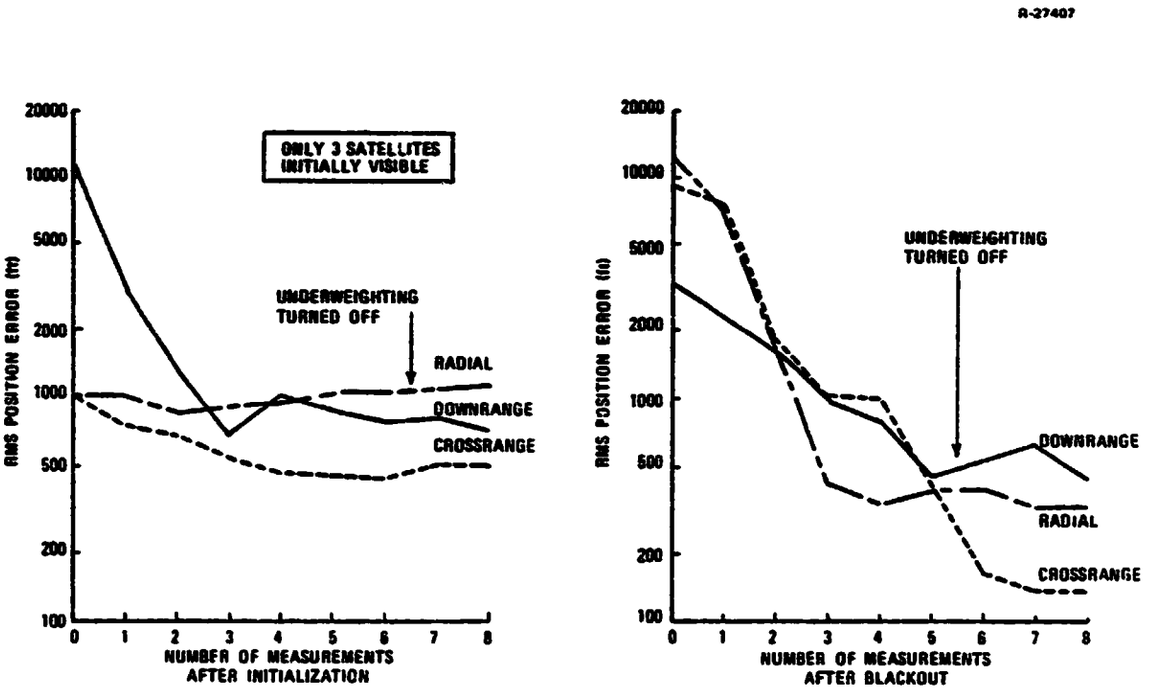

Figure 2.3-7 Initial Error Reduction with GPS (Based on Good Visibility Prior to Uploading)

Tables 2.3-4 thru 2.3-6 contain error budgets prior to blackout, after blackout, and at the terminal 20 kft of altitude points, both for the good visibility situation and the reduced visibility situation. After blackout, the results

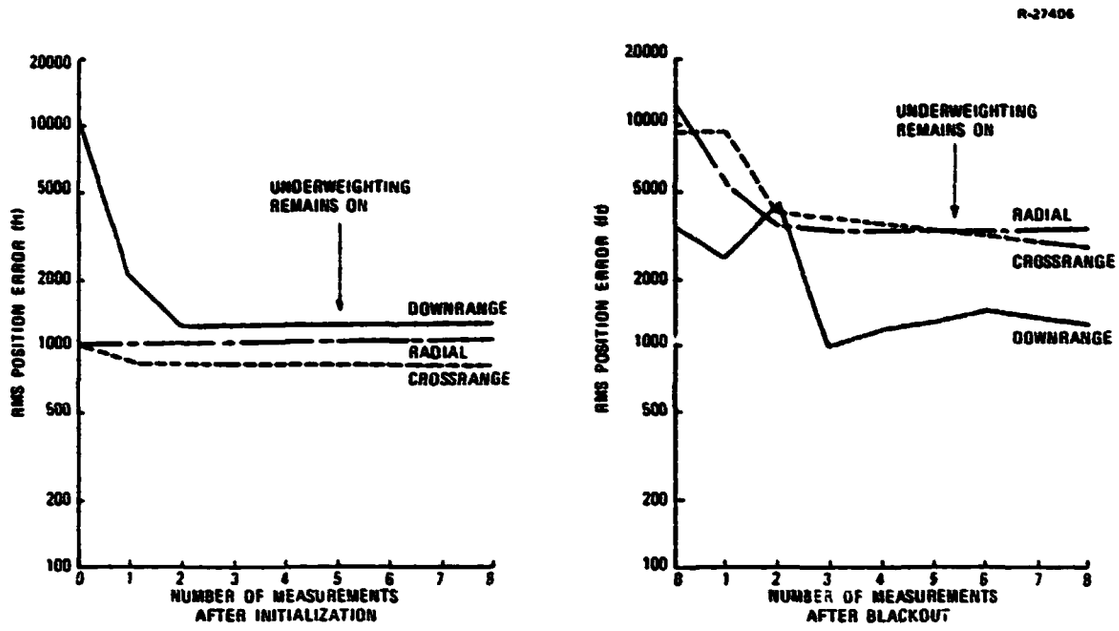

Figure 2.3-8 Initial Error Reduction with GPS (Based on Reduced Visibility After Uploading)

TABLE 2.3-4

GPS-AIDED DEORBIT NAVIGATION ERROR BUDGETS PRIOR TO BLACKOUT

T4301

	ERROR GROUP	RMS POSITION ERROR (FT) DR	CR	R	RMS VELOCITY ERROR (FPS) DR	CR	R
BASED ON GOOD VISIBILITY PRIOR TO UPLOADING	INITIAL CONDITIONS	0	0	1	0.01	0.01	0.01
	MEASUREMENT NOISE	7	5	14	0.05	0.05	0.06
	INERTIAL MEASUREMENT UNIT	1	1	1	0.02	0.04	0.04
	ORBITER CLOCK	8	8	35	0.12	0.14	0.26
	SATELLITE STATES	133	100	300	0.03	0.04	0.42
	RSS	133	101	302	0.14	0.16	0.50
BASED ON REDUCED VISIBILITY AFTER UPLOADING	INITIAL CONDITIONS	539	110	82	0.57	0.17	0.13
	MEASUREMENT NOISE	52	8	14	0.07	0.10	0.22
	INERTIAL MEASUREMENT UNIT	962	53	48	1.21	0.22	0.30
	ORBITER CLOCK	442	1039	652	0.40	0.37	0.13
	SATELLITE STATES	—	—	—	—	—	—
	RSS	1189	1046	659	1.40	0.47	0.42

TABLE 2.3-5
GPS-AIDED DEORBIT NAVIGATION ERROR BUDGETS AFTER BLACKOUT

T-1023

	ERROR GROUP	RMS POSITION ERROR (FT) DR	CR	R	RMS VELOCITY ERROR (FT) DR	CR	R
BASED ON GOOD VISIBILITY PRIOR TO UPLOADING	INITIAL CONDITIONS	2976	9088	11915	14.35	24.43	34.86
	MEASUREMENT NOISE	58	42	83	0.05	0.04	0.17
	INERTIAL MEASUREMENT UNIT	1329	1950	2619	4.46	5.78	8.15
	ORBITER CLOCK	195	132	338	0.19	0.12	0.67
	SATELLITE STATES	410*	210*	827*	0.16	0.17	1.62
	RSS	3292	9299	12233	15.02	25.11	35.84
BASED ON REDUCED VISIBILITY AFTER UPLOADING	INITIAL CONDITIONS	2965	9109	11942	14.59	24.49	35.08
	MEASUREMENT NOISE	154	133	194	0.12	0.11	0.39
	INERTIAL MEASUREMENT UNIT	1475	1968	3654	4.73	5.77	9.24
	ORBITER CLOCK	1013	343	1552	0.31	1.25	2.40
	SATELLITE STATES	—	—	—	—	—	—
	RSS	3467	9326	12586	15.34	25.19	36.36

*SATELLITE CLOCKS CONSISTENT WITH RECENT TEST DATA WOULD YIELD POSITION ERROR CONTRIBUTIONS 10-20 TIMES SMALLER.

are about the same in either case, as the errors are dominantly due to initial platform misalignments with a lesser amount due to the IMU. Because there is very little sensed acceleration prior to blackout, the initial platform alignments are not observable and thus cannot be estimated during this time interval from the GPS measurements. The IMU errors are not estimated by the filter, so their contribution during blackout cannot be reduced by GPS measurements prior to blackout.

Platform alignment errors grow somewhat from their initial values up to the end of the blackout period, due to gyro drift contributions. After blackout, the filter begins to estimate the alignments and to reduce the rms alignment

TABLE 2.3-6

GPS-AIDED DEORBIT NAVIGATION ERROR BUDGETS
AT 20,000 FT ALTITUDE

T-1024

	ERROR GROUP	RMS POSITION ERROR (FT)			RMS VELOCITY ERROR (FPS)		
		DR	CR	R	DR	CR	R
GOOD VISIBILITY PRIOR TO UPLOADING	INITIAL CONDITIONS	1	1	0	0.07	0.06	0.06
	MEASUREMENT NOISE	11	10	14	0.08	0.07	0.05
	INERTIAL MEASUREMENT UNIT	2	2	0	0.07	0.13	0.07
	ORBITER CLOCK	18	22	35	0.18	0.16	0.24
	SATELLITE STATES	314*	329*	425*	0.05	0.02	0.30
	RSS	314	330	427	0.22	0.23	0.39
REDUCED VISIBILITY AFTER UPLOADING	INITIAL CONDITIONS	1267	317	1143	1.44	0.36	1.44
	MEASUREMENT NOISE	265	71	171	0.13	0.09	0.32
	INERTIAL MEASUREMENT UNIT	2474	678	1364	2.85	0.68	2.56
	ORBITER CLOCK	1617	1945	3811	4.01	1.04	3.79
	SATELLITE STATES	—	—	—	—	—	—
	RSS	3226	2085	4209	5.12	1.30	4.80

*SATELLITE CLOCKS CONSISTENT WITH RECENT TEST DATA WOULD YIELD POSITION ERROR CONTRIBUTIONS 10-20 TIMES SMALLER

error , as Table 2.3-7 shows. Sensed acceleration during and after blackout is largely in the downrange direction, with a lesser amount in the radial direction, and very little in the crossrange direction, so alignment observability is best in the crossrange direction and worst in the downrange direction, which the table confirms.

2.3.8 Effect of the Duration of Blackout

Previous Figs. 2.3-3 through 2.3-6 show the error growth during the blackout period as a function of time. An earlier emergence from blackout would cause errors to peak at the lower values plotted for times before 37.3 min. Time and

TABLE 2.3-7

PLATFORM ALIGNMENT ERRORS FOR GPS-AIDED DEORBIT NAVIGATION

T-1141

EVENT	GOOD VISIBILITY PRIOR TO SATELLITE UPLOADING			REDUCED VISIBILITY AFTER SATELLITE UPLOADING		
	RMS MISALIGNMENTS ($\widehat{SEC}$)			RMS MISALIGNMENTS ($\widehat{SEC}$)		
	DR	CR	R	DR	CR	R
INITIAL CONDITIONS	284	284	284	284	284	284
PRIOR TO FIRST MEASUREMENT AFTER BLACKOUT	290	291	292	292	293	294
EIGHT MEASUREMENTS AFTER BLACKOUT	112	46	77	151	51	130
AT 20 KFT ALTITUDE	47	38	39	52	53	39

altitude are related in a nonlinear way during blackout, however, so it is not directly obvious from the previous figures how error growth would be reduced if the altitude (nominally 145 kft) assumed for the end of blackout were raised.

The other way in which the blackout interval could be reduced, by lowering the altitude (nominally 300 kft) assumed for the onset of blackout, would have a less obvious effect on the error growth. A separate investigation is necessary to examine each variation in the altitude for the onset of blackout. Figures 2.3-9 and 2.3-10 show how errors grow during blackout as a function of altitude, so that the effect of ending blackout at a higher altitude is easily assessed, and how the errors at the end of blackout (the nominal 145 kft) reduce if blackout begins at altitudes lower than 300 kft. A general conclusion is that an early emergence from blackout would clearly reduce errors, but that a delay in the onset of blackout would be helpful only if the delay were to an altitude below 240 kft.

R-27414

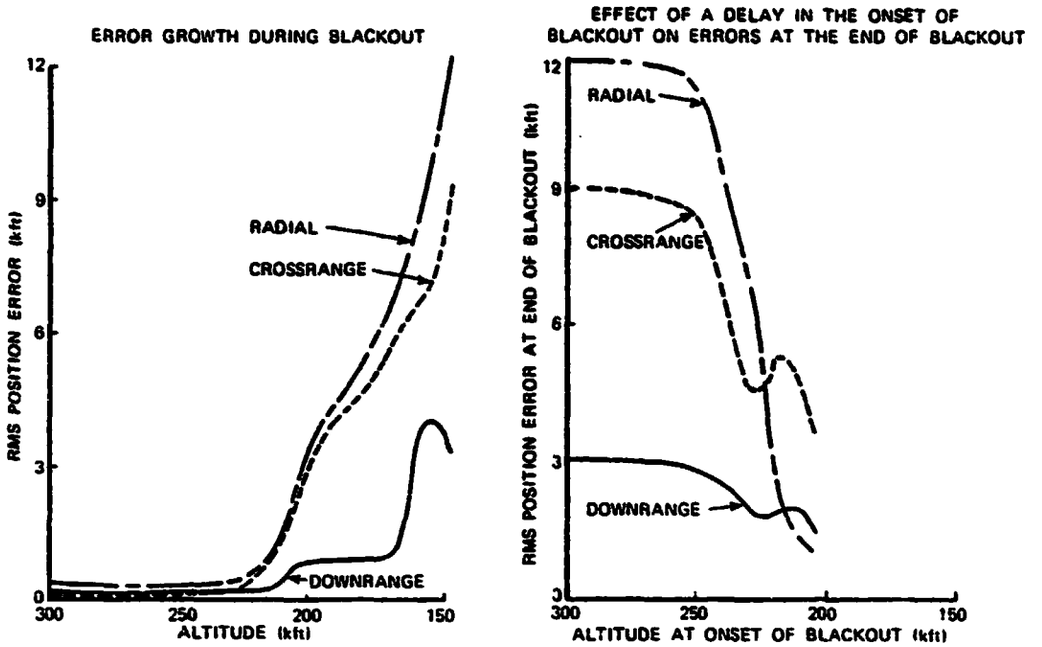

Figure 2.3-9 Sensitivity of Aided Navigation Results to the Duration of Blackout -- Position Errors

R-27412

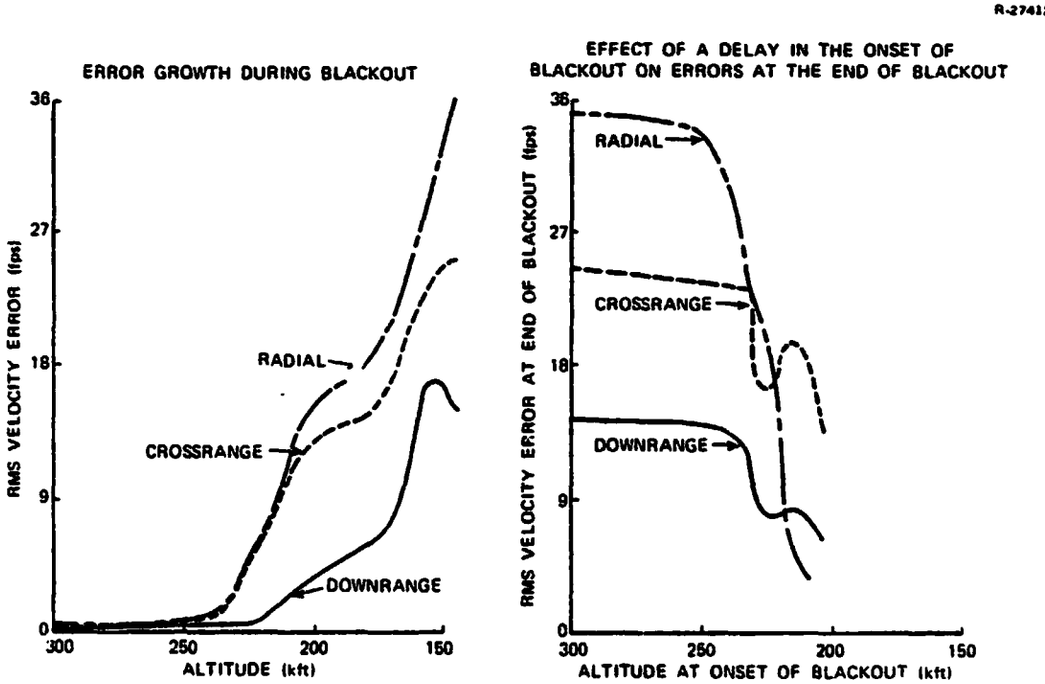

Figure 2.3-10 Sensitivity of Aided Navigation Results to the Duration of Blackout -- Velocity Errors

2.3.9 Effect of Misalignment States in the Filter

A possible simplification of the deorbit navigation filter would be to omit the three platform alignment states. These states cannot possibly be estimated until after blackout, because before blackout there is inadequate sensed acceleration to have platform misalignment cause any effect, and during blackout there are no measurements. The misalignment states are useful, however, in quickly reducing the navigation errors after blackout, as Fig. 2.3-11 shows. The reason for this behavior is that with alignment states present, the filter correctly accounts for the cross correlations in position and velocity error components that build up during blackout, making subsequent identification of errors an easier process.

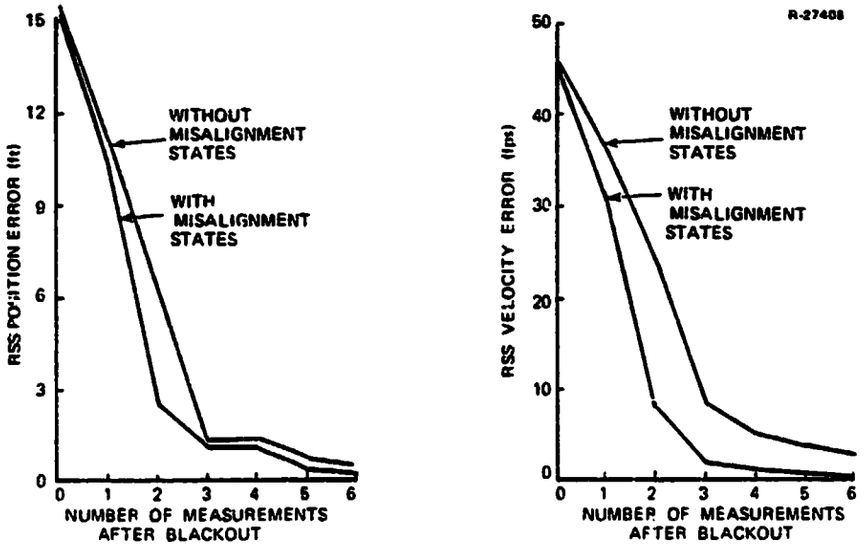

Figure 2.3-11 Effect of Misalignment States in the Filter (Based on Good Visibility Prior to Uploading)

2.3.10 Effect of Adding Drag Updates and a Baro-Altimeter

One way to control the error buildup during blackout and to assist in recovery after blackout in a reduced visibility situation is to add drag updating and baro-altimeter measurements. Both of these aids are useful in reducing errors in the plane of motion, especially in the radial direction.

Drag updating begins around 282 kft of altitude, just after blackout begins, and continues past the nominal end of blackout down to 100 kft of altitude. One update is assumed each 3.6 seconds in this analysis. Baro-altimeter measurements do not begin until 31 kft of altitude is reached, and continue to the 20 kft point at which this study stops.* Baro-altitude measurements are also assumed at 3.6 second intervals. Because these additional aids are most useful under reduced visibility conditions, such conditions are assumed to exist. Reduced visibility conditions here follow satellite uploading, so that questions of satellite clock quality are obviated.

Figure 2.3-12 shows the error growth during blackout when drag updating is used, while Fig. 2.1-18 shows the initial error reduction following the blackout period. Table 2.3-8 gives error budgets after blackout and at 20 kft of altitude when drag updates and baro-altimeter measurements are used. Note especially the reductions in radial position and velocity errors when the additional aids are used in conjunction with even reduced visibility GPS measurements.

*After the initial series of Shuttle test flights, the air data system will be sufficiently well calibrated to permit operation at higher altitudes, possibly up to 85-100 kft.

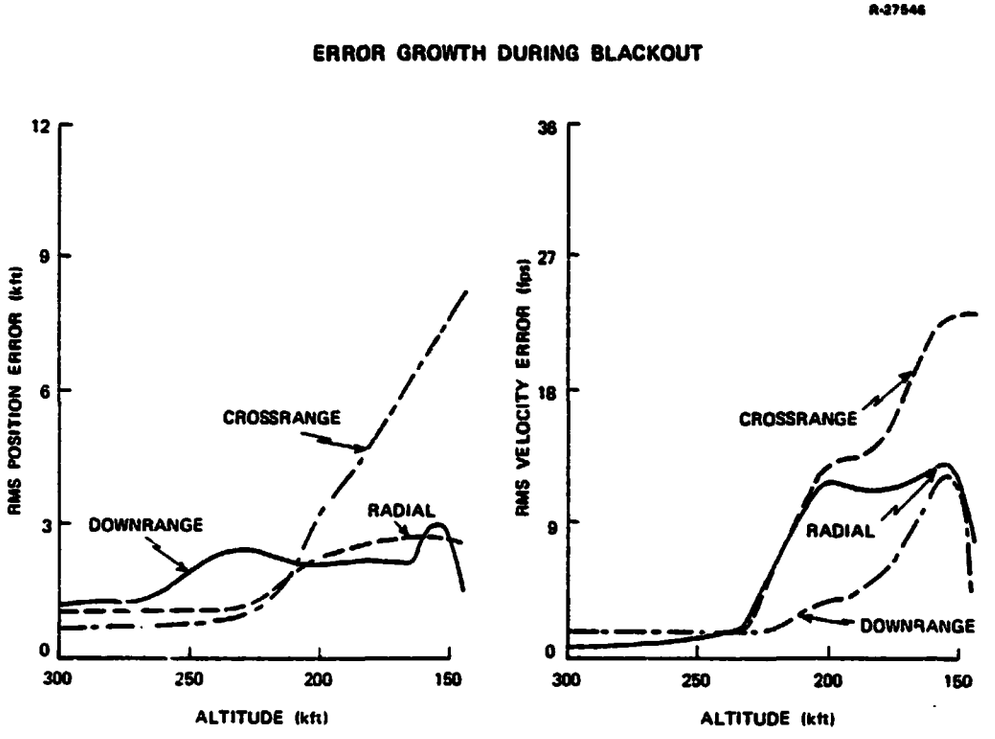

Figure 2.3-12 GPS + Drag Update + Baro-Altimeter Aided Deorbit Navigation (Error Growth During Blackout)

2.3.11 Deorbit Navigation Conclusions

An important aspect of deorbit navigation concerns visibility coverage for the deorbit mission with Phase I GPS. It is shown in section 2.2.2 that good visibility is obtained only about five hours each day, with reduced visibility obtained for a 12-16 hour interval each day. For the remaining 8-12 hours each day, satellite visibility during deorbit is poor to nonexistent. This study shows that GPS aiding alone produces good deorbit navigation results during periods of good visibility, while acceptable results with reduced visibility may be obtained by adding drag updating and baro-altimeter aids.

TABLE 2.3-8

GPS + DRAG + BARO-ALTIMETER AIDED NAVIGATION ERROR BUDGETS
(BASED ON REDUCED VISIBILITY AFTER UPLOADING)

T-1036

	ERROR GROUP	RMS POSITION ERROR (FT)			RMS VELOCITY ERROR (FPS)		
		DR	CR	R	DR	CR	R
AFTER BLACKOUT	INITIAL CONDITIONS	1366	7897	1661	4.12	21.98	6.72
	GPS MEASUREMENT NOISE	83	180	110	0.06	0.22	0.18
	INERTIAL MEASUREMENT UNIT	621	1890	874	1.63	5.57	2.78
	ORBITER CLOCK	124	279	1477	0.16	2.96	1.13
	DRAG UPDATE STATES	343	459	1153	1.08	1.24	2.50
	BARO-ALTIMETER STATES	—	—	—	—	—	—
	RSS	1547	8140	2654	4.56	22.91	7.78
AT 20,000 FT ALTITUDE	INITIAL CONDITIONS	358	64	293	0.42	0.06	0.28
	GPS MEASUREMENT NOISE	126	19	56	0.15	0.08	0.18
	INERTIAL MEASUREMENT UNIT	1249	188	245	1.65	0.18	1.15
	ORBITER CLOCK	2144	382	401	0.32	0.15	0.63
	DRAG UPDATE STATES	76	11	29	0.09	0.01	0.07
	BARO-ALTIMETER STATES	678	55	640	0.72	0.06	0.77
	RSS	2601	434	849	1.88	0.26	1.55

Provided the time between measurements is on the order of one min or less, a sequential receiver cycling among visible GPS satellites is adequate. The navigation results are insensitive to the actual time between measurements, if transient error reduction is considered on a "number-of-measurements" basis rather than on a time basis.

Error buildup during the blackout period is severe with GPS aiding alone. It may be reduced either by shortening the blackout interval or by adding drag updating.

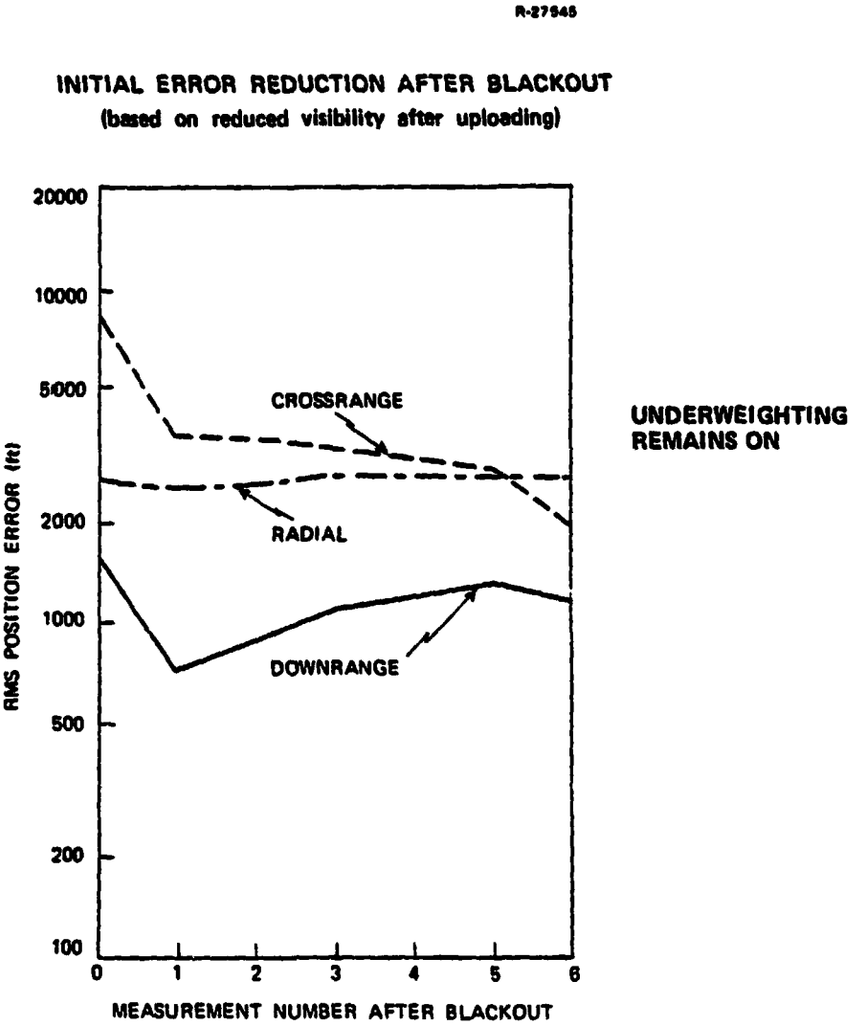

Figure 2.3-13 GPS + Drag Update + Baro-Altimeter Aided Deorbit Navigation (Post Blackout Error Reduction)

With good satellite visibility prior to satellite ephemeris uploading, and assuming the modeled 5-state rubidium satellite clock accuracy, "steady-state" errors are dominated by satellite ephemeris errors. With reduced visibility after uploading, "steady-state" errors are much larger and are dominated by the Orbiter clock and IMU.

Platform alignment states in the deorbit navigation filter are of limited utility in the early stages of deorbit, but help in rapid transient error reduction following blackout. The addition of drag updates and baro-altimeter measurements to the GPS measurements substantially reduces errors at low altitudes, especially in the radial direction.

2.4 ORBITAL NAVIGATION

2.4.1 Introduction

Orbital navigation performance with Phase I GPS is treated in this section in a manner similar to that used for deorbit navigation in the previous section. There are key differences. No IMU information is utilized on orbit, as sensed acceleration levels are generally below the IMU threshold. Instead, low-level venting thrusts are the dynamical error drivers and must be modeled. The satellite constellation and orbital trajectory are discussed along with the visibility results in previous Section 2.2.3. In this section, the orbital navigation filter in the GPS receiver is discussed, as is the truth model used to evaluate the filter performance. The nominal results are presented, followed by a set of results for a situation slightly modified to assess error build-up during periods of no satellite visibility. Finally, conclusions are summarized.

2.4.2 Orbital Navigation Filter

There are fundamental differences between orbital and deorbit navigation that call for changes in the navigation filter. The filter for orbital navigation remains an 11-state

Kalman filter with underweighting, but the three platform alignment states used during deorbit are not useful on orbit. Vehicle dynamics on orbit, besides those due to the accurately predictable earth gravitational field, are primarily due to venting effects, and these are below the threshold of the IMU. In place of the three platform alignments states, the orbital filter has three thrust acceleration states, modeled as first-order Markov processes in downrange-crossrange-radial coordinates. This approach is similar to that used in Section 3.3 of Ref. 21.

Discussions with JSC (Ref. 22) related that the Shuttle venting details are not yet firm, but that rms values in the 0.5 to 1.0 lb of thrust range (1 lb of thrust is 5μg's of acceleration on a 200,000 lb vehicle) are probable. Venting thrusts will probably be dominately along the Orbiter body forward-aft and "vertical" axes with a smaller amount in the port-starboard direction. Expecting that the forward-aft body axis will be near the orbital plane more often that not, and using some conservation in filter design, the rms thrust values used in the filter are those of Table 2.4-1. Venting thrusts may be highly correlated in Orbiter body coordinates, but they will be less so in the orbital coordinates of downrange-crossrange-radial. The first-order Markov process time constants assumed for thrust in Table 2.4-1 reflect that fact.

2.4.3 Orbital Navigation Truth Model

The truth model for GPS-aided orbital navigation is similar to that used for deorbit navigation with a few exceptions. Due to the very low level of sensed acceleration on orbit, the IMU states are not important. Hence, the 20 IMU states are removed from the truth model. For the same reason, one of the MTU states, an acceleration sensitive clock state,

TABLE 2.4-1

THRUST PROCESS PARAMETER VALUES USED IN THE ORBITAL NAVIGATION FILTER

T-1152

THRUST PROCESS PARAMETER	AXIS		
	DR	CR	R
Time Constant (sec)	600	300	600
RMS Initial Thrust (lb)	1.5	0.5	1.5
Thrust Process Noise Intensity (lb/$\sqrt{sec}$)	0.0866	0.0408	0.0866

is removed, reducing the MTU model to five states. And of course, the 11 filter states in the truth model correspond to those just discussed, incorporating the three thrust states in place of the three platform alignment states used for deorbit studies.

The data base for the orbital navigation truth model, where the two models have corresponding states, is entirely the same as that used for deorbit and summarized in Table 2.3-3. The truth model values for the thrust states are shown in Table 2.4-2. Thr thrust state time constants used in the filter are kept, but the initial rms state values and the corresponding process noises are reduced by 1/3.

2.4.4 Orbital Navigation Results

Position and velocity error results of a truth model evaluation of GPS aiding on orbit, assuming a recent satellite uploading, are presented in Figs. 2.4-1 and 2.4-2. As the

TABLE 2.4-2

THRUST PROCESS PARAMETER VALUES USED IN THE ORBITAL NAVIGATION TRUTH MODEL

T-1156

THRUST PROCESS PARAMETER	AXIS		
	DR	CR	R
Time Constant (sec)	600	300	600
RMS Initial Thrust (lb)	1.0	0.33	1.0

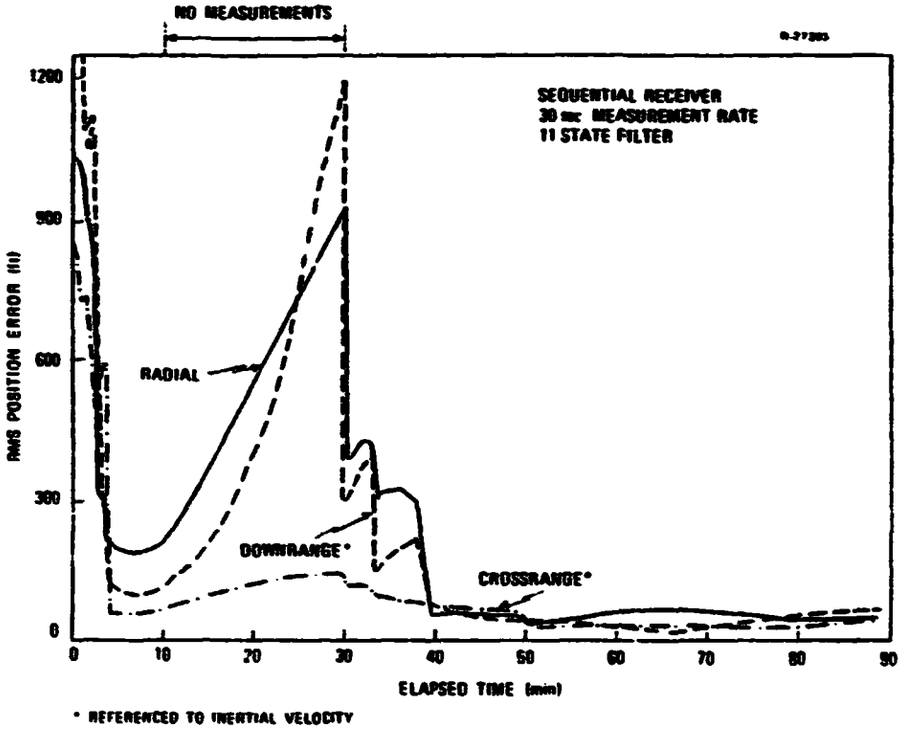

Figure 2.4-1 Orbital Navigation: RMS Position Error Versus Time

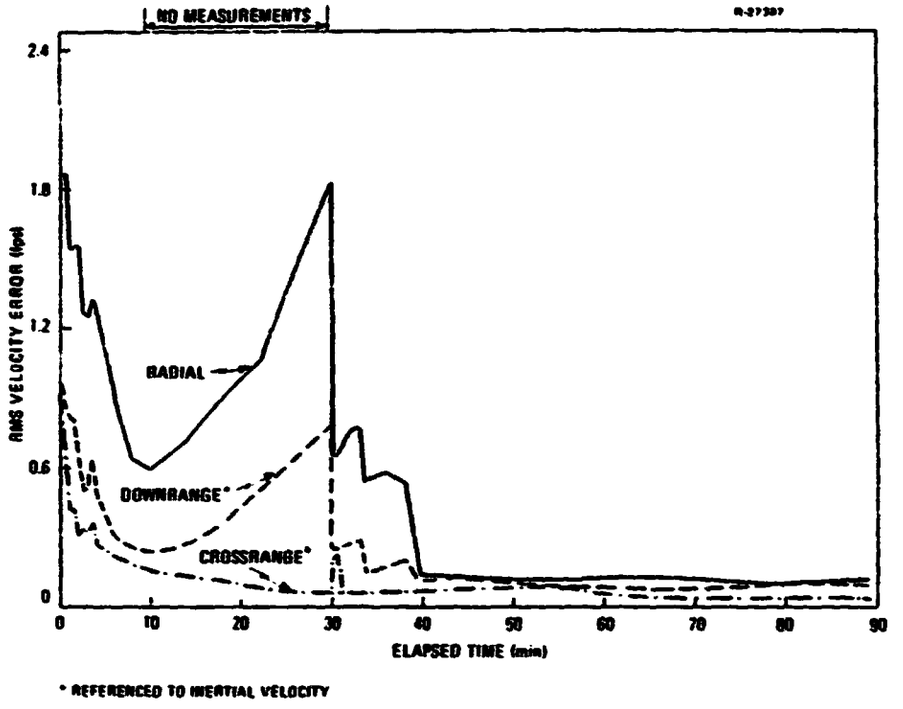

Figure 2.4-2 Orbital Navigation: RMS Velocity Error Versus Time

figures show, initial errors are reduced during the first 10 min segment of fading satellite visibility. The errors grow during the next 20 min segment of no visibility, and then they fall again as visibility improves. An error budget at 89 min is presented in Table 2.4-3. After more than one orbit, errors prior to a segment of no visibility would be smaller than those at 10 min of Figs. 2.4-1 and 2.4-2. In the figures, the effect of the large initial errors was not yet overcome before the 20 min segment of no visibility was encountered.

2.4.5 Results for a Modified Measurement Schedule

To see how large orbital navigation errors would become during a typical period of no satellite visibility after

TABLE 2.4-3
ORBITAL NAVIGATION ERROR BUDGET
(89 MINUTES)

T-1026

ERROR SOURCE GROUP	POSITION ERROR (FT)			VELOCITY ERROR (FPS)			CLOCK ERROR	
	DR	CR	R	DR	CR	R	PHASE (FT)	FREQUENCY (FPS)
INITIAL CONDITIONS	0	0	0	0	0	0	0	0
MEASUREMENT NOISE	21	16	16	.04	.02	.04	21	.04
THRUST PROCESS	7	7	4	.03	.02	.03	8	.02
CLOCK	27	16	27	.09	.03	.10	23	.08
SATELLITE ERRORS	59	38	31	.02	.02	.04	62	.02
RSS	68	45	45	.10	.04	.12	69	.09
VECTOR RSS	93			0.16				

first stabilizing during a period of good visibility, the orbital navigation results were redone after adjusting the previous measurement schedule so it simulates such a situation. Figure 2.4-3 shows the adjusted visibility pattern and measurement schedule shifted from that in Section 2.2 "end-around" by 50 min.

Position and velocity error results of a truth model evaluation of GPS aiding for this visibility situation on orbit, assuming, as before, recent satellite uploadings, are presented in Figs. 2.4-4 and 2.4-5. The figures show that position errors are reduced to reasonably stable low values after about 10 min, while velocity errors require about 20 min. Note from Fig. 2.4-3 that 4 satellites do not become visible until about 10 min of elapsed time, largely explaining the initial error behavior.

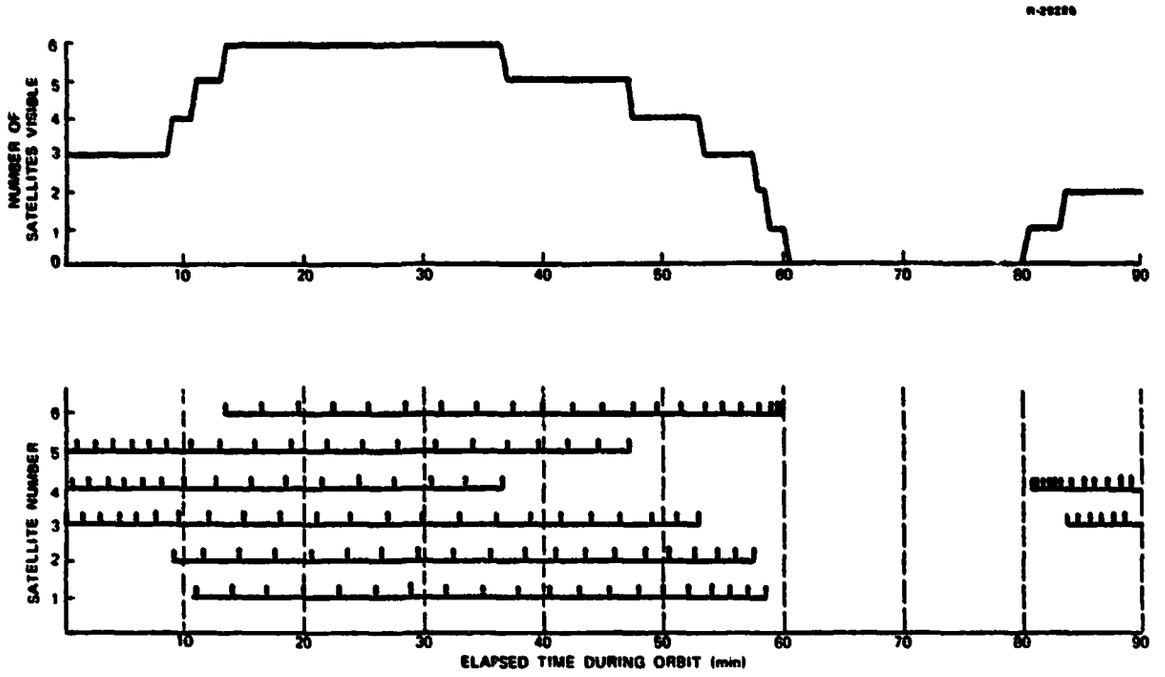

Figure 2.4-3 Revised Orbital Satellite Visibility and Measurement Schedule

Downrange position error and radial velocity error grow most rapidly during periods of no visibility. In the results previously reported, rms downrange position error grew to 1200 ft and rms radial velocity error grew to 1.82 fps during the 20 min period of no visibility. Here, as Figs. 2.4-4 and 2.4-5 show, rms downrange position error grows to 870 ft while rms radial velocity error grows to 1.34 fps during the 20 min period of no visibility that occurs after GPS aiding has had time to overcome the effect of the large initial navigation errors. The present results are expected to be typical of error growth during periods of no visibility on orbit using Phase I GPS.

2.4.6 Orbital Navigation Conclusions

GPS appears particularly well suited to Shuttle orbital navigation. Even Phase I GPS with its limited coverage should

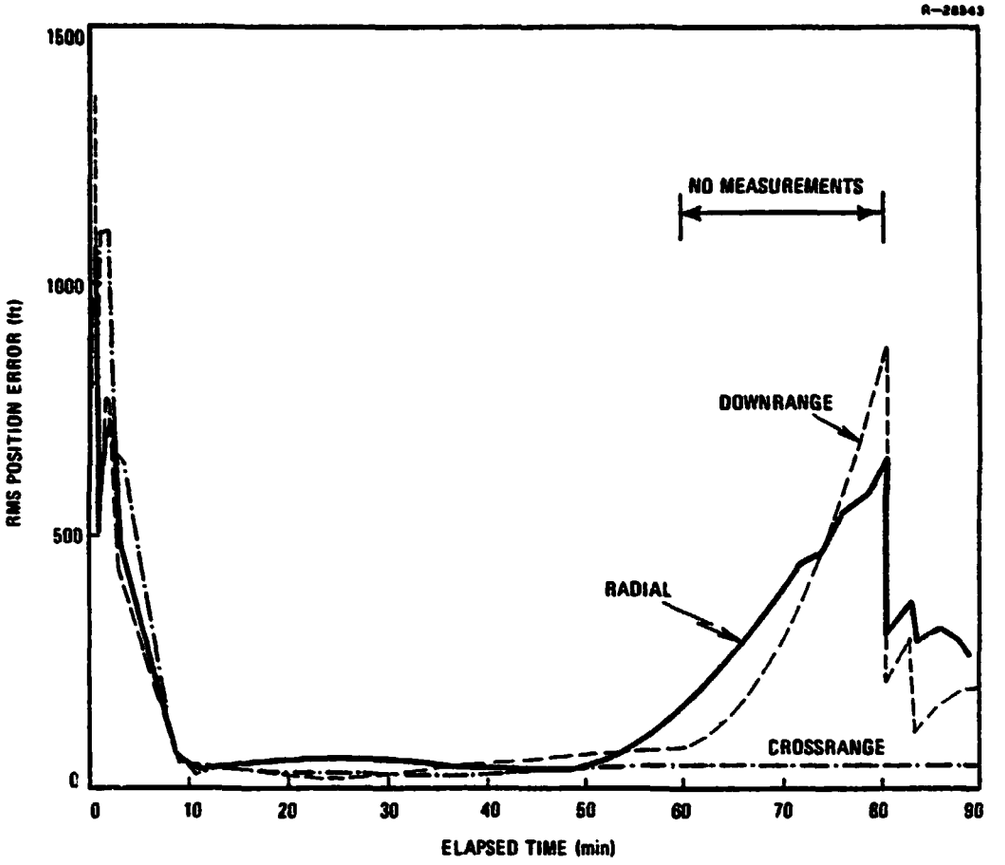

Figure 2.4-4 Orbital Navigation: RMS Position Error Versus Time

provide good satellite visibility over some segment of almost every orbit, whatever the orbital inclination. During periods of good visibility subsequent to a satellite uploading interval, rms orbital navigation errors should reduce to less than 100 ft in position and 0.2 fps in velocity. After 20 min of no visibility following a period of good visibility, rms navigation errors should grow into the 600-900 ft range in position and be less than 1.5 fps in velocity.

An additional conclusion evident in the detailed examination of the truth model results is that while the filter

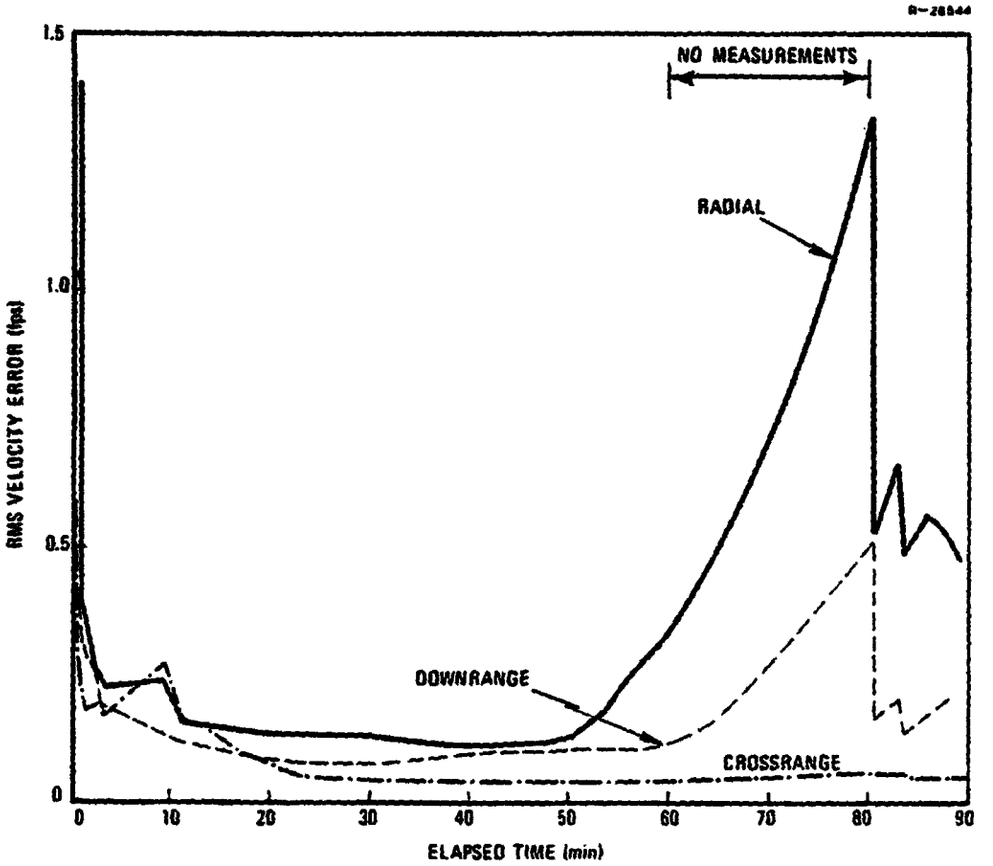

Figure 2.4-5 Orbital Navigation: RMS Velocity Error Versus Time

does not do well in estimating the thrust states, it uses the thrust states to compensate for correlated frequency noise in the Orbiter MTU, making for a slight improvement in velocity estimation.

3. SINGLE SATELLITE GPS ORBITAL NAVIGATION

3.1 INTRODUCTION

This chapter presents results of a study of orbital Space Shuttle navigation using a single GPS satellite. The study meets several practical objectives. It demonstrates the minimum capability of GPS for Shuttle navigation in a worst case situation. While the current schedule for GPS satellite launches calls for several satellites to be available in the time frame projected for GPS user equipment implementation aboard the Shuttle, schedule changes or satellite failures could conceivably result in only one or two operational satellites during some Shuttle flights with a GPS receiver. This study provides a valuable preliminary examination necessary for guiding decisions on the use of GPS for orbital navigation with an incomplete satellite system. Even if several satellites are always available, this study still is useful for the insights it provides. The results from a single satellite study bring out fundamental relationships in the satellite navigation system, thus leading to a better understanding of the complex interactions of the multisatellite navigation system.

3.2 METHODOLOGY

In all of the results reported here, the single GPS satellite was assumed to be in a typical GPS circular orbit of 63 deg inclination at a radius of approximately 4.164 earth radii. The Shuttle was also assumed to be in a circular orbit,

always at 150 nm altitude (1.044 earth radii), sometimes at a 38 deg inclination typical of some early missions, and sometimes at a 63 deg inclination, matching that of the GPS satellite, to consider extreme Shuttle-GPS geometry. Right ascension and mean anomaly of the Shuttle orbit relative to the GPS satellite orbit were varied.

A preparatory satellite visibility study indicated that typical visibility periods of 45 minutes and gaps of 55 minutes could be expected. Variations in initial mean anomalies made little difference when 12 hour periods were considered. Variations in right ascensions, however, could cause gaps as large as 104 minutes and visibility periods as short as 6 minutes in extreme cases. This preliminary analysis helped establish the reasonable Shuttle-GPS satellite orbital relationships for the navigation performance study.

An 8-state suboptimal GPS navigation filter and a 14-state truth model are used for error analysis. The states of the filter and of the truth model are presented in Table 3.2-1. Detailed development of the models and state variables is contained in Refs. 3 and 4, and in Chapter 2. A 14-state truth model is sufficient for the present analysis because only one satellite is considered; some small error contributing factors are not modeled.

Many simplifications are possible in this single satellite study since simulation of a particular mission is not being attempted. Circular orbits are assumed with no maneuvering on orbit, and no gravity errors per se are included. Satellite ephemeris and clock errors are also absent, as they are minor contributors (Ref. 4) and are reasonably difficult

TABLE 3.2-1
FILTER AND TRUTH MODEL STATES

Shuttle Filter		Truth Model	
Position	3	Position	3
Velocity	3	Velocity	3
Clock		Thrust	3
Phase	1	Clock	
Frequency	1	Phase	1
		Frequency	1
		Aging	1
		Random Frequency	1
		Random Frequency Rate	1
Total	8	Total	14

Position and velocity are in ECI (earth centered inertial) coordinates in both the Filter and the Truth Model.

to model over 12 hour periods, especially when uploading is considered.*

The truth model contains three thrust states to account for venting and other unmodeled acceleration effects. The navigation filter has velocity white noise added to prevent it from being overly optimistic, since it has no thrust state error contributions.

*Satellite ephemeris and clock errors are minor for the single satellite study, but would be significant contributors for a multiple satellite study where greater navigation accuracy was possible.

3.3 PROCEDURE

Three situations of varying Shuttle-to-GPS-satellite geometry are used in producing the navigation resuts reported here. These three situations are termed Cases 1, 2, and 3. As is mentioned above, in all cases the GPS satellite is in a circular, 63 deg inclination orbit at the appropriate radius to yield a 12 hr orbital period. The Shuttle orbit is also circular in all cases, at an altitude of 150 nm, so that it has a period of 90 min. In each case, a 12 hr span of GPS-aided navigation is simulated, with measurements at 2 min intervals whenever the satellite is visible. (The satellite is assumed visibile if it is at least 10 deg above the Shuttle horizon.) The initial conditions in each case have the Shuttle and the GPS satellite at their respective ascending nodes crossing the earth's equatorial plane. In Cases 1 and 2, the Shuttle is in a 38 deg inclination orbit. In Case 1, the Shuttle right ascension is initialized to be equal to the initial right ascension of the GPS satellite, so that the Shuttle starts directly beneath the satellite. In Case 2, the Shuttle right ascension is moved by 60 deg, so it does not start directly beneath the GPS satellite. Case 3 is selected to make the orbit planes for the Shuttle and the GPS satellite coincide, so that cross-range information is not present in the GPS measurements. Thus, in Case 3, the Shuttle orbit has a 63 deg inclination, and, as in Case 1, the Shuttle starts directly beneath the satellite. Table 3.3-1 summarizes the geometry for these three cases.

Data bases used for the navigation filter and for the associated truth model are summarized in Tables 3.3-2 and 3.3-3. These values have all been used in prior GPS-aided Shuttle navigation studies, and the tables give references to their prior usage.

TABLE 3.3-1
SHUTTLE-GPS SATELLITE GEOMETRY COMPARISON BY CASE

ORBIT PARAMETER	SPACECRAFT	CASE		
		1	2	3
Inclination (deg)	Shuttle	38	38	63
	Satellite	63	63	63
Initial Right Ascension (deg)	Shuttle	0	-60	0
	Satellite	0	0	0

TABLE 3.3-2
FILTER DATA BASE

ERROR SOURCE	STANDARD DEVIATION	DATA SOURCE
Measurement Noise		
Pseudo Range	12 ft	
Pseudo Range-Rate	0.05 fps	
		Ref. 2
Clock Process Noise		
Phase	0.1 ft	
Frequency	3.0×10^{-5} fps	
Velocity White Noise	2.89×10^{-3} fps	

RMS ERRORS FOLLOWING INITIALIZATION (no measurements)

Type	Radial	Downrange	Crossrange	Data Source
Position (ft)	2500	25000	2500	
Velocity (fps)	26.3	3.3	3.3	
RMS Clock Errors Phase 1200 ft Frequency 0.25 fps				Ref. 2

TABLE 3.3-3
TRUTH MODEL DATA BASE

ERROR SOURCE	STANDARD DEVIATION	DATA SOURCE
Measurement Noise		
Pseudo Range	12 ft	Ref. 4
Pseudo Range-Rate	0.05 fps	
Clock Process Errors		
Initial Phase	1130 ft	Refs. 3 and 4 and Chapter 2
Initial Frequency	0.142 fps	
Aging	3.86×10^{-6} ft/sec^2	
Random Frequency	20.2 fps	
Random Frequency-Rate	1.37 ft/sec^2	

Thrust Process	Axial Parameter Values			
	Radial	Down Range	Cross Range	
Time Constant (sec)	600	600	300	Chapter 2
RMS Initial Thrust (lb)	1.0	1.0	.33	
Process Noise (lb/$\sqrt{}$sec)	.0578	.0578	.0272	
RMS Initial Conditions				
Position (ft)	1040	11300	866	Ref. 4
Velocity (fps)	12.5	1.09	.094	

3.4 RESULTS AND ANALYSIS

Large initial errors are assumed at the start of observation for all cases under consideration. Truth model rms position errors are assumed to be approximately 1000 ft radial, 11,000 ft downrange, and 900 ft crossrange at initialization. Figure 3.4-1 displays error development for all three cases during the initial phase of the simulations. In all cases, the position errors have stabilized within 200 min (i.e., by the third visibility period). For Cases 1 and 3 where the first visibility period is short (18 min), rms downrange position errors grow to about 20,000 ft during the first visibility gap. The longer (36 min) initial visibility in Case 2 prevents rms downrange error from reaching 10,000 ft in the first gap.

Steady state stabilized position errors for the three cases are presented in Fig. 3.4-2. RMS downrange position errors predominate and have maximum values, near 4,000 ft, at the end of the nonvisibility propagation phase. RMS radial errors are less than 900 ft and actually begin to decline after about 45 min (one-half an orbit) of nonvisibility. Radial and downrange errors fall below 500 ft rms in all cases at some point within the satellite visibility periods. Crossrange rms position error remains consistently below 500 ft for the first and second cases, with oscillations at a period of one half the orbital period.* In Case 3, where the orbital geometry is such that the Shuttle orbit is always in plane with the single satellite orbit, no crossrange information is obtained. Crossrange rms error therefore demonstrates a slow but steady growth due to thrusting, in addition to its oscillation.

*Crossrange error has a period equal to the orbital period. The graphs demonstrate a frequency doubling effect because they concern rms statistics on the error and not actual error values.

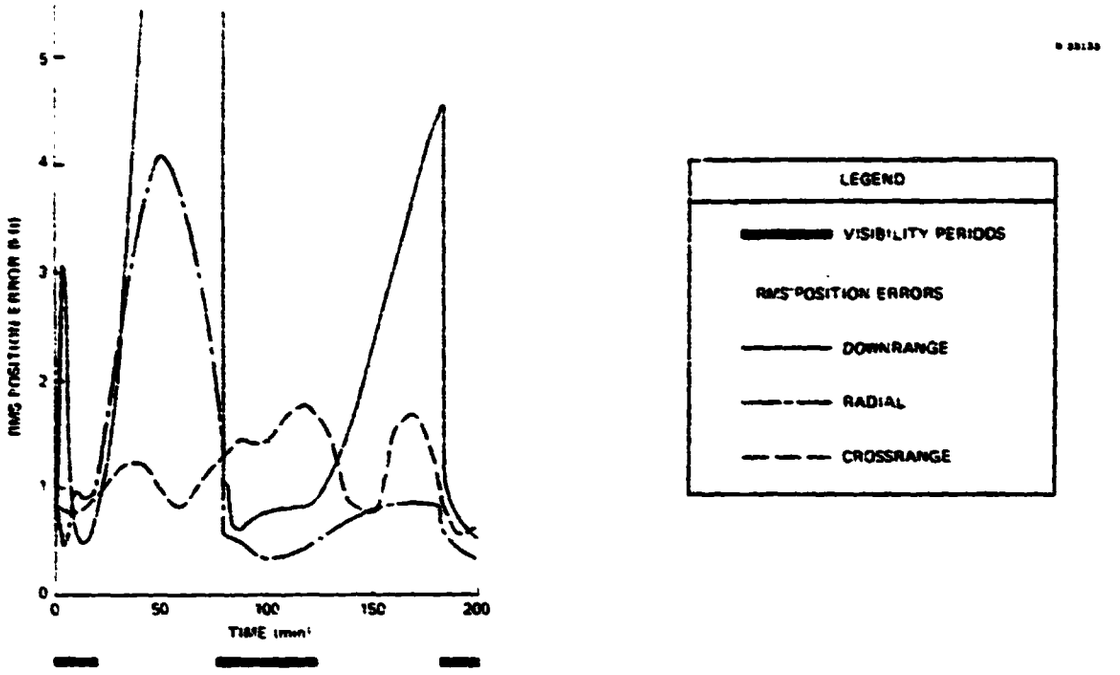

(a) Case 1

(b) Case 2

(c) Case 3

Figure 3.4-1 Initial Phase RMS Position Errors

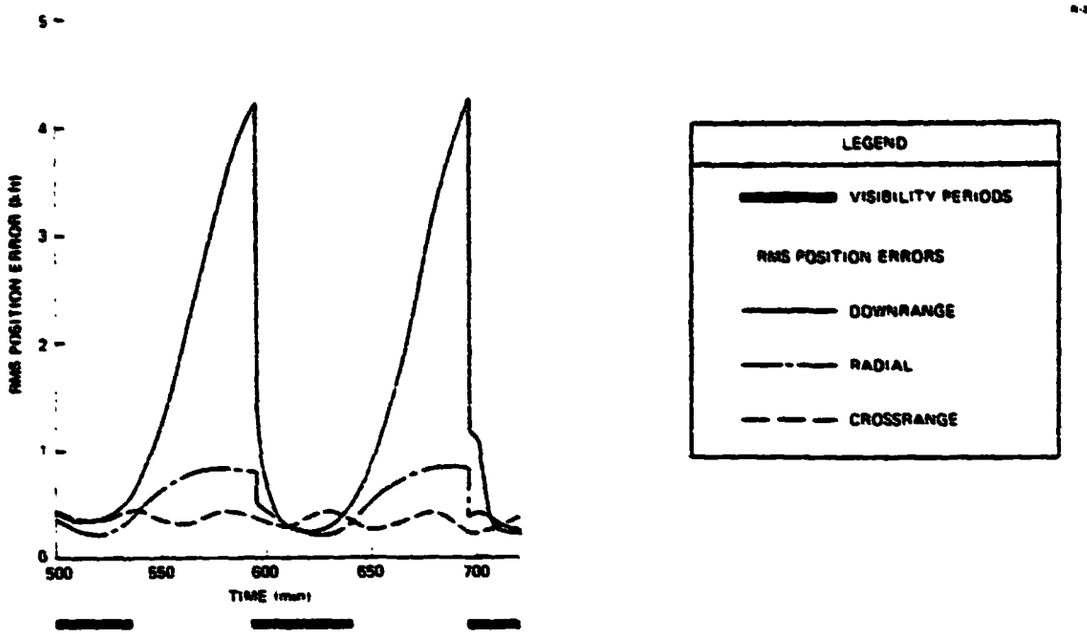

(a) Case 1

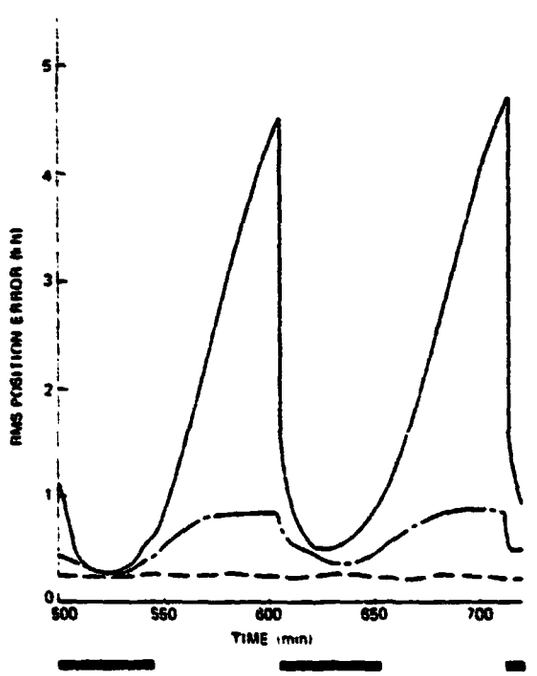

(b) Case 2

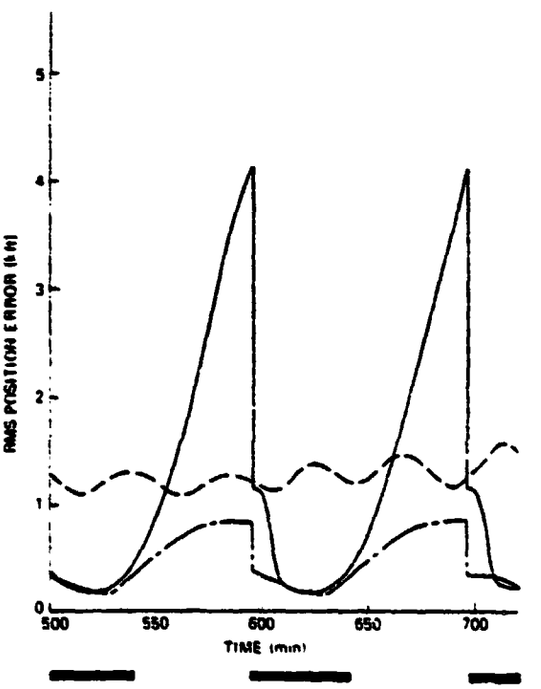

(c) Case 3

Figure 3.4-2 "Steady State" RMS Position Errors

Initial phase and steady state rms velocity errors for Case 1 appear in Fig. 3.4-3. The shape of these graphs when compared with Case 1 position errors in Figs. 3.4-1a and 3.4-2a illustrates important relationships between velocity and position error growth. Radial velocity and downrange position error curves display almost identical development. This correspondence is also observable when comparing the downrange velocity with radial position error curves. It can be noted that the major rms radial velocity errors peak at about 4.5 fps and all velocity errors drop to below 0.5 fps during part of the visibility segment.

Clock rms phase and frequency errors for Case 1 are presented in Figs. 3.4-4 and 3.4-5, respectively. The phase errors increase slowly to the 1300 ft rms range when the satellite is not visible and decrease to about 300 ft rms during visibility periods. Frequency error graphs demonstrate a quick rise to 0.34 fps rms when visibility is lost and lower values of 0.2 fps rms during visibility. Some of the abruptness of changes in frequency error as indicated by the truth model may be caused by the differences between the simplistic Shuttle filter two state clock and the truth model five state clock.

An important consideration of the single satellite navigation results is the source of the errors. Error budgets for Case 1 at a time near maximum error, and at a time during good visibility, identify the important error sources. Table 3.4-1 presents these error budgets. As can be seen, initial conditions contribute little to velocity or position errors at this stage, about 10 hours after initiation of the GPS filter. Measurement errors are also a minor consideration during both visibility and nonvisibility time periods. At 590 min, when propagated errors in position and velocity are large, the

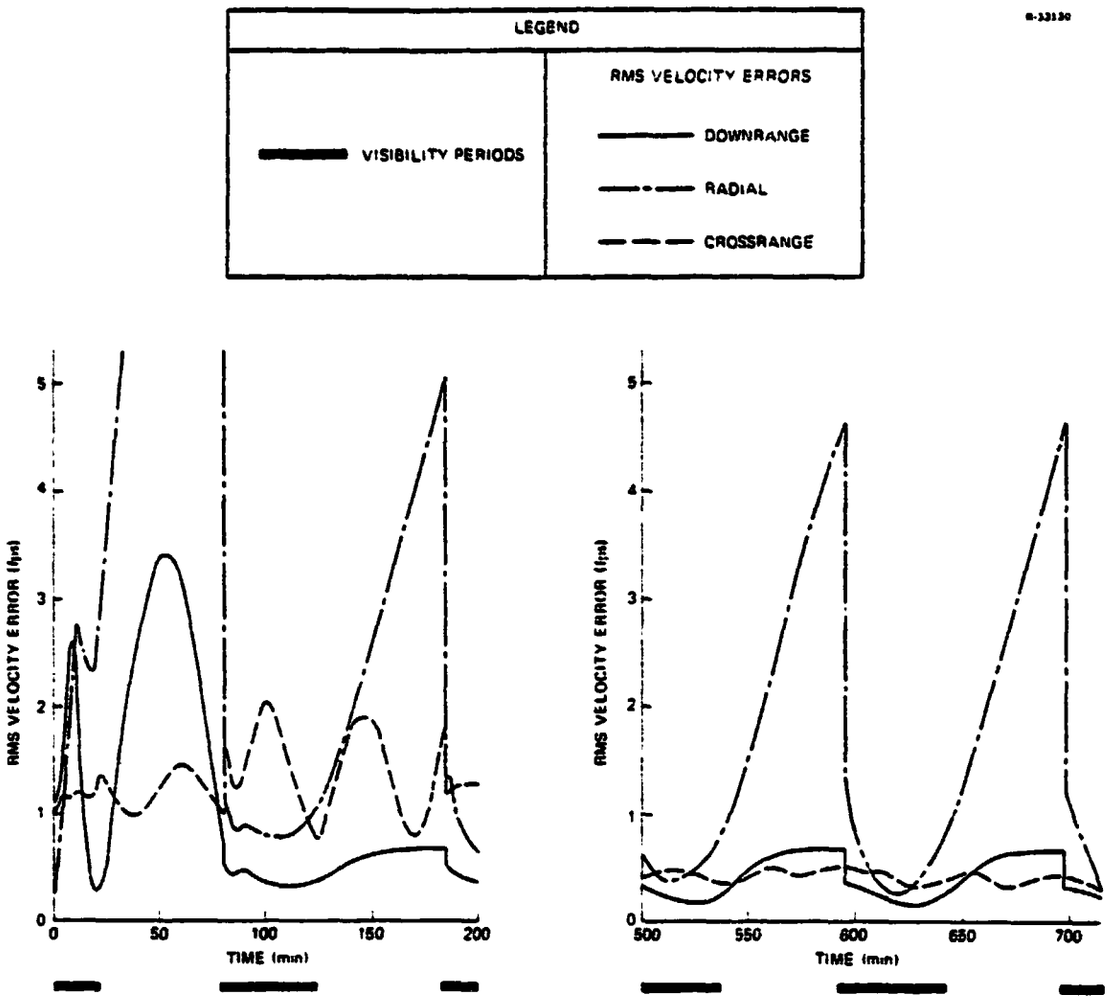

a) Initial Phase b) Steady State

Figure 3.4-3 RMS Velocity Errors (Case 1)

predominant influence is thrust. When the satellite is visible (610 min), thrust errors remain a major consideration, but clock errors become a dominant error contributor. An improvement in clock accuracy would cause a major improvement in position and velocity errors only during visibility periods when accuracy is already fairly good.

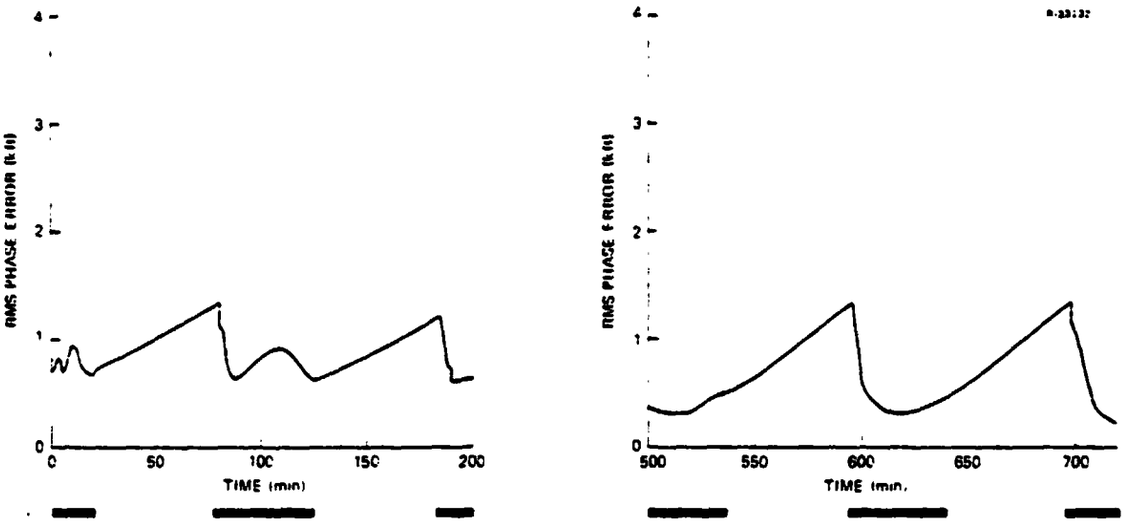

a) Initial Phase b) Steady State

Figure 3.4-4 Clock Phase Errors (Case 1)

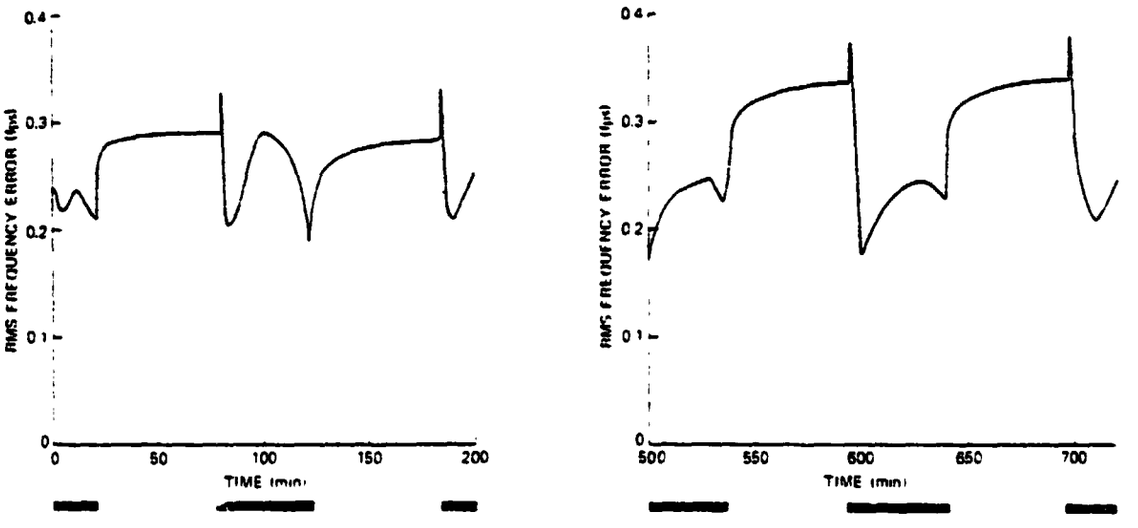

a) Initial Phase b) Steady State

Figure 3.4-5 Clock Frequency Errors (Case 1)

TABLE 3.4-1

ERROR BUDGETS FOR TRUTH MODEL 1 (AFTER SEVERAL ORBITS)

TIME	SOURCE	POSITION (ft)			VELOCITY (fps)			CLOCK	
		R	DR	CR	R	DR	CR	PHASE (ft)	FREQ (fps
590 min (near end of period of no visibility)	ICs	1	12	15	0.01	0.00	0.01	2	0.00
	Measure-ment	21	216	70	0.25	0.02	0.07	260	0.06
	Thrust	804	3970	253	4.32	0.64	0.27	798	0.16
	Clock	87	839	301	0.97	0.10	0.29	935	0.29
	RSS	809	4060	400	4.44	0.64	0.40	1260	0.33
			4160			4.50			
610 min (middle of period of visibility)	ICs	3	4	6	0.01	0.00	0.02	6	0.00
	Measurement	74	54	55	0.09	0.07	0.06	72	0.02
	Thrust	201	185	177	0.22	0.17	0.32	232	0.11
	Clock	245	229	226	0.31	0.23	0.35	258	0.19
	RSS	326	299	292	0.39	0.29	0.48	354	0.22
			530			0.68			

3.5 CONCLUSIONS

The key to accurate orbital navigation with a single GPS satellite is controlling error growth when the satellite is not visible. To some extent, this error growth can be controlled by limiting the duration of the visibility gaps themselves, through constraints on the vehicle orbit. A second method for controlling error growth is to reduce the size of Shuttle vehicle thrust errors due to venting, to gravitational modeling errors, and to other unmodeled or incorrectly modeled acceleration sources. Any other system improvement -- in GPS receiver clock quality or in measurement accuracy -- would do very little to reduce peak navigation errors during visibility gaps.

When a single GPS satellite is visible, navigation errors are reduced to levels comparable to TDRSS navigation errors as reported in Ref. 23. Visibility gaps with the two satellite TDRSS are relatively small, and no error growth characteristics comparable to those reported here are evident in the TDRSS results. However, it is not clear from the reference that the assumed level of unmodeled vehicle acceleration is as high in the TDRSS simulation results as is assumed in this GPS study.

In summary, a venting Shuttle vehicle may be navigated on orbit with only a single GPS satellite to useable accuracy provided that: (1) the orbit plane of the Shuttle does not coincide with that of the GPS satellite, and (2) exceptionally long visibility gaps, possible for some orbital geometries, are avoided.

4. POST BLACKOUT NAVIGATION WITH PHASE III GPS

A major benefit of carrying GPS user equipment aboard the Space Shuttle is the timely provision of accurate navigation data following reentry blackout. Chapter 2 of this report presents navigation accuracy results for Shuttle deorbit with the Phase I GPS constellation of six satellites that provides coverage for deorbit for about a six hour period each day. This chapter considers navigation following reentry blackout with the Phase III GPS constellation of 24 satellites. Comparable accuracy would be anticipated if the Phase III GPS constellation were reduced to as few as 18 satellites.

There are three additional changes from the scenario assumed for Chapter 2. First, a new Shuttle GPS antenna coverage pattern (provided by Rockwell International for the Space Shuttle GPS panel) is used here. Second, the effect on navigation accuracy of incorporating a ground GPS transmitter to augment the satellite constellation is evaluated. (Chapter 5 treats ground transmitters in considerably more detail.) Third, this study assesses the effect on navigation accuracy of three user clock (oscillator) types: the standard quartz clock, a quartz clock compensated for acceleration sensitivity, and a rubidium clock.

Section 4.1 documents a variety of background elements concerning deorbit navigation, principally those that are treated here in the same way as they were in past studies. The deorbit trajectory, the initial conditions on the navigation system, the quality of the IMU, the duration of reentry blackout, and the details of the navigation filter are all

discussed. Section 4.2 treats the issue of visibility, incorporating the new antenna patterns, the Phase III GPS constellation, and the matter of measurement scheduling. Section 4.3 deals with the three user clock types included in the study, and Section 4.4 presents the navigation results and conclusions.

4.1 BACKGROUND

Many of the elements used in this study of deorbit navigation were introduced and documented in Chapter 2 and in earlier work. Capsule descriptions of these elements are given here, and references to the earlier studies are provided.

The overall methodology of evaluating aided navigation errors is discussed in Chapter 4 of Ref. 3. In capsule, a covariance simulation of a suboptimal navigation filter is performed using a reference trajectory and an assumed measurement schedule. The filter gains are stored and used as input to a more comprehensive "truth model" covariance analysis program that produces the navigation accuracy results.

The Shuttle trajectory used here is taken from a JSC-supplied trajectory tape and is an OFT-1 trajectory with a landing at Edwards AFB runway 17. It is discussed in Chapter 2. The same conservative assumptions about the duration of reentry blackout are made here, blackout being assumed from 300 kft to 145 kft of altitude, a period of nearly 15 min. During this segment, no GPS measurements are assumed possible.

The navigation filter is an eight-state filter incorporating three position error states, three velocity error states, one clock phase error state, and one clock frequency error state. This filter is the minimum necessary to process

GPS pseudo range and pseudo range-rate measurements. The current Shuttle GPS Panel baseline navigation filter adds either three platform misalignments or three acceleration error states.

The IMU error model data base used in the truth model is the same as was used in the previous deorbit navigation studies, and corresponds to the IMU specifications for a period of time greater than 15 hrs since the last calibration. GPS measurement noises in both the navigation filter and in the truth model analysis program are 12 ft for pseudo range and 0.05 fps for pseudo range-rate.*

Since the Phase III GPS constellation offers generally excellent orbital visibility that results in excellent orbital navigation, the initial navigation errors in position, velocity and the clock upon entry into reentry blackout are assumed to be negligibly small. The initial IMU platform misalignments, however, are not small. As in past studies, these misalignments, observable on orbit only by comparison with star tracker outputs, are assumed to be 284 seconds of arc (1σ) about each of the three, space stable platform axes.

The GPS satellite ephemeris and clock errors treated by the NESA program (Ref. 3) in some previous studies are not included in the truth model analysis of this study. Phase III GPS satellites are assumed to carry cesium clocks resulting in uploaded ephemeris errors that produce pseudo range errors of five feet or less (1σ) to the user. These errors are negligible in the context of the current study.

*A pseudo range-rate accuracy of 0.05 fps assumes a doppler count of approximately one second.

4.2 VISIBILITY

There are three major issues affecting GPS satellite visibility from the shuttle during deorbit: 1) the receiving antenna gain pattern, 2) the GPS satellite constellation, and 3) the time relationship between the deorbit trajectory and the satellite constellation.

At the time this analysis was performed, the baseline the antenna configuration consisted of two antennas, one topside with its maximum gain or symmetry axis pointing "straight up" in Shuttle body coordinates, the other a bottom antenna with its symmetry axis pointing straight down. The bottom antenna has a conical gain pattern; that is, antenna gain is a function only of the angle between the direction to the signal source and the direction of the antenna symmetry axis. For visibility purposes. such an antenna is treated as it if can receive all signals originating from directions within a circular cone about the symmetry axis. The topside antenna is more complex. It has an elliptical visibility pattern in Shuttle coordinates. It is assumed to receive all signals originating inside of an elliptical cone about its symmetry axis.

Table 4.2-1 contains the limits of visibility for these two antennas in terms of half-cone angles for two differing sig-nal strength criteria. The primary zone, within which antenna gain will always exceed -1 dBiC (decibels with respect to an isotropic antenna for right hand circularly polarized signals), is the zone in which usable signal reception is confidently assumed. In the larger secondary zone, usable signals might well be received, but the confidence is lower. The primary zone is used in all of the results in this study.

TABLE 4.2-1

BASELINE ANTENNA VISIBILITY LIMITS
(HALF-CONE ANGLES IN DEGREES)

ANTENNA	PRIMARY ZONE -1 dBiC POINT		SECONDARY ZONE -4 dBiC POINT	
	FORE-AFT	LATERAL	FORE-AFT	LATERAL
Topside	80°	63°	89°	75°
Bottom	83°	83°	87°	87°

(See Figure 5.2-2, showing a slight variant of these specifications, for a better visualization).

The Phase III GPS satellite constellation of 24 satellites has eight satellites uniformly spaced 45 deg apart in each of three orbital planes inclined at 63 deg* to the equator and separated by 120 deg in right ascension. The satellites are in circular orbits at about four earth radii so they complete one orbit in just under 12 hrs and repeat their ground tracks once every sidereal day. Table 4.2-2 gives a set of right ascension and anomaly values for the 24 satellites at one instant.

Missing from Table 4.2-2 is the "satellite epoch," the absolute time at which given orbital elements are valid. While there are baseline values for this epoch, they mean little to the present study. Rather, what is important is the time relationship between the satellite constellation and the deorbit trajectory. As part of the preliminary visibility studies, this time relationship was varied in a search for the

*Recent changes put the inclination for Phase III at 55 deg and reduced the number of satellites to 18. Only minor differences in visibility, mostly improvement for this study, will result from the change in inclination.

TABLE 4.2-2

PHASE III GPS SATELLITE CONSTELLATION RIGHT ASCENSIONS AND INITIAL ANOMALIES

ORBIT PLANE 1 RIGHT ASCENSION 0 deg		ORBIT PLANE 2 RIGHT ASCENSION 120 deg		ORBIT PLANE 3 RIGHT ASCENSION 240 deg	
SATELLITE NUMBER	ANOMALY	SATELLITE NUMBER	ANOMALY	SATELLITE NUMBER	ANOMALY
1	0	9	15	17	30
2	45	10	60	18	75
3	90	11	105	19	120
4	135	12	150	20	165
5	180	13	195	21	210
6	225	14	240	22	255
7	270	15	285	23	300
8	315	16	330	24	345

poorest visibility following reentry blackout. Visibility with the 24 satellites of the Phase III constellation is generally excellent, and navigation accuracy given excellent visibility is quite adequate for any Orbiter vehicle (as opposed to payload) navigation purpose.

Figure 4.2-1 illustrates the worst case deorbit visibility encountered. As the key to the figures indicates, the thick line implies that a satellite is visible to the topside antenna (within the -1 dBiC gain pattern limit) while the thin line implies visibility to the bottomside antenna. Following the indicated blackout segment of the deorbit trajectory, only three Satellites, Numbers 3, 4, and 15, are visible to the Space Shuttle. A little more than two minutes after the blackout, several other satellites become visibile, due to an attitude change of the Orbiter.

An important fact illustrated by Fig. 4.2-1 is that almost all of the satellites visible after blackout (with the

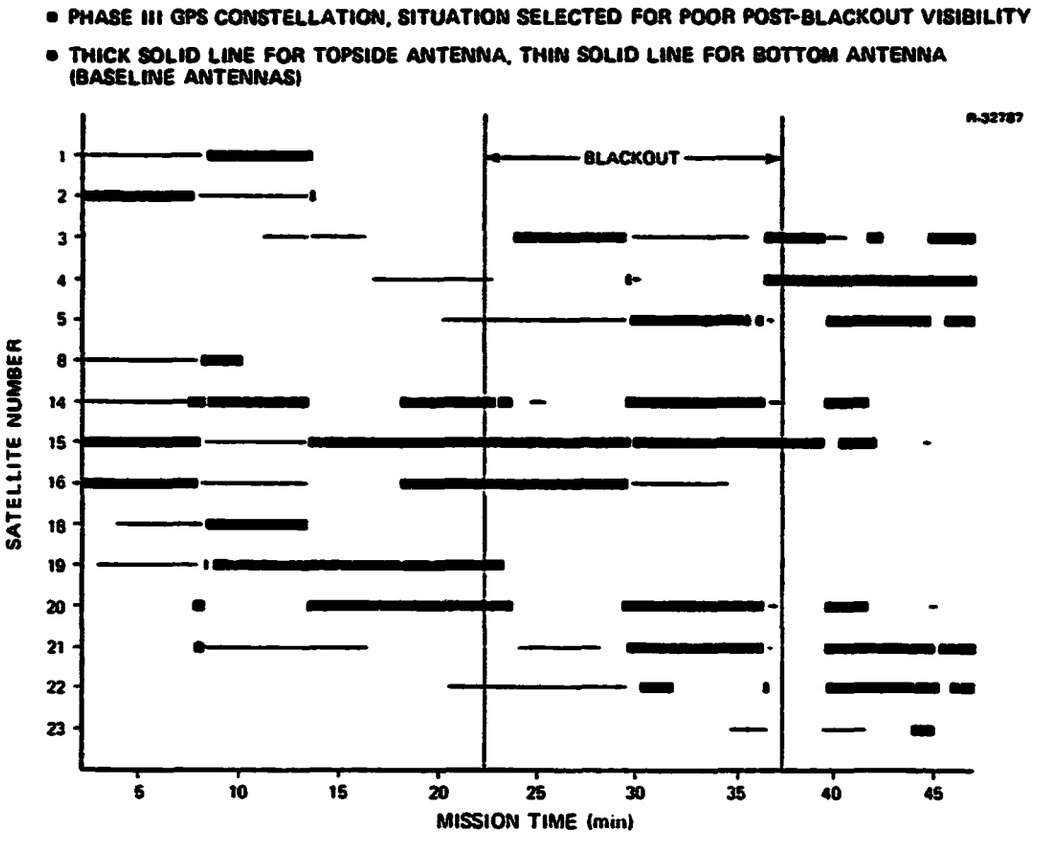

Figure 4.2-1 Worst Case Deorbit Visibility Following Blackout

exception in this case of Satellite 23) are visible for some time segment prior to blackout. This means that if the GPS receiver/processor has storage space for the precision ephemeris data on all 24 satellites (or a large enough subset of them), then precision GPS measurements may be taken after blackout without spending the 30 seconds on each satellite necessary to acquire the ephemeris data (see Chapter 6). This pre-acquisition of ephemeris data will require special consideration in the satellite selection algorithm, but will reduce the critical time-to-first fix following blackout by 60 sec for a two channel receiver, assuming four satellites are required for the fix.

From the visibility results shown in Fig. 4.2-1, a measurement schedule was prepared that takes into account the time to acquire and track the signal from each satellite, omitting the 30 sec ephemeris data acquisition time. Figure 4.2-2 shows this measurement schedule in terms of satellite availability. Measurements were scheduled at 6 sec intervals to the available satellites.

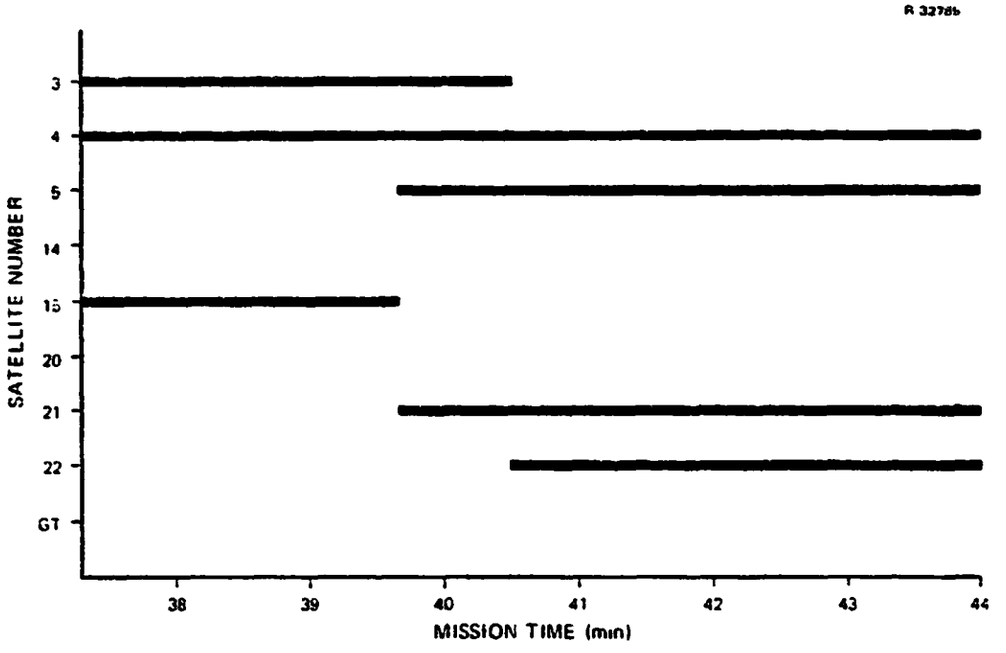

Figure 4.2-2 Measurement Schedule After Blackout (Worst Case Visibility)

To evaluate performance sensitivity to Shuttle antenna coverage, satellite availabilities for a reduced antenna coverage situation are also used to generate performance results. Figure 4.2-3 shows these reduced coverage availabilities, which correspond to antennas with conical viewing limits of 55 deg half angles. With reduced coverage, only two satellites are available immediately following blackout.

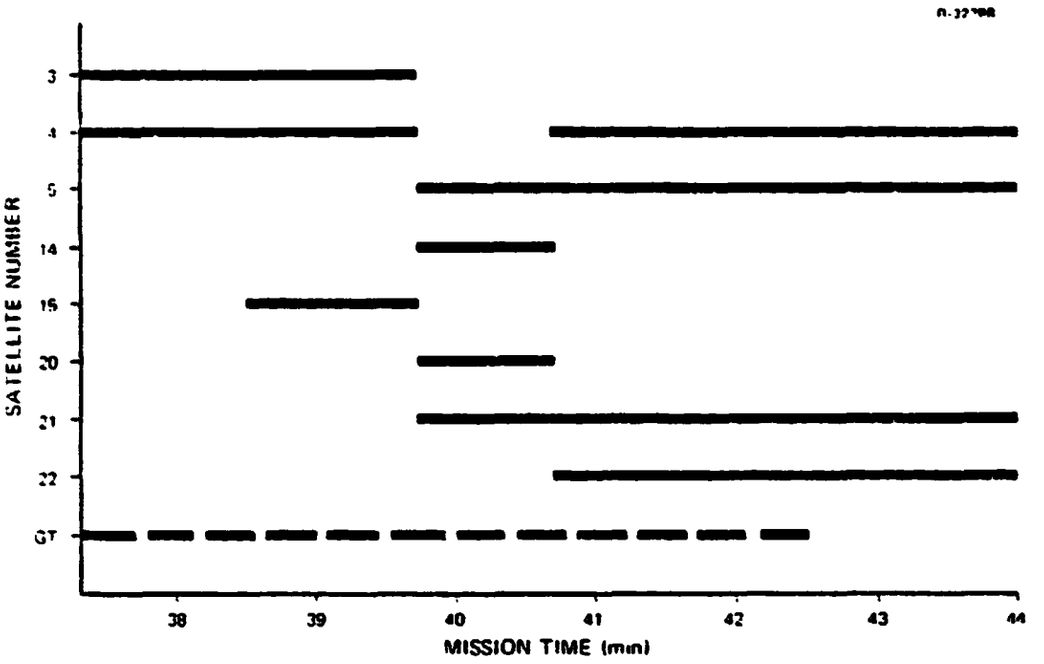

Figure 4.2-3 Reduced Coverage Satellite Availability After Blackout (Including Ground Transmitter)

Because of the low coverage with reduced visibility, the possibility of using a ground GPS transmitter is considered in some cases. Figure 4.2-3 also shows when the ground transmitter (assumed located under the Orbiter trajectory at San Simeon) would be available. No antenna limitations on ground transmitter visibility are assumed, due to the potentially high power of the ground transmitter; only line of sight limitations from the transmitter to the Orbiter are taken.

4.3 CLOCK QUALITY

Three different clock types are included in this study. Figure 4.3-1 illustrates the quality of two of them -- the ordinary (uncompensated) quartz clock and the rubidium clock -- in

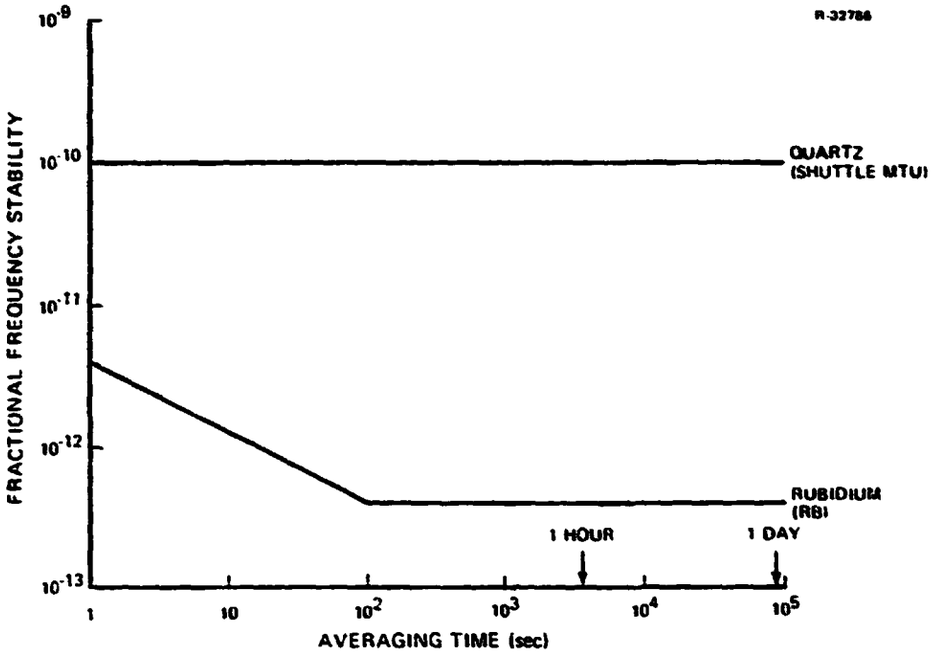

Figure 4.3-1 Quartz and Rubidium Oscillator Quality

an unaccelerated environment. Clock modeling is discussed in Chapter 4 of Ref. 3. The same five-state clock model (with different data bases) is used to simulate both the quartz and the rubidium oscillators.

An additional source of clock error arises from acceleration sensitivity. Ref. 6 discusses such sensitivity. A quartz crystal has an axis of sensitivity to non-gravitational acceleration, and the frequency error produced by the oscillator is typically 1 part in 10^9 per g of acceleration along the sensitive axis. Accelerations normal to the sensitive axis produce little or no effect.

Rubidium clocks depend for long term (10 sec and up) stability on the atomic rubidium standard, but they use a quartz crystal oscillator for short term (1 sec and less) stability.

The rubidium cell is put into an outer loop about the quartz crystal, and the time constant of this loop (from 1 to 10 sec) determines the intermediate term stabiliity. The rubidium cell is not subject to appreciable acceleration sensitivity, being at least two orders of magnitude less sensitive than is the quartz crystal. Tracking stability of the GPS receiver depends upon short term stability of the oscillator, so quartz and rubidium clocks are equal in this respect. But the ability of a sequential receiver to "tie together" measurements at different times depends on the long term stability of the oscillator, so rubidium oscillators provide an improvement over quartz oscillators in this respect. In particular, a rubidium oscillator can maintain a good time reference through the blackout period of 15 min, so that only three satellites are necessary to obtain a good "fix" after blackout.

Much of the error that a quartz crystal clock would acquire during the blackout period would arise from the acceleration sensitivity. As Ref. 24 points out, this sensitivity may be calibrated and accounted for by mounting an accelerometer with the crystal and building a compensation control system about the oscillator. Figure 4.3-2 diagrams such a control system. Alternately, for the Space Shuttle, acceleration compensation could be accomplished in the GPS receiver/processor software using acceleration and attitude inputs from the IMU's.

The quality of such compensation is potentially quite good. Figure 4.3-3 shows experimental results reported in Ref. 24, while Figure 4.3-4 indicates the range of frequencies over which the compensation is valid (the primary limitation being the accelerometer and not the math model). For navigation purposes, as previously remarked, it is the long term (low frequency) stability that is important. Because of this potential for improving the quartz clock, the third type of clock considered here is an acceleration compensated quartz oscillator.

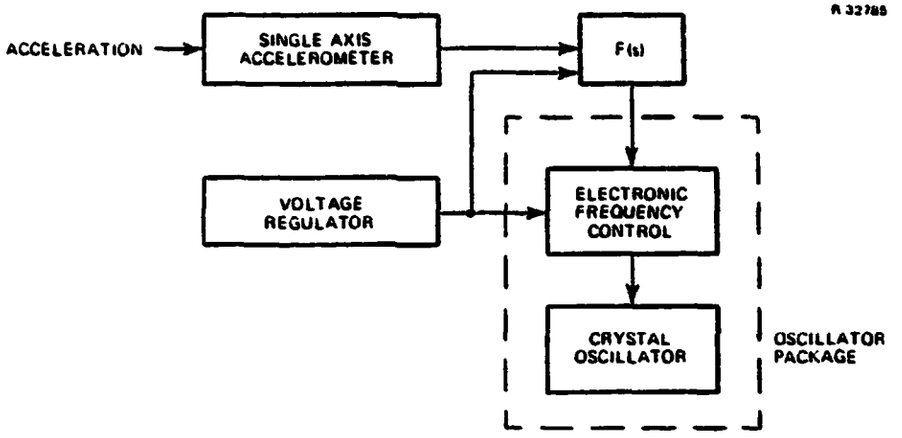

Figure 4.3-2 Acceleration Compensated Quartz Oscillator

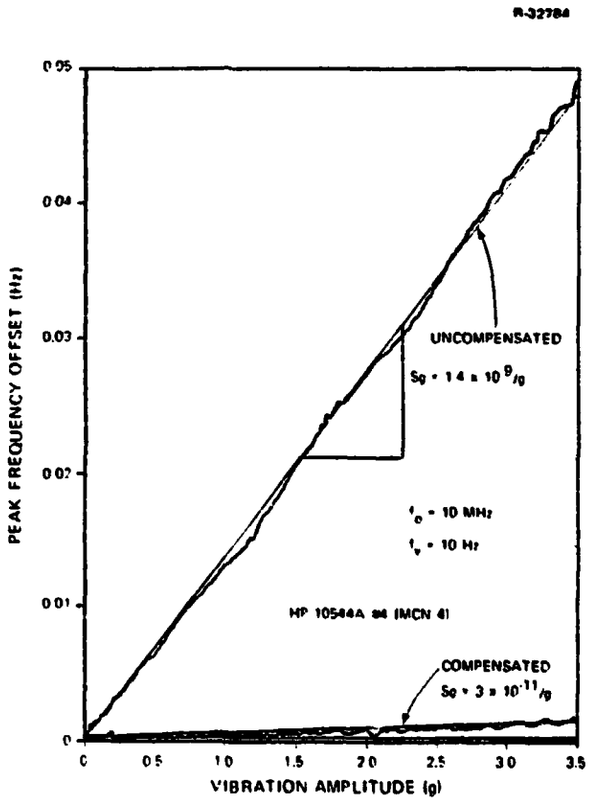

Figure 4.3-3 Acceleration Compensation Test Result (Ref. 24)

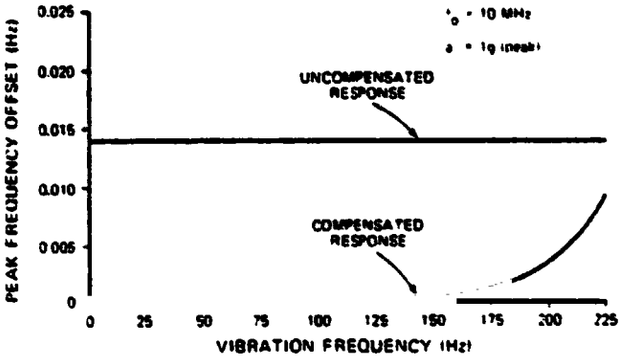

Figure 4.3-4 Acceleration Compensation Frequency Dependence (Ref. 24)

A frequency error of one part in 10^9 is equivalent to a pseudo range-rate error of about 1 ft/sec (since the speed of light is about 10^9 ft/sec). Since acceleration levels on the Orbiter during deorbit are limited to three g's or less, and since compensation is good to 2%, the remaining acceleration sensitivity of a compensated quartz or rubidium oscillator for navigation purposes may be ignored.

4.4 POST BLACKOUT NAVIGATION RESULTS

The combination filter covariance/truth model covariance analysis programs were run on several different post-blackout scenarios varying the post-blackout GPS transmitter availability and the user clock type. Fortunately, the results may be summarized without having to look in detail at the case conditions and output covariances versus time for each scenario. A series of tables will suffice.

Table 4.4-1 shows the clock errors after blackout. These errors change very little in the time period following

TABLE 4.4-1
POST-BLACKOUT CLOCK ERRORS*

RMS CLOCK ERROR	QUARTZ	COMPENSATED QUARTZ	Rb
PHASE (FT)	900 (40)	125 (30)	8
FREQUENCY (FT/SEC)	1.3 (0.25)	0.25 (0.20)	0.005

blackout until the fourth emitter (satellite or ground transmitter) is acquired, whereupon the filter obtains the information necessary to correct the relatively large errors of the quartz oscillators, and the values in parentheses are obtained. This table shows that the dominant portion of the quartz clock errors accumulated during the blackout are due to acceleration sensitivity of the clock, for the only difference between the quartz clock and the compensated quartz clock is the acceleration sensitivity.

Table 4.4-2 is an error budget for Shuttle position and velocity errors following the blackout period before any GPS measurements are taken. The budget assumes that an ordinary quartz oscillator is used in taking GPS measurements prior to the blackout period. If a compensated quartz or rubidium oscillator were used prior to blackout, the budget line items for the clock and for the clock acceleration term would change to smaller values, but the totals would be unaffected, since clock errors do not contribute significantly to post-blackout navigation error until after GPS measurements are processed by the filter.

TABLE 4.4-2
POST-BLACKOUT ERROR BUDGET PRIOR TO MEASUREMENTS

ERROR GROUP	RMS ERRORS					
	POSITION (FT)			VELOCITY (FPS)		
	DR	CR	R	DR	CR	R
Measurement Noise*	366	252	670	0.33	0.12	1.28
Platform Alignment†	3018	9073	12030	14.60	24.58	35.28
IMU	1305	1933	2600	4.41	5.74	8.11
Clock*	103	104	319	0.11	0.07	0.59
Clock Acceleration*	10	10	30	0.01	0.01	0.06
RSS	3310	9280	12330	15.26	25.24	36.19
Vector RSS		15790			46.69	

*These errors have propagated from pre-blackout conditions.

†Platform alignment error is initial value. Subsequent growth during blackout is included in IMU error group.

In fact, the only significant contributors to post-blackout navigation errors (before GPS measurements are taken) are the initial IMU platform alignments going into blackout and the IMU component (gyro and accelerometer) errors accumulated during blackout. Gyro errors during blackout increase the IMU platform misalignment errors, but the budgeted navigation errors due to platform misalignments refer to those errors due only to the initial values of the misalignments, with the errors due to subsequent growth being lumped into the IMU entry.

Tables 4.4-3 and 4.4-4 show how navigation errors decrease after the acquisition of independent emitters following blackout. In this general scenario, the navigation error is not a strong function of time, per se, or of the number of

TABLE 4.4-3

POST-BLACKOUT NAVIGATION ERRORS AFTER ACQUISITION OF 1ST AND 2ND EMITTERS

RMS VECTOR ERROR	BEFORE MEASUREMENT	AFTER MEASUREMENTS TO 1 EMITTER	AFTER MEASUREMENTS TO 2 EMITTERS
Position (ft)	16,000	13,000	5,000
Velocity (ft/sec)	47	40	14

TABLE 4.4-4

POST-BLACKOUT NAVIGATION ERRORS AFTER ACQUISITION OF 3RD AND 4TH EMITTERS

CLOCK TYPE	RMS VECTOR ERROR	AFTER MEASUREMENTS TO	AFTER MEASUREMENTS TO
QUARTZ	Position (ft)	1500	60
	Velocity (ft/sec)	2.0	1.5
COMPENSATED QUARTZ	Position (ft)	180	40
	Velocity (ft/sec)	1.3	1.3
Rb	Position (ft)	30	25
	Velocity (ft/sec)	1.0	1.0

measurements (several measurements to one emitter being possible), but is primarily a function of the number of different emitters to which measurements have been made. The results from which Table 4.4-3 was compiled show, by implication, that there is no substantial variation in navigation error with user clock type when only one or two emitters have been acquired. In Table 4.4-4, on the other hand, the clock type is explicit, and variations in navigation error are noted. The clock type is especially important when three emitters have been acquired. This is to be expected. Without accurate time information

(the "normal" case) it takes four GPS satellites to determine a user fix. With accurate time information, three satellites suffice.

The only time (in this limited study) when an accurate user clock is important is when only three emitters are available following blackout. In the same context, the only time a ground GPS transmitter is useful is when three satellites are available and an uncompensated quartz oscillator is used, or when two satellites are available and a compensated quartz or rubidium oscillator is used.

Table 4.4-5 is an error budget following acquisition of the third GPS emitter. It shows the dominance of the clock errors when an uncompensated quartz clock is used. Table 4.4-6 is an error budget following acquisition of the fourth emitter. After the fourth emitter has been acquired, position errors are reduced to small values, but velocity errors are not correspondingly small. The dominant source of the velocity errors is platform misalignment. (The IMU entry is also mostly platform misalignment growth during blackout.) The eight-state baseline navigation filter does not recognize platform alignment errors and thus can do little to mitigate their effects. A significant reduction in post-blackout velocity errors would require the addition of three platform misalignment states to the navigation filter.* Additionally, a compensated quartz or rubidium clock would help. Measurement noise contributions to velocity errors will fall as the number of measurements increases, while the other error contributions will not.

*These misalignment states have subsequently been incorporated into the baseline filter design.

TABLE 4.4-5

ERROR BUDGET FOLLOWING ACQUISITION OF THE 3RD EMITTER
(UNCOMPENSATED QUARTZ OSCILLATOR)

ERROR GROUP	RMS ERRORS					
	POSITION (FT)			VELOCITY (FPS)		
	DR	CR	R	DR	CR	R
Measurement Noise	25	29	39	0.41	0.55	0.25
Platform Alignment	3	2	1	0.40	0.32	0.06
IMU	1	0	0	0.13	0.10	0.03
Clock	83	100	139	0.15	0.15	0.23
Clock Acceleration	633	769	1065	0.80	0.76	1.41
RSS	639	766	1074	1.00	1.01	1.45
Vector Rss		1470			2.04	

TABLE 4.4-6

ERROR BUDGET FOLLOWING ACQUISITION OF THE 4TH EMITTER
(UNCOMPENSATED QUARTZ OSCILLATOR)

ERROR GROUP	RMS ERRORS					
	POSITION (FT)			VELOCITY (FPS)		
	DR	CR	R	DR	CR	R
Measurement Noise	19	11	29	0.60	0.11	0.34
Platform Alignment	8	3	15	0.84	0.39	0.25
IMU	2	1	0	0.24	0.11	0.08
Clock	3	1	6	0.16	0.12	0.24
Clock Acceleration	9	3	44	0.49	0.37	0.54
RSS	22	12	53	1.19	0.58	0.73
Vector RSS		58			1.51	

5. GPS GROUND TRANSMITTERS FOR SPACE SHUTTLE SUPPORT

During ascent and entry of the Space Shuttle, GPS satellite visibility may be inadequate to support accurate navigation. Depending upon the type of clock used in the GPS receiver, either three satellites (for an atomic clock) or four satellites (for a quartz crystal clock) must be in view of the Orbiter antennas to accurately navigate during these dynamic flight phases. Before the Phase III GPS constellation reaches initial operational capability (18 satellites) in 1986* there will at most times be fewer than three satellites visible to the Orbiter. Even after the Phase III constellation is complete, the external fuel tank will block the downward GPS antennas on the Orbiter during ascent. Since the Orbiter flies "upside down" during ascent, the fuel tank may severely impact satellite visibility.

This chapter examines some of the issues involved in using GPS ground transmitters to augment the satellite constellation and support Shuttle navigation during ascent and entry. Section 5.1 briefly examines some of the issues involved, while Sections 5.2 and 5.3 present results for the entry and ascent phases, respectively. Section 5.4 contains a summary of conclusions regarding the use of ground transmitters.

5.1 GROUND TRANSMITTER ISSUES

A wide range of design, performance, and support issues would need resolution to establish the feasibility of GPS ground

*Restructuring of the GPS program may result in a final Phase III constellation of 18 satellites, to be operational in 1987.

transmitters as an aid to the Space Shuttle during ascent and entry. This report addresses a subset of those issues regarding the use of the satellite signals, a subset that comes generally under the headings of signal availability, signal usability, and navigation accuracy. In particular, the following questions are examined:

- How many ground transmitters would be required, and where would they best be placed?
- What demands would ground transmitters place on the antenna management and tracking loop functions of the Orbiter GPS receiver processor assembly (R/PA)?
- What Orbiter navigation accuracy could be expected to result from the use of ground transmitters?

The first question, that of number and placement of ground transmitters, depends, in turn, on a range of further issues, including:

- fixed versus mobile transmitters
- the range (variety) of ascent or entry trajectories to be accommodated
- the type and quality of the R/PA clock
- the GPS antenna coverage of the Orbiter
- the interim GPS satellite constellation(s)
- the attitude dynamics of the Orbiter

The number of transmitters required might also be expected to be related to the navigation accuracy demanded of the system, but the actual relationship here is a simple one: depending on the type of clock in the R/PA, if three or four signals are available, navigation accuracy will be good; if fewer than three

or four signals are available, then (GPS-based) navigation accuracy will be less than adequate unless the navigation system Kalman filter can take advantage of changing transmitter-to-Orbiter geometry. So the question of number and placement of ground transmitters generally is resolved on matters of signal availability (visibility) alone.

The second question, that of the demands a ground transmitter signal places on the receiver, is partly a matter of visibility -- Is the signal available to one antenna long enough to be acquired and tracked? -- is partly a matter of signal dynamics -- Can the tracking loops follow the signal dynamics, especially the geometrical range acceleration arising from high Orbiter velocities relative to nearby ground transmitters? -- and is partly a matter of signal strength relationships -- Can the ground transmitter signal strength be selected so as to be usable over the large relative variation in range to the Orbiter and yet not interfere with other ground transmitters or with the satellite signals? These questions may be answered with visibility charts, range dynamics computations, and range ratio computations.

The third question, that of expected accuracy, is not addressable with just the visibility analysis tools useful for the other issues considered here. The source of the GPS signals has far less impact on Shuttle accuracy than does the number of such signals, so previous results for post-blackout entry accuracy will give a good idea of the accuracy to be expected in this flight phase if GPS ground transmitters were substituted for satellites. Only limited performance analysis has been done for the ascent phase, so no comparable accuracy estimates are presented here for that phase.

5.2 ENTRY

In investigating the use of ground transmitters to support entry, it would be desirable to have a full range of entry trajectories available so that variations in signal availability could be considered. Unfortunately, only one entry trajectory tape, for a landing at Edwards Air Force Base (EAFB) (the tape used in all previous deorbit studies and discussed in Section 2.2.2), was available for this study. The problem of signal availability is determined by the relative locations of the ground transmitters to the trajectory, so by assuming numerous ground transmitter sites, one trajectory can be made to show a wide variety of situations. Figure 5.2-1 is

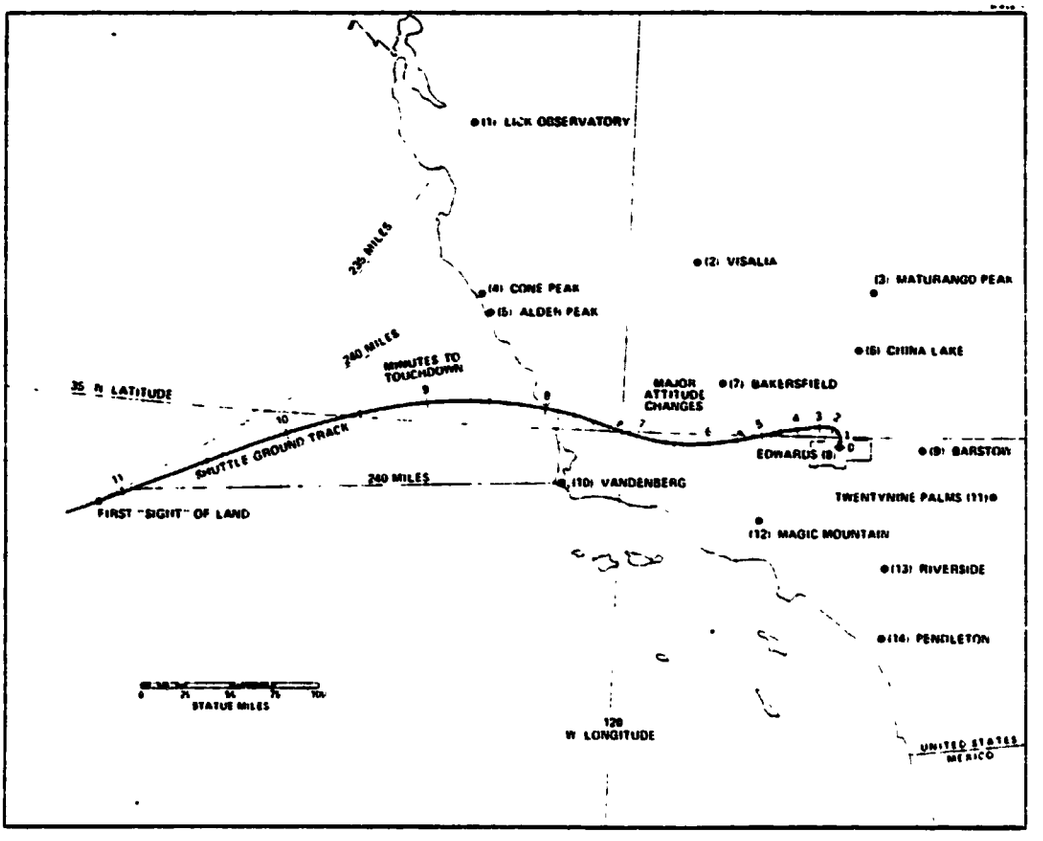

Figure 5.2-1 Deorbit Ground Transmitter Locations

a map showing the ground track of the trajectory utilized for this study and the locations of the 14 ground transmitter sites simulated. The numbers labeling the tic marks along the trajectory ground track are minutes to touchdown.

Due to the mountainous terrain in the wide vicinity of the landing site, high elevation locations were often chosen for the ground transmitters to avoid the question of terrain blockage of visibility. Some of the exact locations assumed might not be practical, but equivalent, practical locations are almost surely available. In all cases in this entry study it is assumed that the Orbiter is visible to the ground transmitter if the Orbiter is over five degrees above the local horizon at the transmitter. This does not, however, necessarily imply signal availability. In addition to the Orbiter being visible to the ground transmitter, the ground transmitter must be within the beamwidth of the Orbiter GPS antennas in order for the signal to be received.

Figure 5.2-2 illustrates the antenna coverage assumed for the Orbiter for the entry study (Ref. 25). This is approximately the same coverage assumed for the deorbit analysis in Chapter 4. (The ascent study, done later, uses different antenna patterns resulting from model tests at JSC. Test results were not available when the entry study was done.) For ground transmitter visibility during entry, it is the bottom antenna that is of primary importance. Note that the bottom antenna pattern assumed is an axisymmetrical "conical" pattern, while the top antenna pattern is an asymmetrical "elliptical" pattern.

The maximum range of visibility from a ground transmitter to the Orbiter is about 240 nm, and Fig 5.2-1 illustrates the point of first contact for three of the ground

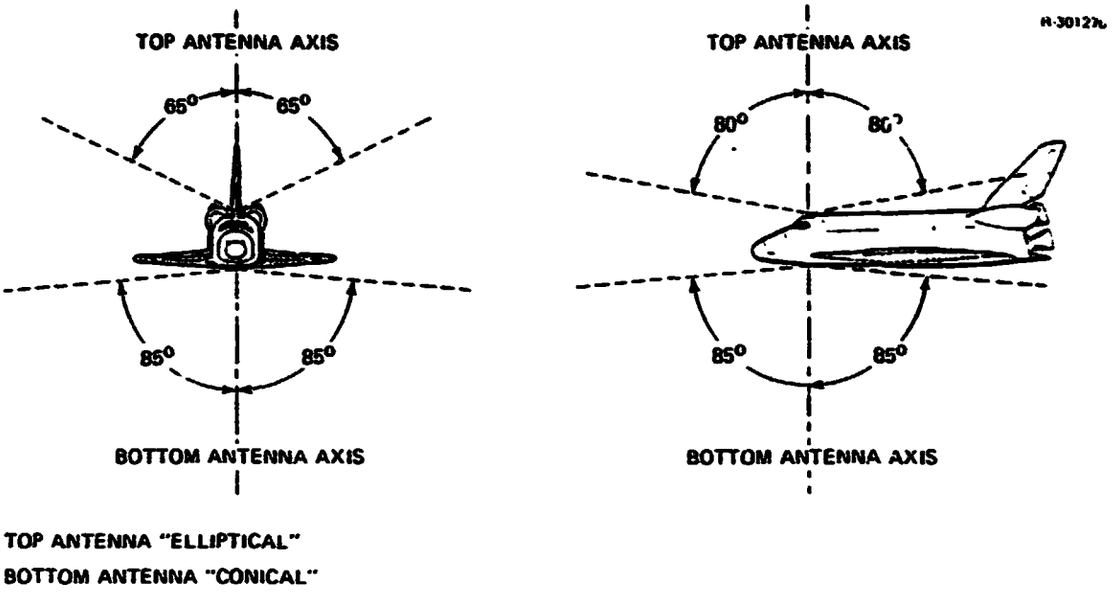

Figure 5.2-2 Antenna Coverage Assumed for Entry (-1 dBi Gain Limits)

transmitters. This point occurs following the (assumed) exit of down-looking L-band communications blackout. (GPS signals as well as TACAN signals are in the L-band.) Only the final 12 min or so of the trajectory prior to landing need be considered for ground transmitter aiding.

Figure 5.2-3 summarizes the visibility situation for all 14 ground transmitter sites. As the key describes, the narrow lines indicate periods when the Orbiter is below the five deg elevation minimum to be visible from the ground transmitter. During the wide portions of the lines, the Orbiter is visible to the ground transmitter, but the ground transmitter is not always visible to the Orbiter GPS antennas. During the unshaded portions of the wide lines, the ground transmitter is not visible to either Orbiter GPS antenna. During the solid portions of the wide lines, the ground transmitter is visible to the bottom antenna, and during the cross hatched portions of the line, it is visible to the top antenna.

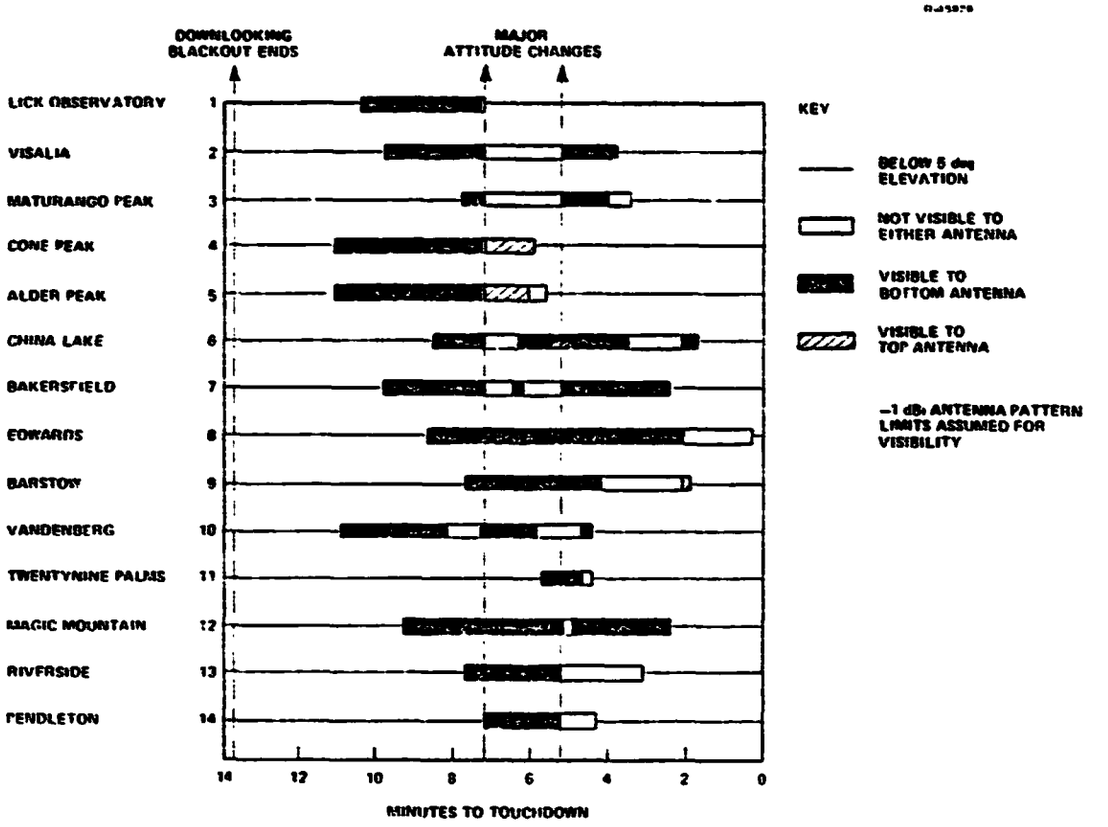

Figure 5.2-3 Entry Visibility of Ground Transmitters

In preparation for landing, the Orbiter undergoes two sharp attitude changes, noted in Fig. 5.2-3, that produce numerous simultaneous changes in the ground transmitter visibilities. In general, these attitude changes are not totally predictable as to timing or amount, but the figure illustrates the type of unpredictable visibility situation that must be dealt with during a typical entry.

All of the 14 ground transmitters would not be needed to support entry, as only three or four signals are necessary for accurate navigation. If no signals were available from the GPS satellite constellation, then three to five ground

transmitters would be necessary for the specific trajectory studied, depending on the receiver clock and on the period of coverage desired. Generally speaking, a period of about two minutes of simultaneous availability of three signals as early in the trajectory as possible would provide most of the potential benefit to be derived from ground transmitters (assuming an atomic clock in the R/PA). The sites at Cone Peak, Edwards, and Magic Mountain would provide such signal availability.

If a range of entry trajectories were to be considered, and fixed ground transmitters were to be used, then, of course, more than three would be required. If the entry trajectory were known sufficiently in advance, the use of mobile ground transmitters could be considered. There are two ways to use mobile transmitters. One involves locating the mobile transmitter and synchronizing its clock by reference to the GPS satellite system. During GPS Phase II, this might take the better part of a day to accomplish, as the six (or fewer) satellites are not visible to ground locations except for a period of a few hours a day. A second way to set up mobile transmitters would be to locate them at previously surveyed sites and depend on atomic time standard accuracy to maintain clock synchronization to each other (and to the satellite system, if necessary). In this mode, mobile transmitters might be set up in a period of a few hours. In either case, mobile transmitters might not be able to support contingency entries.

A second vantage point on ground transmitter visibility is provided in Table 5.2-1. This table ignores the effect of the Orbiter antennas in limiting visibility of the ground transmitters and assumes the transmitters are visible if the Orbiter is above five degrees elevation when viewed from the transmitter. The duration of the visibility period is noted for each of the 14 ground transmitter sites, as is the peak

TABLE 5.2-1

GROUND TRANSMITTER VISIBILITY RANGES
(ANTENNA EFFECTS NOT INCLUDED)

GROUND TRANSMITTER NO.	LOCATION	VISIBILITY DURATION (MIN)	PEAK ELEVATION (DEG)	AZIMUTH VARIATION (DEG)
1	LICK OBSERVATORY	3.2	8.0	64
2	VISALIA	6.0	11.5	103
3	MATURANGO PEAK	4.4	7.0	43
4	CONE PEAK	5.2	20.8	124
5	ALDER PEAK	5.5	25.2	127
6	CHINA LAKE	5.0	11.9	49
7	BAKERSFIELD	7.4	28.5	156
8	EDWARDS	8.4	27.4	96
9	BARSTOW	5.8	9.0	13
10	VANDENBERG	6.5	30.1	170
11	TWENTYNINE PALMS	1.3	5.2	6
12	MAGIC MOUNTAIN	6.9	19.6	77
13	RIVERSIDE	4.6	7.8	38
14	PENDLETON	2.9	6.0	27

elevation of the Orbiter, and its variation in azimuth as viewed from the transmitter. The elevation and azimuth variation values are related to navigation accuracy. In particular, accuracy in the vertical direction depends on the elevation angles, higher angles producing better accuracy.

Variations in azimuth during the viewing period can improve overall accuracy. Since the ground transmitter observations are assumed to be processed by a Kalman filter that has access to IMU-sensed velocity information, the cumulative effect of two measurements in different directions is much stronger than two measurements in a single direction. That is, one ground transmitter viewed from two different directions during the trajectory has about the same effect as two independent ground transmitters in different directions. This

aspect of navigation accuracy with ground transmitters was not studied explicitly, but it might be concluded that even fewer than three ground transmitters could support navigation during entry. Fewer than three transmitters would not support accurate navigation at the earliest opportunity, however, for to be effective with less than three transmitters requires waiting until substantial changes in the Orbiter-to-transmitter geometry have occurred.

Accuracy results from the Chapter 4 study on this same trajectory are appropriate for the first establishment of accurate navigation following entry blackout. Table 5.2-2 (a repeat of Table 4.4-3 and 4.4-4) summarizes these results. Following the blackout, typical navigation errors would be 16,000 ft. and 47 ft/sec. Regardless of the type of clock used in the R/PA, these errors will be reduced when the first two (independent) GPS signals are processed, as the first part of the table shows. The results after processing the third and fourth independent GPS signals depend on the type of clock in the R/PA, as the second part of the table shows. The acceleration-compensated quartz clock refers to a quartz crystal oscillator which is compensated by special added hardware (or

TABLE 5.2-2

POST-BLACKOUT NAVIGATION ERRORS
FOLLOWING ACQUISITION OF
FIRST AND SECOND EMITTERS

RMS VECTOR ERROR	BEFORE MEASUREMENT	AFTER MEASUREMENTS TO 1 EMITTER	AFTER MEASUREMENTS TO 2 EMITTERS
Position (ft)	16,000	13,000	5,000
Velocity (ft/sec)	47	40	14

TABLE 5.2-2 (Cont.)
(THIRD AND FOURTH EMITTERS)

CLOCK TYPE	RMS VECTOR ERROR	AFTER MEASUREMENTS TO 3 EMITTERS	AFTER MEASUREMENTS TO 4 EMITTERS
QUARTZ	POSITION (FT)	1500	60
	VELOCITY (FT/SEC)	2.0	1.5
QUARTZ+	POSITION (FT)	180	40
	VELOCITY (FT/SEC)	1.3	1.3
Rb	POSITION (FT)	30	25
	VELOCITY (FT/SEC)	1.0	1.0

through R/PA software) so as to reduce its acceleration sensitivity by about an order of magnitude. The "Rb" heading refers to a rubidium time standard. Such an atomic clock has a negligible acceleration sensitivity for navigation purposes. This table illustrates that accurate navigation will be achieved when the third or fourth independent signal is processed, depending on the type of clock in the R/PA.

One more result of the entry ground transmitter study is given in Table 5.2-3, where the ratios of the minimum and maximum ranges from the Orbiter to the various ground transmitters during the periods of potential visibility are expressed in terms of an equivalent power ratio ($20 \log_{10}$ rmax/rmin). The various C/A codes used for GPS signals can interfere with each other if they do not have the proper signal power relationships. The peak cross correlation of one C/A code to another is -21.6 dB (Ref. 26), which means that if one signal is close to 21.6 dB stronger than another, it will interfere

TABLE 5.2-3
GROUND TRANSMITTER SLANT RANGE VARIATIONS

D-45838

GROUND TRANSMITTER		SLANT RANGE ABOVE 5 DEG ELEVATION		
NO.	LOCATION	MAX (MI)	MIN (MI)	POWER RATIO (dB)
1	LICK OBSERVATORY	230	180	2.1
2	VISALIA	230	97	7.5
3	MATURANGO PEAK	186	82	7.1
4	CONE PEAK	242	65	11.4
5	ALDER PEAK	242	55	12.9
6	CHINA LAKE	210	52	12.1
7	BAKERSFIELD	232	35	16.4
8	EDWARDS	212	2	(40.5)
9	BARSTOW	196	51	11.7
10	VANDENBERG	240	42	15.1
11	TWENTYNINE PALMS	152	124	1.8
12	MAGIC MOUNTAIN	220	48	13.2
13	RIVERSIDE	192	84	7.2
14	PENDLETON	185	124	3.5

PEAK C/A CODE CROSS CORRELATION (WITH DOPPLER SHIFT) = -21.6 dB

with the acquisition process for the other code. As long as the power ratio of the minimum and maximum ranges for a single transmitter is safely below this figure, it would be possible to select a noninterfering transmitter power level that is constant. When the power ratio climbs to within a few dB of 21.6 dB, however, such a power level setting is not possible, and either:

- the transmitter power level must be dynamically adjusted in response to range to the Orbiter during entry.
- the transmitter power level may be kept constant but will be inadequate for acquisition at maximum range.

- the transmitter power level may be kept constant but will interfere with other signals at minimum range.

As the table shows, only the transmitter located at the landing site poses any interference problems.

One final issue of signal usability was not investigated as part of the entry study. It concerns the dynamics of the signals from the ground transmitters and the stress they place on the receiver tracking loops. This stress is considerable and would substantially affect the receiver design, as is shown in the next Section, where it is considered for the ascent phase.

5.3 ASCENT

Figure 5.3-1 (Ref. 27) illustrates the range of allowable launch azimuths from the Kennedy Space Center. Three ascent trajectories (Ref. 28) were available for this study that reasonably span the range of those allowable. Two are termed northward launches, one to a nearly limiting 55 deg orbital inclination, and another to a more normal 40.5 deg orbital inclination (sometimes referred to as 40 deg inclination). A third trajectory is eastward, to a 28 deg orbital inclination. This eastward ascent exhibits about the poorest ground transmitter visibility of all launches due to the scarcity of locations for ground transmitters in this direction.

A total of 17 ground transmitter sites were selected for study although only 14 were used at any one time. Figure 5.3-2 maps the three ascent trajectory ground tracks and shows the ground transmitter locations, although it omits the names of the ground transmitters. The length of the trajectory ground

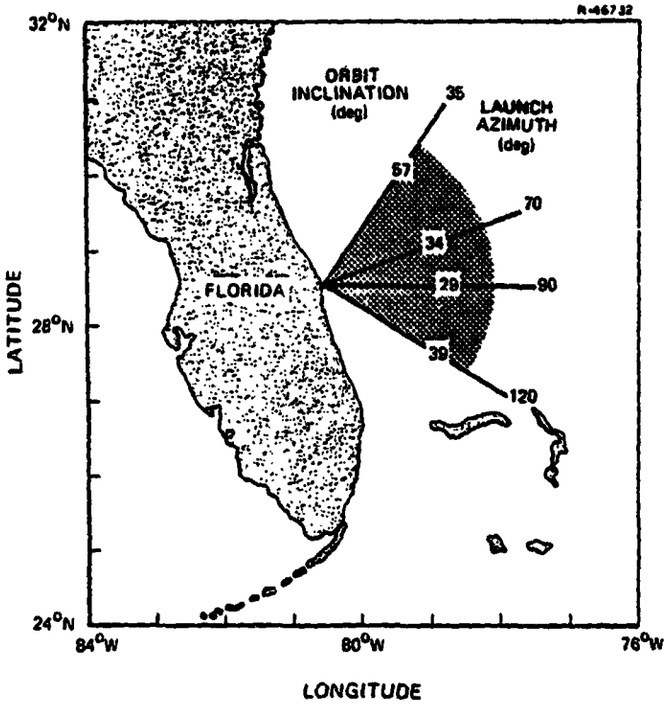

Figure 5.3-1 Allowable Orbit Inclinations and Launch Azimuths from Kennedy Space Center

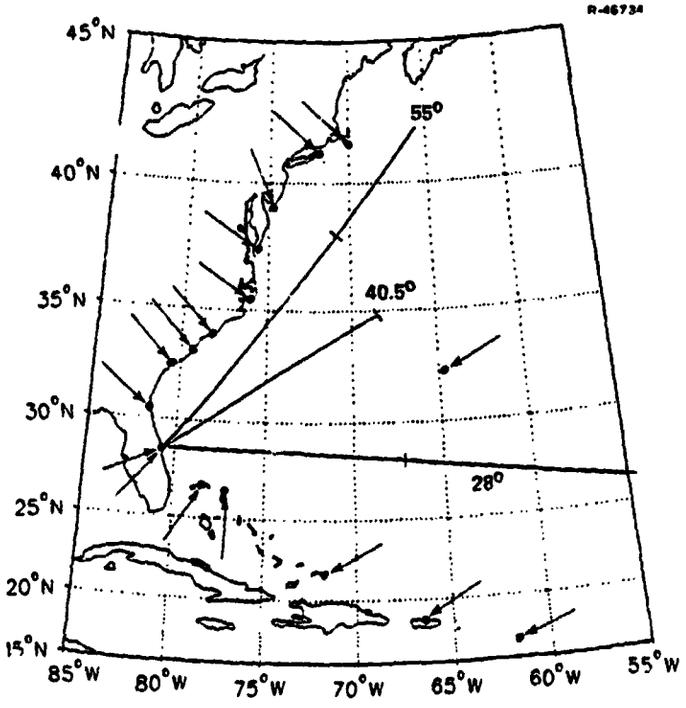

Figure 5.3-2 Map of Ascent Trajectory Ground Tracks And GPS Ground Transmitter Study Locations

tracks is indicative of how much of the trajectory was available for study. In the 40.5 deg inclination case, only that portion of the trajectory prior to Orbiter main engine cutoff (MECO) was available. Post-MECO data was available for the other two trajectories.

To correlate the locations of the ground transmitters with the names of the ground transmitter sites given in the sequel, it should be noted that the transmitters are always listed from north-most to south-most, and Bermuda is an obvious reference point included in all lists. Bermuda is just slightly north of Savanna Beach, Georgia, which appears at an equal latitude in the figure. Cape Kennedy and Patrick AFB are so close to one another as to be indistinguishable on the map in the figure, where two arrows point to the same location.

There are no terrain visibility restrictions for any of these ground transmitter sites, and so the visibility criterion used in the entry study was slightly relaxed here -- during ascent the Orbiter must be above three degrees above the horizon at the ground transmitter to be visible to the ground transmitter. Of course, the ground transmitter must also be within the receiving antenna beamwidth of the Orbiter for signal reception. Figure 5.3-3 illustrates the visibility situation for ground transmitters during ascent. Note that the antenna pattern has also been altered from that used in the entry study. Now an 80 deg half-cone angle, conical antenna is assumed as nominal (Ref. 29), while a full hemispherical coverage, 90 deg half-cone angle antenna is used as an alternate to study the sensitivity of the visibility results to antenna coverage.

Ground transmitters were studied for entry primarily to assist during GPS Phase II when no satellites are available

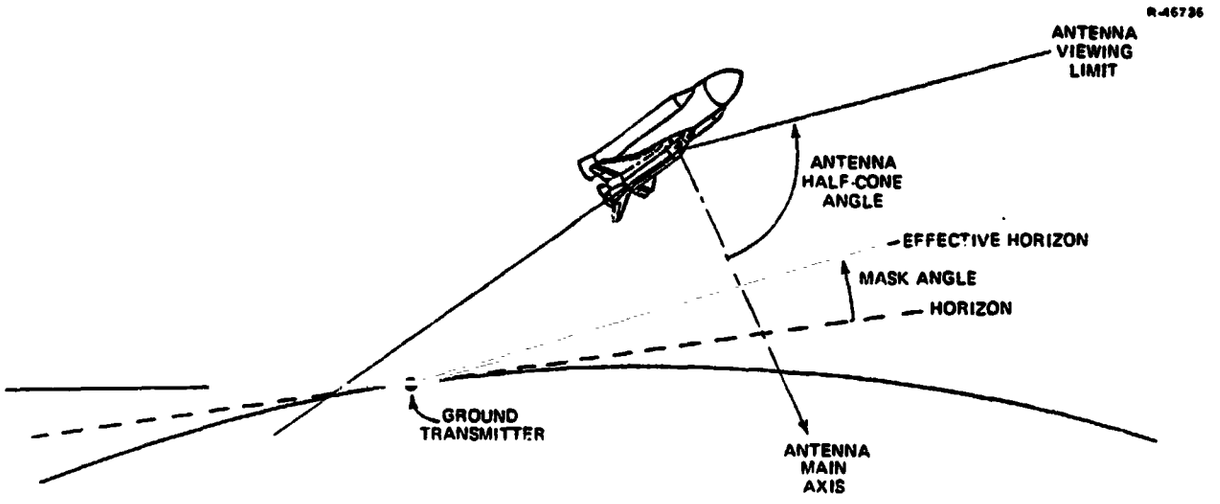

Figure 5.3-3 GPS Ground Transmitter Visibility Geometry During Ascent

for significant portions of each day. For the ascent study, the external fuel tank will block satellite visibility to the downward antenna even during GPS Phase III when satellites are constantly available. But satellites are sometimes visible to the upward antenna during ascent, so the contribution of the satellites to the ascent signal availability must be examined. The visibility criteria for satellite signals are illustrated in Fig. 5.3-4. Because satellite signals have limited strength the horizon mask angles are more conservative for satellites than for ground transmitters.

Figures 5.3-5 through 5.3-7 summarize the ground transmitter visibility situations for the three ascent trajectories. The key to these figures is almost the same as that for Fig. 5.2-3, except that three deg elevation is now the visibility

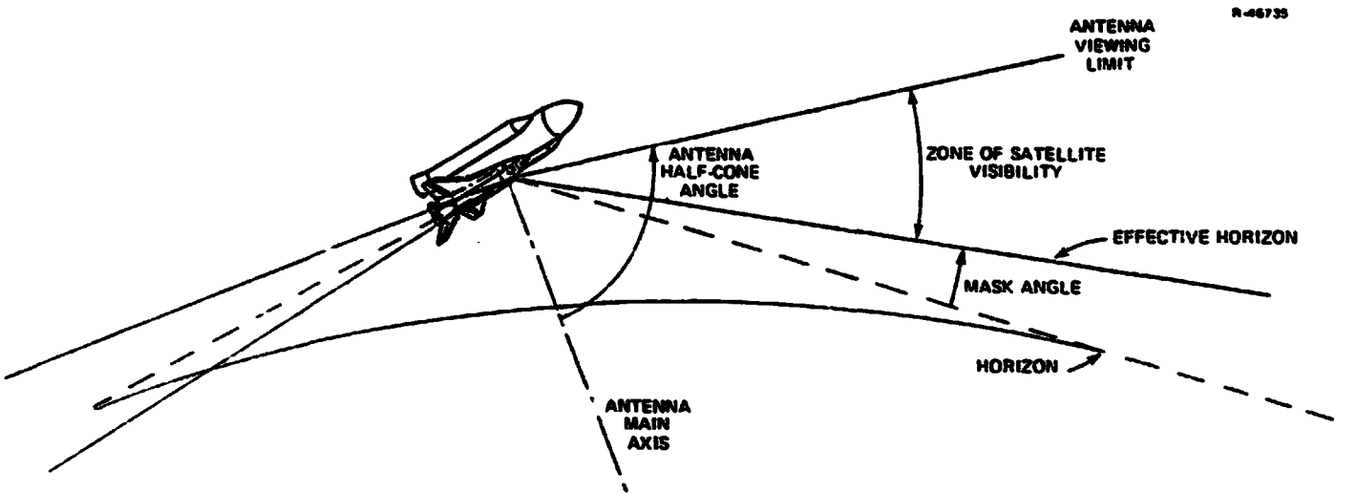

Figure 5.3-4 GPS Satellite Visibility Geometry During Ascent

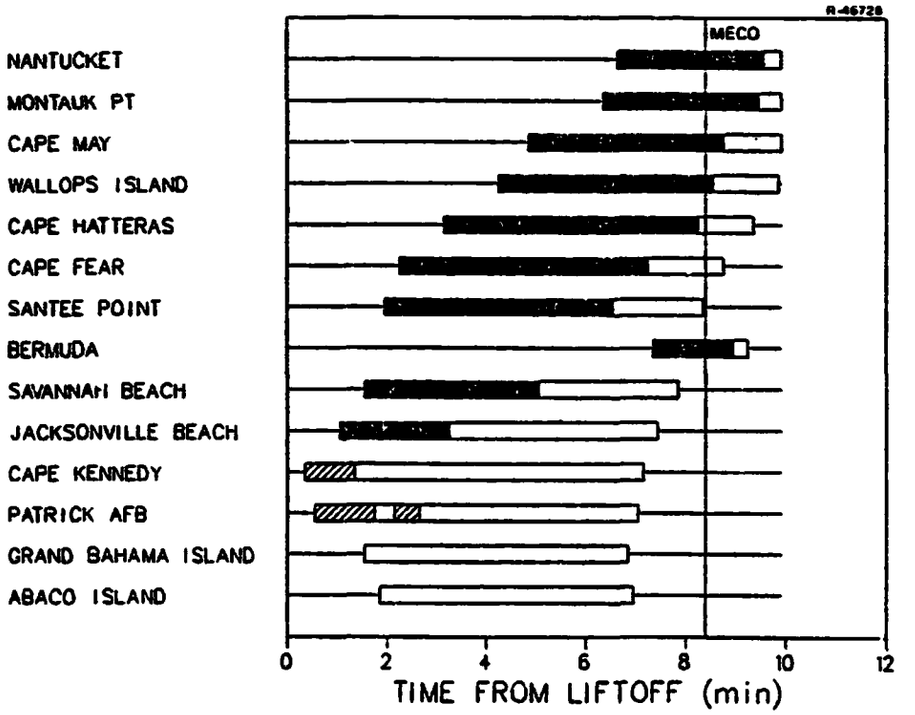

Figure 5.3-5 Ground Transmitter Visibility For KSC Ascent (55 Deg Inclination Orbit)

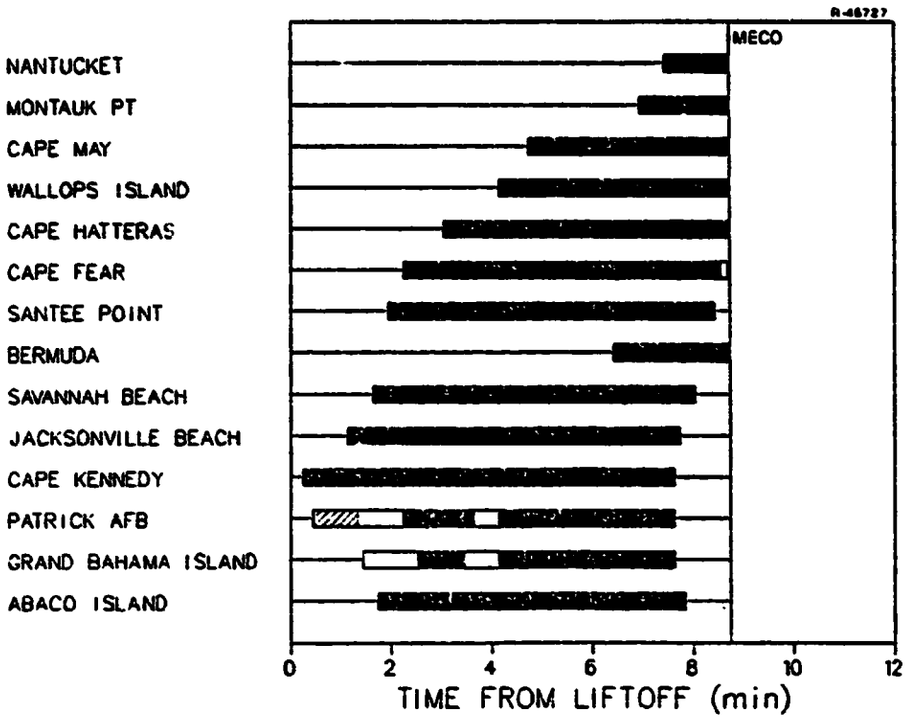

Figure 5.3-6 Ground Transmitter Visibility For KSC Ascent (40 Deg Inclination Orbit)

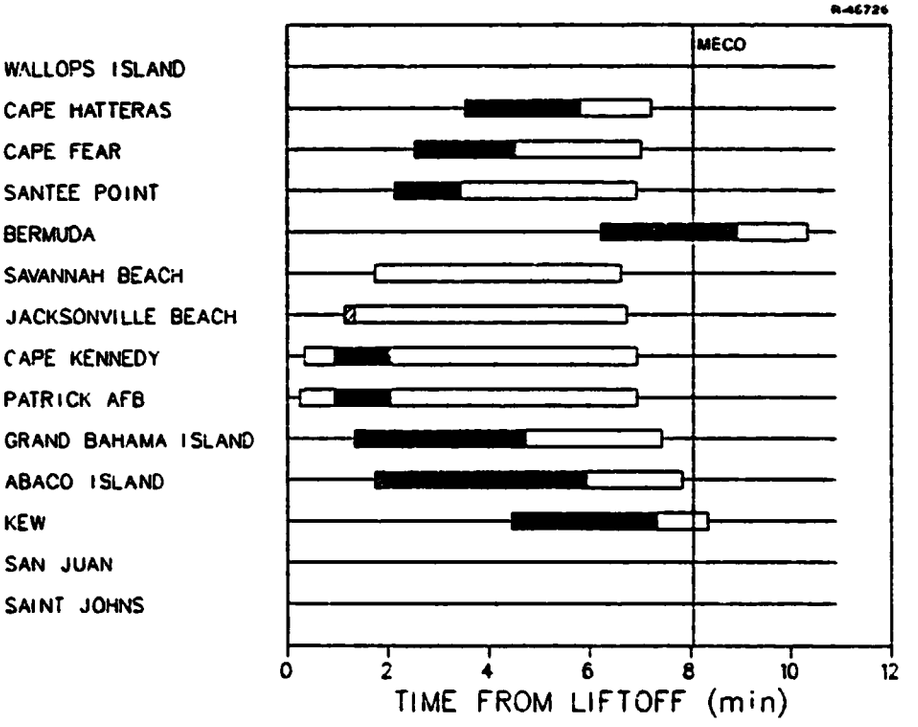

Figure 5.3-7 Ground Transmitter Visibility For KSC Ascent (28 Deg Inclination Orbit)

criteria, and the roles of the top and bottom antennas have been interchanged, since the Orbiter flies "upside down" during ascent. The solid portions of the wide bars thus imply visibility to the top antenna. The cross hatched portions of the wide bars imply visibility to the bottom antenna without regard for blockage by the external fuel tank. Thus, these cross hatched segments should be regarded as periods of no visibility, since the tank does block the bottom antenna.

Figure 5.3-6 shows the excellent ground transmitter coverage for ascent to a 40 deg inclination orbit. Figures 5.3-5 and 5.3-7 show that coverage reduces for extreme launches, especially for the eastward launch. Generally speaking, to support accurate navigation when it is needed during ascent would require three signals available during roughly the five to seven min period following liftoff. The Montauk Point, Cape Hatteras, Bermuda, and Abaco Island sites would probably cover all launch azimuths with marginal capability (assuming no satellite visibility).

The eastward launch suffers the poorest ground transmitter coverage. Figure 5.3-8 shows how this coverage would dramatically improve if the receiving antenna beamwidth could be enlarged to full hemispherical coverage.

Figures 5.3-9 and 5.3-10 show what GPS satellite visibility might be available to the 40 and 28 deg inclination ascents with the 24 satellite, Phase III constellation. Unlike the case with ground transmitters, satellite visibility varies depending on the time of day, being roughly similar in each eight hour period. (It takes the earth eight hours to rotate the 120 deg separation between the three GPS satellite orbital planes.) Thus, the figures give two time variables, one for time since liftoff in minutes, and one for time of day (called

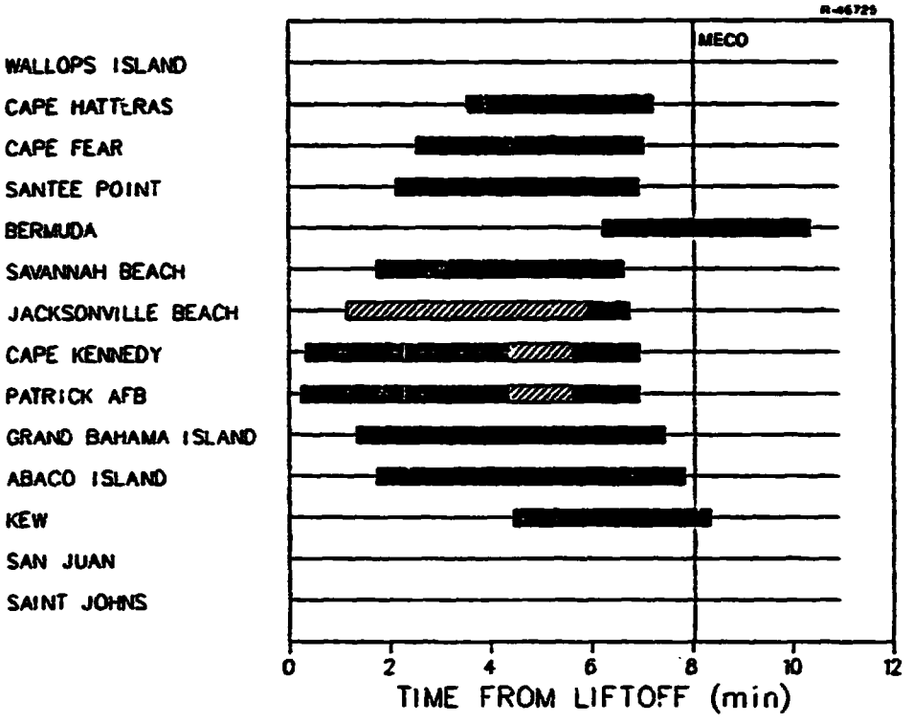

Figure 5.3-8 Ground Transmitter Visibility For KSC Ascent (28 Deg Inclination Orbit) (90 Deg Half-Cone Antennas)

offset time) in hours. The figures show the number of satellites visible to the (80 deg half-cone) top antenna during ascent, with a blank space indicating no satellites visible.

Figure 5.3-9 shows that for a northward launch to a 40 deg orbital inclination no satellites are ever visible after about four min after launch. Satellite visibility for a more northward launch would be even worse; thus, the 55 deg results are not shown. Clearly, no satellite visibility can be expected in the critical five to seven minute period following launch. Figure 5.3-10 shows an improving situation for an eastward

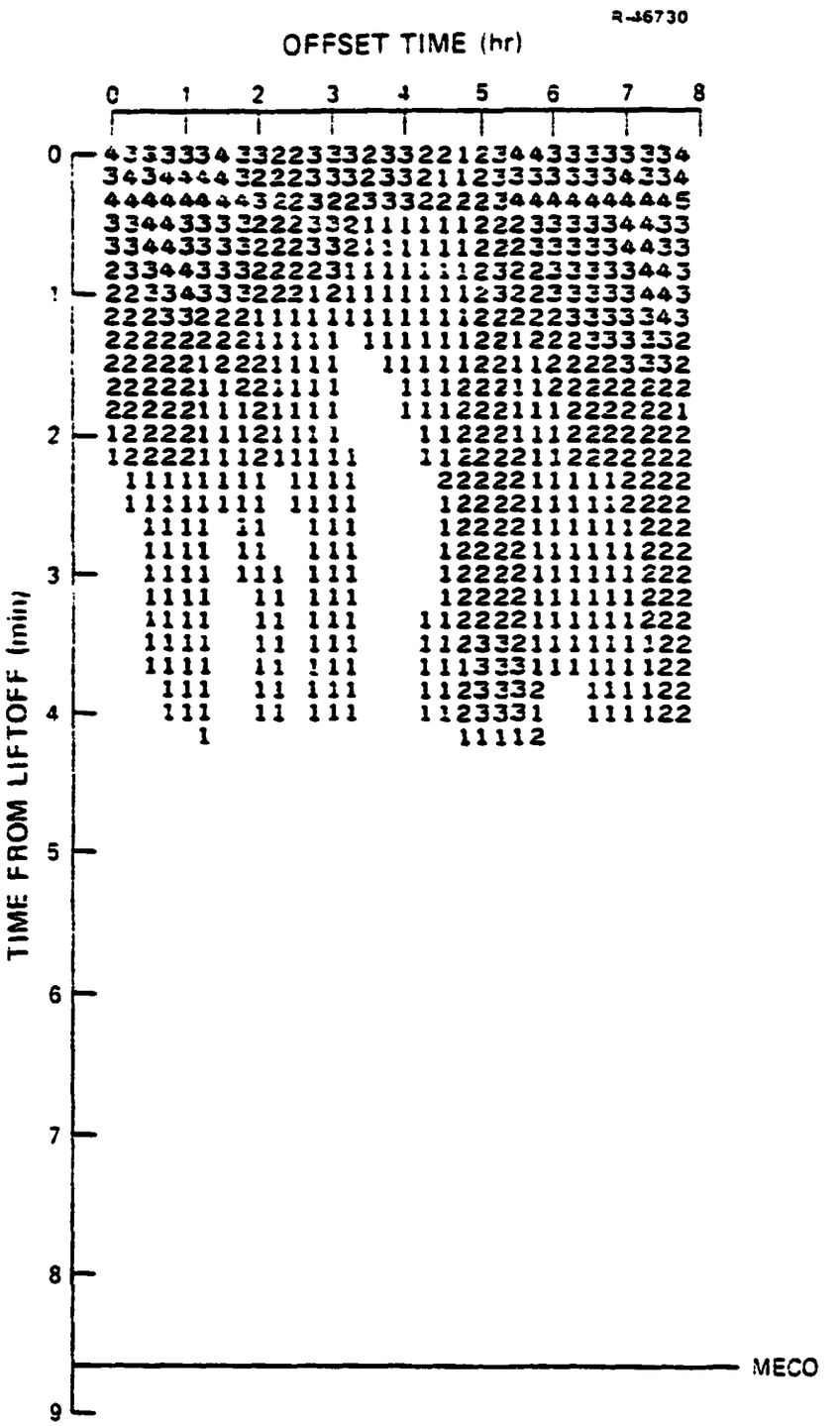

Figure 5.3-9 GPS Satellite Visibility During Ascent (40.5 Deg Inclination Orbit)

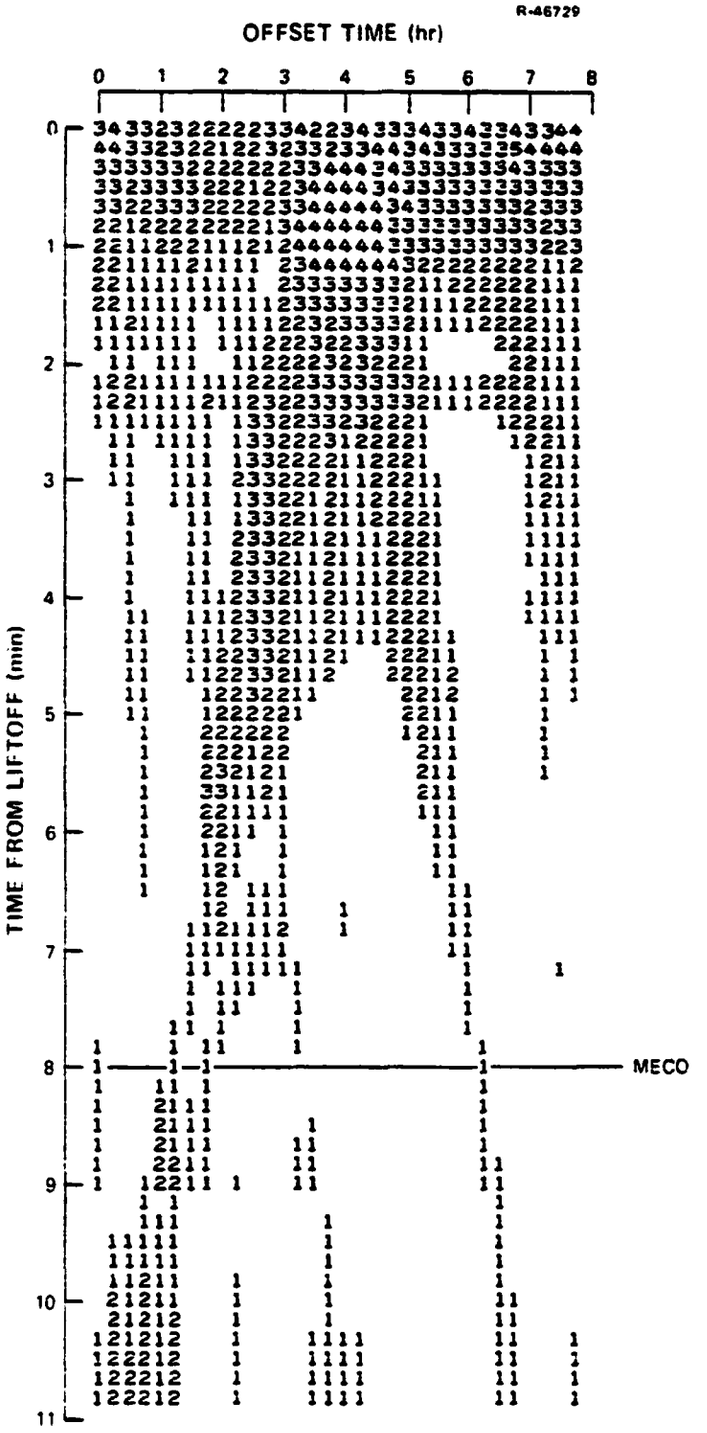

Figure 5.3-10 GPS Satellite Visibility During Ascent (28 Deg Inclination Orbit)

launch. Still, there are significant portions of each day when no satellites may be seen during the critical period, even though one or two are often available.

Travelling at high speed close to a ground transmitter site produces a large range acceleration that puts severe demands on the receiver tracking loops. Figure 5.3-11 shows a time history of range acceleration for the ascent trajectory to the 55 deg orbital inclination and the Wallops Island ground transmitter site. The curve peaks out at over 13 g's and spends most of the period of visibility higher than three g's. The receiver tracking loops will have to accomodate three g's to account for Orbiter acceleration levels, but it would strongly affect receiver design to demand higher levels.

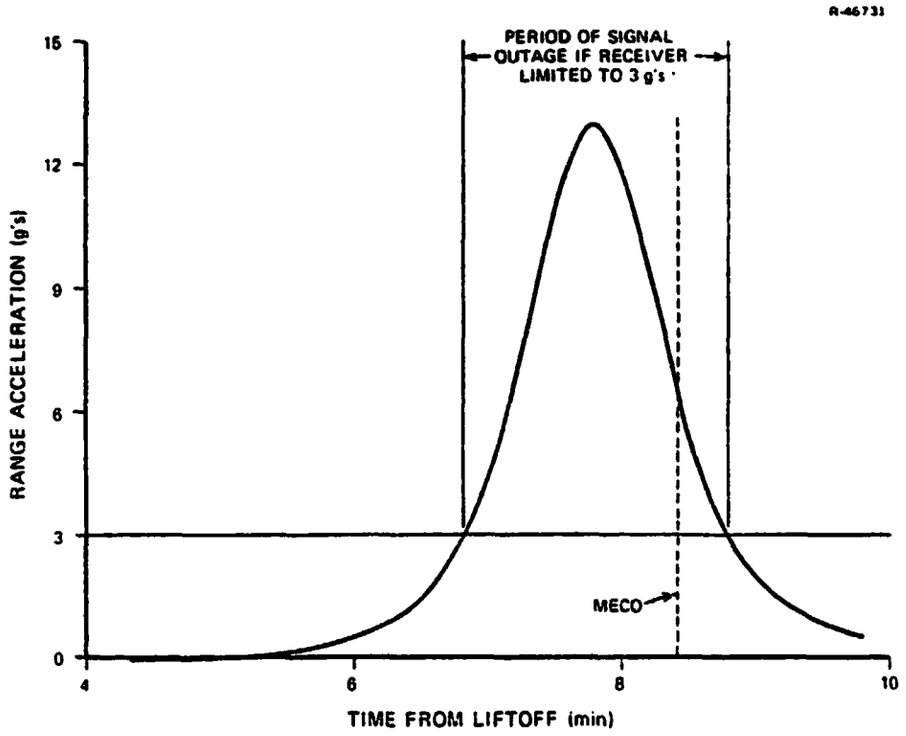

Figure 5.3-11 Example Plot of Range Acceleration During Ascent

5.4 CONCLUSIONS OF THE GROUND TRANSMITTER STUDY

Several conclusions summarize the results of the two ground transmitter studies for ascent and entry. They are:

Satellite Visibility

During entry, satellite visibility will be adequate once the full Phase III GPS constellation is established. Substantial periods of no visibility will exist during Phase II. During ascent, northward launches can expect no satellites visible to the baseline antenna system even after the Phase III constellation is in place. Eastward launches may occasionally have one or two satellites in view.

Ground Transmitter Visibility

Three ground transmitters would be adequate to support any particular entry trajectory, with four or five being necessary to support a range of trajectories to one landing site. An additional ground transmitter would be required if a quartz crystal clock were used in the R/PA instead of an atomic clock. Four ground transmitters would provide adequate support for ascents from Kennedy Space Center.

Ground Transmitter Power Levels

In general, it would not be a problem to select constant power levels for ground transmitters that would not interfere with other GPS signal sources for the Space Shuttle during either ascent or entry. Some care would have to be used with a transmitter at the landing site for entry. Signal interference to other (aircraft) users of GPS is a possibility.

Ground Transmitter Signal Dynamics

Signal dynamics for ground transmitter signals during either ascent or entry are severe. Receivers designed for the baseline three g's of signal acceleration would generally be unable to use ground transmitter signals. Design of receiver tracking loops not aided by IMU information and capable of tracking at the 10g's and higher levels necessary is very difficult and would have a major program impact.

Alternatives to Ground Transmitters

During entry, there appears to be no alternative to ground transmitters other than to "give up" on GPS navigation until the Phase III constellation is sufficiently established to provide adequate satellite visibility, probably in 1986 or 1987. During ascent, there are likewise no alternatives until Phase III is established. Once the satellites are in place, alternatives to ground transmitters include widening the topside antenna field view, mounting a GPS antenna on the external fuel tank, or changing the attitude profile of the Orbiter so the satellites become visible to the unshaded topside antenna.

6. GPS RECEIVER SUBSYSTEM ANALYSIS

The objective of GPS is navigation, but its methods are those of communication, and there are several GPS user equipment communication issues that impact navigation capability. The user equipment communication issues may be broken into two general areas: signal acquisition/reacquisition and signal tracking. Each of these areas is treated in this chapter.

6.1 GPS SIGNAL ACQUISITION/REACQUISITION

This section discusses the issues involved in acquiring/reacquiring a GPS signal and the time required to establish a navigation fix. The discussion includes an explanation of the need for an indirect method of acquiring the P-code, as well as the functional dependence of time-to-acquire/reacquire on signal-to-noise density, C/N_0, and on residual line-of-sight dynamics. The nature and complexity of the GPS acquisition process results from the GPS signal structure. The relevant properties of the signal structure are discussed in the next section, followed by a discussion of the actual acquisition/reacquisition process including navigation fix times.

6.1.1 GPS Signal Structure

The Global Positioning System (GPS) Navigational Signal is a composite waveform consisting of a Protected (P) Signal and a Clear/Acquisition (C/A) Signal transmitted in phase quadrature. The C/A-signal is designed for commercial and other users not requiring the highest accuracy and desiring to

use low cost equipment. From a military standpoint, its primary function is in providing a method of acquiring the protected code. The protected code is designed for both the highest navigation accuracy and for high anti-jam protection. The C/A-signal, by design, is easy to acquire but is highly susceptible to jamming. On the other hand, the P-signal, having been designed to resist jamming*, is nearly impossible to acquire directly without á priori range information; hence, the need for an indirect acquisition procedure.

Each signal transmitted by a given satellite (P and C/A) consists of a carrier wave modulated by both 50 Hz data and a bi-phase digital ranging code. The data consists of space vehicle ephemerides, system time-of-day, C/A to P handover information†, etc. The bi-phase digital codes are derived from a class of digital codes known as pseudo-random noise sequences (PRN sequences). The spread spectrum nature of the codes makes them ideal for highly accurate ranging while providing high anti-jam (A/J) protection.

The PRN sequence used for the C/A ranging code is composed of ≈1000 nsec (300m) chips with a code repetition period (i.e., code length) of 1023 chips (1 msec). Whereas, the PRN sequence for the P-code is composed of ≈100 nsec (30m) chips with a code repetition period of 6×10^{12} chips (7 days). The narrower chip width gives the P-code a factor of ten improvement in ranging accuracy over the C/A code. The longer code period gives the P-code added protection against jamming while denying its use to unauthorized users. The sequences

*The P-code has a seven day period which, while making direct acquisition quite difficult, is the very feature which gives the P-code its anti-jam resistance.

†The Handover information enables acquisition of the P-signal with a minimum of search time.

are similar in that they have very sharp autocorrelation functions: i.e., if a PRN sequence is correlated with a replica of itself that differs by more than a chip, then the resulting signal has essentially zero power. Thus, for a GPS receiver to detect a GPS RF signal, it must correlate the incoming signal with a replica of the code delayed by less than a chip. Otherwise, the effective signal-to-noise ratio, SNR, is ≈-30dB for the P-code (-20 dB for the C/A-code). This compares with a SNR as great as 40 dB for perfect correlation. Therefore, a transmitted signal modulated by a PRN sequence is inherently nonobservable to a receiver that does not know the repetition time of the PRN sequence.

6.1.2 GPS Signal Acquisition and Reacquisition

The term acquisition denotes the synchronization of carrier and code phases of the user GPS receiver with the satellite transmitted P-code. The acquisition procedure is therefore the first step in establishing a navigation fix. The user must demodulate the GPS data after closed loop tracking is achieved. This demodulated data is then decoded and combined with pseudo range and pseudo delta range measurements in an appropriate algorithm before computing a navigation fix. The time required to perform this entire operation is called the time-to-first-fix, TTFF, and is composed of the acquisition time, the data demodulation time, tracking time, and the navigation fix time.

The structure of the GPS signal is such that two distinct methods of acquiring it are available to the user: direct and normal. For the direct method, á priori information is utilized to define a time-frequency uncertainty region for the P-signal. This region is then searched to determine the signal's code position and carrier frequency so that tracking may

be initiated. Because the P-signal is designed to be secure, direct acquisition may require unsatisfactorily long acquisition times unless accurate á priori information is available to the user.

For the normal method, á priori information is employed to define a time-frequency uncertainty region for the C/A-signal. This region is then searched to determine the code position and carrier frequency so that tracking can begin. The tracking operation (for the C/A-signal) and associated data demodulation continues until the handover word (which is present in the data signal) is recovered -- handover words are present in the GPS data every six seconds. This word provides the information required to acquire the P-signal directly in a reasonable length of time. A brief, direct acquisition of the P-signal is the final step in the normal method. When the á priori information available to the user is not extremely accurate, the normal method will provide substantially better acquisition times than the direct method.

There are several factors which affect the acquisition time of a receiver. An obvious factor is the quality of the á priori information about range delay and doppler shift of the GPS signal. This factor is determined by uncertainties in the position and velocity of the user relative to the satellite, and by uncertainties in the time and frequency of the user's clock. Other factors influencing acquisition time include the received SNR, the desired probability of a correct acquisition, the search pattern used to check each cell in the time-frequency uncertainty region, and the structure of the acquisition receiver.

The á priori range-velocity uncertainty defines a code position-frequency uncertainty region which must be searched

by the receiver*. The acquisition procedure is initiated by testing a code position and a doppler frequency. This test is accomplished by replicating the received signal as it would exist under the assumption that the test parameters are correct. In the simplest case, this signal is then correlated with the actual received signal, bandpass filtered, and then signal power detected. If the assumed doppler frequency is incorrect, the mixed signal will not pass the bandpass filter. Similarly, if the assumed code position is incorrect by more than a chip, the SNR will be -20dB for the C/A-code (-30 dB for the P-code). If the test parameters are close to the correct values, the SNR will be as great as 40 dB. If the cross-correlation of the received signal and the locally-generated signal estimate (with the assumed code position and doppler frequency) do not pass a predetermined energy threshold, those signal parameters are rejected, and the local signal estimate is sequentially stepped through the uncertanty region until the energy exceeds the threshold. When the threshold is exceeded, operation is switched to the tracking mode.

Assuming a low cost GPS set in which all tests must be performed serially†, Fig. 6.1-1 depicts the time to acquire a C/A-signal for a 300 meter range uncertainty as a function of doppler uncertainty and C/N_o, i.e., GPS signal strength at the receiver input. The results assume probability of detection, $P_D=0.9$, and probability of false alarm, $P_F=10^{-4}$. Each curve within the family of 5 curves is composed of three regions designated by a solid curve, a dashed curve, and a dotted curve.

---

*If previous receiver operation has not provided GPS system time, then an additional range uncertainty equal to the time error must be included. This is typically small compared with the range uncertainty.

†This assumes there are not multiple channels available which could be employed to perform testing in parallel.

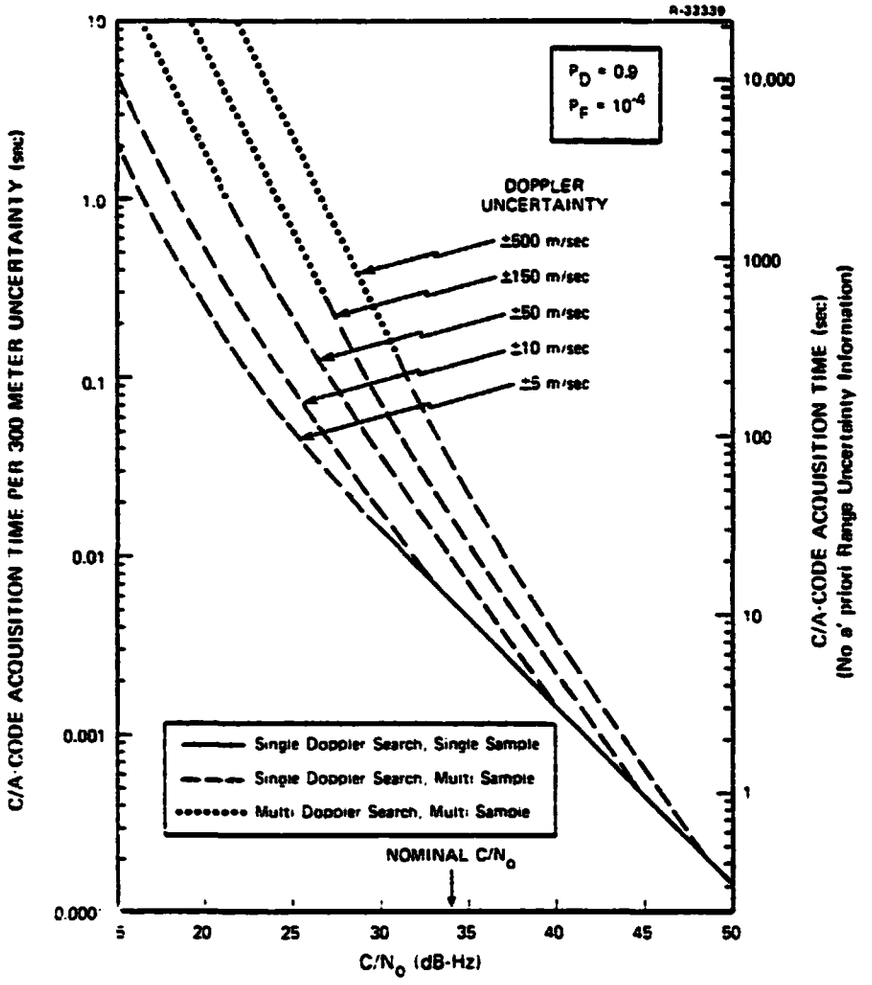

Figure 6.1-1 Time to Acquire/Reacquire the C/A-Code as a Function of C/N_0, and Position and Velocity Uncertainties

The dashed and dotted curves employ slight variations of the acquisition procedure defined above in order to optimize acquisition performance under weak signal conditions*. For a 600 meter uncertainty, the times indicated in the table double,

*The solid curve assumes only a single doppler frequency is searched. As C/N_0 decreases, a sequence of independent samples at the output of the detector are required as the basis for detection, (dashed curve). The number of samples available depends on how long the doppler accuracy will keep the test code within a half chip of the received code. A further decrease in C/N_0 requires multiple doppler regions to be searched in addition to multiple code position, (dotted curve).

etc. It should be noted that, in the worst case, no á priori range information is required for C/A acquisition; i.e., since the signal is periodic, the time uncertainty is limited to the code period, 1023 msec. Thus, with no á priori range information a maximum 1023 chips must be tested (and typically codes are tested every 1/2 chip) for a total number of 2046 tests. In Fig. 6.1-1 a scale has been added for the total acquisition time (right hand side) for one C/A channel as a function of C/N_o assuming no á priori range information.

Figure 6.1-2 is analogous to Fig. 6.1-1; it depicts

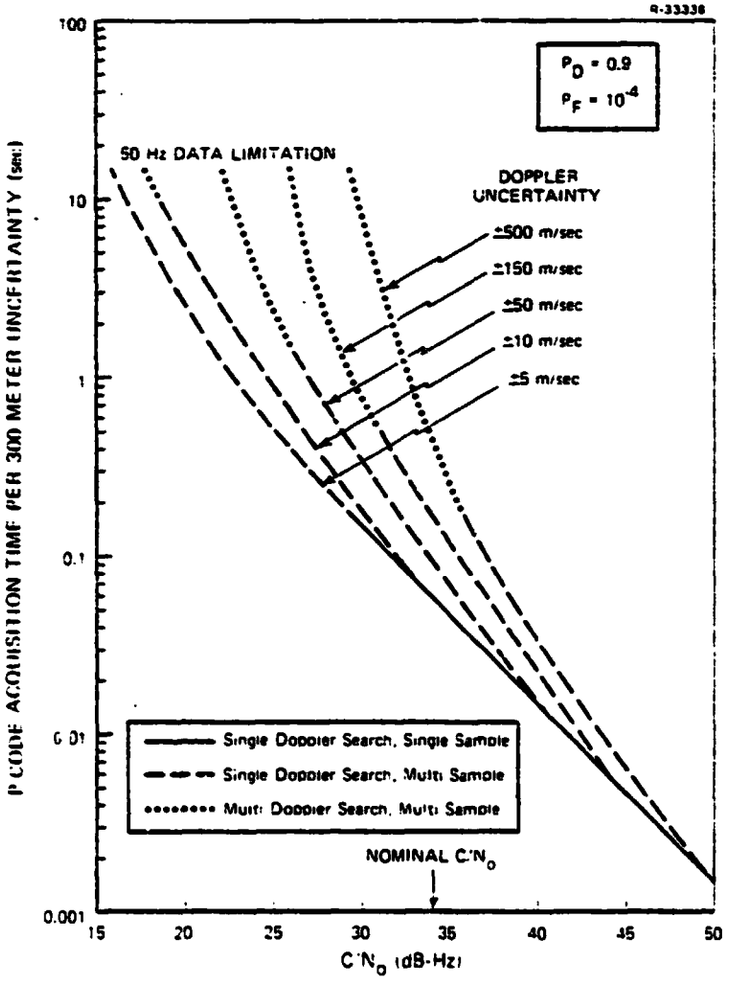

Figure 6.1-2 Time to Acquire/Reacquire the P-Code as a Function of C/N_o, and Position and Velocity Uncertainties

the time to acquire a P-signal for a 300 meter range uncertainty as a function of doppler uncertainty and C/N_o. Again, the times double for a 600 meter uncertainty. Since the P-code has a 7-day period, there is no corresponding right hand scale depicting acquisition time if no á priori range information is known; i.e., the time would be prohibitive.

These acquisition times can be combined with the data demodulation time, tracking time, and the navigation fix time to provide the time-to-first-fix (both normal and direct). The data demodulation time is the time required to demodulate the entire data block (1500 bits) in order to recover the necessary satellite data for utilization in the navigation algorithm. Since the data is transmitted at a 50 Hz rate, this operation requires exactly 30 seconds following bit synchronization (<1 sec). The tracking time governs the accuracy of pseudo range and pseudo delta range measurements. Its value depends on the receiver bandwidths; values of 2 to 6 seconds are reasonable. Finally, the navigation fix time, which depends upon the user's computation capabilities and the fix algorithm, will typically require approximately 1 second.

Table 6.1-1 lists the times associated with the individual factors that make up the time-to-first-fix for the P-signal. Several points should be noted:

- If the range-doppler uncertainty is small enough to allow P-code acquisition in less than ~8 seconds (see Fig. 6.1-2), then direct acquisition is faster than normal acquisition
- The time required to demodulate the data block (30 seconds) can make up the major portion of time-to-first-fix, TTFF

TIME 6.1-1

TIME-TO-FIRST-FIX FOR THE P-SIGNAL

ACQUISITION PHASE	NORMAL ACQUISITION	DIRECT ACQUISITION
Acquire Carrier and C/A-Code Phase (Depends on Position and Velocity Uncertainties)	$T_{C/A,\ ACQ}$ (Fig. 6.1-1)	---
Obtain Bit Synch and Frame Synch	< 1.0 Sec	---
Demodulate and Decode Handover Word	6.0 Sec	---
Acquire P-Code	< 1.0 Sec	$T_{P,\ ACQ}$ (Fig. 6.1-2)
Demodulate Data Block (1500 Bits @ 50 Hz)	30 Sec	30 Sec
Derive Pseudo Range and Pseudo Delta Range Measurements (Depends on Receiver Bandwidths)	$T_{Tracking}$†	$T_{Tracking}$†
Sum of Previous Times	T_{SUB}	T_{SUB}
N=4 in Low Cost Sequential Set (N=1 in 4 Channel Set)	$T_{SUB} \times N$	$T_{SUB} \times N$
Perform Navigation Fix (Depends on User Computer and Fix Algorithm)	∿ 1 Sec	∿ 1 Sec

†$T_{Tracking}$ Governs the Accuracy of the Correlation Process and Therefore the Measurement Accuracy (Values of 2 Sec to 6 Sec are Reasonable).

- A low cost sequential set (1 channel set) affects TTFF by introducing a factor of four increase in TTFF* relative to a four channel set.

*Less the time required to perform the navigation fix.

An example may help to clarify the discussion. Assume the signal-to-noise density (C/N_o) is 30 dB-Hz, the total velocity uncertainty is ±150m/sec, the total range uncertainty is 3000 meters (~2 miles), and the user has a single channel receiver. Then, assuming also 4 seconds to derive pseudo range and pseudo delta range, both normal and direct acquisition would take ~169 seconds; 120 seconds of which are required to demodulate the data block. The direct approach would be faster if C/N_o increased or if doppler uncertainty and/or range uncertainty decreased.

The term reacquisition denotes the resynchronization of carrier and code phases of the user GPS receiver with the satellite transmitted P-code that must be accomplished whenever the tracking loops lose lock. Because closed loop tracking has already been achieved, demodulated GPS data is available to the user attempting reacquisition. Since GPS data changes slowly, this available data may be employed in the navigation algorithm once closed loop tracking has been re-established. Consequently, when the outage is brief, the normal reacquisition-fix-time would be the acquisition time of the P-signal (Fig. 6.1-2) plus ~4 sec to derive pseudo range and pseudo delta range measurements, plus the navigation fix time. (This value is multiplied by four if a sequential single channel set is used.) Reacquisition-fix-time is naturally shorter than the time-to-first-fix since the necessity of data demodulation has been eliminated and since the position and velocity uncertainties are small. When outage is sufficiently long, faster reacquisition can be accomplished by first locking-up the C/A-signal and then reacquiring the P-code by the handover word; this is referred to as the indirect reacquisition method. Table 6.1-2 lists the times associated with the factors that make up the reacquisition-fix-time for the P-signal for both the normal and indirect reacquisition methods. This table differs from Table 6.1-2 primarily in there being no time required to demodulate the data block.

TABLE 6.1-2
REACQUISITION-FIX-TIME FOR THE P-SIGNAL

REACQUISITION PHASE	NORMAL REACQUISITION	INDIRECT REACQUISITION
Acquire Carrier and C/A-Code Phase (Depends on Position and Velocity Uncertainties)	---	$T_{C/A,\ ACQ}$ (Fig. 6.1-1)
Obtain Bit Synch and Frame Synch	---	< 1 Sec
Demodulate and Decode Handover Word	---	6 Sec
Acquire P-Code	$T_{P,\ ACQ}$ (Fig. 6.1-2)	< 1 Sec
Derive Pseudo Range and Pseudo Delta Range Measurements (Depends on Receiver Bandwidths)	$T_{Tracking}$†	$T_{Tracking}$†
Sum of Previous Times	T_{SUB}	T_{SUB}
N=4 in Low Cost Sequential Set (N=1 in 4 Channel Set)	$T_{SUB} \times N$	$T_{SUB} \times N$
Perform Navigation Fix (Depends on User Computer and Fix Algorithm)	∿ 1 Sec	∿ 1 Sec

†$T_{Tracking}$ Governs the Accuracy of the Correlation Process and Therefore the Measurement Accuracy (Values of 2 to 6 Seconds are Reasonable)

6.1.3 Acquisition/Reacquisition Summary

The complexity of the acquisition/reacquisition process results from the structure of the GPS signal; namely, unless both the pseudo-random code modulating the GPS signal as well as the time when the code repeats are known to a receiver, the GPS signal is inherently non-observable; i.e., buried in the noise. To account for the GPS signal structure, there are two methods available for performing both acquisition and reacquisition: the normal and indirect method for reacquisition.

The time required to first establish a navigation fix is referred to as time-to-first-fix, TTFF. TTFF for the P-signal is tabulated in Table 6.1-1 for both the normal and direct methods of acquisition. The normal method requires acquisition of the C/A signal; the acquisition time is shown in Fig. 6.1-1 in terms of C/N_o and position and velocity uncertainties. The direct method of acquisition requires acquisition of the P-signal; this acquisition time is shown in Fig. 6.1-2.

When the GPS receiver loses lock, resynchronization of the carrier and code phases with the transmitter P-signal must be accomplished before the next navigation fix can be obtained. The time required to obtain the navigation fix is referred to as reacquisition-fix-time. Reacquisition-fix-time for the P-signal is tabulated in Table 6.1-2 for both the normal and indirect methods of reacquisition. The normal method requires reacquisition of the P-signal; this time is given in Fig. 6.1-2 as a function of C/N_o and position and velocity uncertainties. The indirect method of reacquisition requires reacquisition of the C/A-signal; this time is given in Fig. 6.1-1.

The method used to acquire/reacquire a GPS signal will depend on the range and velocity uncertainties as well as on the signal-to-noise density, C/N_o. In particular, if uncertainties and C/N_o are such that the P-code can be acquired within 6-8 seconds, then the direct acquisition process will be faster than the normal method. Similarly, if the P-code can be reacquired within 6-8 seconds, then the normal reacquisition process will be faster than the indirect method.

6.2 GPS SIGNAL TRACKING ANALYSIS

The analysis reported in this chapter was done when the phased approach to putting GPS aboard the Shuttle was being considered. The most attractive candidate for a receiver for the experimental phase is called GPSPAC, under development by Magnavox for use in satellites. While the phased development approach and the experiment plan have been abandoned, the receiver analysis results of this chapter are presented because they are still relevant. In fact, it is possible that a derivative of the GPSPAC could still be a candidate for the Shuttle GPS receiver.

The baseline navigation system for the Space Shuttle will require measurements from a variety of navigation aids in order to maintain accurate position and velocity estimates, including navigation updates from a ground tracking system during orbital operations. One of the greatest potential benefits of GPS to the Space Shuttle is the possibility of obtaining accurate, autonomous navigation across the entire flight regime from a single navigation aid. Unfortunately, none of the GPS user equipment under development is versatile enough to fulfill all potential Space Shuttle navigation requirements without either software or hardware modifications. However, the GPSPAC receiver being developed by Magnavox is sufficiently attractive in terms of both its operational flight envelope and its potential availability to warrant a more detailed evaluation. The results of a preliminary analysis of the GPSPAC receiver design are presented in this chapter with emphasis on the changes required to meet the Space Shuttle navigation requirements.

The five modules present in most user equipment designs are identified in Fig. 6.2-1. The heart of the equipment

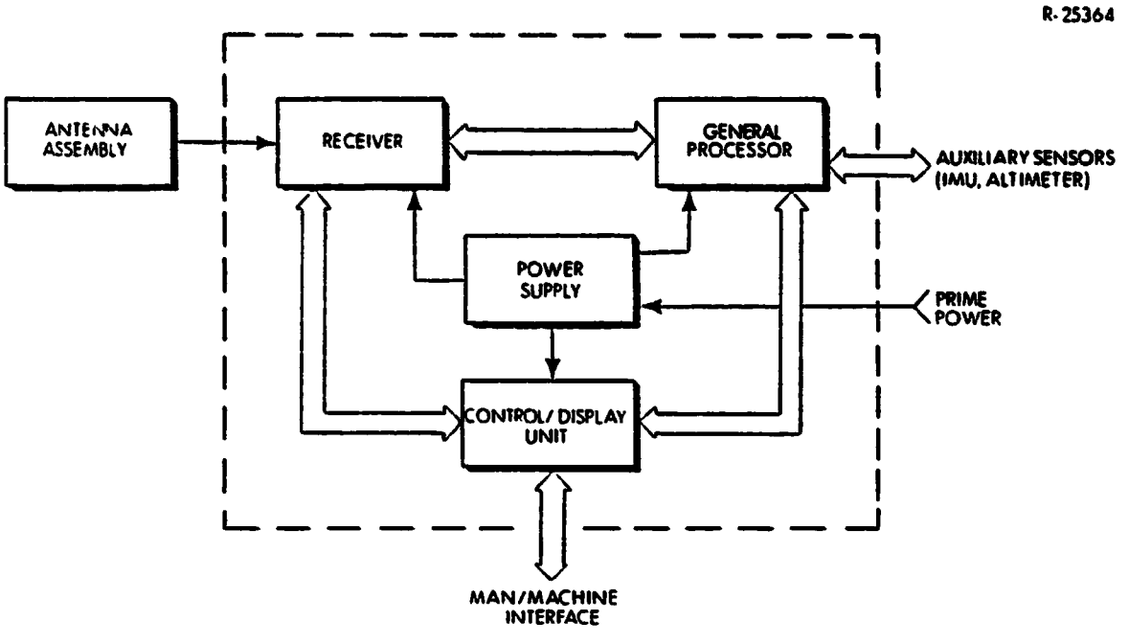

Figure 6.2-1 Major Elements of GPS User Equipment

is the receiver subsystem which tracks the GPS signal and generates range and range-rate measurements. In addition to the measurements, the receiver subsystem outputs system data transmitted by the satellites. In a high dynamics environment, the receiver tracking loops are generally rate-aided with processed IMU outputs generated by the data processor. The data processor also incorporates the GPS measurements into the navigation solution. In most user equipment designs, this is accomplished with a Kalman filter which is also capable of processing measurements from auxiliary sensors such as an altimeter or IMU.

The GPSPAC receiver is a two channel, space-rated set designed for a low dynamics environment. Measurements from four different satellites are obtained by sequencing between the satellites at well-defined intervals. The performance specifications require the receiver subsystem to maintain signal lock at orbital velocities and in the presence of accelerations as

large as 16 m/sec^2. Rate-aiding would not be possible without a software modification. The general processor uses a Kalman filter, but IMU data could not be incorporated into the navigation solution without a software modification.

It is apparent that the GPSPAC receiver subsystem as presently designed could operate satisfactorily during orbital operations for the Space Shuttle. The remainder of this chapter investigates potential receiver performance during re-entry.

6.2.1 Receiver Subsystem

Much of the nature and complexity of GPS receiver structures derives from the nature of the GPS signal. Generally, the satellite signals consist of RF carrier waves bi-phase modulated (±90°) with pseudo-random codes and 50 baud (bit-per-second) data. The carrier is tracked for user-to-satellite relative velocity information. The codes are tracked to provide user-to-satellite pseudo ranges (i.e., actual range plus user clock bias error). The 50 baud data has information concerning satellite ephemerides, etc.

Although there can be substantial variation in the design of an appropriate receiver, some essential elements are common to most proposed designs. Noncoherent delay-locked loops are used for locking to the pseudo-random code transmitted by each satellite, and Costas carrier tracking loops are used for locking to the doppler-shifted suppressed carrier. The pseudo ranges obtained from the code tracking provide the positional fix, while the range-rate estimates obtained from the Costas loop provide the velocity fix. The carrier phase reference obtained from the Costas loop is also used in the data demodulation, which is accomplished using 20 msec integrate-and-dump circuits.

The proposed GPSPAC receiver (Ref. 30) utilizes a single IF (Intermediate Frequency) and VCO (Voltage Controlled Oscillator) which is common to both the carrier and code tracking loops. Figure 6.2-2 provides a block diagram of the receiver subsystem. The common IF design is accomplished by time multiplexing the two tracking loops. In particular, the pseudo-noise (PN) demodulator (1 in the figure) is time shared between two distinct modes. In mode 1, the PN demodulator mixes an on-time version of the locally generated P-code with the incoming IF signal. This, in effect, provides a reconstructed carrier which is utilized by the Costas loop for phase tracking*. In mode 2, the PN demodulator alternately mixes the input signal with an early and late version of the P-code. This results in a code phasing error signal which is used by the delay-locked loop for code phase alignment. The common IF design eliminates dedicated code channel hardware. However, as will be discussed, dynamic errors can result while the PN demodulator is in mode 2 and the Costas loop is coasting.

The VCO (3 in the figure) is used in a Costas-type phase-locked loop to track the carrier signal phase. The code loop clock is also derived (4 in the figure) from the same carrier tracking VCO. The common VCO design eliminates the effect of vehicle dynamics on the code loop; i.e., when the Costas loop is tracking the carrier (mode 1) the code clock is inherently locked in frequency to the received code. However, it remains to align the code phase (mode 2) to derive the range measurement.

*In actuality, the carrier is still suppressed by the data; however, the data is removed by subsequent inphase/quadrature multiplication (2 in the figure).

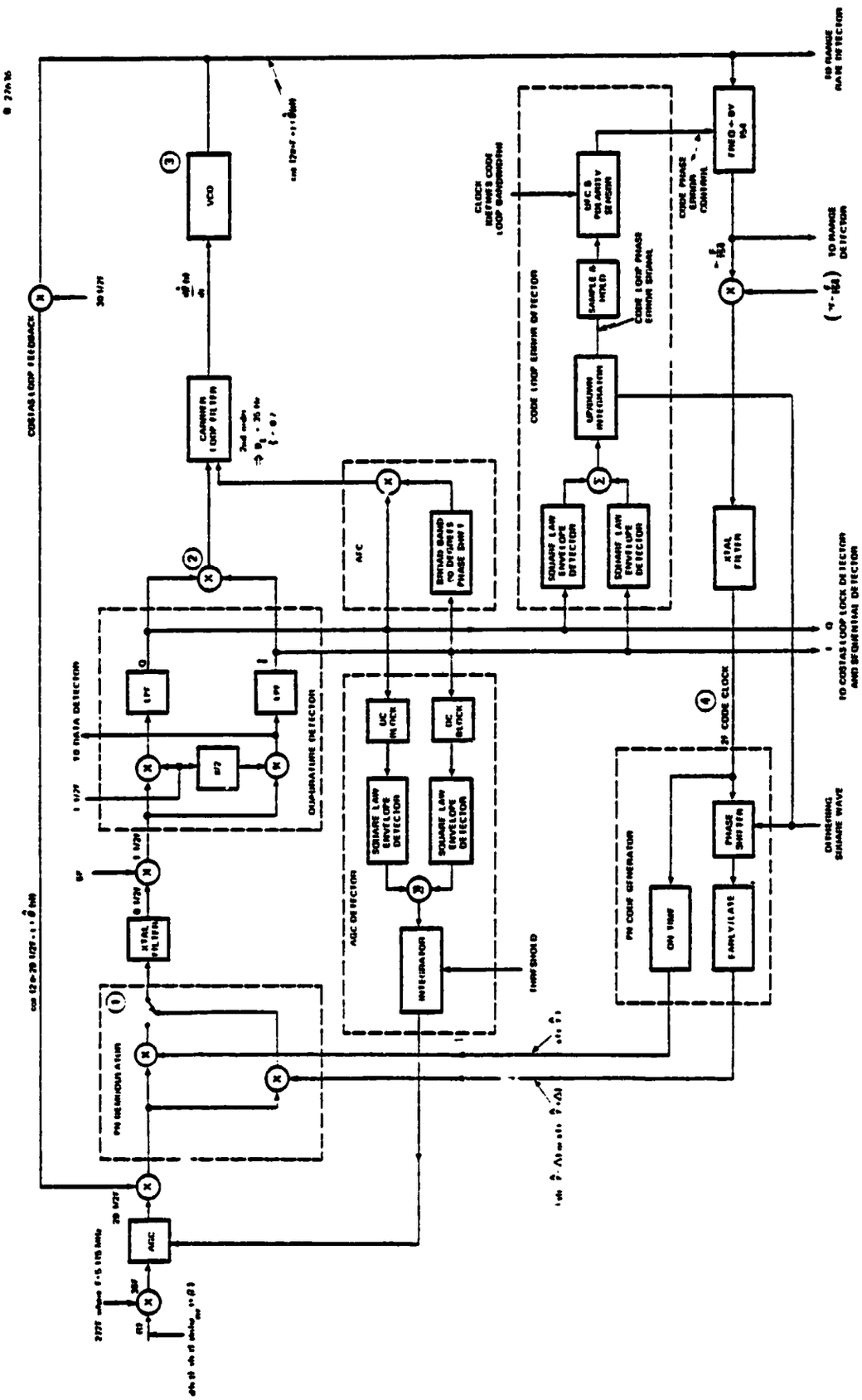

Figure 6.2-2 Receiver Block Diagram

The receiver mode of operation is first to establish carrier tracking while the PN demodulator is in mode 1. Having locked to the received carrier signal, the PN demodulator then switches to mode 2 during which time code phase alignment is accomplished. (The Costas loop coasts via a prediction of the carrier signal during this period.) Once aligned, the PN demodulator may switch back to Costas loop operation (mode 1) to remove any carrier tracking errors (due to vehicle dynamics) which may have occurred while in mode 2.

A model for the Costas loop is shown in the upper half of Fig. 6.2-3. The loop provides the coherent phase reference for data demodulation and range-rate determination. Because of its improved acquisition performance compared with that of a third-order loop, the Costas loop employs a second-order loop (35 Hz bandwidth, 0.707 damping coefficient). However, use of a second-order loop can result in sizeable phase tracking errors during acceleration unless some form of rate-aiding is employed. (See Section 6.2.2)

A model for the code loop is shown in the lower half of Figure 6.2-3. The loop provides code phase alignment for range determination. The code loop clock is derived from the carrier tracking VCO by dividing the VCO output (consisting of some IF frequency plus carrier loop doppler) by the code/carrier ratio (154) to obtain the doppler-shifted code frequency. This signal is then mixed with a reference to produce the 10.23 MHz P-code clock which in turn is used during mode 2.

During mode 2 a code phase error signal is derived by alternately modulating the input signal with an early and late version of the P-code. This technique is referred to as τ-dithering and has the major advantage over the early-late

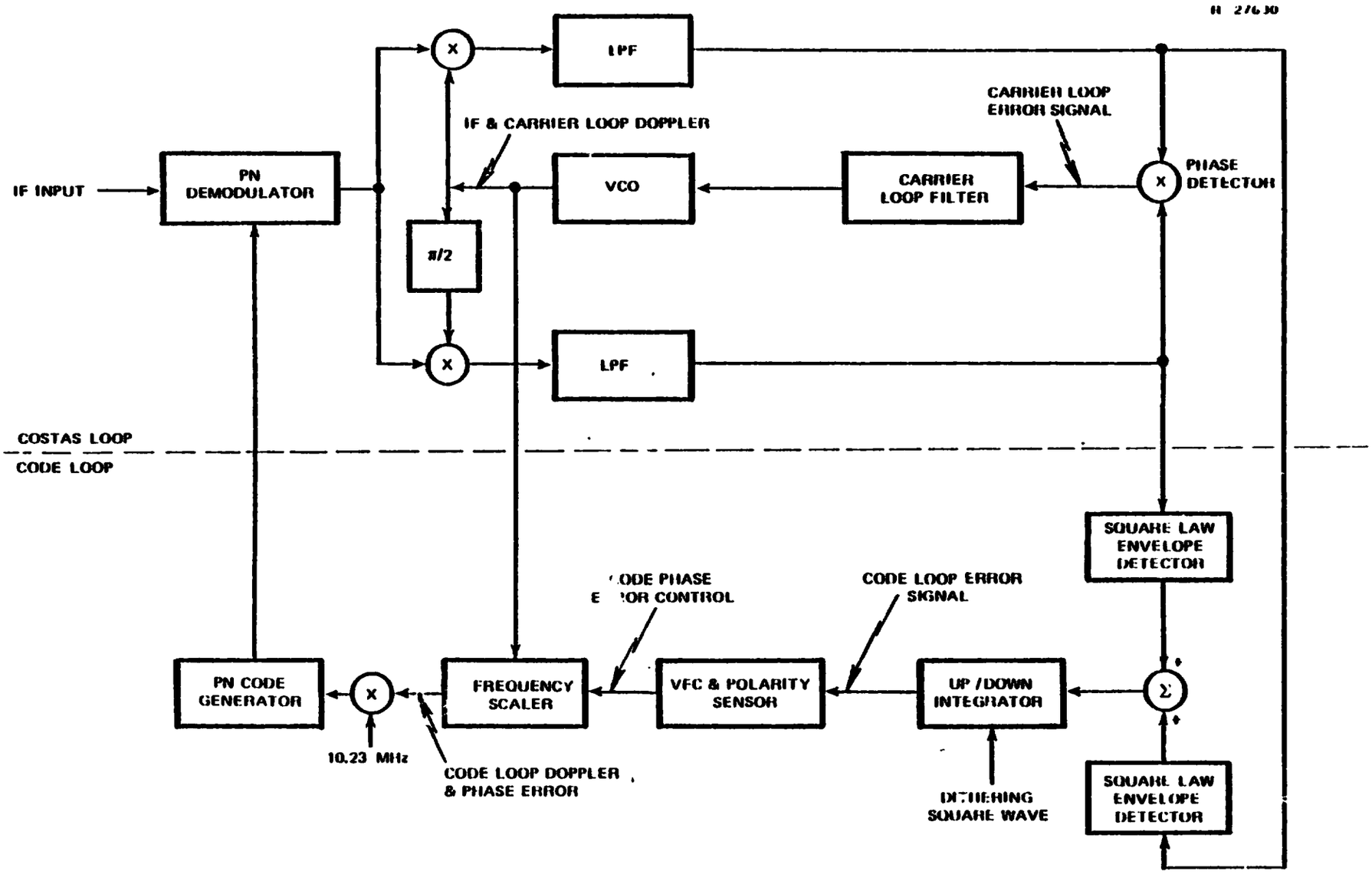

Figure 6.2-3 Simplified Receiver Block Diagram

delay-locked loop approach that it employs only one correlation channel. Thus, this implementation minimizes hardware, while eliminating the problems associated with two channel gain imbalances. However, the time sharing of the early and late channels does result in an approximate 3 dB degradation in the code loop signal-to-noise ratio. In so much as the system need not consider ultra low signal-to-noise operation (i.e., high anti-jam operation), this seems to be a reasonable tradeoff. The code phase error signal consists of an amplitude modulation of the carrier occurring at the dithering rate (25 Hz). The amplitude difference of the two components (early and late) is proportional to the code phase error; whereas, the sign of the two components (relative to the τ-dither reference signal) contains the polarity of the code phase error.

The code phase error signal is detected by the code loop during mode 2. The baseband envelope detected signal is passed through an up/down integrator which is controlled by the τ-dither reference. The polarity of the integrator output indicates whether a positive or negative phase adjustment to the code loop clock is required. The magnitude of the integrator output is input to a VFC (Voltage to Frequency Converter). The VFC output provides a phase correction to the code loop clock. This correction is applied at a fixed rate; the rate defines the code loop bandwidth.

6.2.2 Error Analysis

The essential elements which make up the GPS receiver are a Costas carrier tracking loop used for locking to the doppler shifted carrier, and a noncoherent delay-locked loop for locking to the pseudo random code transmitted by each satellite. The performance of each loop can be specified in terms of rms phase and delay jitter, respectively. In turn, each is a function of two components, input noise and user dynamics.

The phase-locked loop requires a higher signal-to-noise density ratio, S/N_0, than the delay-locked loop to maintain lock. Thus, one need only investigate the performance of the phase-locked loop to determine the minimum S/N_0 of the receiver. (This assumes that a phase-locked loop is needed to provide a coherent reference for data demodulation. Otherwise, if data demodulation is not required, the AFC frequency acquisition function of the GPSPAC receiver -- which can operate in a lower S/N_0 than the Costas loop -- will dictate the minimum S/N_0.)

With regard to user dynamics, the receiver configuration has eliminated the effect of vehicle dynamics on code loop performance by employing a common VCO design. Thus, user dynamics impact the performance of the GPS receiver by affecting the Costas loop. Coupled with the previous observation on minimum S/N_0, this suggests that preliminary analysis need only be concerned with the performance characteristics of the Costas loop. A complete, rigorous investigation into the performance of the receiver should be performed at a later time.

The total allowable rms phase error of the Costas loop depends on the receiver function under consideration. A predefined range-rate accuracy will define a maximum rms phase error; this allowable error is referred to as the track threshold. However, independent of the track threshold, the loss-of-lock threshold defines an inherent upper bound on the rms phase error; loss-of-lock threshold is reached at an rms phase error of $\sigma_\phi = 0.25$ radians. (The Costas loop implementation tracks a double frequency carrier which would then have a 0.5 radian rms error; 0.5 radian is considered the loss-of-lock threshold for a phase-locked loop.)

The total rms error of the Costas loop is composed of two terms. The first, σ_{ϕ_n}, is a result of input noise, and the second, σ_{ϕ_d}, is due to user dynamics. The total rms error is given by

$$\sigma_\phi = \left(\sigma_{\phi_n}^2 + \sigma_{\phi_d}^2\right)^{1/2} \qquad (6.2\text{-}1)$$

As is shown in the following section, for a fixed S/N_o narrowing the loop bandwidth will tend to improve tracking performance by decreasing the effective noise. However, the useable bandwidth is bounded from below by the user's dynamic motion; this is discussed in Section 6.2-2.

Oscillator instability errors have also been investigated, and, for the nominal Costas loop bandwidth, the rms phase error was found to be on the order of 1 mrad. With regard to vibration-induced fluctuations, these need not be a serious problem in the system under consideration. Note, in particular, that the Costas loop noise bandwidth is rather wide (B_L = 35 Hz) and phase fluctuations below the loop cutoff are tracked out by the loop. If necessary, it would be a relatively simple matter to provide damping and isolation to a small oscillator for mechanical vibration frequencies above, say, 10 Hz.

Noise Error - The Costas loop error variance is of the form

$$\sigma_\phi^2 = \left[\frac{N_o}{S} B_L\right] S_L^{-1} \qquad (6.2\text{-}2)$$

where B_L is closed-loop single-sided bandwidth, S/N_o is the equivalent signal-to-noise density assuming all correlation losses and other factors, and S_L is defined to be the squaring loss associated with a squaring type phase-locked loop (such as a Costas loop). The squaring loss would be equal to unity for the common phase-locked loop. However the GPS data modulation results in a suppressed carrier which can only be tracked by a squaring-loop method.

The squaring loss is defined by

$$S_L = \left[1 + K_L \frac{N_o}{S} \frac{B_{LP}}{2}\right]^{-1} \qquad (6.2\text{-}3)$$

where K_L is a function of the type of low-pass filter employed (see Fig. 6.2-3) and B_{LP} is the 3 dB single-sided bandwidth of the low-pass filter. K_L is equal to 5/6 assuming the low-pass filters are third-order Butterworth. Thus, the noise variance is given by

$$\sigma_{\phi_n}^2 = \frac{N_o}{S} B_L \left[1 + \frac{5}{6} \frac{N_o}{S} \frac{B_{LP}}{2}\right] \qquad (6.2\text{-}4)$$

The value for B_{LP} is constrained by the presence of the 50 baud data. Given that

$$B_{LP} = 200 \text{ Hz}$$

$$B_L = 35 \text{ Hz}$$

and

$$\sigma_\phi \text{ unlock} = 0.25 \text{ radians}$$

eq. 6.2-4 can be solved for the minimum equivalent signal-to-noise density in the absence of other disturbances. This is roughly $(S/N_o)_{min}$ = 28 dB-Hz; Fig. 6.2-4 plots σ_{ϕ_n} versus S/N_o. Thus, the minimum signal-to-noise density at the receiver input, $S/N_{o\ input}$, (allowing for such factors as cable losses) is somewhere in the vicinity of 30 dB-Hz.* In the presence of dynamic errors, larger values of S/N_o are required to maintain lock; this is discussed in the following section.

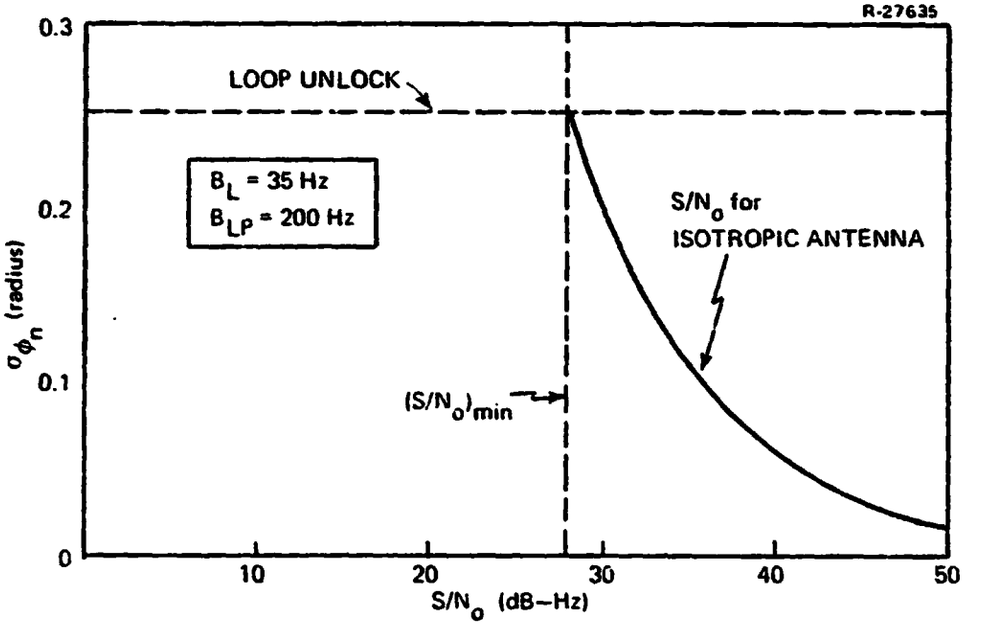

Figure 6.2-4 RMS Phase Error Versus Signal-to-Noise Density

Dynamic Errors - The phase error for a phase-locked loop (in the frequency domain) is given by the expression,

*Given a 35 Hz filter bandwidth, these values can be converted to the more familiar signal-to-noise ratio by subtracting 15.5 dB.

$$\theta_e(s) = \frac{s\theta_i(s)}{s + K_o K_d F(s)} \qquad (6.2\text{-}5)$$

where F(s) is the carrier loop filter (Fig. 6.1-2), K_d is the phase detector gain, K_o is the VCO gain constant, and $\theta_i(s)$ is the Laplace transform of the input phase.

If the input is a step change in frequency of magnitude $\Delta\omega$ (equivalent to a step change in velocity), then $\theta_i(s)$ is a phase ramp; i.e., $\theta_i(s) = \Delta\omega/s^2$. The steady-state error is given by the final value theorem of Laplace transforms,

$$\lim_{t\to\infty} y(t) = \lim_{s\to 0} s\,Y(s) \qquad (6.2\text{-}6)$$

Thus,

$$\lim_{t\to\infty} \theta_e(t) = \lim_{s\to 0} \frac{\Delta\omega}{s+K_o K_d F(s)} = \frac{\Delta\omega}{K_v} \qquad (6.2\text{-}7)$$

Where K_v is the dc loop gain and is given by the expression

$$K_v = K_o K_d F(0) \qquad (6.2\text{-}8)$$

The resulting error is the steady state velocity error, σ_{ϕ_v}. For an active filter in a second-order loop, F(0) = A, where A is the dc gain of an operational amplifier.

When the error is due to a doppler shift (and not to an actual difference between transmitter and receiver frequencies). σ_{ϕ_v} is given by

$$\sigma_{\phi_V} = \frac{2\pi f_c}{c} \frac{\dot{r}}{K_V} \text{ radians} \qquad (6.2\text{-}9)$$

where $\dot{r}$ is the relative range-rate along the line-of-sight and c is the speed of light. The loop gain, K_V, has not been specified; however, it can be shown that a reasonable choice for the loop gain is on the order of 10^4 to 10^5.

Assuming a value of $K_V = 5 \times 10^4$, Fig. 6.2-5 shows the linear relationship between σ_{ϕ_V} and $\dot{r}$. (For different values of K_V the slope scales inversely with K_V.) The maximum velocity uncertainty before the loop unlocks is obviously a function of S/N_o (see Eqs. 6.2-1, 6.2-2). This relationship is shown in Fig. 6.2-6. For S/N_o less than ~28 dB-Hz the loop unlocks due to noise alone; i.e., independent of velocity uncertainty. The steady state analysis would indicate that as the signal level increases larger velocity errors can be tolerated -- up to a maximum of 373 m/sec for the high S/N_o case. (This result is conditioned on there being no other dynamics involved and on a loop gain of 5×10^4). Since velocity errors are expected to be on the order of 10 m/sec, Fig. 6.2-6 implies that the velocity uncertainty has negligible impact on defining $(S/N_o)_{min}$. However, it should be noted that if such a large velocity step were applied, the loop would actually skip cycles for a while following the input transient, before locking up again. While the carrier loop is cycle slipping. velocity measurements are meaningless. The maximum velocity step which can be tolerated without cycle slipping is proportional to the carrier loop bandwidth; for a bandwidth of 35 Hz, the velocity step must be less than ~7 m/sec.

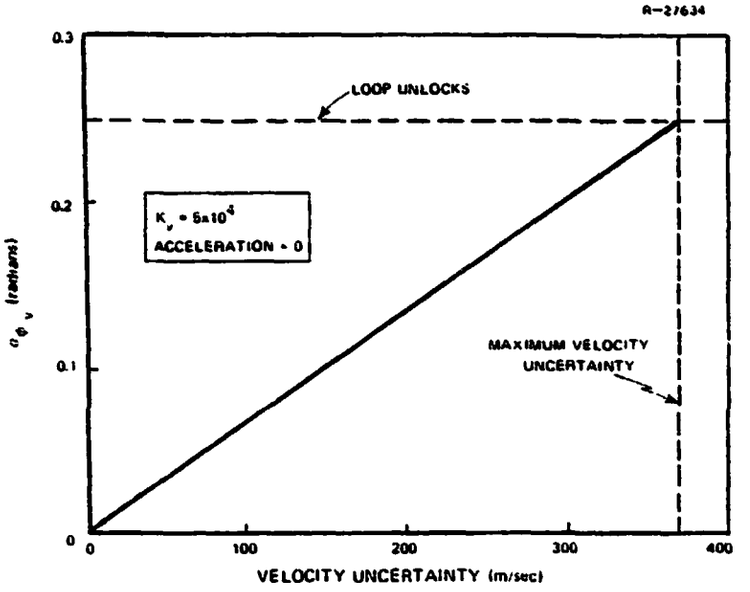

Figure 6.2-5 RMS Phase Error Due to Velocity Uncertainty

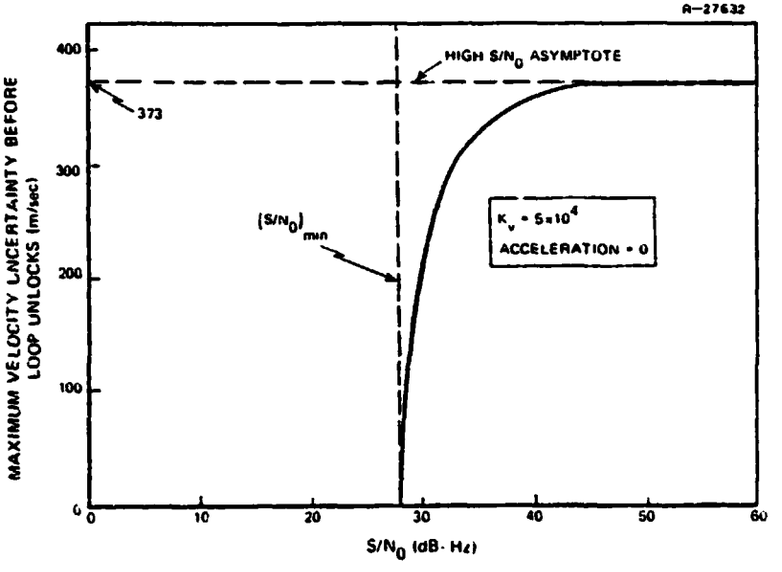

Figure 6.2-6 Maximum Velocity Uncertainty Before Loop Unlocks Versus S/N_0

For sufficiently large gain the steady state velocity error can be made quite small. However, a second-order loop, will produce a steady state phase error due to acceleration even for infinite gain. In particular, for infinite gain the phase error (defined by Eq. 6.2-5) in a second-order loop can be written in the form

$$\theta_e(s) = \frac{s^2\theta_i(s)}{s^2 + 2\,\xi\omega_n s + \omega_n^2} \qquad (6.2\text{-}10)$$

where ω_n is the natural frequency of the loop and ξ is the damping coefficient. If the input frequency is changing linearly at a rate $\dot{\Delta}\omega$ rad/sec^2 due to an acceleration, then the input phase is $\theta_i(s) = \dot{\Delta}\omega/s^3$. This leads to the steady state acceleration error, σ_{ϕ_a},

$$\sigma_{\phi_a} = \lim_{t\to\infty} \theta_e(t) = \lim_{s\to 0} \frac{\dot{\Delta}\omega}{s^2 + 2\xi\omega_n s + \omega_n^2} \qquad (6.2\text{-}11)$$

$$= \frac{\dot{\Delta}\omega}{\omega_n^2}$$

The natural frequency, ω_n, can be related to the bandwidth of the loop by the expression

$$\omega_n = 2B_L / \xi\left(+ \frac{1}{4\xi}\right) \qquad (6.2\text{-}12)$$

where the damping coefficient is given as $\xi = 0.707$. Thus, substituting this expression into Eq. (6.2-11)

$$\sigma_{\phi_a} = \frac{2\pi f_c}{c} \frac{9}{8} \frac{\ddot{r}}{(2B_L)^2} \text{ radians} \qquad (6.2\text{-}13)$$

where $\ddot{r}$ is relative acceleration along the line-of-sight.

Assuming a bandwidth of 35 Hz, Fig. 6.2-7 shows the linear relationship between σ_{ϕ_a} and $\ddot{r}$. (The slope scales inversely with B_L^2). Again, the maximum allowable acceleration uncertainty before the loop unlocks is a function of S/N_o. This relationship is shown in Fig. 6.2-8. Notice that even for infinite S/N_o the maximum acceleration uncertainty must be less than 32.5 m/sec^2 (assuming no additional phase error due to velocity errors). The acceleration tolerance of the Costas loop can be increased beyond those values indicated by Fig. 6.2-8 by either:

- Rate-aiding the receiver
- Increasing the loop bandwidth, B_L
- Replacing the second-order loop with a third-order loop.

The phase error due to acceleration decreases with increasing B_L since σ_{ϕ_a} is proportional to $1/B_L^2$. The disadvantage of an increased B_L is primarily a decrease in noise tolerance. A B_L of 43 Hz seems to be a reasonable compromise. This would provide marginally acceptable loss-of-lock performance in a 5 g environment. The advantage of a third-order loop is that it has zero steady state phase error due to uncompensated acceleration errors. However, the pull-in behavior when the VCO is not initally tracking the signal is less stable than that of a second-order loop. This disadvantage could potentially be offset by the AFC acquisition circuitry in the receiver (Fig. 6.2-2).

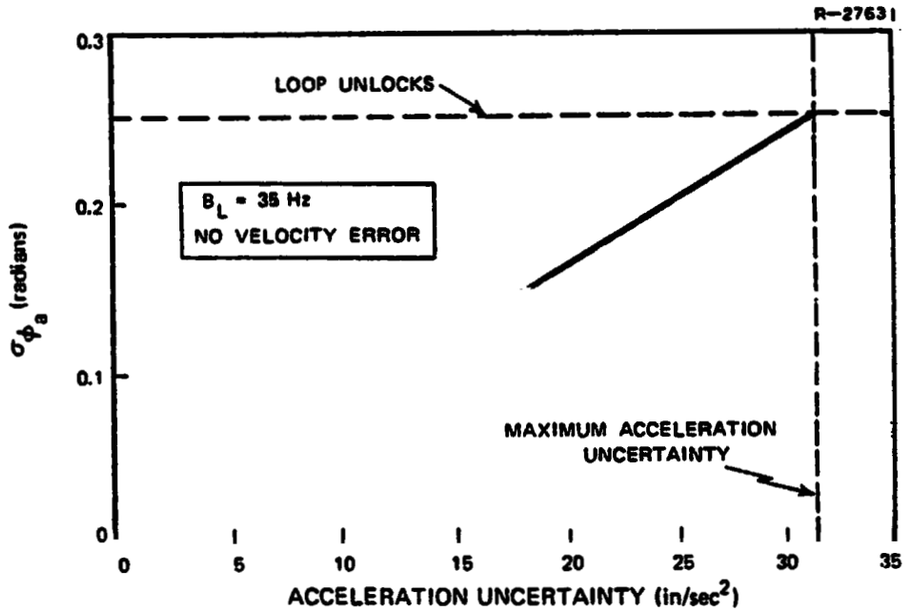

Figure 6.2-7 RMS Phase Error Due to Acceleration Uncertainty

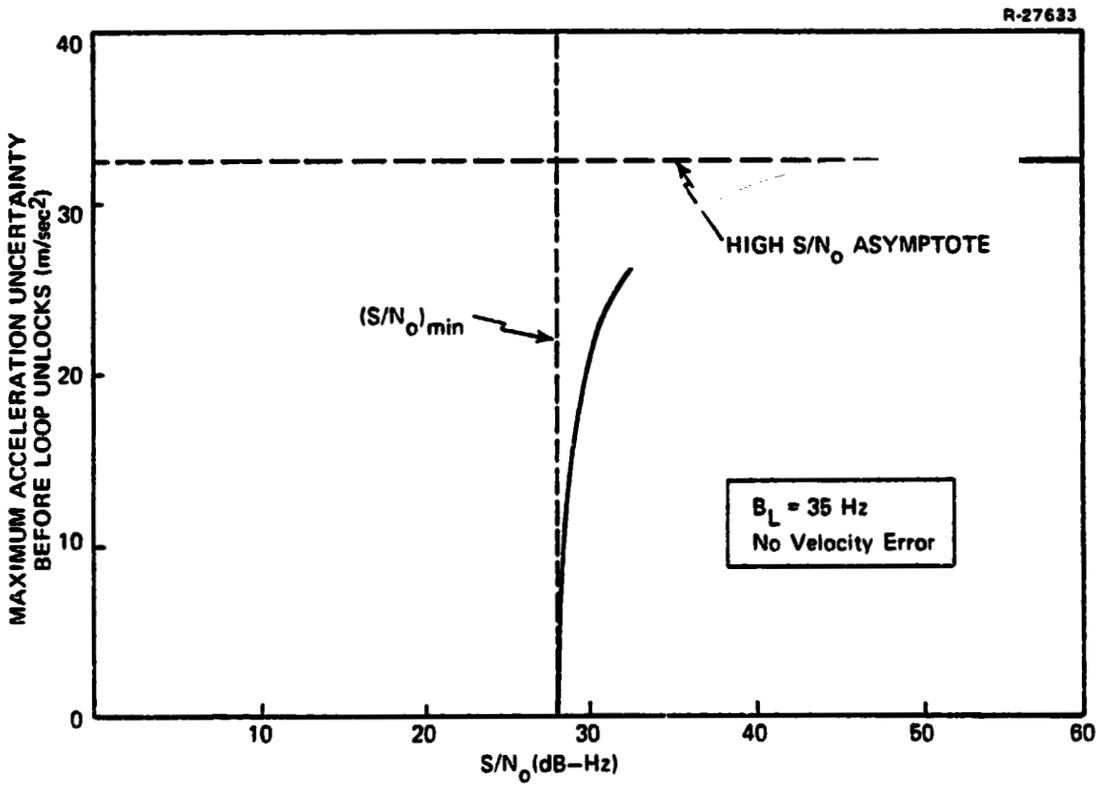

Figure 6.2-8 Maximum Acceleration Uncertainty Before Loop Unlocks Versus S/N_o

6.2.3 Summary

The proposed GPSPAC receiver utilizes a single IF and VCO which is common to both the carrier and code tracking loops. The common IF design is accomplished by time-sharing the two tracking loops. Further hardware is eliminated by generating the code phasing error signal using τ-dithering. The advantages of this implementation are:

- The common VCO design eliminates vehicle dynamics from the loop as well as minimizing hardware
- τ-dithering minimizes hardware while eliminating the problems associated with two channel gain imbalances.

The disadvantages are:

- The common IF design can result in errors due to vehicle dynamics during the time interval dedicated to the code loop
- There is a 3 dB degradation in the code loop signal-to-noise due to τ-dithering.

The Shuttle performance specifications require subsystem operation in a 5 g environment. The dynamic error analysis presented in Section 6.2.2 indicates the acceleration tolerance of the GPSPAC in this environment is, at best, marginal. The acceleration tolerance can be increased by either:

- Rate-aiding the receiver
- Increasing the loop bandwidth
- Replacing the second-order loop with a third-order loop.

Increasing the loop bandwidth to 43 Hz would keep the Costas loop in lock for acceleration uncertainties as great as 5 g while raising the minimum usable signal-to-noise by only 1 dB. A third-order loop has zero steady states phase error due to acceleration; however, its pull-in behavior is not as stable as that of a second-order loop. Further analysis is required to determine the most desirable alternative.

7. SUMMARY AND CONCLUSIONS

This report addresses a number of system implementation and performance issues associated with the possible use of GPS as a navigation aid for the Space Shuttle. While each of the preceding seven chapters has a separate conclusions section, the more important results and conclusions of this study are summarized here for convenience.

7.1 NAVIGATION WITH PHASE I AND II GPS

Depending upon the final schedules for both the Orbiter and for the GPS system, there may be a period of several years when GPS user equipment is aboard the Shuttle but the fully operational, Phase III GPS constellation of satellites is not yet in place. The reduced coverage provided by the Phase II GPS constellation of six (or perhaps even fewer) satellites places some serious limitations on the ability of the Shuttle to navigate with GPS. The visibility (satellite signal availability) studies presented in this report are an important prelude to the navigation accuracy studies. Visibility patterns depend upon receiving antenna coverage, as well as on masking by the earth, and vary considerably with Shuttle flight phase and, for the incomplete Phase I and II constellations, with "time of day."

Figure 7.1-1 shows a typical visibility product for the reentry phase, assuming a six satellite constellation. The vertical axis is time during the flight phase, while the horizontal axis is essentially "time-of-day." Since three or four satellites are necessary for reasonable navigation during

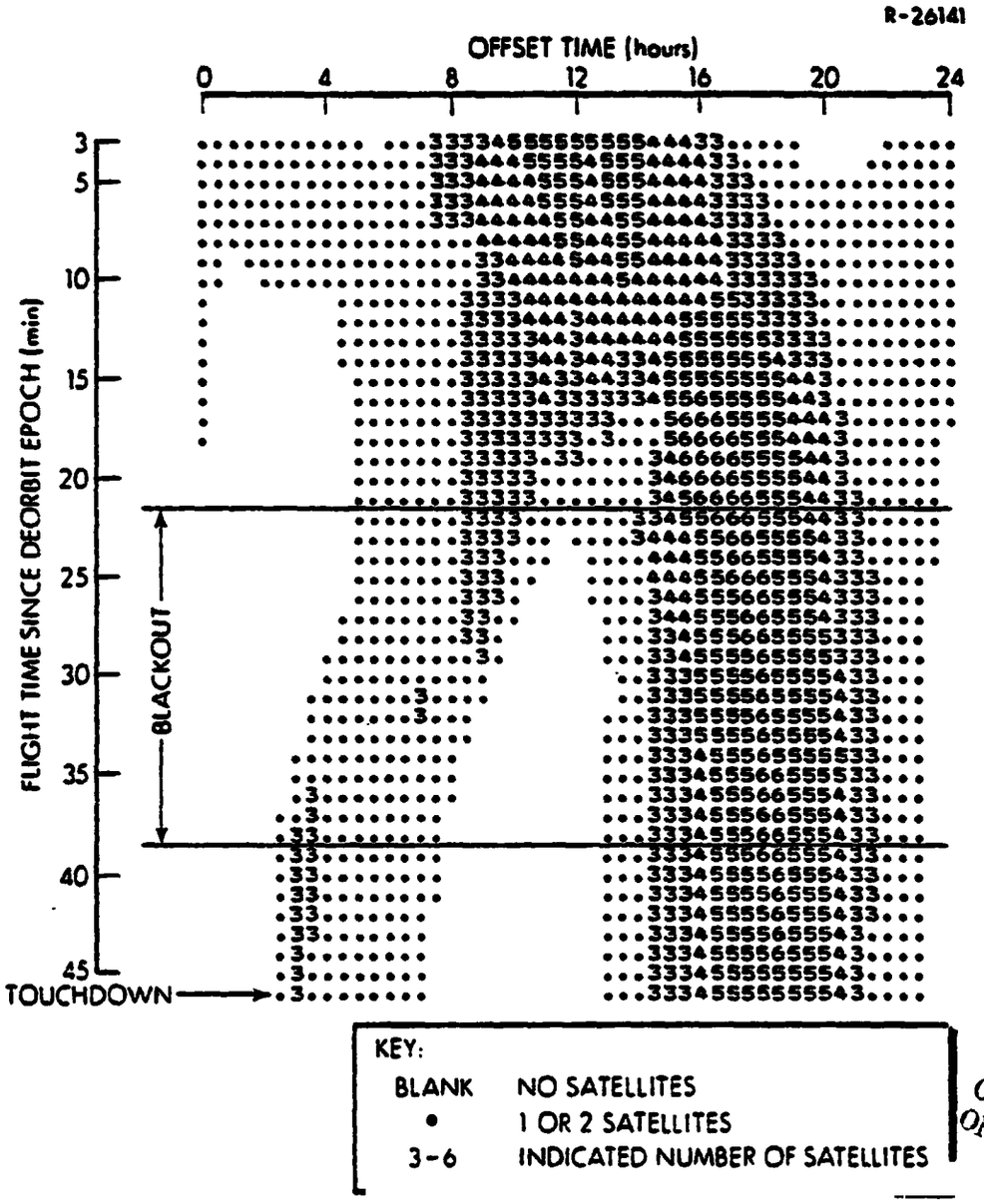

Figure 7.1-1 Satellite Visibility During the Deorbit Phase as a Function of Offset Time

a dynamic flight phase, the figure illustrates that the early GPS constellations will be capable of supporting reentry only during a short portion of each day.

C-3

On-orbit visibility patterns demonstrate a periodicity roughly comparable to the orbital period. Figure 7.1-2 shows a statistical summary for a particular orbit (at one time slated for mission OFT-5) with a six satellite constellation. Three or more satellites (which will provide high accuracy orbital navigation) are available more than half of the time. Possible changes to the Phase II constellation to reduce it to four satellites would reduce the three-satellite visibility to about one third of the time.

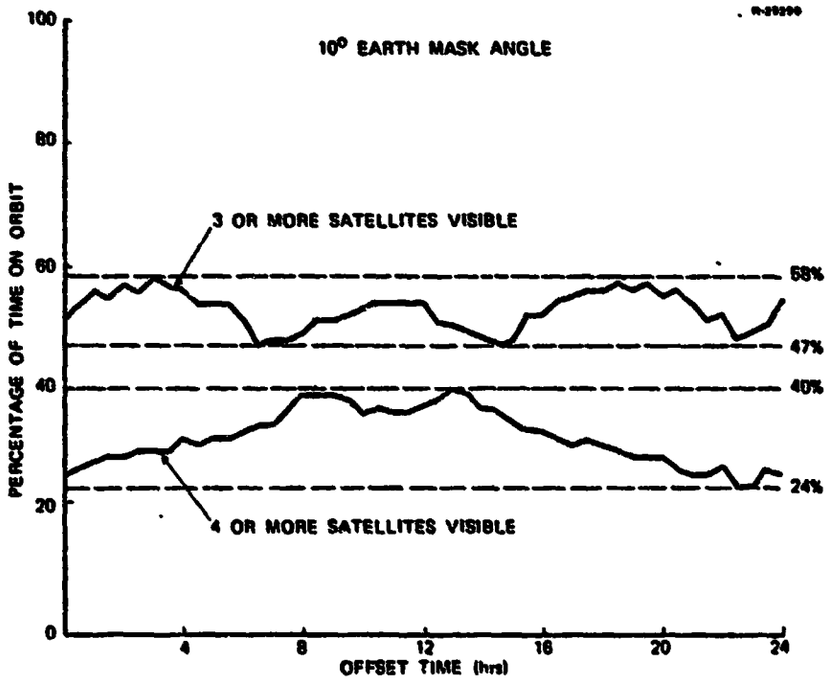

Figure 7.1-2 Percentage Visibility for Typical Orbit as Function of Offset Time

Given one of the good visibility situations possible during reentry, the simulation results in Chapter 2 indicate that reasonable navigation accuracy is achievable. Figure 7.1-3 shows a typical result, with errors growing to about

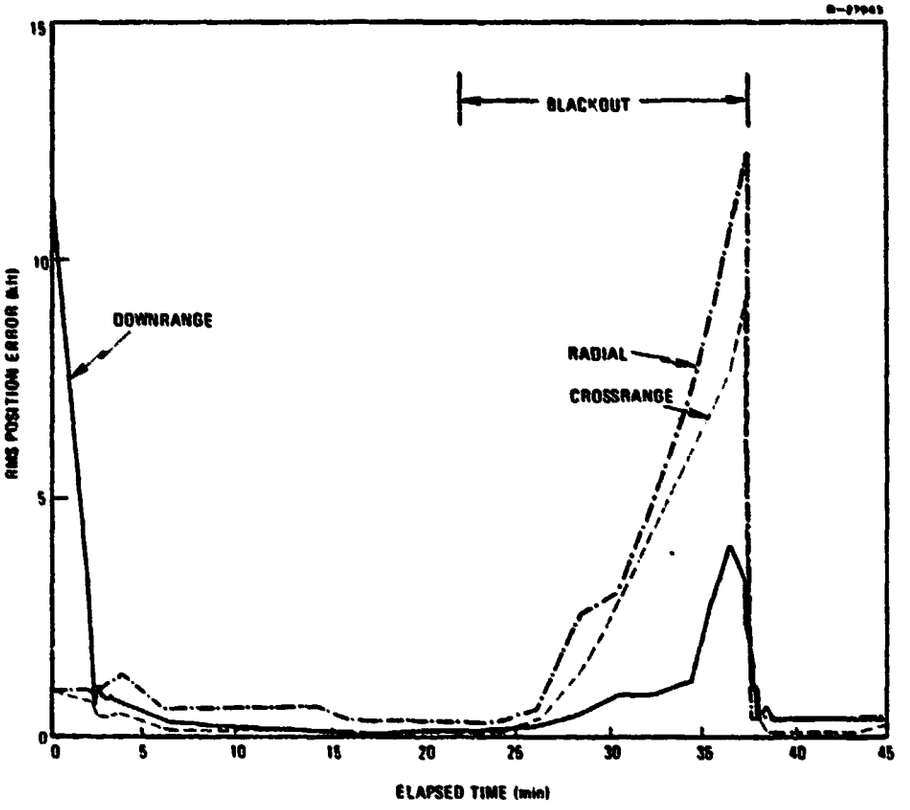

Figure 7.1-3 RMS Position Error versus Time for GPS-Aided Deorbit Navigation with Good Visibility Prior to Satellite Uploading

13000 ft (1σ) during the reentry blackout period during which no GPS signals are assumed available, but being well controlled at other times. Various navigation filter mechanizations were evaluated in this study, with an eleven state filter (incorporating IMU platform misalignments along with the usual vehicle vector position and velocity and the clock phase and frequency states) proving adequate. Drag update measurements (part of the current Shuttle baseline) could control the error buildup during blackout.

Orbital navigation performance, on the other hand, is generally quite good at all times, even with only a six satellite constellation. Figure 7.1-4 shows a typical result. Here too, errors grow during periods when no satellite signals are available, but they grow much more slowly and typically peak at less than 1000 ft (1σ). Low level thrusting on orbit due to venting of liquids and to attitude jet usage is the dominant contributor to this error growth. During periods of good visibility (three or more satellites in view) orbital navigation errors are in the area of 100 ft (1σ) in position and 0.2 ft/sec (1σ) in velocity.

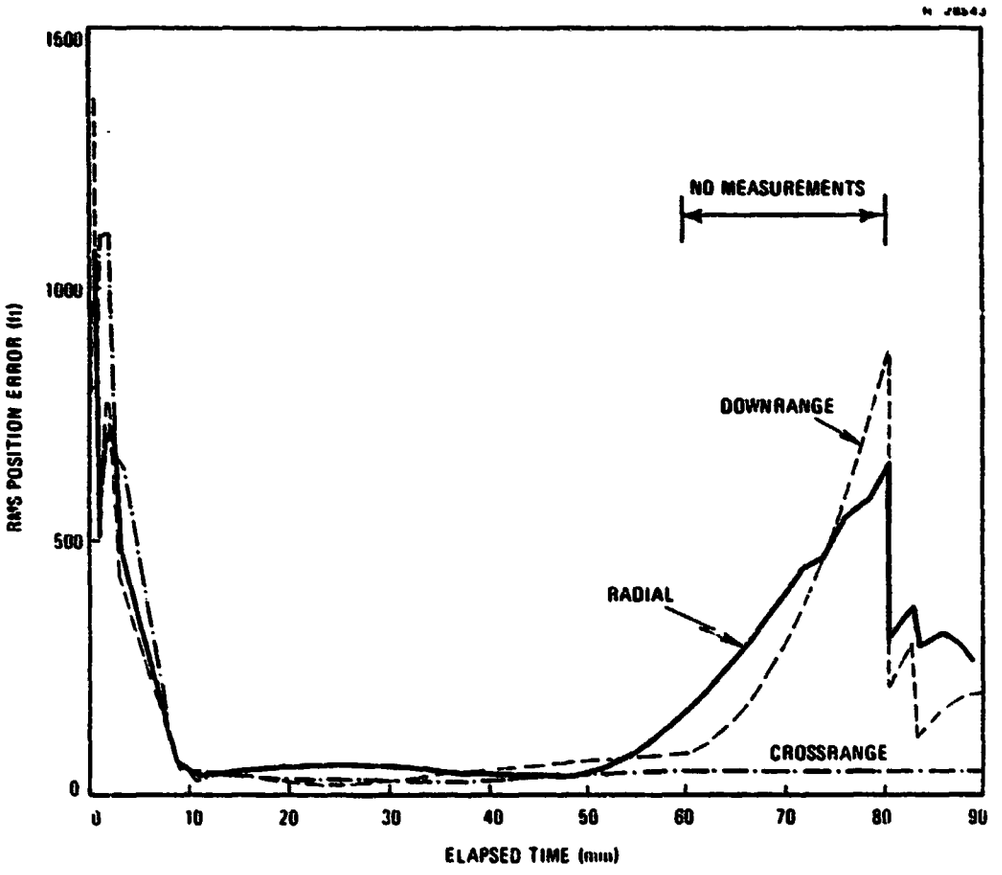

Figure 7.1-4 Orbital Navigation: RMS Position Error Versus Time

Surprisingly, even a single GPS satellite could provide useful navigation information to the Space Shuttle on orbit. Figure 7.1-5 illustrates a typical situation. During periods when the satellite is visible, denoted by the solid bar beneath the time scale, position errors are reduced to the 300-600 ft (1σ) level. During periods of no visibility, downrange position errors climb to 4500 ft. The situation when the Shuttle orbit is coplanar with the GPS satellite orbit is a singular one, not typical, wherein crossrange errors would not be controlled. Velocity errors in the typical case range from about 0.5 ft/sec during periods of visibility to 4.5 ft/sec when the satellite is out of view.

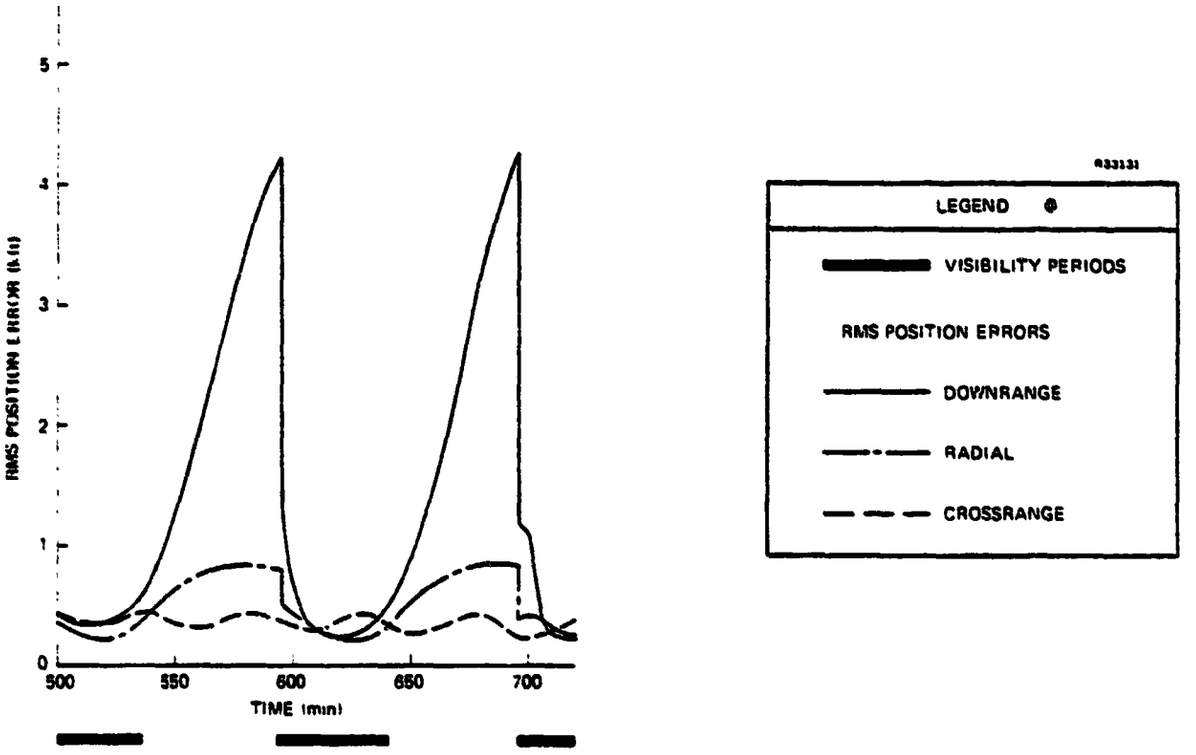

Figure 7.1-5 Typical Single Satellite Navigation Errors

7.2 POST-BLACKOUT NAVIGATION WITH PHASE III GPS

The post-blackout period during Shuttle reentry is one of the most severe for GPS user equipment and may drive many of the ultimate specifications for the antenna/preamp/receiver/processor equipments. Even with a 24 satellite, Phase III constellation, only three GPS satellites may be visible to the Orbiter GPS antennas following blackout. Further, it is undesirable to wait 30 or 60 extra seconds while a one or two channel sequential receiver demodulates navigation data from four satellites. The performance results presented in Chapter 4 verified that an atomic time standard will substitute for one satellite, in terms of visibility, while processor storage for navigation data from all 24 satellites will usually solve the data gathering time problem. Table 7.2-1 summarizes typical post-blackout navigation performance after each of the first four GPS measurements (to different satellites) are processed by a sequential (single channel) receiver, and parameterizes on the clock type. Beyond the conclusions already noted, it was also discovered that the post-blackout velocity errors cannot be further reduced below the 1.0 ft/sec level unless IMU platform misalignments are modeled in the navigation filter.

7.3 GPS GROUND TRANSMITTERS FOR SPACE SHUTTLE SUPPORT

Before the full GPS constellation of satellites is available, there will rarely be enough coverage to provide GPS navigation during reentry. Even with the full constellation, antenna blockage by the main fuel tank will hamper GPS use during ascent. Ground GPS transmitters to augment the satellite constellation would be a way of filling these coverage gaps. Several transmitters would be required to support either ascent or reentry, use of transmitters might interfere with the

TABLE 7.2-1
POST-BLACKOUT NAVIGATION PERFORMANCE

CLOCK TYPE	RMS VECTOR ERROR	AFTER PROCESSING GPS MEASUREMENTS TO			
		1 SATELLITE	2 SATELLITES	3 SATELLITES	4 SATELLITES
Quartz	Position (ft)	13000	5000	1500	60
	Velocity (ft/sec)	40	14	2	1.5
Rubidium	Position (ft)	13000	5000	30	25
	Velocity (ft/sec)	40	14	1.0	1.0

satellite signals to the Orbiter or to other GPS users, would impose severe design restraints in the Orbiter receiver due to the high signal dynamics associated with nearby signal sources. Other alternatives (such as varying the Orbiter attitude profile) may be available to solve the ascent problem, and the reentry problem is a temporary one. For all these reasons, ground transmitters do not appear desirable for Shuttle support.

7.4 GPS RECEIVER SUBSYSTEM ANALYSIS

GPS signal acquisition and reacquisition processes may be time consuming for a sequential receiver with only one or two channels. The time required to establish a navigation fix is referred to as the time-to-first-fix (TTFF), and may depend on the users á priori knowledge of position and time as well as on the signal-to-noise density ratio. Figure 7.4-1 summarizes one important component of TTFF, the time required to acquire the C/A code.

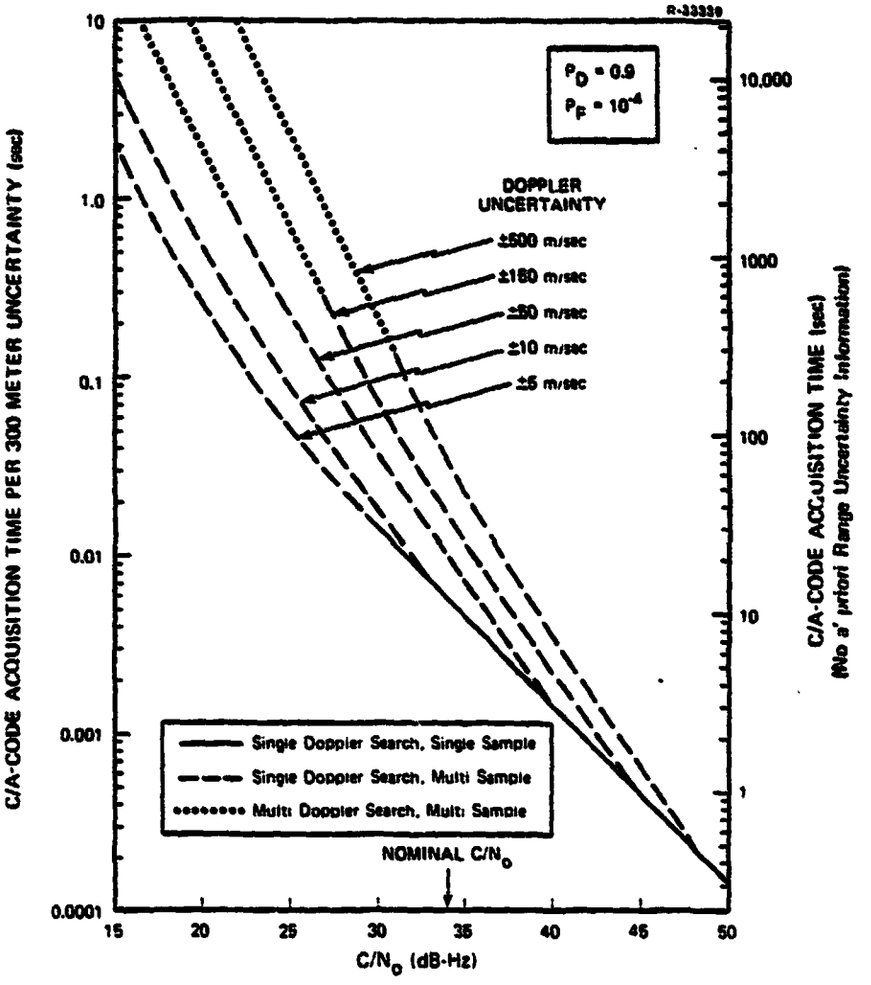

Figure 7.4-1 Time to Acquire/Reacquire the C/A-Code as a Function of C/N_0, and Position and Velocity Uncertainties

To the C/A acquisition time must be added about 10 sec to process the C/A signal sufficiently to acquire the precise P-code and to track the P-code for a navigation measurement. An additional 30 sec is required if the navigation data message superimposed on the codes must be interpreted. It must be remembered that four such measurements are typically

required for a navigation fix, but that the receiver may have more than one channel working at a time.

The receiver signal tracking process was addressed by considering a specific design, that of the GPSPAC receiver currently being designed for space application. That receiver utilizes a single IF and VCO common to both the carrier and code tracking loops, time sharing the two loops. This design minimizes hardware and eliminates vehicle dynamics from the loop, but it allows vehicle dynamics to upset the carrier loop while the code loop is occupying the common IF stage, and it results in a 3 dB degradation in the code loop signal-to-noise. The dynamic analysis indicates that the loops are, at best, marginal for the Orbiter acceleration environment. They may be improved by rate-aiding the receiver (by using IMU outputs), by increasing the loop bandwidth, or by going to a third-order loop instead of the second-order loop currently envisioned.

APPENDIX A
RELATIVISTIC EFFECTS ON THE SPACE SHUTTLE GPS CLOCK

This chapter describes the relativistic effects on the rubidium time standard being considered for incorporation into the Space Shuttle GPS user equipment set. The relativistic effects are reviewed and then numerically evaluated for ascent, reentry blackout, and elliptical orbit flight segments. While the relativistic effects are generally small enough to ignore for purposes of navigating the Orbiter, under certain conditions they are large enough to be the dominant source of clock error if uncompensated. At these times, some adjustment should be made in the operation of the GPS-aided navigation algorithm. The simplest approach is to properly compensate for the relativistic effects at all times in the state propagation routines. It should be noted that the effects treated here are with reference to a ground-based observer at the north pole and are not adequate to compensate the Shuttle receiver clock relative to the various GPS satellite clocks.

A.1 RELATIVISTIC EFFECTS ON CLOCKS

An atomic time standard is a "proper clock" to an observer that travels with the clock. For that observer, the clock runs at a constant frequency within its statistical limits of stability. To an outside observer, however, there are two relativistic effects that produce deterministic deviations from constancy in the clock frequency. One effect is known as "time dilatation" or as "second-order Doppler effect" and is related to the velocity of the clock with respect to the observer. A moving clock appears to run more slowly than a

clock at rest with respect to the observer. The second effect is known as "gravitational redshift" and is related to the difference in gravitational potential between the clock and the observer. A clock at a lower gravitational potential than the observer ("downhill" from the observer) appears to run more slowly than a clock at the observer's potential.

The normalized frequency offset observed for the clock due to the above effects is given approximately by (Ref. 31)

$$\frac{\Delta f}{f_o} = \frac{\Delta U}{c^2} - \frac{v^2}{2c^2} \qquad \text{(A.1-1)}$$

In this expression ΔU is the difference in gravitational potential between the clock and the observer, v is the magnitude of the velocity of the clock relative to the observer, and c is the velocity of light (in vacuo).

One interesting result of Eq. A.1-1 is that all clocks fixed on the geoid appear to run at the same rate when viewed from the north pole. On the geoid, the gravitational potential changes with latitude, but so does the velocity imparted by the earth's rotation, and the effects on clock frequency cancel.

For purposes of evaluating the relativistic effects on a GPS user clock it is useful to scale the normalized frequency offset into units of velocity (pseudo range-rate) by multiplying Eq. A.1-1 by the speed of light. The integral of the scaled, normalized frequency offset is the "accumulated

phase offset" to be denoted by ϕ and measured in units of distance (pseudo range).* Thus:

$$\frac{d\phi}{dt} = \frac{c\Delta f}{f_o} = \frac{\Delta U}{c} - \frac{v^2}{2c} \qquad \text{(A.1-2)}$$

The derivative, $d\phi/dt$, is referred to as the "phase rate offset."

Since a GPS user clock is synchronized in phase and frequency to GPS system time through the GPS measurements, nominal differences between the user clock and system time are not important. It is only changes in the clock behavior relative to GPS system time (during periods when GPS satellite signal availability is inadequate to maintain clock synchronization) that are important. For the Space Shuttle there are three different periods in which significant relativistic effects could potentially accrue.

One such period is the segment from launch to main engine cutoff (MECO). Because the external tank will obstruct the bottomside GPS antenna, and because the Shuttle flies upside-down during this period, no satellite signals may be available to either GPS antenna. The Orbiter gravitational potential and Orbiter velocity change markedly during launch, of course.

A second such period may occur during reentry when radio blackout will deny GPS signals to the antennas. Again, Orbiter gravitational potential and Orbiter velocity are changing rapidly at this time.

*Since the speed of light is roughly one foot per nanosecond, a one foot phase offset corresponds to a one nanosecond time offset, and a phase rate offset of one foot per second corresponds to a frequency offset of one part in 10^9.

The third period potentially impacted by relativistic effects on the GPS clock is a segment of an elliptic orbit with little or no satellite visibility. Since GPS user equipment is expected to be aboard the Shuttle in mid-1981 when only six GPS satellites will be in place, there will be significant visibility gaps on orbit. A complete visibility gap of one-half an orbit (about 45 minutes) will be possible. For a circular orbit, both the gravitational potential and the Orbiter velocity are constant, so there is no relativistic fluctuation in the clock frequency. Elliptic orbits do, however, produce relativistic fluctuations.

A.2 SPACE SHUTTLE ASCENT AND REENTRY BLACKOUT

To evaluate the relativistic effects on the clock during ascent and reentry blackout, it is necessary to have, in addition to Eq. A.1-2, an expression for the gravitational potential in the vicinity of the earth and relevant trajectory characteristics of the orbiter during these periods. The gravitational potential is given approximately by

$$U = -\frac{\mu}{r} \quad , \qquad \text{(A.2-1)}$$

where μ is the earth's gravitational constant, and r is the radial distance from the center of the earth to the point in question.

Calculation shows that the gravitational redshift of the clock is of little importance during ascent and reentry blackout. Table A.2-1 summarizes these results.

An OFT-1 simulated trajectory (Ref. 32) was used for the ascent segment. Total elapsed time from launch to MECO

TABLE A.2-1
GRAVITATIONAL REDSHIFT DURING ASCENT AND REENTRY BLACKOUT

PERIOD	EVENT	RADIAL DISTANCE (r) (ft)	PHASE RATE OFFSET (dφ/dt) (ft/sec)
ASCENT	LAUNCH	2.09099×10^{7}	0.0000*
	MECO	2.12903×10^{7}	0.0122
REENTRY BLACKOUT	ENTER	2.12097×10^{7}	0.0000*
	EXIT	2.10480×10^{7}	-0.0052

*Assumed point of clock calibration.

for this trajectory is 527 sec. The peak redshift phase rate offset is 0.0125 ft/sec, occurring at about 370 sec after launch, when the trajectory is at its maximum altitude for this segment. Altitude decreases somewhat before MECO, leading to the smaller offset value reported in Table A.2-1. The accumulated phase error from launch to MECO due to the redshift is less than 5 ft.

The standard deorbit trajectory first discussed in Section 2.2.2 was also used for the reentry blackout calculations. It is not certain just when the blackout will occur, so a conservative assumption was made that blackout will begin at 300 kft of altitude and end at 145 kft of altitude. A period of 890 sec elapses between these two altitudes. The peak redshift occurs at exit from blackout and is noted in Table A.2-1. The accumulated phase offset during blackout due to the redshift would be less than 3 ft.

The second-order Doppler shift effects during ascent and reentry blackout are not so small. Figure A.2-1 plots the

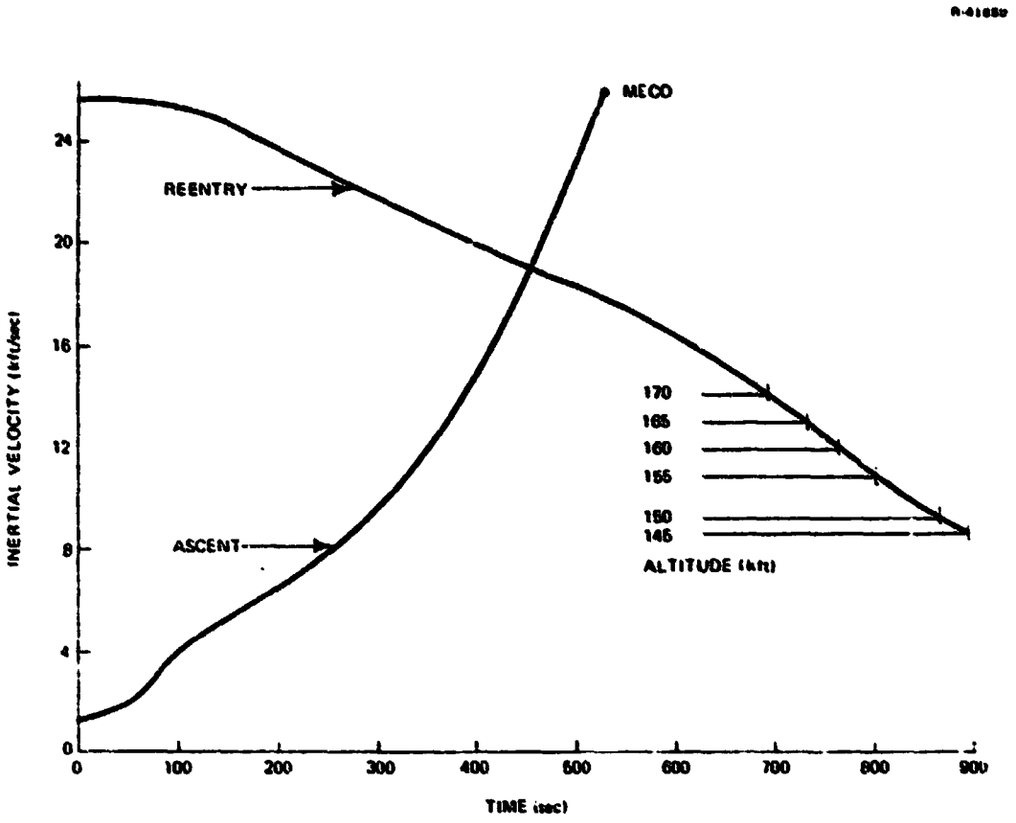

Figure A.2-1 Velocity versus Time for Ascent and Reentry Blackout

inertial velocity magnitude during these two flight segments. Because exit from blackout is uncertain, various terminal altitudes are noted on this and subsequent figures. (The initial altitude for blackout is still taken as 300 kft). Figure A.2-2 shows the resulting clock frequency offset due to the second-order Doppler shift, and Fig. A.2-3 plots the integrated clock phase offset. For both these latter figures the sign of the offsets during ascent is negative.

For purposes of comparison, the statistical phase error is plotted in Fig. A.2-4 for a typical rubidium clock calibrated to GPS system time aboard the Orbiter. Only one hour of elapsed time is shown in Fig. A.2-4, as longer time

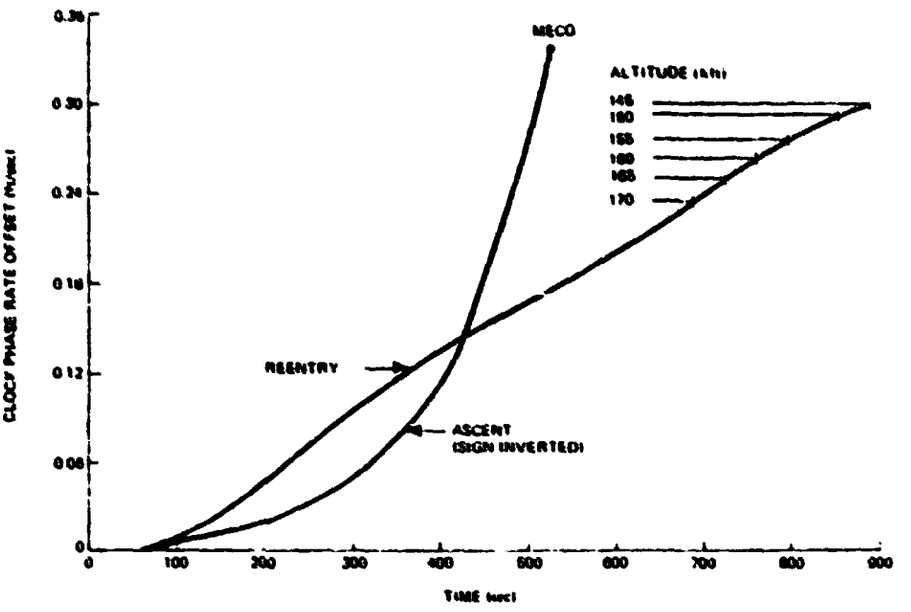

Figure A.2-2 Clock Phase Rate Offset Due to Second-Order Doppler Shift for Ascent and Reentry Blackout

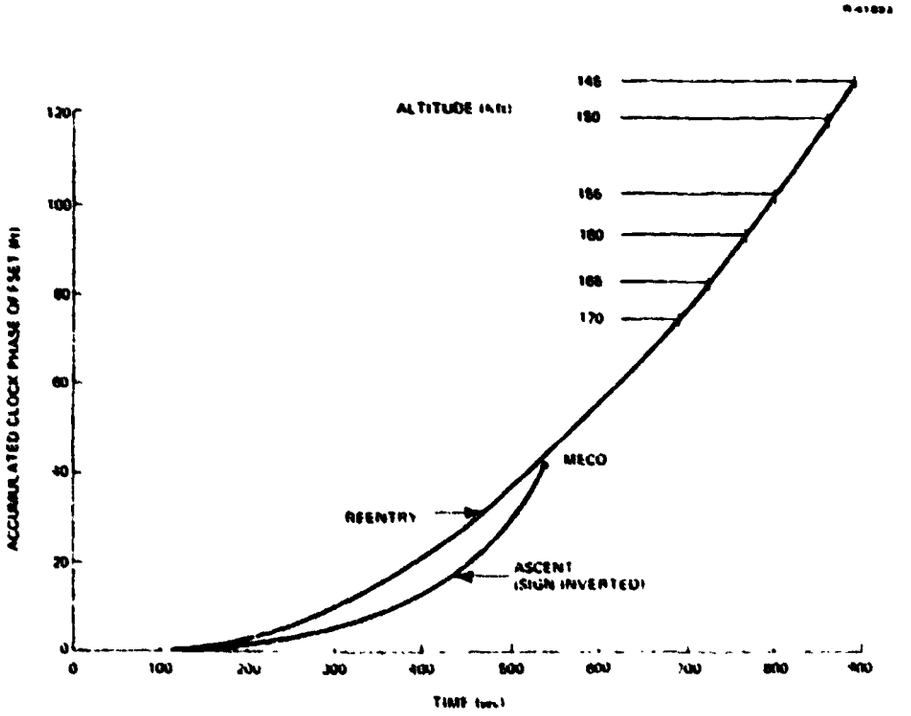

Figure A.2-3 Accumulated Clock Phase Offset Due to Second-Order Doppler Shift for Ascent and Reentry Blackout

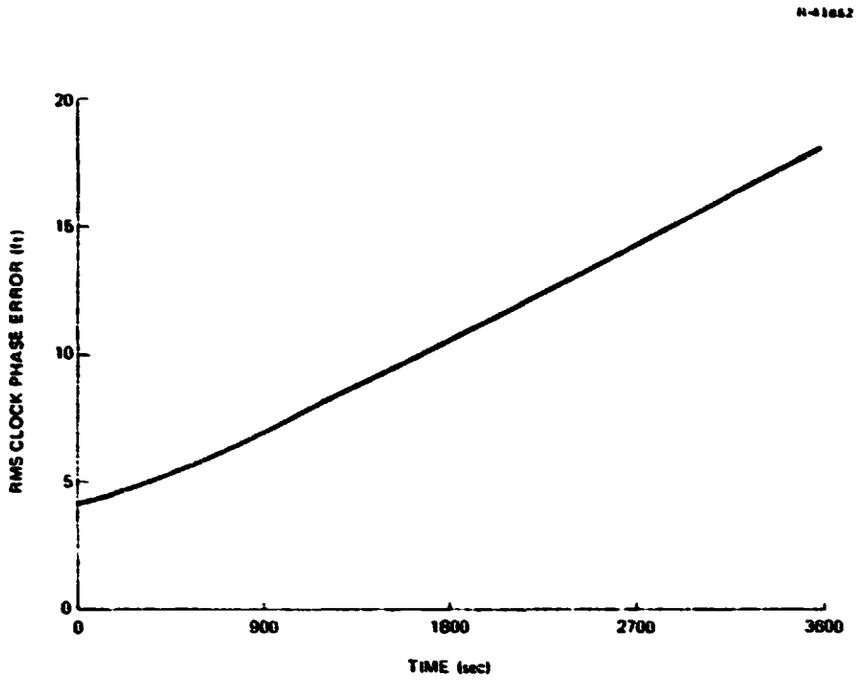

Figure A.2-4 Statistical Performance of a Rubidium Oscillator Calibrated to GPS Time Aboard the Orbiter

periods are generally not of interest for Orbiter navigation purposes. Over this short time period the statistical stability of the clock is much better than Fig. A.2-4 would indicate. The (1σ) clock errors shown are almost totally the result of errors in the initial calibration of the clock to GPS system time. Excellent satellite visibility and geometry, use of both the L_1 and L_2 satellite signals for ionospheric delay compensation, and use of Phase III GPS satellites should allow a user clock calibration on orbit to about 4 ft in phase and about 0.0046 ft/sec in frequency (1σ). These values, along with a five state stochastic model of typical rubidium oscillator performance, were used to generate Fig. A.2-4.

Clearly the relativistic clock effects during ascent and reentry blackout are larger than the expected errors due

to clock instability and calibration error. The subject of what to do about the relativistic effects is postponed until the effects on an elliptic orbit are examined.

A.3 RELATIVISTIC EFFECTS ASSOCIATED WITH ELLIPTIC ORBITS

The gravitational redshift is not important compared to the second-order Doppler shift during ascent and reentry blackout. On orbit, however, the two effects are of equal importance.

The square of the total velocity of a spacecraft in an elliptical earth orbit is given approximately by

$$v^2 = \mu\left(\frac{2}{r} - \frac{1}{a}\right) \quad , \qquad \text{(A.3-1)}$$

where "a" is the semimajor axis of the orbit. Since the clock is to be calibrated in orbit, it is only variations in the square of the velocity that produce second-order Doppler shift effects. These variations are inversely proportional to the radial distance of the orbiter, as Eq. A.3-1 states. The variations in the gravitational redshift are also inversely proportional to the radial distance, as Eqs. A.1-2 and A.2-1 jointly state. Inserting Eqs. A.2-1 and A.3-1 into expression A.1-2 for the total phase rate offset, it is apparent that the total effect is the sum of equal amounts of redshift and second-order Doppler shift, and the resultant effect is given by

$$\frac{d\phi}{dt} = \frac{2\mu}{c}\left(\frac{1}{r_o} - \frac{1}{r(t)}\right) \qquad \text{(A.3-2)}$$

In this expression, r_o is the radial distance to the spacecraft at the time of clock calibration, and the explicit dependence

of the radial distance to the spacecraft upon time has been noted.

It would be convenient to have a closed form expression for the dependence of the phase rate offset upon time. Equation A.3-2 does not provide such an expression because there is no closed form expression for the radial distance to a body in an elliptical orbit as a function of time. Equation A.3-2 is the "next best" expression, involving only the radial distance. A similarly useful expression is derived for the phase offset in the remainder of this section.

Clearly, the phase offset is the integral of Eq. A.3-2

$$\phi(t) = \frac{2\mu}{c}\left(\frac{t}{r_o} - \int_0^t \frac{dt}{r(t)}\right) , \qquad (A.3-3)$$

which may be rewritten as

$$\phi(t) = \frac{2\mu}{c}\left(\frac{t}{r_o} - \int_{r_o}^{r(t)} \frac{dr}{r(dr/dt)}\right) . \qquad (A.3-4)$$

For a body in an elliptical orbit of semimajor axis "a" and eccentricity "e",

$$\frac{dr}{dt} = \pm \sqrt{\mu\left[\frac{2}{r} - \frac{1}{a} - \frac{a(1-e^2)}{r^2}\right]} , \qquad (A.3-5)$$

which expresses dr/dt in terms of r for use in Eq. A.3-4. The upper (+) sign holds for that portion of the orbit from perigee to apogee, while the lower (-) sign holds for the remaining half.

The indicated integration in Eq. A.3-4 may be performed analytically by use of Eq. A.3-5. The result is

$$\phi(t) = \frac{2\mu}{c} \left\{ \frac{t}{r_o} \pm \sqrt{\frac{a}{\mu}} \left[\cos^{-1} \left(\frac{r(t)-a}{ae} \right) - \cos^{-1} \left(\frac{r_o-a}{ae} \right) \right] \right\} \tag{A.3-6}$$

This result is valid only over segments of an orbit wholly contained between apogee and perigee or vice versa.

To see how large $\phi(t)$ may grow in one half of an orbit, consider that the spacecraft is at apogee at time zero. That is

$$r_o = a(1 + e) \tag{A.3-7}$$

Then

$$\phi(t) = \frac{2\mu}{c} \left\{ \frac{t}{a(1+e)} - \sqrt{\frac{a}{\mu}} \cos^{-1} \left(\frac{r(t)-a}{ae} \right) \right\} \tag{A.3-8}$$

One half of an orbital period, T/2, later, the spacecraft is at perigee where

$$r(T/2) = a(1-e) \quad , \tag{A.3-9}$$

and

$$T = 2\pi a \sqrt{\frac{a}{\mu}} \quad . \tag{A.3-10}$$

Thus, at perigee

$$\phi(T/2) = - \frac{2\pi\sqrt{a\mu}}{c} \frac{e}{1+e} \quad , \tag{A.3-11}$$

$$\frac{d\phi}{dt}(T/2) = - \frac{4\mu}{ac} \left(\frac{e}{1-e^2}\right) \quad . \qquad \text{(A.3-12)}$$

For a numerical example, consider a deorbit trajectory with an apogee at 400 nm altitude and a perigee at the earth's surface. For this orbit (an extreme elliptical orbit for the Space Shuttle)

$$a = 2.214086 \times 10^7 \text{ ft},$$

$$e = 5.488599 \times 10^{-2},$$

$$T = 5517 \text{ sec (92 min)}.$$

and

$$\phi(T/2) = -185.6 \text{ ft},$$

$$\frac{d\phi}{dt}(T/2) = -0.1423 \text{ ft/sec}.$$

Again, comparison with Fig. A.2-4 shows that the relativistic effects are larger by far than the likely clock errors due to instability.

A.4 CLOCK COMPENSATION FOR RELATIVISTIC EFFECTS

Comparing the relativistic clock effects during ascent, reentry blackout, or elliptical orbit with the statistical clock performance figures, it is clear that the inherent stability of the clock will not be achieved without compensation for the relativistic effects. For purposes of Orbiter navigation, however, the relativistic clock offsets should be tolerable without compensation, even though limited satellite visibility and poor geometry can multiply clock errors by a factor of 10 or more in producing navigation position and velocity errors (Chapter 4).

If, as is a virtual certainty, a Kalman (or Kalman-like) filter is used to process GPS measurements, then some accounting for the relativistic effects will be necessary for proper filter operation. The clock phase and frequency variances of the navigation filter will have to be sized to accommodate any uncompensated relativistic effects. To do otherwise would be to produce unrealistically small clock variance estimates at certain times, leading to improper filter operation and probably to the rejection of good measurement data at critical times. It is simpler to incorporate deterministic compensation for the relativistic effects than to (improperly) adjust the filter clock variances on special occasions.

The equations for compensating the clock for the relativistic effects are easily derived. Using ϕ to represent the clock phase (measured in units of distance) as before, and using f here to represent the clock phase rate (measured in units of velocity) then, clearly

$$\frac{d\phi}{dt} = f \quad , \tag{A.4-1}$$

$$\frac{df}{dt} = \frac{\mu}{cr^2}\frac{dr}{dt} - \frac{v}{c}\frac{dv}{dt} \quad . \tag{A.4-2}$$

In discrete form

$$f_1 = f_o + \frac{\mu}{cr^2}\Delta r - \frac{v}{c}\Delta v \quad , \tag{A.4-3}$$

$$\phi_1 = \phi_o + \frac{1}{2}(f_o + f_1)\Delta t, \tag{A.4-4}$$

where ϕ_o, f_o are the phase and phase rate before the time step Δt, and ϕ_1, f_1 are the phase and phase rate after the time step. The new terms Δr and Δv refer to changes in the radial distance and in the total inertial velocity during the interval.

The addition of these simple compensation equations to the GPS R/PA navigation state propagation algorithm will reduce relativistic effects to a negligible level and will preserve the inherent capability of the onboard atomic time standard.

APPENDIX B
GPS DILUTION OF PRECISION

This chapter is a tutorial introduction to the subject of measures of dilution of precision (DOP) for the NAVSTAR Global Positioning System. Geometric (GDOP), position (PDOP), time (TDOP), horizontal (HDOP), and vertical (VDOP) dilutions of precision are discussed. After defining the DOP's for the normal case of measurements to four GPS satellites, the case of more than four measurements is treated. Coordinate invariance of GDOP, PDOP, and TDOP is demonstrated, and the singular situation when all satellites lie on a cone with apex at the user is introduced. To obtain a quantitative feel for the DOP's, a particular one-parameter geometric situation is examined in detail, and minimum values for the DOP's are established.

Section B.1 summarizes the motivation for performing DOP analysis. Section B.2 defines several measures of dilution of precision and also reviews the manner in which the GPS receiver generates and processes ranging measurements. Measurements to more than four satellites may be made, and Section B.3 addresses this issue. Some measures of dilution of precision do not depend on the coordinate systems used to compute them, a fact demonstrated in Section B.4. Certain geometrical situations are singular - they do not yield enough information to allow the user to solve for his position -- and Section B.5 identifies such situations. Section B.6 is devoted largely to an examination of one family of geometrical situations, a family with interesting properties for minimization of dilution of precision.

B.1 INTRODUCTION

The NAVSTAR Global Positioning System (GPS) is a satellite-based radio ranging navigation system scheduled to be operational in the mid-1980's. The transmitters are located in satellites in circular orbits of about four earth radii, having orbital periods of 12 hr and ground tracks that repeat once per day. Twenty-four satellites are planned for the operational GPS constellation, with fewer (five or six) to be initially available. Ranging signal transmission is in the L band, so signal reception is limited to "line-of-sight" visibility between user and satellite. (Clouds and weather will not block the signals, but the earth, the user's own vehicle, and other obstructions may.)

GPS users will need to measure one-way range (offset by user clock errors) to four or more satellites to determine their position. Since generally more than four satellites will be visible, a choice of satellites usually must be made. This choice, and the user position and time errors that result from it, depends upon the geometry of the satellites with respect to the user. The effect of the geometry is generally to dilute the precision available in any single ranging measurement, producing amplified user position and time errors. Errors along particular spatial orientations may be reduced instead of amplified, but the effect is still known as dilution of precision (DOP).

B.2 DEFINITION OF DILUTION OF PRECISION

A GPS receiver measures what are termed "pseudo ranges" to a number of GPS satellites (usually four, but possibly more) and then solves for the receiver position and time. Errors in the pseudo range measurements cause errors in the determined

position and time that are functions of the receiver-to-satellite geometry. Geometric dilution of precision (GDOP) and its relatives are scalar measures of the effect of measurement geometry in translating the pseudo range errors into receiver position and time errors. The dilution of precision values are useful because they reduce the effect of a complex geometric situation into a single number. The various DOP's have nothing to do, however, with the pseudo range measurement errors themselves, and they accurately describe the effect of measurement geometry only when certain restrictive assumptions concerning the statistics of the pseudo range errors are satisfied. This chapter is a tutorial attempt to explain the DOP's and demonstrate some of their properties.

A good place to begin this discussion is with an explanation of the measurement process itself. Figure B.2-1 is a conceptual diagram of the pseudo range measurement process. Each GPS satellite carries a clock that drives a signal generator producing a unique, pre-determined function of time. The receiver also incorporates a clock that drives a signal generator capable of mimicking any of the satellite signal generators. A key conceptual difference between the receiver and the satellite is that the receiver is capable of retarding the signal generator output by a variable time difference, ρ. The retarded, self-generated signal is compared in the receiver to the received satellite signal, and the time difference is continuously adjusted to keep the two signals in synchronism. At any time when the two signals are sufficiently in synch, a measurement of pseudo range may be made by simultaneously noting both the time difference, ρ, and the receiver time, t_r.

The GPS pseudo range measurement is essentially a measure of the time difference between transmission (from the satellite) and receipt (by the user) of the GPS signal. The

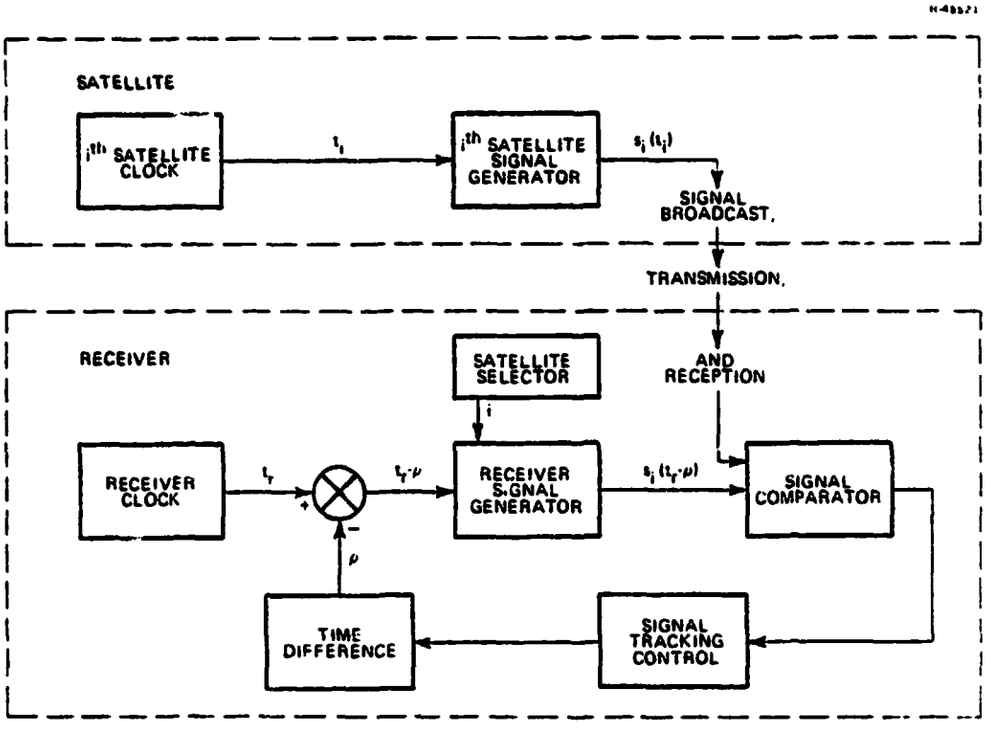

Figure B.2-1 Conceptual Diagram of GPS Pseudo-Range Measurement Process

measured time difference is the time it took the signal to travel from the satellite to the receiver, plus any offset in the receiver clock with respect to the satellite clock (plus any uncompensated signal processing delays in either the transmitter or the receiver). Assuming that the signal travels at the constant speed of light (making various corrections for ionospheric and tropospheric effects) and that the speed of light has been used to scale time intervals so they are measured in units of distance*, then

*The speed of light is nearly one foot per nanosecond, so a time interval of one nanosecond is measured as a pseudo-range of about one foot.

$$\rho_i = \sqrt{(x_r-x_i)^2 + (y_r-y_i)^2 + (z_r-z_i)^2} + \delta t_{ri}. \quad \text{(B.2-1)}$$

In this equation, ρ_i is the pseudo range to the i^{th} satellite; (x_i, y_i, z_i) are the position coordinates of the i^{th} satellite at the time, $t_r-\rho_i$, the signal was "sent"; (x_r, y_r, z_r) are the position coordinates of the receiver at the time, t_r, the signal was "received"); and δt_{ri} is the offset of the receiver clock with respect to the i^{th} satellite clock. The radical term is, of course, the true range from the satellite to the receiver.

Information transmitted along with the satellite signals allows the receiver to estimate both the position coordinates of any satellite at any time and the offset of any satellite clock with respect to GPS system time. The satellite clock offsets may be used to adjust the measured pseudo ranges so that they reflect the offset of the receiver clock from GPS system time, effectively removing the subscript i from δt_{ri} in Eq. B.2-1.

Equation B.2-1 thus contains four unknowns related only to the receiver position and clock offset: $(x_r, y_r, z_r, \delta t_r)$. Simultaneous measurements of pseudo range to four satellites will then allow the receiver to solve for its position and clock offset, provided that the measurement geometry is such that the four measurements supply four independent pieces of information.

The question remains: How are errors in the measured pseudo ranges related to errors in determined receiver position and clock offset? Differentiation of Eq. B.2-1 leads to an approximate linear relationship for th· errors

$$-\Delta\rho_i = u_{ix}\,\Delta x_r + u_{iy}\,\Delta y_r + u_{iz}\,\Delta z_r + \Delta t_r, \qquad \text{(B.2-2)}$$

where $\Delta\rho_i$ is the error in the i^{th} pseudo range, (Δx_r, Δy_r, Δz_r) are the coordinates of the resultant error in receiver position, and Δt_r is the resultant error in receiver clock offset. The new symbols, (u_{ix}, u_{iy}, u_{iz}), of Eq. B.2-2 are the components of the unit vector from the receiver toward the i^{th} satellite

$$\hat{u}_i = \begin{pmatrix} u_{ix} \\ u_{iy} \\ u_{iz} \end{pmatrix} = R_i^{-1} \begin{pmatrix} x_i - x_r \\ y_i - y_r \\ z_i - z_r \end{pmatrix}, \qquad \text{(B.2-3)}$$

where

$$R_i = \sqrt{(x_i - x_r)^2 + (y_i - y_r)^2 + (z_i - z_r)^2}\ . \qquad \text{(B.2-4)}$$

Clearly

$$\hat{u}_i^T\,\hat{u}_i = u_{ix}^2 + u_{iy}^2 + u_{iz}^2 = 1\ . \qquad \text{(B.2-5)}$$

The four necessary equations of the form of Eq. B.2-2, corresponding to pseudo range measurements to four satellites, may be combined into one matrix equation

$$A\,\vec{\Delta x} = \vec{\Delta\rho}\ , \qquad \text{(B.2-6)}$$

where

$$\vec{\Delta x} = \begin{pmatrix} \Delta x_r \\ \Delta y_r \\ \Delta z_r \\ \Delta t_r \end{pmatrix}\ , \qquad \text{(B.2-7)}$$

$$\vec{\Delta\rho} = \begin{pmatrix} -\Delta\rho_1 \\ -\Delta\rho_2 \\ -\Delta\rho_3 \\ -\Delta\rho_4 \end{pmatrix} , \qquad \text{(B.2-8)}$$

and

$$A = \begin{pmatrix} u_{1x} & u_{1y} & u_{1z} & 1 \\ u_{2x} & u_{2y} & u_{2z} & 1 \\ u_{3x} & u_{3y} & u_{3z} & 1 \\ u_{4x} & u_{4y} & u_{4z} & 1 \end{pmatrix} . \qquad \text{(B.2-9)}$$

(Note the inclusion of the minus signs in the definition of the vector of measurement errors, $\vec{\Delta\rho}$, for notational convenience.)

The statement that the four pseudo range measurements are independent is equivalent to the statement that the matrix A is invertible. Assuming such to be the case, the receiver errors are given by

$$\vec{\Delta x} = A^{-1} \vec{\Delta\rho} . \qquad \text{(B.2-10)}$$

The discussion now becomes statistical. Assuming that the expected (or mean) values of the pseudo range measurements are all zero, then the same is true of all elements of the receiver error vector, $\vec{\Delta x}$. Furthermore, the covariance of the receiver errors is given by

$$P = E\{\vec{\Delta x}\ \vec{\Delta x}^T\} = A^{-1}\ E\{\vec{\Delta\rho}\ \vec{\Delta\rho}^T\}\ A^{-T} , \qquad \text{(B.2-11)}$$

where E is the ensemble expectation operator, and A^{-T} is the transpose of the inverse of A. Assuming that the pseudo range

errors are independent of each other and have a common variance, σ^2, or

$$E\{\vec{\Delta\rho}\ \vec{\Delta\rho}^T\} = \sigma^2\ I \qquad \text{(B.2-12)}$$

(with I the 4×4 identity matrix), then the receiver error covariance matrix is given by

$$P = \sigma^2(A^TA)^{-1}\ . \qquad \text{(B.2-13)}$$

Assuming, further, that the pseudo range errors are normally distributed, then so are the receiver position and time errors, and Eq. B.2-13 provides a complete statistical description of the resultant receiver errors due to pseudo range errors.

To focus on the effect of the measurement geometry instead of on the pseudo range errors, the receiver error covariance matrix will be normalized by replacing the pseudo range variance, σ^2, in Eq. B.2-13 by unity. Thus,

$$P = (A^TA)^{-1}\ . \qquad \text{(B.2-14)}$$

To reduce further to a single number, define the geometric dilution of precision as

$$GDOP = \sqrt{tr(P)}\ , \qquad \text{(B.2-15)}$$

where the symbol tr stands for the trace of its matrix argument, that is, for the sum of the diagonal entries. GDOP is thus the root sum square (rss) of the errors in receiver position (on all three axes) and time offset, normalized to unit variance pseudo range errors.

GDOP is a useful descriptor of the geometric situation when all four receiver errors are of importance. Often this is not the case, and related DOP's are more useful. When only the three position errors are important, the useful descriptor is position dilution of precision

$$PDOP = \sqrt{P_{11} + P_{22} + P_{33}} , \qquad (B.2\text{-}16)$$

which is the (normalized) rss radial position error. If only the time is of importance, then time dilution of precision is given by

$$TDOP = \sqrt{P_{44}} , \qquad (B.2\text{-}17)$$

and is simply the (normalized) one-sigma clock offset error.

To go further requires particularization of the calculations to a local coordinate system at the receiver. If the coordinate system is chosen so that the z-axis is along the local vertical (putting the x- and y-axes in the horizontal plane), then horizontal and vertical dilutions of precision are defined as

$$HDOP = \sqrt{P_{11} + P_{22}} , \qquad (B.2\text{-}18)$$

$$VDOP = \sqrt{P_{33}} . \qquad (B.2\text{-}19)$$

B.3 MORE THAN FOUR MEASUREMENTS

The discussion to this point has proceeded as if exactly four independent pseudo range measurements were always made. With fewer than four measurements, Eqs. B.2-2 cannot be solved due to insufficient data. Conversely, with more than four measurements, there is no exact solution to the overdetermined

set of these equations. With any number of measurements, the equations may be put in the form of Eq. B.2-6, by altering Eqs. B.2-8 and B.2-9 so that the number of rows of A and $\vec{\Delta\rho}$ equals the number of measurements. With other than four measuremen's, the matrix A is not square. With fewer than four measurements, additional information of some sort is necessary. With more than four measurements, the standard procedure is to multiply Eq. B.2-6 by A^T to obtain

$$A^T A \, \vec{\Delta x} = A^T \, \vec{\Delta\rho} \ . \qquad \text{(B.3-1)}$$

The matrix $A^T A$ is a 4×4, and, if it is invertible (if the more than four measurements contain at least four independent ones), then Eq. B.3-1 may be "solved" to yield

$$\vec{\Delta x} = (A^T A)^{-1} \, A^T \, \vec{\Delta\rho} \ . \qquad \text{(B.3-2)}$$

This solution for the receiver error vector will, in general, not satisfy any of the original equations, but it represents the well-known "least squares" solution to the overdetermined set of equations, minimizing the sum of the squares of the amounts by which the equations are not satisfied. This least squares method of solving for the <u>errors</u> in determined position due to <u>errors</u> in pseudo-range measurements is only appropriate if the position estimate itself was obtained from the pseudo range measurements by the least squares process.

Making the same statistical assumptions about the (now more than four) pseudo range errors as were previously made yields the same formal results; namely, that Eq. B.2-13 and its normalized form Eq. B.2-14 are still valid, and the definitions of the DOP's are unchanged. Thus, the dilution of precision concept is useful in describing the situation involving more than four measurements, with the basic definitions virtually unchanged.

B.4 COORDINATE INVARIANCE OF GDOP, PDOP, AND TDOP

As was remarked earlier, in order to compute the horizontal or vertical dilutions of precision an appropriate coordinate system must be used. It might be expected that GDOP, PDOP, and TDOP do <u>not</u> depend upon which coordinate system is chosen for the computations. This coordinate invariance is demonstrated here.

Assume that the computations have already been performed in one coordinate system with the notation previously given. Assume a second coordinate system related to the first by the orthonormal 3×3 rotation matrix M, so that the unit vectors from the receiver toward the satellites are given by $\hat{v}_i$ in the new coordinates, where

$$\hat{v}_i = M\,\hat{u}_i \ , \tag{B.4-1}$$

and M satisfies

$$M^{-1} = M^T \ . \tag{B.4-2}$$

What was termed the A matrix in the original coordinates will become the B matrix in the new coordinates. Clearly

$$B = \begin{pmatrix} v_{1x}' & v_{1y}' & v_{1z}' & 1 \\ v_{2x}' & v_{2y}' & v_{2z}' & 1 \\ \cdot & \cdot & \cdot & \cdot \\ \cdot & \cdot & \cdot & \cdot \\ \cdot & \cdot & \cdot & \cdot \\ v_{nx}' & v_{ny}' & v_{nz}' & 1 \end{pmatrix} , \tag{B.4-3}$$

where the general case of measurements to n satellites is considered. Reflection shows that

$$B = AM_4^T \ , \tag{B.4-4}$$

where the new, 4×4 matrix M_4 is given in partitioned form by

$$M_4 = \left(\begin{array}{c|c} M & \vec{0} \\ \hline 0 & 1 \end{array}\right) . \qquad \text{(B.4-5)}$$

Like M, M_4 is orthonormal and satisfies

$$M_4^{-1} = M_4^T . \qquad \text{(B.4-6)}$$

The normalized receiver error covariance matrix in the new coordinates becomes Q, where

$$Q = (B^T B)^{-1} . \qquad \text{(B.4-7)}$$

Clearly,

$$\begin{aligned} Q &= (M_4 A^T A M_4^T)^{-1} , \\ &= M_4 \, P \, M_4^T . \end{aligned} \qquad \text{(B.4-8)}$$

If P is partitioned as

$$P = \left(\begin{array}{c|c} P_3 & \vec{p} \\ \hline \vec{p}^T & P_{44} \end{array}\right) , \qquad \text{(B.4-9)}$$

then Q is given as

$$Q = \left(\begin{array}{c|c} M P_3 M^T & M\vec{p} \\ \hline \vec{p}^T M^T & P_{44} \end{array}\right) . \qquad \text{(B.4-10)}$$

As the 4,4 element of Q is identical to P_{44}, it is clear that TDOP is the same when computed in the second coordinate system as it is when computed in the first. As for PDOP, in the first system

$$PDOP^2 = tr(P_3) \ , \qquad (B.4\text{-}11)$$

while in the second,

$$PDOP^2 = tr(M\ P_3\ M^T) \ . \qquad (B.4\text{-}12)$$

The trace function has the general property that

$$tr(CD) = tr(DC) \qquad (B.4\text{-}13)$$

for any matrices C and D whenever their dimensions give sense to both products. (I.e., if C is n×m, then D must be m×n.) Thus

$$tr(M\ P_3\ M^T) = tr(P_3\ M^T\ M) = tr(P_3) \ , \qquad (B.4\text{-}14)$$

and PDOP is the same in both coordinate systems.

The identical argument applied to the full 4×4 P matrix shows that GDOP is the same when computed in either system. Or, the fact that

$$GDOP^2 = PDOP^2 + TDOP^2 \ , \qquad (B.4\text{-}15)$$

combined with the invariance of PDOP and TDOP will demonstrate the coordinate invariance of GDOP.

B.5 SINGULAR MEASUREMENT GEOMETRY

It has been remarked that for certain geometrical conditions the pseudo range measurements might not yield four independent pieces of information. In this singular case, it is not possible to solve Eqs. B.2-1 for the receiver position

and clock offset. Also, Eq. B.2-6 will not be solvable for the receiver error vector due to errors in the pseudo range measurements. The A matrix will be of rank three or less, and A^TA will be singular and have no inverse. In the case of exactly four measurements, A itself will be singular. The question is: For what geometries does this singular condition occur?

The often heard answer is that if all the satellites lie on any (circular) cone with apex at the receiver then the geometry is singular. This fact, and its converse, will be demonstrated here.

It is easy to show that if the satellites all lie on a cone with apex at the receiver, then the A matrix is of rank three (or less), and A^TA is singular. By the results of the previous section, it is clear that it makes no difference what coordinate system is used to express the A matrix; if it is of rank three in one coordinate system, then it is of rank three in all coordinate systems. Supposing all the satellites to lie on a cone with apex at the receiver, select the axis of the cone as the z-axis of the coordinate system. Then the unit vectors from the receiver toward the satellites will all have identical z components equal to the cosine of the half-cone angle, α. This geometry is illustrated in Fig. B.5-1. The A matrix now looks like

$$A = \begin{pmatrix} u_{1x} & u_{1y} & \cos\alpha & 1 \\ u_{2x} & u_{2y} & \cos\alpha & 1 \\ \vdots & \vdots & \vdots & \vdots \\ u_{nx} & u_{ny} & \cos\alpha & 1 \end{pmatrix} . \quad \text{(B.5-1)}$$

Clearly the last two columns of A are scalar multiples of one another, so A can be of rank three at most, and A^TA must be singular.

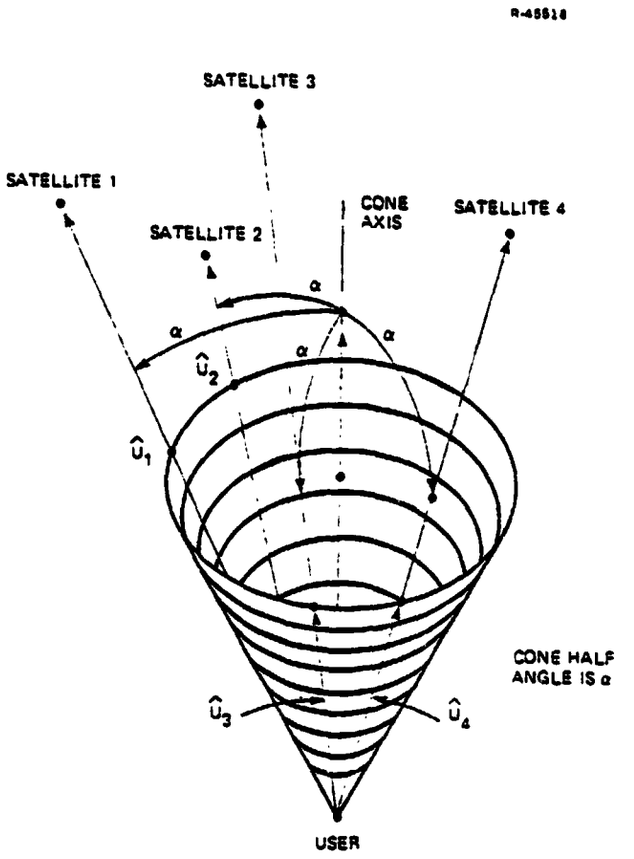

Figure B.5-1 Singular Geometry -- Satellites Lie on a Cone With Apex at the User

The converse statement, that if A is of rank three (or less), then all the satellites lie on a cone with apex at the receiver, is not much harder to show. If A is of rank three, only three of its rows may be linearly independent. (The case when fewer than three rows are linearly independent will be an obvious extension.) As it makes no difference how the rows are numbered, move these three rows to the top. The remaining dependent row (or rows) may then be expressed as linear combinations of the top three rows. That is, for k = 4,...,n there are constants λ_{k1}, λ_{k2}, and λ_{k3} such that

$$(u_{kx}\ u_{ky}\ u_{kz}\ 1) = \lambda_{k1}(u_{1x}\ u_{1y}\ u_{1z}\ 1) + \lambda_{k2}(u_{2x}\ u_{2y}\ u_{2z}\ 1) + \lambda_{k3}(u_{3x}\ u_{3y}\ u_{3z}\ 1) \ . \qquad \text{(B.5-2)}$$

Examination of the fourth component of this equation reveals that

$$\lambda_{k1} + \lambda_{k2} + \lambda_{k3} = 1 \ . \qquad \text{(B.5-3)}$$

Any <u>three</u> vectors must lie on a cone with apex at the origin. (This is equivalent to the statement that any three points on the unit sphere must lie on some small circle.) So the unit vectors to the satellites involved in the top three rows of the A matrix must lie on some cone. Take the axis of this cone as the z-axis of the coordinate system, then the z components of the first three rows must equal the cosine of the half cone angle, or

$$u_{1z} = u_{2z} = u_{3z} = \cos\alpha \ . \qquad \text{(B.5-4)}$$

Equations B.5-2 and B.5-3 now show that the z components of all the rows of A must be equal,

$$\lambda_{k1}u_{1z} + \lambda_{k2}u_{2z} + \lambda_{k3}u_{3z} = u_{kz} = \cos\alpha \qquad \text{(B.5-5)}$$

hence all the satellites must lie on a cone with apex at the receiver.

When the satellites do all lie on a cone, then the various DOP's do not exist. When the satellites are nearly on such a cone, then the DOP's exist but will, in general, be large. It might happen that VDOP, HDOP, or TDOP will be of reasonable size in this case, but GDOP and PDOP will be large.

B.6 'N IMPORTANT EXAMPLE SITUATION

The reason for defining the various DOP's is to reduce complex geometrical situations to a single number, or to a few numbers, with direct relevance to GPS navigation and time accuracy. Equations B.2-15 through B.2-19 defining the DOP's accomplish that objective. but they give no immediate insight into the relationship between the DOP's and the geometry.

One way to use the DOP's is to calculate them for every alternative geometry in a given situation and choose the satellites for tracking which yield the best DOP values. For example, if nine satellites are visible to a receiver but only four are to be used, the DOP's may be calculated for each of the 126 ways four satellites could be selected from the nine visible, and the set of four to be used could be taken as the one with the appropriate minimum DOP. No geometrical insight is needed for this exhaustive process.

To decide the acceptability of a single DOP in a non-exhaustive situation, or to otherwise shorten the computationally burdensome process of exhaustively computing DOP's, it is useful to have a quantitative feel for the relationship between geometrical situations and the DOP's, and for the potential ranges of the DOP's.

It would be ideal if there were some simply understandable, closed-form expression for the DOP's in terms of obvious parameters describing the geometrical situation, without reference to unnecessary, complicating details such as the orientation of the coordinate system in which the DOP is computed. In the simplest case for which the DOP's exist, that of measurements to four satellites, there are eight independent

parameters necessary to describe the orientations of the unit vectors toward the satellites. If one is considering GDOP, PDOP, or TDOP, where the coordinates of computation are not relevant, then the number of independent parameters may be reduced to five. Describing a single unit vector by two independent parameters, however, is not simple; it involves either trigonometric functions of two angles or square roots of direction cosine parameters. After inserting several of these expressions into the matrix multiplication and inversion processes used to compute DOP's, the results would be too complex to be easily understandable. So the process of gaining a quantitative feel of the relationship of the DOP's to the geometry will begin with the close analysis of a constrained geometrical situation having only one free parameter.

This situation is most easily described with reference to a locally level coordinate system. Let one satellite, the first one, be directly overhead (along the z-axis). The other three satellites are separated from one another in azimuth by 120 deg, and all have the same, unspecified coelevation (which may vary from zero to 180 deg). The common coelevation angle, α, of the three satellites is the only variable parameter of this situation. For completeness, assume that the vector from the receiver to the second satellite has an azimuth of zero, the third satellite has an azimuth of +120 deg, and the fourth satellite has an azimuth of -120 deg. Figure B.6-1 illustrates this geometry.

Of course, the geometry need not be referenced to any local level frame to consider GDOP, PDOP, or TDOP. It may simply by described by saying that the vectors toward three of the satellites are evenly spread around a cone of half-angle α, while the vector toward the fourth satellite lies on the axis of the cone (pointing either into or out of the cone).

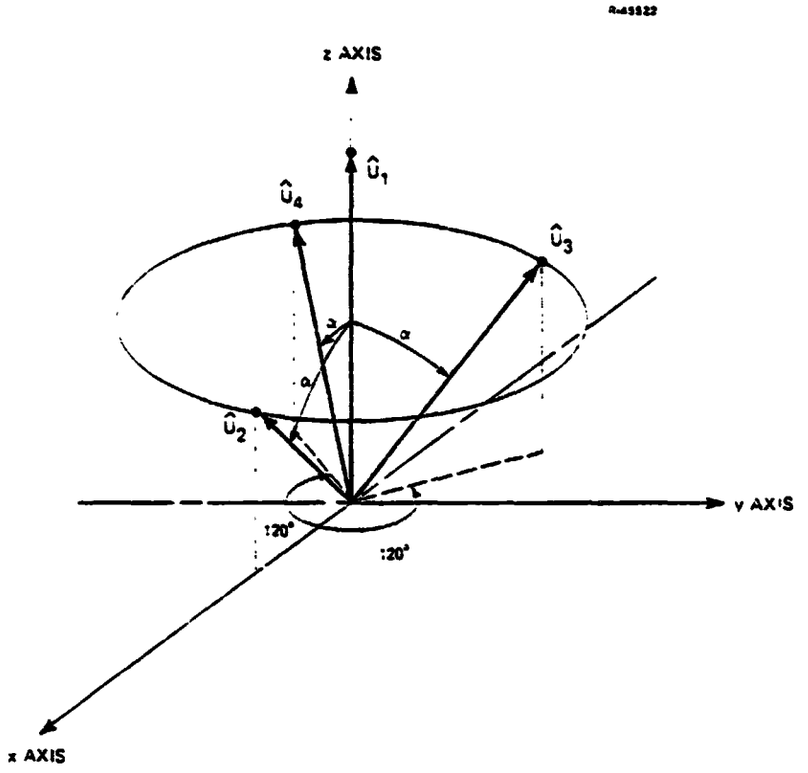

Figure B.6-1 Single Parameter (Constrained) Geometry Situation

The unit vectors toward the four satellites are given by

$$\hat{u}_1 = \begin{pmatrix} 0 \\ 0 \\ 1 \end{pmatrix} \quad , \quad \hat{u}_2 = \begin{pmatrix} \sin \alpha \\ 0 \\ \cos \alpha \end{pmatrix} \quad ,$$

$$\hat{u}_3 = \begin{pmatrix} -(1/2)\sin \alpha \\ (\sqrt{3}/2)\sin \alpha \\ \cos \alpha \end{pmatrix} \quad , \quad \hat{u}_4 = \begin{pmatrix} -(1/2)\sin \alpha \\ -(\sqrt{3}/2)\sin \alpha \\ \cos \alpha \end{pmatrix} \cdot \qquad \text{(B.6-1)}$$

The A matrix of Eq. B.2-9 becomes

$$A = \begin{pmatrix} 0 & 0 & 1 & 1 \\ \sin\alpha & 0 & \cos\alpha & 1 \\ -(1/2)\sin\alpha & (\sqrt{3}/2)\sin\alpha & \cos\alpha & 1 \\ -(1/2)\sin\alpha & -(\sqrt{3}/2)\sin\alpha & \cos\alpha & 1 \end{pmatrix} , \tag{B.6-2}$$

whereupon

$$A^TA = \begin{pmatrix} (3/2)\sin^2\alpha & 0 & 0 & 0 \\ 0 & (3/2)\sin^2\alpha & 0 & 0 \\ 0 & 0 & 1+3\cos^2\alpha & 1+3\cos\alpha \\ 0 & 0 & 1+3\cos\alpha & 4 \end{pmatrix} . \tag{B.6-3}$$

It follows that the normalized receiver error covariance matrix, the inverse of A^TA, is given by

$$P = \begin{pmatrix} \frac{2}{3\sin^2\alpha} & 0 & 0 & 0 \\ 0 & \frac{2}{3\sin^2\alpha} & 0 & 0 \\ 0 & 0 & \frac{4}{3(1-\cos\alpha)^2} & -\frac{1+3\cos\alpha}{3(1-\cos\alpha)^2} \\ 0 & 0 & -\frac{(1+3\cos\alpha)}{3(1-\cos\alpha)^2} & \frac{1+3\cos^2\alpha}{3(1-\cos\alpha)^2} \end{pmatrix} \tag{B.6-4}$$

The various DOP's are given by

$$HDOP = \frac{2}{\sin \alpha} \sqrt{\frac{1}{3}} \quad , \qquad (B.6\text{-}5)$$

$$VDOP = \frac{2}{(1-\cos \alpha)} \sqrt{\frac{1}{3}} \quad , \qquad (B.6\text{-}6)$$

$$PDOP = \frac{2}{(1-\cos \alpha)} \sqrt{\frac{2}{3(1+\cos \alpha)}} \quad , \qquad (B.6\text{-}7)$$

$$TDOP = \frac{1}{(1-\cos \alpha)} \sqrt{\frac{1+3 \cos^2 \alpha}{3}} \quad , \qquad (B.6\text{-}8)$$

$$GDOP = \frac{1}{(1-\cos \alpha)} \sqrt{\frac{9 + \cos \alpha + 3 \cos^2 \alpha + 3 \cos^3 \alpha}{3(1+\cos \alpha)}} \quad . \qquad (B.6\text{-}9)$$

An issue of immediate interest is the situation in which these DOP's are minimized and the minimum values thus obtained. It is readily apparent that HDOP is minimized when α is 90 deg, putting three of the satellites in the horizontal plane. The values of the DOP's for this situation are

$$HDOP = 2 \sqrt{\frac{1}{3}} \simeq 1.1547,$$

$$VDOP = 2 \sqrt{\frac{1}{3}} \simeq 1.1547,$$

$$PDOP = 2 \sqrt{\frac{2}{3}} \simeq 1.6330,$$

$$TDOP = \sqrt{\frac{1}{3}} \simeq 0.5774,$$

$$GDOP = \sqrt{3} \simeq 1.7321.$$

The situation in this constrained case which "minimizes" VDOP would have α be 180 deg, putting three satellites directly

below the receiver and one above. This situation is a singular one, however, causing HDOP, PDOP, and GDOP to blow up.

A single situation simultaneously minimizes PDOP, TDOP, and GDOP. It has α at about 109.47 deg (so that $\cos \alpha = -1/3$), meaning that the three satellites are all about 20 deg below the horizon. In this situation the four unit vectors toward the satellites all terminate at the vertices of a regular tetrahedron, illustrated in Fig. B.6-2. This situation is completely symmetric in that each unit vector makes the same angle, 109.47 deg, with each of the other unit vectors. While the minimization taking place in this example is only that of selecting the single parameter in a constrained, one-parameter geometrical situation, the resultant minimum situation illustrated in Fig. B.6-2 happens to be a global minimum for PDOP, TDOP, and GDOP. That is, no better values for these DOP's can be obtained by any other arrangement of four satellites, a fact stated here without proof. The values of the DOP's in this situation are

$$\text{HDOP} = \sqrt{\frac{3}{2}} \simeq 1.2247$$

$$\text{VDOP} = \sqrt{\frac{3}{2}} \simeq 0.8660$$

$$\left.\begin{aligned} \text{PDOP} &= \frac{3}{2} = 1.5000 \\ \text{TDOP} &= \frac{1}{2} = 0.5000 \\ \text{GDOP} &= \sqrt{\frac{5}{2}} \approx 1.5811 \end{aligned}\right\} \text{Absolute minimum for 4 satellites}$$

Of course, this global minimum situation would be impossible to obtain near the surface of the earth, for the earth itself would block visibility to the three satellites below the horizontal plane. A better picture of how the DOP's

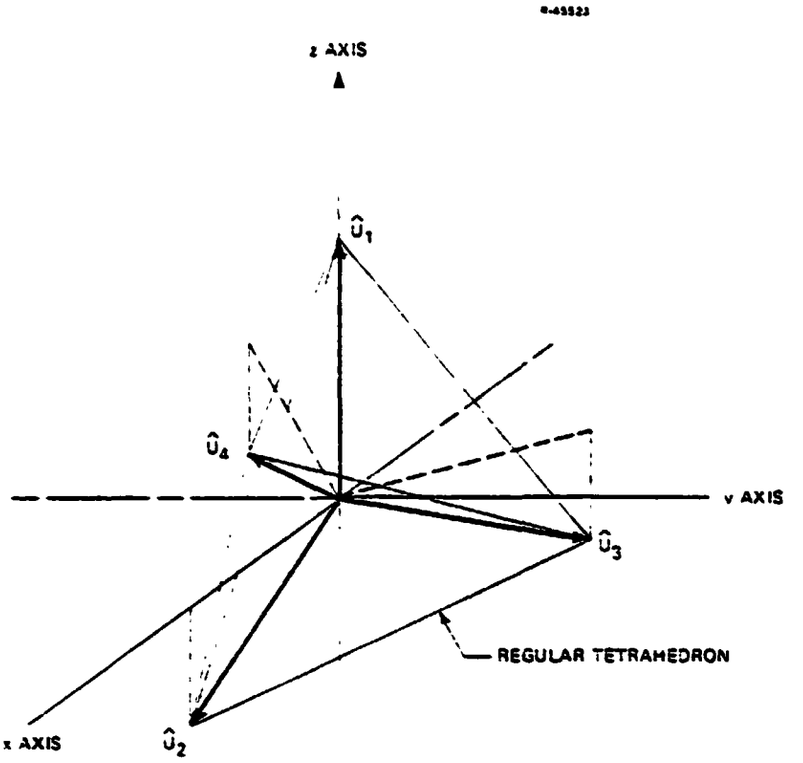

Figure B.6-2 Global Minimum for Four-Satellite GDOP, PDOP, and TDOP

vary with the coelevation angle is given in Fig. B.6-3 (a and b), which plots the DOP's versus the coelevation angle.

Leaving, for a paragraph, the one-parameter geometry and taking up the topic of global minimums for the DOP's, a global minimum for HDOP is approached as a singular limit of a situation where the unit vectors to the four satellites approach the plus and minus x and y axes in the horizontal plane. The limit of HDOP in this situation is 1.0, but the limiting situation is singular, so HDOP does not exist.* Similarly, a global minimum for VDOP would be the limit of a singular situation

*The DOP's could be redefined using matrix pseudo-inverses instead of ordinary inverses. Then, in some singular situations, certain of the DOP's would still be well defined, as would HDOP in the situation indicated.

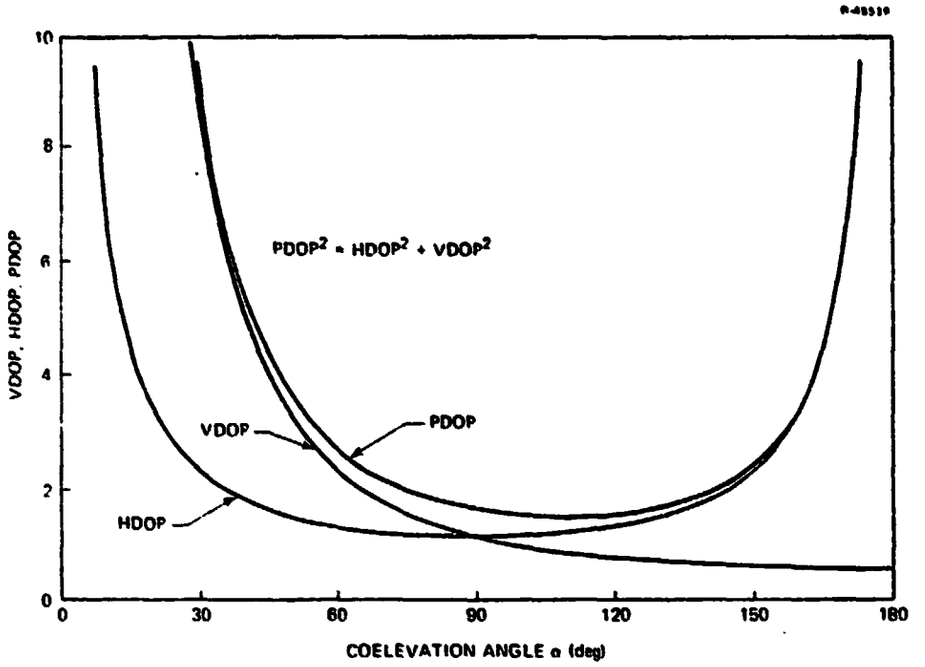

Figure B.6-3(a) Variation of VDOP, HDOP, and PDOP with Coelevation Angle for a One-Parameter Geometrical Situation

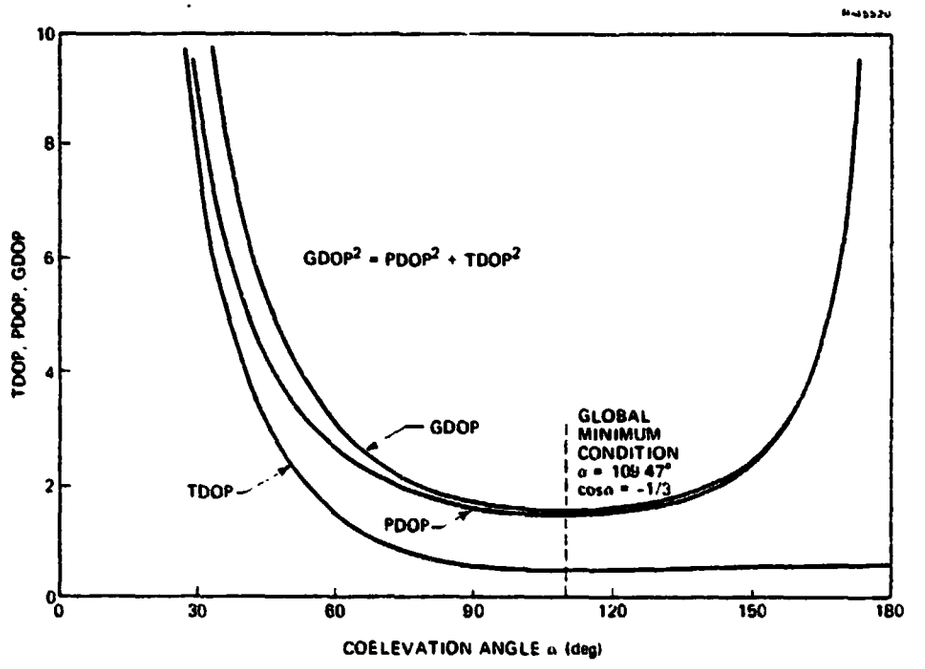

Figure B.6-3(b) Variation of TDOP, PDOP, and GDOP with Coelevation Angle for a One-Parameter Geometrical Situation

with two satellites along the positive vertical (z) axis and two along the negative vertical axis. The limit of VDOP in this situation is 0.5.

Returning again to the one-parameter geometry, Fig. B.6-3(b) has utility beyond its example purposes. It frequently happens that satellite visibility to a user is restricted to some cone with apex at the user. This could be because the earth masks satellites, leaving the user with an 80 to 85 deg half-angle cone of visibility, corresponding to a 10 or 5 deg mask angle above the horizon.* Or, it could be because the user has an antenna with a conical reception pattern, as, for example, a hemispherical antenna. In any event, if the user is restricted to a cone of satellite visibility of half angle 109.5° or less, then the best possible four satellite geometry is the single parameter geometry shown in Fig. B.6-1, and Fig. B.6-3(b) shows the best obtainable TDOP, PDOP, and GDOP. The values quoted earlier for the half-cone angle of 90° are thus lower bounds for users on the surface of the earth, or with hemispherical antennas, making measurements to four satellites.

*This cone could be larger if the user were high above the earth, such as for the Space Shuttle.

REFERENCES

1. Crawford, B.S., and Duiven, E.M., "Space Shuttle Post Entry and Landing Analysis," The Analytic Sciences Corporation, Technical Report TR-302-1, July 1973.

2. Jones, H.L., and Crawford, B.S., "Space Shuttle Entry and Landing Navigation Analysis," The Analytic Sciences Corporation, Technical Report TR-302-2, July 1974.

3. Jones, H.L., and Luders, G., "Space Shuttle Navigation Analysis," The Analytic Sciences Corporation, Technical Report TR-548-1, December 1975.

4. Jones, H.L. et al., "Space Shuttle Navigation Analysis," The Analytic Sciences Corporation, Technical Report TR-548-2, September 1976.

5. Jones, H.L. et al., "Quarterly Progress Report for the Period Ending 30 November 1976," The Analytic Sciences Corporation, Progress Report PR-1001-3, December 1976.

6. Macdonald, T.J. et al., "Quarterly Progress Report for the Period Ending 28 February 1977," The Analytic Sciences Corporation, Progress Report PR-1001-6, April 1977.

7. Matchett, G.A., and Rains, R.G., "Quarterly Progress Report for the Period Ending 31 May 1977," The Analytic Sciences Corporation, Progress Report PR-1001-9, June 1977.

8. Matchett, G.A., and Rains, R.G., "Quarterly Progress Report for the Period Ending 31 August 1977," The Analytic Sciences Corporation, Progress Report PR-1001-12, October 1977.

9. Matchett, G.A. et al., "Quarterly Progress Report for the Period Ending 30 November 1977," The Analytic Sciences Corporation, Progress Report PR-1001-15, December 1977.

10. Matchett, G.A. et al., "Quarterly Progress Report for the Period Ending 28 February 1978," The Analytic Sciences Corporation, Progress Report PR-1001-18, March 1978.

REFERENCES (Continued)

11. Matchett, G.A. et al., "Quarterly Progress Report for the Period Ending 31 May 1978," The Analytic Sciences Corporation, Progress Report PR-1001-21, August 1978.

12. Matchett, G.A. et al., "Quarterly Progress Report for the Period Ending 31 August 1978," The Analytic Sciences Corporation, Progress Report PR-1001-24, October 1978.

13. Luders, G., and Matchett, G.A., "Quarterly Progress Report for the Period Ending 30 November 1978," The Analytic Sciences Corporation, Progress Report PR-1001-27, December 1978.

14. Luders, G., and Matchett, G.A., "Quarterly Progress Report for the Period Ending 28 February 1979," The Analytic Sciences Corporation, Progress Report PR-1001-30, April 1979.

15. Matchett, G.A., "Quarterly Progress Report for the Period Ending 31 May 1979," The Analytic Sciences Corporation, Progress Report PR-1001-33, June 1979.

16. Matchett, G.A., "Quarterly Progress Report for the Period Ending 31 August 1979," The Analytic Sciences Corporation, Progress Report PR-1001-36, October 1979.

17. "OFT-1 Deorbit to Landing," Shuttle Trajectory Data Tape No. V05983, NASA Johnson Space Center, Houston, Texas, March 1976.

18. Eckelkamp, R.E., "OFT-1 Nominal Entry - Landing Test Case 1," Informal Memorandum, April 1976.

19. Heck, M. and Mayur, N., "OFT-1 Preliminary Entry Navigation Simulation Results," Johnson Space Center, IN No. 76-FM-65, September 1976.

20. Van Leeuwen, A., Rockwell International, Private Communication, 26 May 1977.

21. Heck, M.L., "Estimation and Prediction of the Orbiting Space Shuttle in the Presence of Random Propulsive Venting," Applied Mechanics Research Laboratory, The University of Texas at Austin, Austin, Texas, AMRL-1069, May 1975.

22. Osburn, R., private communication, NASA Johnson Space Center, Houston, Texas, January 1977.

REFERENCES (Continued)

23. MacLeod, J., and Batson, B., "Space Shuttle Use of the Global Positioning System (GPS)", NASA Johnson Space Center, Houston, Texas, July 1977.

24. Przyjemski, J.M., "A Compensation Technique for Acceleration-Induced Frequency Changes in Crystal Oscillators," NAECON 1978, Vol. 1, p. 55, May 1978.

25. Rosen, E., and VanLeeuwen, A., "SSTS/GPS Navigation System Design Definition Document (Concept Requirement Document)," SD78-SH-0042, Rockwell International, Space Systems Group, October 1978.

26. Spilker, J.J., Jr., "GPS Signal Structure and Performance Characteristics," Navigation, Vol 25, No. 2, Summer 1978.

27. Lyndon B. Johnson Space Center, Space Shuttle, NASA SP-407, 1976.

28. Speer, K., private communication of Orbiter ascent trajectory data tapes from Johnson Space Center.

29. VanLeeuwen, A., et al., "Shuttle GPS Project Update Presented at XIIIth GPS Panel Meeting June 26-27, 1979, Rockwell Space Systems Group-Downey."

30. "Preliminary Design Review of the Receiver/Processor Assembly (R/PA)," Magnavox, Torrance, California, March 1977.

31. Kartaschoff, P., Frequency and Time, Academic Press, London 1978.

32. Langston, L.S., "Trajectory Tape for OFT-1 Updated Reference Flight Profile (Mean of 1950 Coordinate System)," McDonnell Douglas Technical Services Co., Houston Astronautics Division, TM-1.4-7-473, July 1977.